~~CONFIDENTIAL~~

APOLLO

Final Report

(NASA-CR-136676) APOLLO GUIDANCE AND CONTROLS, 3 Final Report (Martin Co.) 333 p
N74-70971
Unclas
00/99 26175

~~This document will not be indexed or announced in Scientific and Technical Aerospace Reports. The document has received partial Descriptive Cataloging Only.~~

~~EXTRA!~~
~~Kee~~

ER 12007-3 JUNE 1961

Guidance and Control System III

~~Available to NASA Offices and NASA Centers Only~~ -

CLASSIFICATION C GE
UNCLASSIFIED ~~FIDENTIAL~~
By authority of [redacted] E.O. 11652
Changed by Date 8-22-7

~~CONFIDENTIAL~~ ~~EXCLUDED FROM THE GDS~~

MARTIN

CONFIDENTIAL

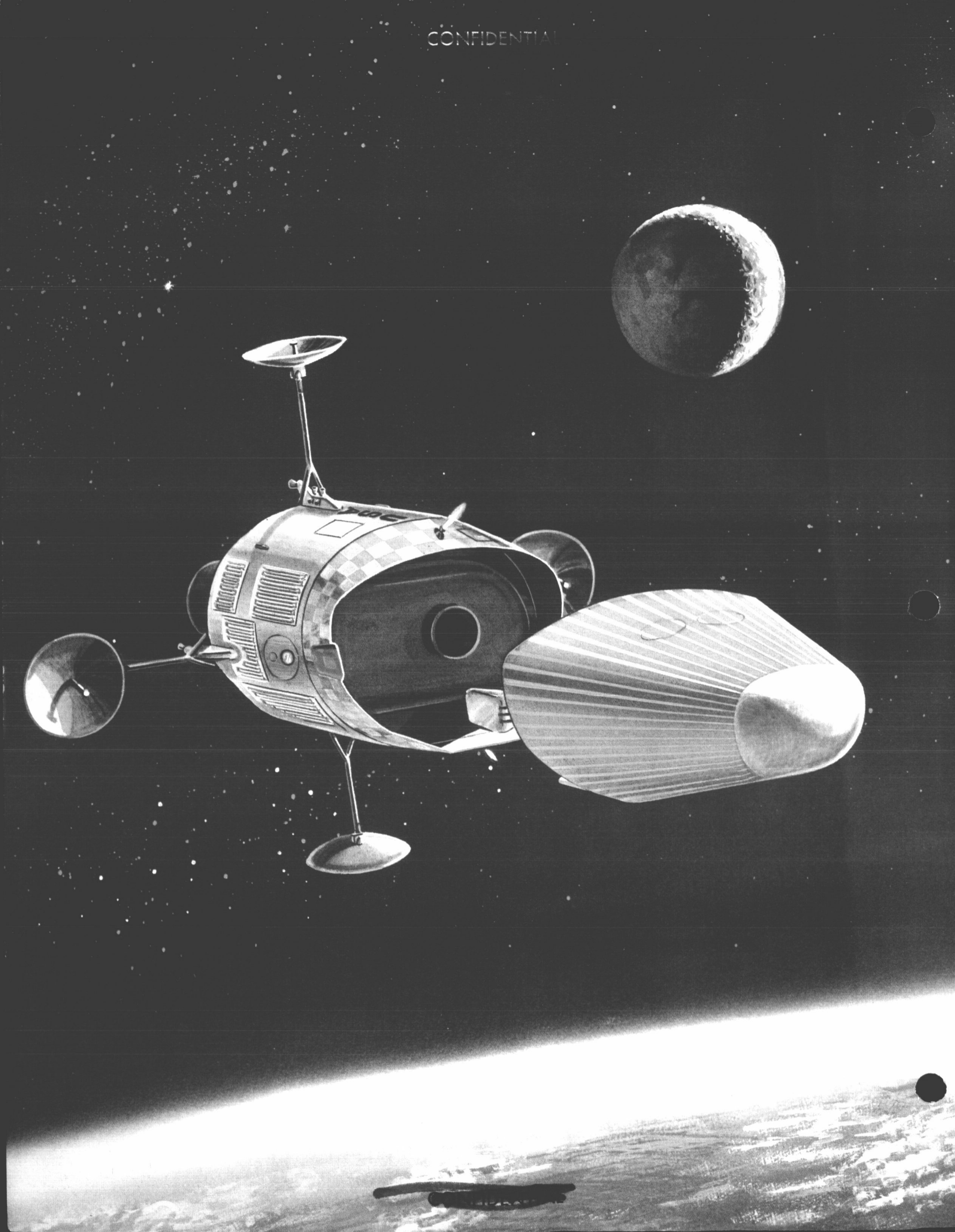

[redacted]

APOLLO

Final Report

Submitted to: NASA Space Task Group.
Contract NAS 5-303, Exhibit A, Item 1.2

Guidance and Controls III

ER 12007-3 JUNE 1961

MARTIN

[redacted]

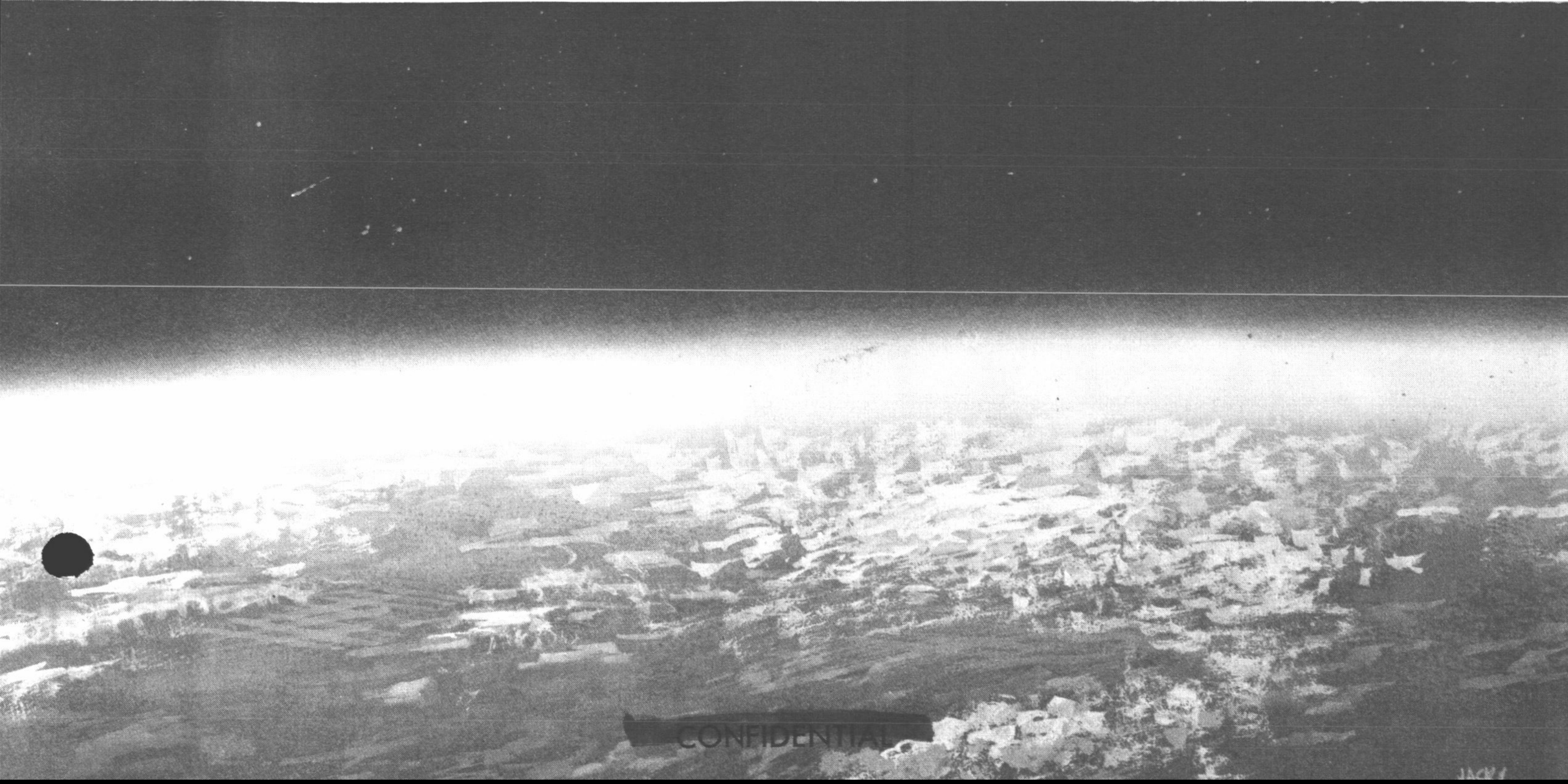

[redacted]

MODEL 410 — THE SYSTEM AND ITS OPERATION

*A BRIEF DESCRIPTION**

Model 410 is the spacecraft system recommended by Martin for the Apollo mission. Its design satisfies the guidelines stated in NASA RFP–302, as well as a more detailed set of guidelines developed by Martin during the Apollo design feasibility study.

We conceive the ultimate Apollo mission to be a manned journey to the lunar surface, arrived at by the preliminary steps of earth orbit, circumlunar and lunar orbit flights. Operational procedures proved out in the early steps will be carried over into the advanced steps, thus establishing a high level of confidence in the success of the lunar flights. With the recommended system, manned lunar orbit missions can be made as early as 1966.

Operational Features

For a circumlunar flight when the moon is at its most southerly declination (Fig. p–1) the launch operation proceeds southeast from Cape Canaveral and down the Atlantic Missile Range. The Saturn C–2 third stage shuts down when orbital velocity is reached at an altitude of 650,000 feet. What follows is a coasting orbit passing over the southern tip of Africa, the Indian Ocean and up the Pacific Missile Range. In this interval the crew checks out all onboard equipment, which has just passed through the accelerations, noise and vibration of the boost phase. If the pilot-commander is satisfied that all systems are working properly, the third stage is restarted and the spacecraft is injected at parabolic velocity northwest of Hawaii. If the pilot-commander is dissatisfied with the condition of the vehicle or crew, he separates from the Saturn S–IV, starts the mission abort engine, re-enters at the point shown in Fig. p–1 and lands at Edwards AFB.

Continuing translunar flight from the point of injection, the trajectory trace swings down over the Caribbean and then west over South America. This particular trajectory passes within 240 naut mi of the moon, then turns back for a direct re-entry some six days after launch. Re-entry occurs southwest of Hawaii some 3300 naut mi from the Edwards AFB landing site.

Tracking. The range coverage provided by present and planned facilities is shown in Fig. p–1 for this trajectory and for a second return trace representing the case when the moon is at the most northerly declination. This second trajectory establishes the 10000-naut mi re-entry range requirement for Apollo to meet the guidelines of operation on every day of the lunar month and of operation into a single landing site.

---

*For more complete descriptions, see ER 12000 or ER 12001.

Abort. During the critical launch and checkout phase, abort will be possible at any time : at the crew's discretion, automatically or by ground command. Up to nine minutes after launch (from Canaveral), the abort landing is restricted to the AMR for a circumlunar flight. Beyond this point the pilot has the option of continuing to any point along the AMR, PMR or into Edwards AFB through the use of the mission abort propulsion system and the inherent downrange maneuverability of the Model–410.

The Selected Spacecraft

The Apollo space vehicle (Model 410 spacecraft plus launching vehicle) is shown in Fig. p–2. The spacecraft—that portion of the space vehicle which makes the flight to the moon—consists of these three modules:

(1) Command module, housing the three crew members during all thrusting periods, e.g., launch from earth, any corrections to the flight path during flight in space, during re-entry and, ultimately, during landing and launch from the moon. It is the operating center from which all control of the flight is made.

(2) Propulsion and equipment module, containing all the propulsion units which operate between the point of final booster separation and re-entry after the lunar flight. It is separated from the command module at 200 naut mi from the earth on the return trip. It is designed with tankage for lunar takeoff and will be offloaded for less ambitious missions.

(3) Mission module—contained within the outer frame of the propulsion and equipment module—providing space during the lunar voyage for scientific observations and crew living functions.

Command Module

With its lifting capability, the Apollo command module represents a step forward in technology over ballistic vehicles, Mercury and (to the best of our knowledge the *Boctók* (*Vostok*). The lift results from the capsule's shape—a blunted cone flattened on the top (see Fig. p–3).

Heating and radiation protection. The Model 410 is shaped conservatively for aerodynamic heating in addition to its relatively high L/D (0.77). By accepting the large convective heat load of a nose radius smaller than that of the Mercury type, the Model 410 shape tends to minimize radiative heat transfer which is less well understood and harder to protect against. The thermal protection system provides excellent protection for the crew from the large aerodynamic heat loads, from space radiation (including solar flares) and from meteorites.

The normal mission radiation dose will not exceed the five rem limit defined by NASA. If the crew should encounter a solar event as severe as that following the May 10, 1959 flare, they would receive a dose of only 67 rem—well within the 100 rem dose limit set by Martin as tolerable during an emergency.

Thermal protection for re-entry is provided by a composite shield of deep charring ablator (nylon phenolic) bonded to superalloy honeycomb panels which are set off and insulated from the water-cooled pressure shell. The control flaps are protected from the high initial heat rate by an ablator bonded directly to the flap. The long-time, lower heating rates are handled by re-radiation from the backside. The aft bulkhead is protected by a fiberglas phenolic honeycomb panel with a foamed polyurethane insulation.

Crew provisions. The crew has access to all electronic and electrical equipment in the command module for maintenance and replacement. Both pilots have two-axis sidestick and foot controllers as well as a manual guidance mode used with the computers inoperative for deep space and re-entry operations.

Cabin pressure is maintained at the equivalent of 5000 feet altitude ("shirt sleeve" environment). Protective suiting is donned only for launching and landing, but need not be inflated except in emergency.

Guidance. The guidance system consists of both automatic and manual star tracking equipment, as well as two inertial platforms and two general purpose digital computers. Two windows, with ablative heat shield covers, are provided for use with tracking instruments.

Flight control. Pitch and yaw attitude control within the atmosphere is provided by flaps driven by hot gas servos. Outside the atmosphere dual reaction controls are used. Roll is controlled at all times by a dual reaction system.

Communications. Communications equipment includes a K_u band for re-entry, a C-band for the pre-reentry and both HF and VHF rescue beacons for landing and recovery.

Landing system. The landing system consists of a steerable parachute, retrorocket combination, enabling the M–410 to avoid local obstacles, trim out wind drift and reduce sinking speed to a nominal three feet per second—low enough for safe landing on any kind of terrain or in very rough seas. In the event of retrorocket failure, accelerations on the crew will not exceed 20 G.

Launch escape propulsion system (LEPS). LEPS is a thrust-vector-controlled, solid rocket system which separates the command module from the rest of the space vehicle in the event of an emergency during launch pad operations or during boost through the atmosphere. In an off-the-pad abort, it lifts the command module to an altitude of more than 4000 feet. During a normal boost trajectory, LEPS is jettisoned at 300,000 feet.

Propulsion and Equipment Module

The propulsion and equipment module (shown in Fig. p–3) contains propulsion devices and equipment which are not necessary for re-entry. Its outer skin serves both as a load carrying structure and as a meteorite shield for the propellant tanks, mission module and other equipment.

Propulsion devices. The mission engine, used for trajectory correction and abort, is a high preformance, modified LR–115 (Pratt & Whitney), developing 15,600 pounds of thrust. A total of 10,450 pounds of liquid hydrogen and liquid oxygen propellants may be carried, sufficient for lunar takeoff.

Four vernier engines, with 300 pounds of thrust each, are used for midcourse correction, ullage impulse to settle the mission engine propellants and for thrust vector control during operation of the mission engine. In addition there are two sets of six control jets which provide 30 pounds of thrust for roll, pitch and yaw control.

Power sources. Spacecraft equipment is powered by fuel cells (2 kw) which under normal conditions, use the boiloff from the mission propulsion system. A supply of independent reactants is provided for emergencies. Battery power is used during re-entry.

Communications. Four large antennas fold out to provide S-band communications and X-band radar altimeter information. VHF communications gear is also provided.

Mission Module

The mission module provides 400 cubic feet of living space during the lunar voyage. It serves as a midcourse work-rest area, providing freedom of movement and privacy. For operations on the lunar surface it will be a base of scientific investigations, and will serve as an airlock. The same "shirt sleeve" environment at 12.2 psi is maintained as in the command module.

The mission module provides the space and flexibility required for effective lunar reconnaissance and scientific experimentation. An Eastman-Kodak camera-telescope has been selected, for example, which has one-meter resolution at lunar orbit altitude of 50 naut mi.

MODEL 410 WEIGHT SUMMARY

Mission	Circumlunar	Lunar Orbit	Lunar Takeoff
Command Module	6954	6954	6954
Propulsion and Equipment Module	7372	13,192	15,618
Launch Escape Propulsion System	185	185	0
Adapter	489	489	0
Effective Launch Weight	15,000	20,820	22,572

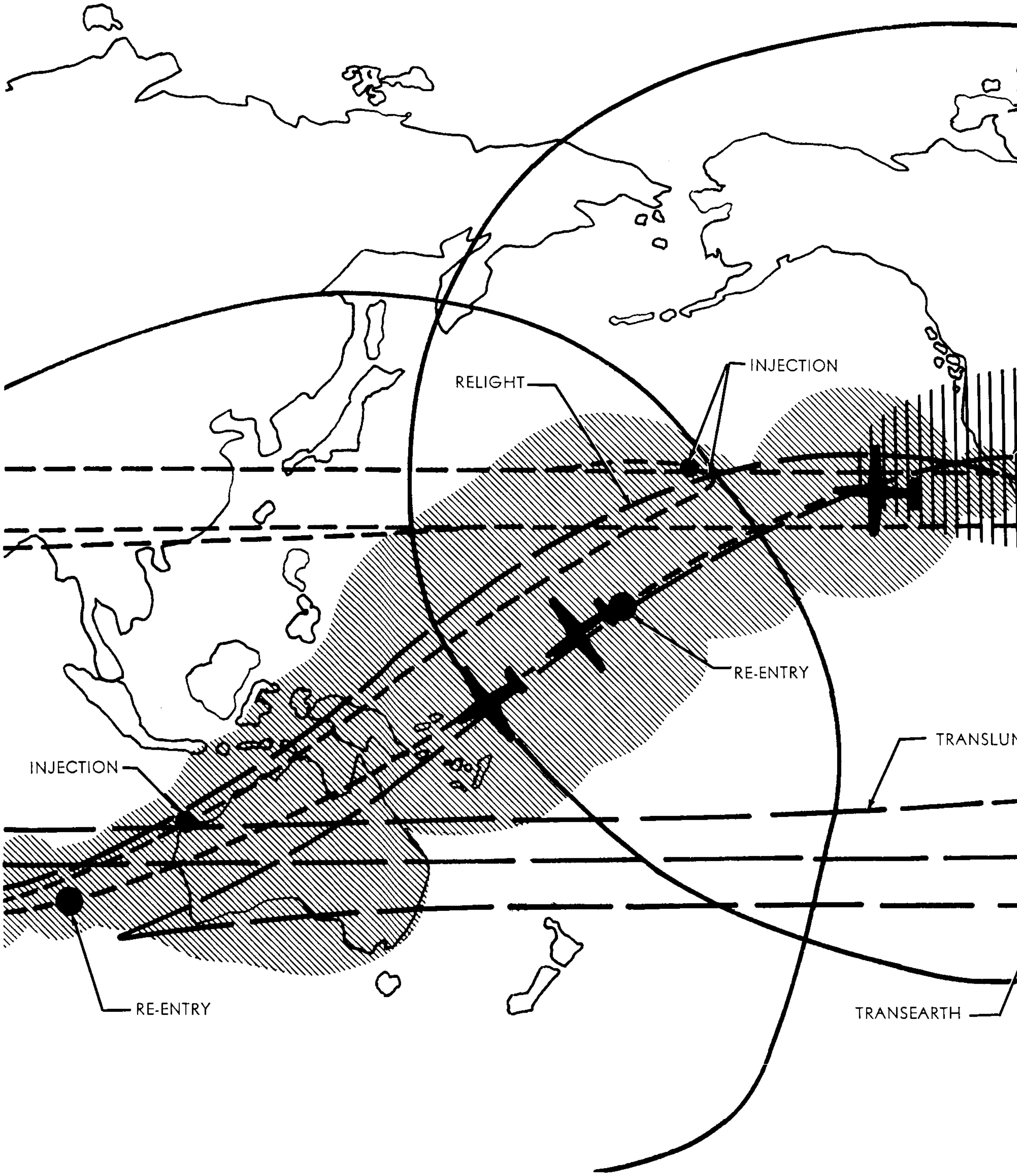
RELIGHT
INJECTION
RE-ENTRY
TRANSLUN
INJECTION
RE-ENTRY
TRANSEARTH

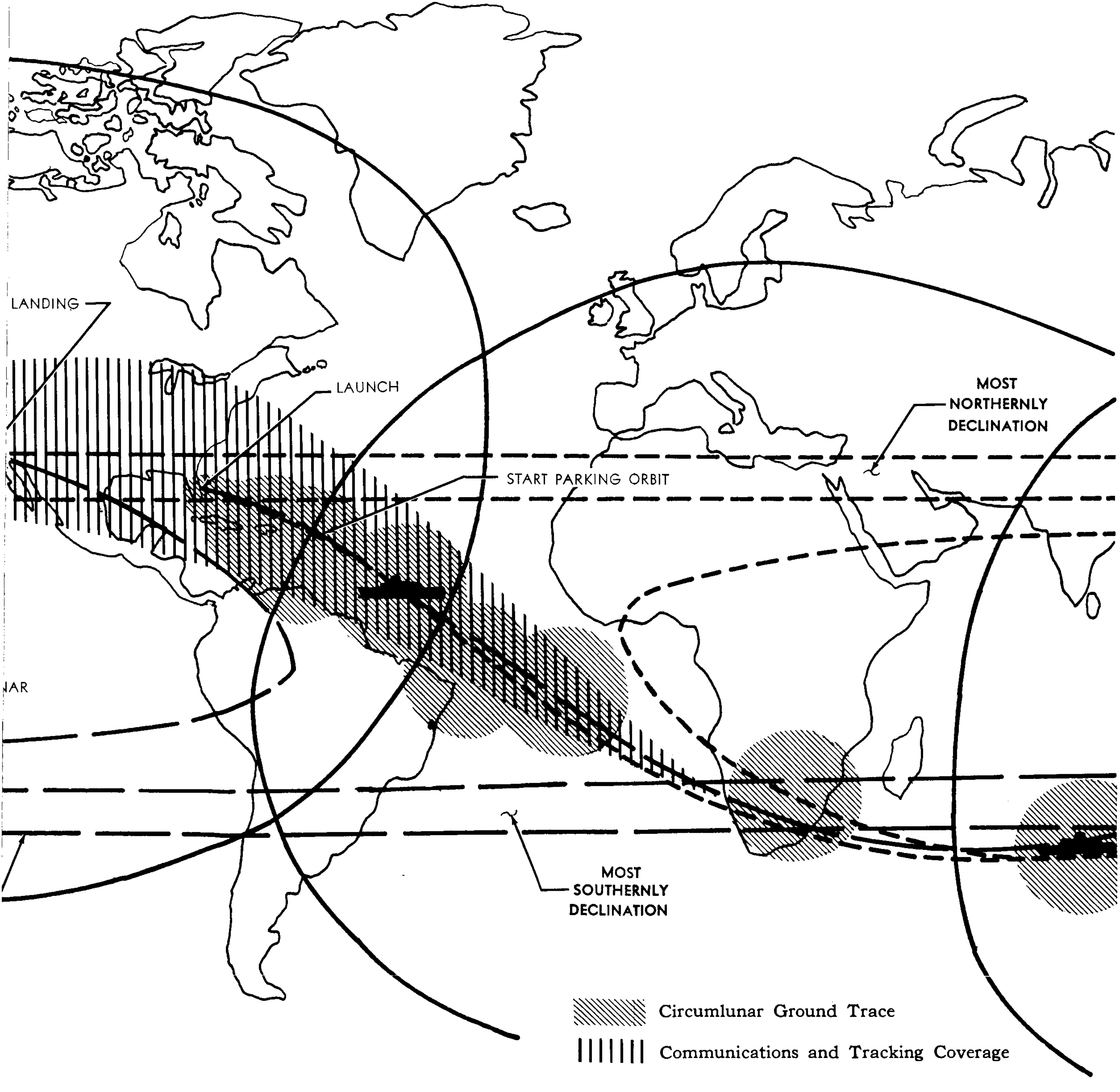
LANDING
LAUNCH
START PARKING ORBIT
MOST NORTHERNLY DECLINATION
AR
MOST SOUTHERNLY DECLINATION
▨ Circumlunar Ground Trace
||||||| Communications and Tracking Coverage

Fig. p–1 Model 410 Circumlunar Trajectory and Range Coverage

MISSION	EFFECTIVE GROSS WEIGHT (lb)	PROPULSION ΔV CAPABILITY (fps) MISSION	PROPULSION ΔV CAPABILITY (fps) VERNIER
CIRCUMLUNAR	15000	1830	525
LUNAR ORBIT	20820	6100	525
LUNAR TAKEOFF	22572	8600	200

VOLUMES (cu ft)	
COMMAND MODULE	350
MISSION MODULE	400
MISSION H_2 TANK	400
MISSION O_2 TANK	122

PROPULSION SYSTEM DATA

PURPOSE	TYPE	ISP. (SEC)	THRUST (lb)
MISSION (1)	H_2—O_2 (ADV. LR115)	427	15600
VERNIER (4)	N_2H_4/UDMH–N_2O_4	315	300 EACH
ATTITUDE CONTROL (14+BACKUP)	N_2H_4/UDMH–N_2O_4	250–315	15 TO 50

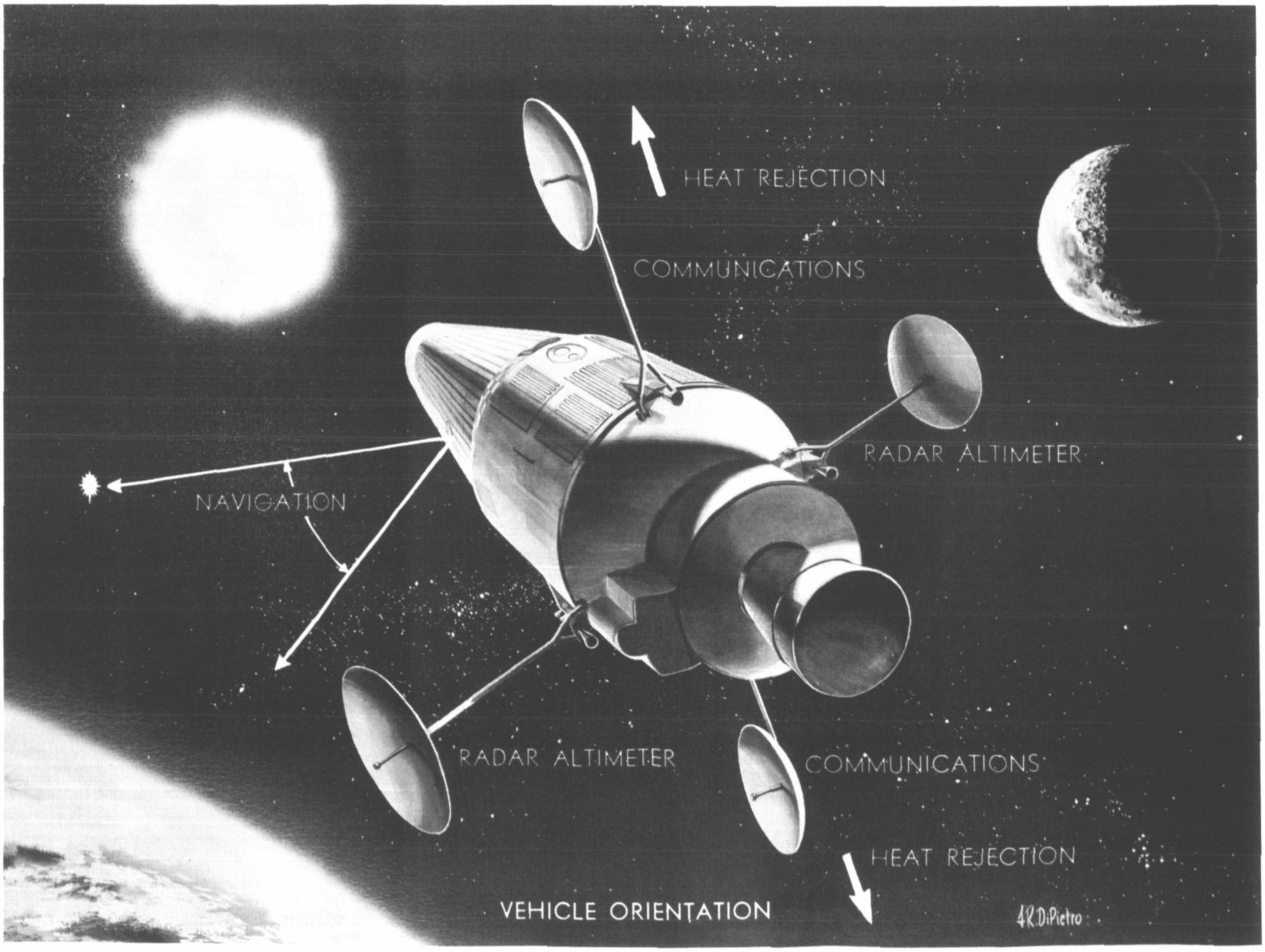
HEAT REJECTION
COMMUNICATIONS
RADAR ALTIMETER
NAVIGATION
RADAR ALTIMETER
COMMUNICATIONS
HEAT REJECTION
VEHICLE ORIENTATION
A.R.DiPietro

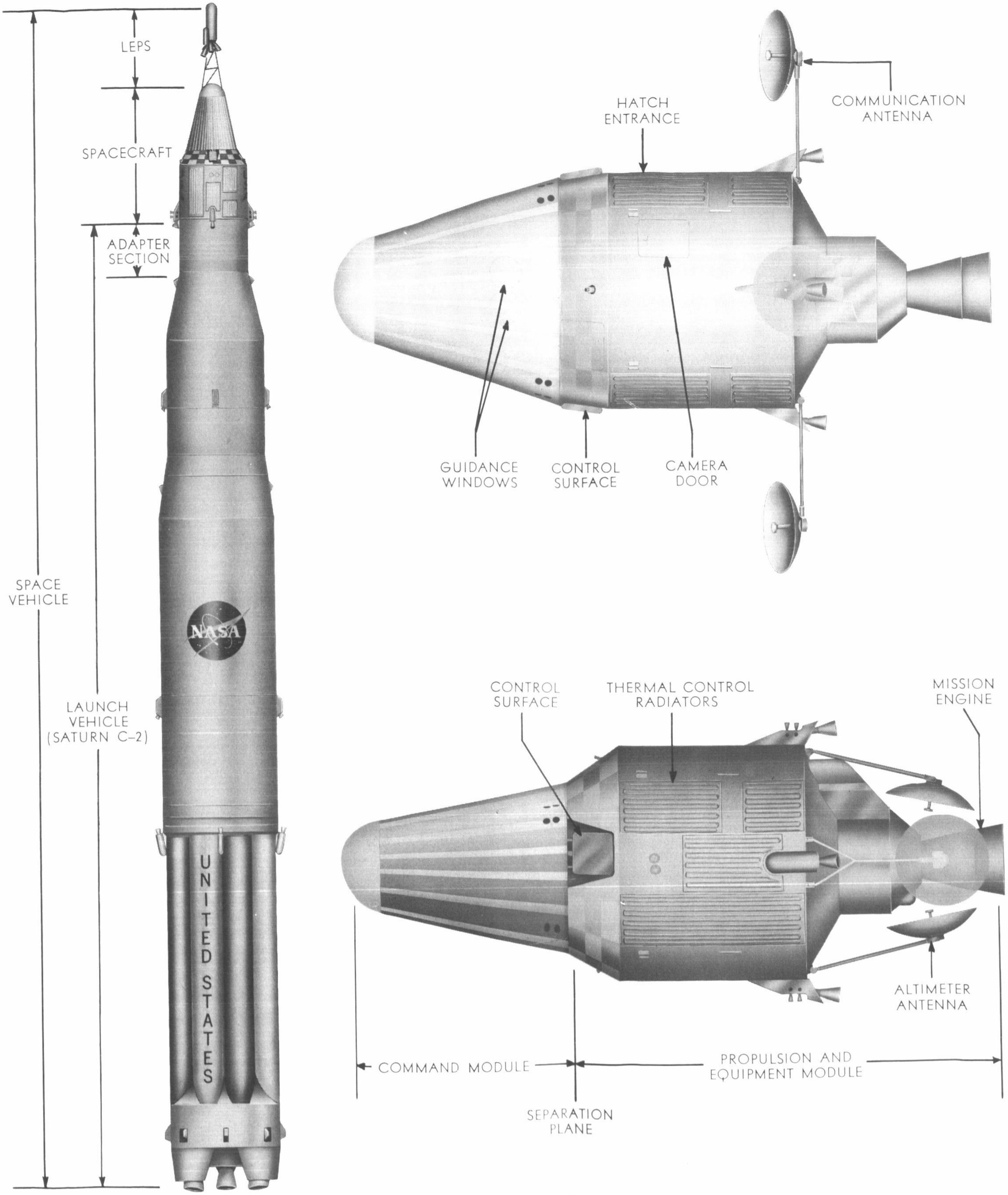
LEPS
SPACECRAFT
ADAPTER SECTION
SPACE VEHICLE
LAUNCH VEHICLE (SATURN C–2)
NASA
UNITED STATES
HATCH ENTRANCE
COMMUNICATION ANTENNA
GUIDANCE WINDOWS
CONTROL SURFACE
CAMERA DOOR
CONTROL SURFACE
THERMAL CONTROL RADIATORS
MISSION ENGINE
ALTIMETER ANTENNA
COMMAND MODULE
PROPULSION AND EQUIPMENT MODULE
SEPARATION PLANE

Fig. p-2. Model 410 Apollo Space Vehicle

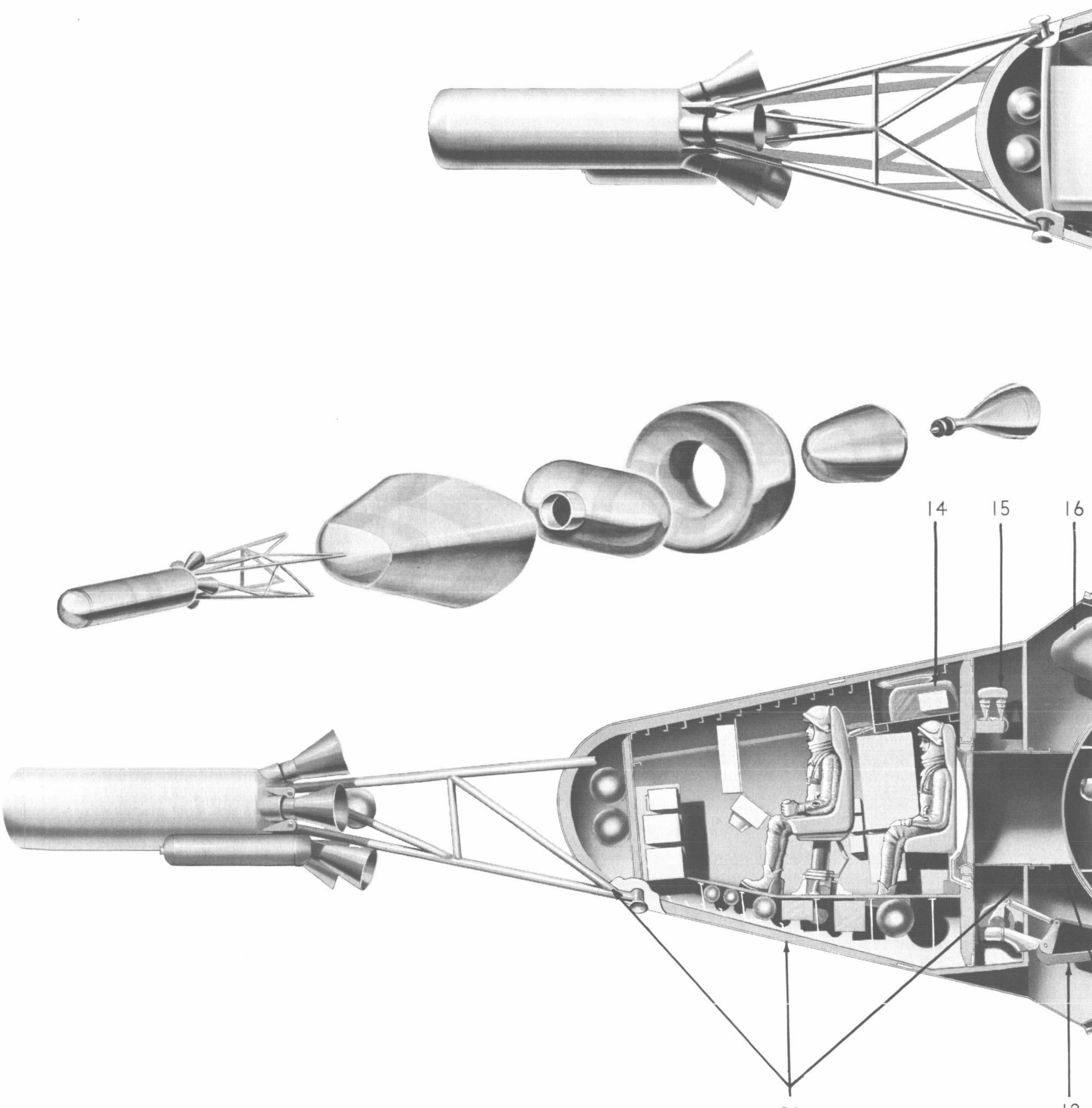

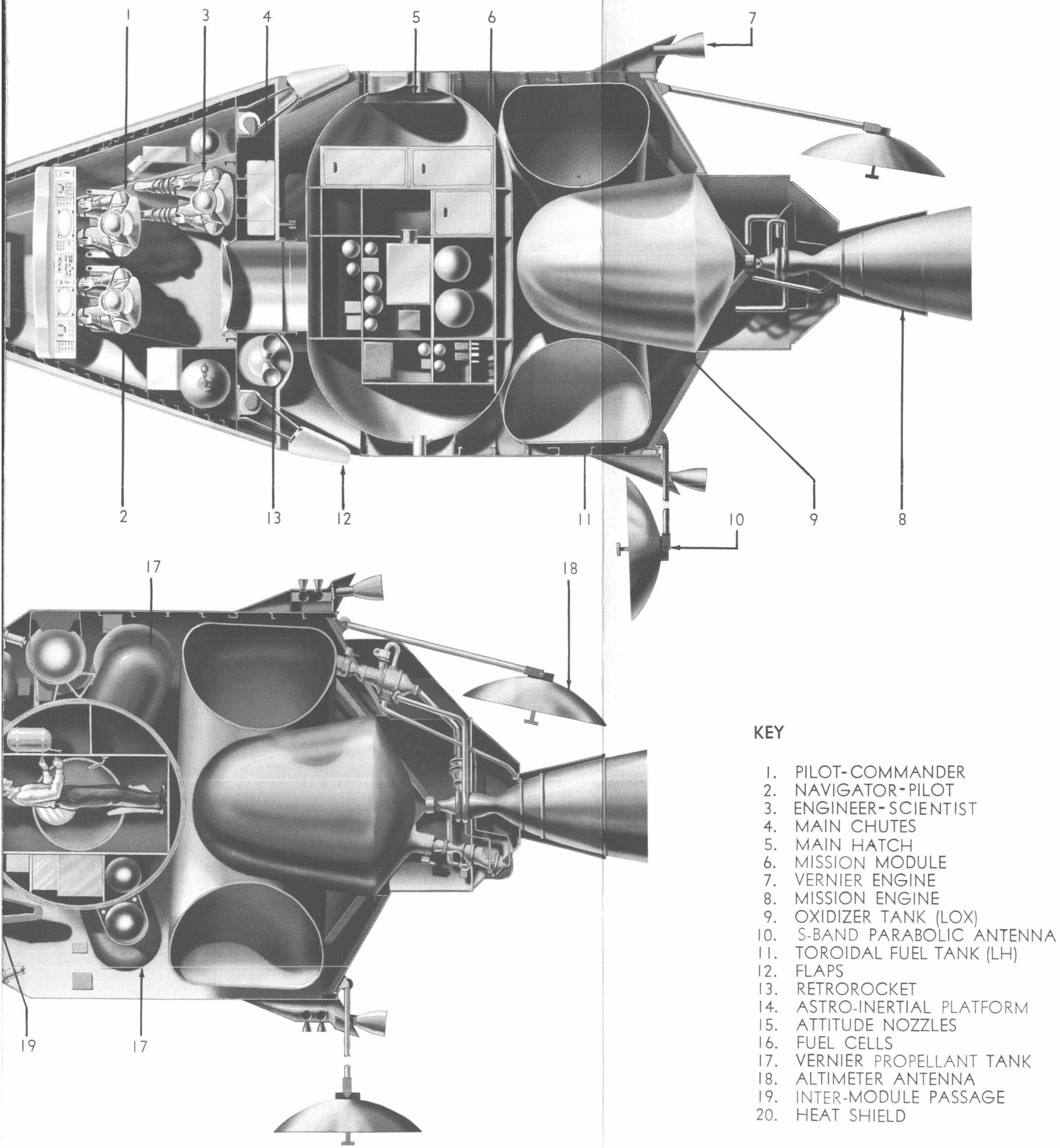

KEY

1. PILOT-COMMANDER
2. NAVIGATOR-PILOT
3. ENGINEER-SCIENTIST
4. MAIN CHUTES
5. MAIN HATCH
6. MISSION MODULE
7. VERNIER ENGINE
8. MISSION ENGINE
9. OXIDIZER TANK (LOX)
10. S-BAND PARABOLIC ANTENNA
11. TOROIDAL FUEL TANK (LH)
12. FLAPS
13. RETROROCKET
14. ASTRO-INERTIAL PLATFORM
15. ATTITUDE NOZZLES
16. FUEL CELLS
17. VERNIER PROPELLANT TANK
18. ALTIMETER ANTENNA
19. INTER-MODULE PASSAGE
20. HEAT SHIELD

Fig. p-3. Model 410 Apollo Inboard Profile

VOLUME III

TABLE OF CONTENTS(cont)

Appendices Page

A. Derivation of Two-Body Guidance Equations A-1
B. Three-Body Series Approximations B-1
C. Martin IBM 7090 Program for Trajectory Computation .. B-1
D. Derivation of Error Equations D-1
E. Astro-Inertial Platform (Litton)..................... E-1
F. Astro-Inertial Platform (Nortronics) F-1
G. Astro-Inertial Platform (Arma) G-1
H. Alternate Platform (Kearfott) H-1
I. Alternate Platform (Minneapolis-Honeywell)........... I-1
J. Astronaut's Sextant (Autonetics)..................... J-1
K. Astro-Sextant (Arma) K-1
L. Digital Computer (Texas Instruments)................. L-1
M. Digital Computer (Litton)............................ M-1
N. Digital Computer (IBM) N-1
O. Equations for Analog Simulations..................... O-1
P. Linear Perturbation Equations for Explicit Hit-Point Steering Analysis P-1
Q. Optimum Trajectory Program Q-1
R. Development of Approximation for Explicit Tangent Steering R-1
S. Apollo Landing Display and Control.................. S-1

TABLE OF CONTENTS (cont)

Page

T. Minimizing Reaction Mass Expenditure During Limit Cycling in a Space Vehicle On-Off Attitude Control System T-1

U. Fuel Expenditure During Limit Cycling with a Pulse Modulated Reaction System V-1

V. Relationship Between the Euler Angle Derivatives and Body Rates V-1

W. Apollo Coasting Autopilot Mechanization W-1

X. Derivation of Longitudinal Transfer Function X-1

Y. Derivation of Transfer Function for Position Rate Integral Control System Y-1

Z. Flight Control Subsystem Reliability Study Z-1

AA. Determination of Rendezvous Equations of Motion AA-1

BB. List of References BB-1

APPENDIX A

DERIVATION OF TWO-BODY GUIDANCE EQUATIONS

I. TIME OF FLIGHT ALONG KEPLER ORBIT

The equation of a Kepler orbit in the form

$$ax + bz + c = (x^2+z^2)^{\frac{1}{2}} \equiv r \qquad (1)$$

can be transformed to $\breve{x}, \breve{z}$ axes, where $\breve{z}$ lies along the major axis. It can be shown (see footnote) that the direction cosines of a vector pointing along the major axis from the directrix toward the origin are:

$$\left.\begin{aligned} l &= \frac{a}{(a^2+b^2)^{\frac{1}{2}}} = \frac{a}{e} \\ m &= \frac{b}{(a^2+b^2)^{\frac{1}{2}}} = \frac{b}{e} \end{aligned}\right\} \qquad (2)$$

The transformation equations

$$\begin{aligned} \breve{x} &= \frac{mx - lz}{c} \\ \breve{z} &= \frac{lx + mz}{c} \end{aligned} \qquad (3)$$

correspond to a rotation and a change of scale, such that equation (1) of the orbit becomes

$$e\breve{z}+1 = (\breve{x}^2+\breve{z}^2)^{\frac{1}{2}} = r \qquad (4)$$

The rotation of axes causes an elliptic orbit to appear as sketched below considering counterclockwise motion positive. The change of scale has the effect of normalizing the distance between the origin (focus) and the directrix to the value 1/e.

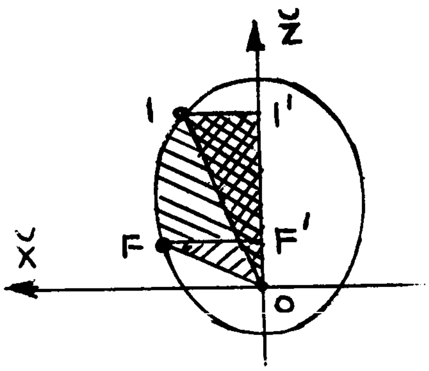

The time of flight between two points on (A.1.4) can be computed simply as the area of the sector subtended by these two points divided by the normalized areal rate characteristic of the orbit. Since we

---

Footnote: "See Martin Engineering Report 10856 (SECRET)," Mathematical Studies Concerning the Application of Q-Matrix Guidance to an Air-Launched Ballistic Missile," by Clagett Bowie.

[redacted]

deal here with rectangular coordinates, and since we will integrate with respect to $\breve{Z}$, the area of the sector would be computed as the area of the four-sided figure 1F1'F', plus the area of the triangle OF'F, minus the triangle 01'1. The tests which must be performed in order to choose appropriate signs and integration intervals are straightforward and will not be discussed here. Instead, we will concentrate upon the derivation of the equations in the forms for various types of orbits.

Equation (4) can be solved explicitly for $\breve{X}$ in terms of $\breve{Z}$ as:

$$\breve{X} = \left(C_2\breve{Z}^2 + C_1\breve{Z} + C_0\right)^{\frac{1}{2}} \qquad (5)$$

where

$C_0 = 1$

$C_1 = 2e$

$C_2 = e^2-1.$

integral of (A.1.5) from $\breve{Z}_1$, to $\breve{Z}_F$ will give the area 1F1'F':

$$A_{1F1'F'} = -\int_{\breve{Z}_1}^{\breve{Z}_F}\left(C_2\breve{Z}^2 + C_1\breve{Z} + C_0\right)^{\frac{1}{2}} d\breve{Z} \qquad (6)$$

Observe that the signs in (A.1.5), (A.1.6) have been chosen so that 1F1'F' will be positive for counterclockwise orbital motion regardless of whether that area lies in the right-or-left-hand plane. Adding and subtracting the triangular areas to (6) gives the total area as

$$A = O_F - O_1$$

where

$$Q = \frac{\breve{X}\breve{Z}}{2} - \int\left(C_2\breve{Z}^2 + C_1\breve{Z} + C_0\right)^{\frac{1}{2}} d\breve{Z} \qquad (7)$$

Evaluating the integral for the three cases $e\left\{\begin{matrix} > \\ = \\ < \end{matrix}\right\}1$ gives for Q:

$$Q = \frac{1}{2B}\left\{e\breve{X} - \frac{1}{|B|^{\frac{1}{2}}}\sin^{-1}\left(B\breve{Z} - e\right)\right\} \qquad ;(e<1)$$

$$(8)$$

$$Q = \frac{}{2B}\left\{e\breve{X} - \frac{1}{|B|^{\frac{1}{2}}}\left[\log 2 + \log\left(|B|^{\frac{1}{2}}\breve{X} - B\breve{Z} + e\right)\right]\right\} \quad (e>1)$$

$$Q = \frac{\breve{X}\breve{Z}}{Z} - \frac{\breve{X}}{3} \qquad ; (e-1) \qquad (8)$$

where

$$B = 1-e^2$$

Finally the areal rate for an orbit given by (1) can be shown (see last preceding footnote) to be

$$\text{Areal rate} = \frac{(cK)^{\frac{1}{2}}}{2} \qquad (9)$$

where K is the product of the Universal Gravitation constant and the mass of the central body. This rate must be non-dimensionalized just as the area itself was; therefore, we divide (9) by c^2:

$$\dot{A} = \frac{(cK)^{\frac{1}{2}}}{2c^2} = \frac{1}{2}\left(\frac{K}{c^3}\right)^{\frac{1}{2}} \qquad (10)$$

The time of flight from point 1 to point F is

$$t_{1-F} = \frac{A}{\dot{A}} = \frac{Q_F - Q_1}{\dot{A}} \qquad (11)$$

II. TANGENT KEPLER ORBITS

A rectangular coordinate frame with origin at the center of the force field is chosen in the desired orbital plane. The positive Z - axis is directed from the origin through pericenter of the target orbit. The X - axis is perpendicular to this and positive in the (counterclockwise) direction of desired motion at pericenter. In this coordinate system the equation of the target orbit can be written

$$e_T(n - Z) = (X^2 + Z^2)^{\frac{1}{2}} \qquad (12)$$

where e_T = eccentricity of the target orbit

$n = r_p\left(\frac{e_T + 1}{e_T}\right)$

r_p = target pericenter radius

The vehicle free-fall trajectory in the same central force field has a focus in common with the target orbit, and its equation can be written more generally as:

$$aX + bZ + c = (X^2 + Z^2)^{\frac{1}{2}} \qquad (13)$$

Let us now solve the points of intersection X_I, Z_I between trajectories (12) and (13):

$$e_T(n - Z_I) = (X_I^2 + Z_I^2)^{\frac{1}{2}} \tag{14}$$

$$aX_I + bZ_I + c = (X_I^2 + Z_I^2)^{\frac{1}{2}} \tag{15}$$

Dividing (14) by (15) give a linear relationship between X_I and Z_I. Solving this for Z_I in terms of X_I and substituting into (14) gives

$$\alpha X_I^2 - 2\beta X_I + \gamma = 0 \tag{16}$$

where

$$\alpha = a^2(e_T^2 - 1) - (e_T^2 + b)^2$$

$$\beta = a[c - e_T n - e_T^2(c + nb)]$$

$$\gamma = e_T^2(c + nb)^2 - (c - e_T n)^2$$

The form of (16) tells us the well-known result that two Keplerian orbits can intersect in 0, 1, or 2 points but no more. Solving (16) explicity for X_I yields.

$$X_I = \frac{\beta \pm E^{\frac{1}{2}}}{\alpha} \tag{17}$$

where

$$E \equiv \beta^2 - \alpha\gamma = c^2(e_T^2 - 1) + 2ce_T n(e_T b + 1) + e_T^2 n^2(a^2 + b^2 - 1) \tag{18}$$

For given target orbit (e_T, n), the quantities a, b, c, defining the vehicle free-fall trajectory determine the sign of E and hence the number of intersections. We seek a combination which makes E=O for this is the case of one tangential intersection.

Considering e_T, n as given (18) set equal to zero would constitute a single equation in the three unknowns a, b, c. Applying the results of Section III of this Appendix, the orbital elements, a, b, c, could be expressed as functions of $X, Z, \dot{X}, \dot{Z}$. Then considering the vehicle position X, Z as known, we would now have a single equation giving a relationship between the two velocity components $\dot{X}, \dot{Z}$ required for tangency. In the absence of any other constraint, there would be an arbitrariness in the solution - - one could choose one

III. ORBITAL ELEMENTS FOR SPECIFIED POSITION AND VELOCITY

Our standard form for a Keplerian orbit

$$ax + bz + c = (x^2 + z^2)^{\frac{1}{2}} \equiv r \qquad (24)$$

can be differentiated to give

$$a\dot{x} + b\dot{z} = \frac{x\dot{x} + z\dot{z}}{r} \qquad (25)$$

A third relationship between the elements a, b, c is found from dynamical considerations. The areal rate for the orbit is

$$A = \frac{(cK)^{\frac{1}{2}}}{2} \qquad (26)$$

where K is the product of the Universal Gravitation Constant and the mass of the central body. The proof of (26) is contained in the document referenced in the preceding footnote. Geometrically, the areal rate is

$$\dot{A} = \frac{r^2\dot{\theta}}{2}$$

where $r^2 = x^2 + z^2$

$$\cot\theta = \frac{z}{x}$$

Therefore in rectangular coordinates

$$\dot{A} = \frac{(\dot{x}z - x\dot{z})^2}{2} \qquad (27)$$

Equating (26) and (27) and squaring leads to

$$c = \frac{(\dot{x}z - x\dot{z})^2}{K} \qquad (28)$$

Finally substituting this into (24), enables us to solve (24) and (25) for a, b:

$$\begin{aligned} a &= \frac{x}{r} + \frac{(\dot{x}z - x\dot{z})\dot{z}}{K} \\ b &= \frac{z}{r} - \frac{(\dot{x}z - x\dot{z})\dot{x}}{K} \end{aligned} \tag{29}$$

The line $ax + bz + c = 0$ is an equation of the directrix corresponding to the focus at O. Denoting the eccentricity by e, then

$$e = (a^2 + b^2)^{\frac{1}{2}} \tag{30}$$

Let l, m denote the direction cosines of a vector pointing along the major axis of the orbit in the direction from the directrix toward O. Then

$$\begin{aligned} l &= \frac{a}{(a^2+b^2)^{\frac{1}{2}}} = \frac{a}{e} \\ m &= \frac{b}{(a^2+b^2)^{\frac{1}{2}}} = \frac{b}{e} \end{aligned} \tag{31}$$

IV. PERICENTER DETERMINATION

As mentioned in Section III of this Appendix, the line

$$ax + bz + c = 0 \tag{32}$$

is an equation of the directrix for the orbit

$$ax + bz + c = (x^2 + z^2)^{\frac{1}{2}} \tag{33}$$

corresponding to the focus at O. Therefore, a line through the origin and perpendicular to (32) is

$$bx - az = 0$$

Solving this for z in terms of x:

$$z = \frac{b}{a}x \tag{34}$$

and substituting into (A.4.2) gives

$$ax + \frac{b^2}{a}x + c = \pm x\left(1+\frac{b^2}{a^2}\right)^{\frac{1}{2}}$$

Making use of the relations developed in Appendix A.3, this can be solved for x to yield

$$x = -\frac{\ell c}{e \pm 1}$$

One sign is for apocenter, the other for pericenter:

$$x_{per} = -\frac{\ell c}{e+1} \qquad (35)$$

Substituting into (34) gives the z-component as

$$z_{per} = -\frac{mc}{e+1}$$

V. VELOCITY AT SPECIFIED POINT ON GIVEN KEPLER ORBIT

The derivative of the standard form for the Kepler orbit gives an equation relating the velocity components:

$$a\dot{x} + b\dot{z} = \frac{x\dot{x} - z\dot{z}}{r}. \qquad (36)$$

Another relationship between the velocity components is given by Kepler's Second Law in the form (Ref. II -6)

$$\dot{x}z - x\dot{z} = (cK)^{\frac{1}{2}} \qquad (37)$$

where K is the product of the Universal Gravitation Constant and the mass of the central body. Equation (36) can be written

$$a_1\dot{x} + a_2\dot{z} = 0 \qquad (38)$$

where

$$\left.\begin{aligned} a_1 &= ar - x \\ a_2 &= br - z \end{aligned}\right\} \qquad (39)$$

Now (37) and (38) can be solved simultaneously for the velocity components to give

$$\left.\begin{aligned} \dot{x} &= \frac{a_2 (cK)^{\frac{1}{2}}}{a_1 x + a_2 z} \\ \dot{z} &= \frac{a_1 (cK)^{\frac{1}{2}}}{a_1 x + a_2 z} \end{aligned}\right\} \qquad (40)$$

component freely and then solve for the other. Let us, however, place another constraint upon the problem. In particular let us specify the magnitude V of the velocity vector. Now

$$\begin{aligned} \dot{x} &= V\cos\Gamma_D \\ \dot{z} &= V\sin\Gamma_D \end{aligned} \qquad (19)$$

where Γ_D is the desired flight path angle for this speed. It turns out that (18) reduces to the form

$$A\tan^2\Gamma_D - 2B\tan\Gamma_D + C = 0 \qquad (20)$$

for Γ_D, where

$$\left.\begin{aligned} A &= \frac{V^2}{K}\left[e_T^2(x^2+\eta^2) - x^2\right] + 2e_T\eta\left[\frac{e_T}{r}(z-\eta)+1\right] \\ B &= x\frac{V^2}{K}\left[e_T^2(z-\eta) - z\right] \\ C &= \frac{V^2}{K}\left[e_T^2(z-\eta)^2 - z^2\right] + 2e_T\eta\left[\frac{e_T}{r}(z-\eta)+1\right] \end{aligned}\right\} \qquad (21)$$

The solution for $\tan\Gamma_D$ is simply

$$\tan\Gamma_D = \frac{B \pm (B^2 - AC)^{\frac{1}{2}}}{A} \qquad (22)$$

The sign ambiguity is easily settled, knowing roughly the desired direction of motion at the tangency point.

For the special case of a circular target orbit, (21) become simply

$$\left.\begin{aligned} A &= \frac{V^2}{K}(r_p^2 - x^2) + 2r_p\left(1 - \frac{r_p}{r}\right) \\ B &= -xz\frac{V^2}{K} \\ C &= \frac{V^2}{K}(r_p^2 - z^2) + 2r_p\left(1 - \frac{r_p}{r}\right) \end{aligned}\right\} \qquad (23)$$

and steering for tangency in this case is tantamount to controlling to the pericenter radius r_p.

APPENDIX B

THREE BODY GUIDANCE

[redacted]

APPENDIX B

Three Body Guidance

A. Restricted Three Body Series Solution; Derivation of Equations

Following along the lines of Ref. 1, the equations of motion in a rotating coordinate system whose origin is at the barycenter are:

$$\ddot{x} - 2\omega\dot{y} - \omega^2 x = -K\left\{\frac{1-\mu}{r_e^3} + \frac{\mu}{r_m^3}\right\}(x+\mu d) + K\frac{\mu d}{r_m^3} \qquad 1(a)$$

$$\ddot{y} + 2\omega\dot{x} - \omega^2 y = -K\left\{\frac{1-\mu}{r_e^3} + \frac{\mu}{r_m^3}\right\} y \qquad 1(b)$$

$$\ddot{z} = -K\left\{\frac{1-\mu}{r_e^3} + \frac{\mu}{r_m^3}\right\} z \qquad 1(c)$$

where

$$r_e = \sqrt{(x+\mu d)^2 + y^2 + z^2}$$

$$r_m = \sqrt{(x+\mu d - d)^2 + y^2 + z^2}$$

$$\mu = \frac{m_m}{m_m + m_e}$$

$$K = G(m_e + m_m)$$

ω = moons orbital angular velocity

[redacted]

The equations are then non-dimensionalized by using the following characteristic quantities:

Length - d - distance between the centers of the earth and moon

Velocity - U - the vacuum velocity at the surface of the earth.

The non-dimensional variables become

$$x^* = x/d\,, \quad y^* = y/d\,, \quad z^* = z/d$$

$$t^* = t\,\frac{U}{d}\,, \quad \omega^* = \omega\left[\frac{d^3}{K(1-\mu)}\right]^{1/2}$$

Introducing these variables

$$\ddot{x}^* - 2\omega^*\dot{y}^*\eta - \omega^{*2}x^*\eta^2 = -\eta^2\left[\frac{1}{r_e^{*3}} + \left(\frac{\mu}{1-\mu}\right)\frac{1}{r_m^{*3}}\right](x^*+\mu) + \eta^2\left[\left(\frac{\mu}{1-\mu}\right)\frac{1}{r_m^{*3}}\right] \qquad 2(a)$$

$$\ddot{y}^* + 2\omega^*\dot{x}^*\eta - \omega^* y^*\eta^2 = -\eta^2\left[\frac{1}{r_e^{*3}} + \left(\frac{\mu}{1-\mu}\right)\frac{1}{r_m^{*3}}\right] y^* \qquad 2(b)$$

$$\ddot{z}^* = -\eta^2\left[\frac{1}{r_e^{*3}} + \left(\frac{\mu}{1-\mu}\right)\frac{1}{r_m^{*3}}\right] z^* \qquad 2(c)$$

where $\eta = \left[\dfrac{K(1-\mu)}{dU^2}\right]^{1/2}$ is a nondimensional parameter.

Since for very high velocities η becomes small, the series

$$f = f_0(t^*) + \sum_{j=1}^{\infty} \eta^j f_j(t^*) \qquad (3)$$

is valid. Substituting these expressions in the D. E. (2) and applying the limit process for $\eta \to 0$ $(U \to \infty)$ gives a series of the form

$$\ddot{x}(t^*) = \ddot{x}_0^* + \eta\,\ddot{x}_1^* + \eta^2\ddot{x}_2^* + \eta^3\ddot{x}_3^* + \cdots$$

To the zero order

$$\ddot{x}_0^* = 0$$

$$\ddot{y}_0^* = 0$$

$$\ddot{z}_0^* = 0$$

To the first order the equations are:

$$\ddot{x}_1^* = 2\omega^* v_i^*$$

$$\ddot{y}_1^* = -2\omega^* u_i^*$$

$$\ddot{z}_1^* = 0$$

Before the series can be carried to higher order, the r^3 terms appearing in the denominator must be expanded and brought into the numerator. The r_e term will be expanded; the r_m term can be handled in like manner.

The $1/r_e^{*3}$ term in components is:

$$\frac{1}{r_e^{*3}} = \frac{1}{\left[(x^*+\mu)^2 + y^{*2} + z^{*2}\right]^{3/2}}$$

$$= \left[(x^*+\mu)^2 + y^{*2} + z^{*2}\right]^{-3/2}$$

Expanding Eq. (4) by the series (3):

$$\frac{1}{r_e^{*3}} = \Big[(x_0^* + \mu + x_1^*\eta + x_2^*\eta^2 + \cdots)^2 + (y_0^* + y_1^*\eta + y_2^*\eta^2 + \cdots)^2 + (z_0^* + z_1^*\eta + z_2^*\eta^2 + \cdots)^2\Big]^{-3/2}$$

Raising to powers and collecting the powers of η :

$$\frac{1}{r_e^{*3}} = \Big\{[(x^*+\mu)^2 + y_0^{*2} + z_0^{*2}] + 2\eta[(x_0^*+\mu)x_1^* + y_0^*y_1^* + z_0^*z_1^*] + \eta^2[2(x_0^*+\mu)x_2^* + x_1^{*2} + 2y_0^*y_1^* + y_1^{*2} + 2z_0^*z_1^* + z_1^{*2}] + \cdots\Big\}^{-3/2}$$

We now assign the symbols A B C to the above expression so that it takes the form:

$$\Big\{A + B + C + \cdots\Big\}^{-3/2} = A^{-3/2}\Big\{1 + \frac{B}{A} + \frac{C}{A} + \cdots\Big\}^{-3/2}$$

Now assign F such that:

$$A^{-3/2}\Big\{1 + F\Big\}^{-3/2} = A^{-3/2}\Big\{1 + \frac{B}{A} + \frac{C}{A} + \cdots\Big\}^{-3/2}$$

Expanding the above expression by the binominal theorem:

$$A^{-3/2}\left\{1+F\right\}^{-3/2} = A^{-3/2}\left\{1-\frac{3}{2}F+\frac{15}{8}F^2-\cdots\right\}$$

Substituting quantities for A, B, C, and F,

$$\frac{1}{r_e^{*3}} = \frac{1}{r_{e_0}^{*3}}\left\{1-\left(\frac{3}{2}\right)\left\{\left[\frac{2\eta[(x_0^*+\mu)x_1^*+y_0^*y_1^*+z_0^*z_1^*]}{r_{e_0}^{*2}}\right.\right.\right.$$

$$\left.+\ \eta^2\frac{[2(x_0^*+\mu)x_2^*+x_1^{*2}+2y_0^*y_2^*+y_1^{*2}+2z_0^*z_2^*+z_1^{*2}]}{r_{e_0}^{*2}}\right.$$

$$\left.+\ \cdots\right\}$$

From the above development all values of η are now in the numerator and the series can be expanded further.

To the second order, the acceleration is:

$$\ddot{x}_2^* - 2\omega^*\dot{y}_1^* - \omega^{*2}x_0^* = -\left[\frac{1}{r_{e_0}^{*3}}+\left(\frac{\mu}{1-\mu}\right)\frac{1}{r_{m_0}^{*3}}\right](x_0^*+\mu)$$

$$+\left(\frac{\mu}{1-\mu}\right)\frac{1}{r_{m_0}^{*3}}$$

$$\ddot{y}_2^* + 2\omega^*\dot{x}_1^* - \omega^{*2}y_0^* = -\left[\frac{1}{r_{e_0}^{*3}}+\left(\frac{\mu}{1-\mu}\right)\frac{1}{r_{m_0}^{*3}}\right]y_0^*$$

$$\ddot{z}_2^* = -\left[\frac{1}{r_{e_0}^{*3}}+\left(\frac{\mu}{1-\mu}\right)\frac{1}{r_{m_0}^{*3}}\right]z_0^*$$

[redacted]

The third order acceleration is given by:

$$\ddot{x}_3^* - 2\omega^*\dot{y}_2^* - \omega^{*2}x_1^* = -\frac{x_1^*}{r_{e_0}^{*3}} + \frac{3(x_0^*+\mu)}{r_{e_0}^{*5}}\left[(x_0^*+\mu)x_1^* + y_0^*y_1^* + z_0^*z_1^*\right]$$

$$-\left(\frac{\mu}{1-\mu}\right)\frac{x_1^*}{r_{m_0}^{*3}} + \left(\frac{\mu}{1-\mu}\right)\frac{3(x_0^*+\mu-1)}{r_{m_0}^{*5}}\left[(x_0^*+\mu-1)x_1^* + y_0^*y_1^* + z_0^*z_1^*\right]$$

$$\ddot{y}_3^* + 2\omega^*\dot{x}_2^* - \omega^{*2}y_1^* = -\frac{y_1^*}{r_{e_0}^{*3}} + \frac{3y_0^*}{r_{e_0}^{*5}}\left[(x_0^*+\mu)x_1^* + y_0y_1^* + z_0^*z_1^*\right]$$

$$-\left(\frac{\mu}{1-\mu}\right)\frac{y_1^*}{r_{m_0}^{*3}} + \left(\frac{\mu}{1-\mu}\right)\frac{3y_0^*}{r_{e_0}^{*6}}\left[(x_0^*+\mu-1)x_1^* + y_0^*y_1^* + z_0^*z_1^*\right]$$

$$z_3^* = -\frac{z_1^*}{r_{e_0}^{*3}} + \frac{3z_0^*}{r_{e_0}^{*3}}\left[(x_0^*+\mu)x_1^* + y_0^*y_1^* + z_0^*z_1^*\right]$$

$$-\left(\frac{\mu}{1-\mu}\right)\frac{z_1^*}{r_{m_0}^{*3}} + \left(\frac{\mu}{1-\mu}\right)\frac{3z_0^*}{r_{m_0}^{*5}}\left[(x_0^*+\mu-1)x_1^* + y_0^*y_1^* + z_0^*z_1^*\right]$$

As an example of the integration envolved consider the first fractional term in the $\ddot{x}_3^*$ equation.

$$-\int_0^{t^*}\frac{x_1^*\,dt^*}{r_e^{*3}} = -\int_0^{t^*}\frac{(u_i^*t^* + x_i^* + \mu)\,dt^*}{\left[(x_i^*+\mu+u_i^*t^*)^2 + (y_i^* + v_i^*t^*)^2 + (z_i^* + w_i^*t^*)^2\right]^{3/2}}$$

where

$$r_{e_0}^* = \left[(x_0^*+\mu)^2 + y_0^{*2} + z_0^{*2}\right]^{3/2}$$

[redacted]

by expanding $r_{e_0}^*$ we obtain the form

$$r_{e_0}^* = \left[a t^{*2} + b t^* + c\right]^{1/2} = X^{1/2}$$

The above integral may now be expressed as:

$$-\int_0^{t^*} \frac{x_i^* dt^*}{r_{e_0}^{*3}} = -u_i^* \int_0^{t^*} \frac{t^* dt^*}{X^{3/2}} - (x_i^* + \mu) \int_0^{t^*} \frac{dt^*}{X^{3/2}}$$

All integrals used are of this form and are tabulated later.

Substitution of initial conditions and integration of the acceleration equations yields the velocity and position components.

The velocity components are:

$$u_0^* = u_i^*$$

$$u_1^* = 2\omega^* v_i^* t^*$$

$$u_2^* = -\frac{3}{2}\omega^{*2} u_i^* t^{*2} + \omega^{*2} x_i^* t^* - (x_i^* + \mu) I_e(3) - u_i^* I_e④ - \left(\frac{\mu}{1-\mu}\right)\left[(x_i^* + \mu - 1) I_m(3) + u_i^* I_m(4)\right]$$

$$u_3^* = -\frac{2}{3}\omega^{*3} v_i^* t^{*3} + \omega^{*3} y_i^* t^{*2} - 2\omega^*\left[y_i^* \mathrm{II}_e ③ + v_i^* \mathrm{II}_e ④ + \left(\frac{\mu}{1-\mu}\right) y_i^* \mathrm{II}_m ③ + \left(\frac{\mu}{1-\mu}\right) v_i^* \mathrm{II}_m ④\right] - \omega^* v_i^* I_e ⑤$$
$$- \left(\frac{\mu}{1-\mu}\right)\omega^* v_i^* I_m ⑤ + 3\omega^* \zeta_e^* \left[u_i^* I_e(9) + (x_i^* + \mu) I_e(8)\right]$$
$$+ \left(\frac{\mu}{1-\mu}\right) 3\omega^* \zeta_m^* \left[u_i^* I_m(9) + (x_i^* + \mu - 1) I_m(8)\right]$$

$$v_0^* = v_i^*$$

$$v_1^* = -2\omega^* u_i^* t^*$$

$$v_2^* = -\frac{3}{2}\omega^{*2} v_i^* t^{*2} + \omega^{*2} y_i^* t^* - y_i^* I_e(3) - v_i^* I_e④ - \left(\frac{\mu}{1-\mu}\right)\left[y_i^* I_m ③ + v_i^* I_m(4)\right]$$

[redacted]

$$v_3^* = \frac{2}{3}\omega^{*3} u_i^* t^{*3} - \omega^{*3} x_i^* t^{*2} + 2\omega^*\left[(x_i^* + \mu)\mathrm{II}_e(3) + u_i^*\mathrm{II}_e(4)\right]$$

$$+ 2\omega^*\left(\frac{\mu}{1-\mu}\right)\left[(x_i^* + \mu - 1)\mathrm{II}_m(3) + u_i^*\mathrm{II}_m(4)\right] + \omega^* u_i^* \mathrm{I}_e(5)$$

$$+ 3\omega^*\zeta_e^*\left[y_i^*\mathrm{I}_e(8) + v_i^*\mathrm{I}_e(9)\right] + \omega^* u_i^*\left(\frac{\mu}{1-\mu}\right)\mathrm{I}_m(5)$$

$$+ 3\omega^*\zeta_m^*\left(\frac{\mu}{1-\mu}\right)\left[v_i^*\mathrm{I}_m(9) + y_i^*\mathrm{I}_m(8)\right]$$

$$w_0^* = w_i^*$$

$$w_1^* = 0$$

$$w_2^* = -z_i^*\mathrm{I}_e(3) - w_i^*\mathrm{I}_e(4) - \left(\frac{\mu}{1-\mu}\right)\left[z_i^*\mathrm{I}_m(3) + w_i^*\mathrm{I}_m(4)\right]$$

$$w_3^* = 3\omega^*\zeta_e^*\left[w_i^*\mathrm{I}_e(9) + z_i^*\mathrm{I}_e(8) + 3\left(\frac{\mu}{1-\mu}\right)\omega^*\zeta_m^*\left[w_i^*\mathrm{I}_m(9)\right.\right.$$

$$\left.\left. + z_i^*\mathrm{I}_m(8)\right]\right.$$

The position components are:

$$x_0^* = x_i^* + u_i^* t^*$$

$$x_1^* = \omega^* v_i^* t^{*2}$$

$$x_2^* = -\frac{1}{2}\omega^{*2} u_i^* t^{*3} + \frac{1}{2}\omega^{*2} x_i^* t^{*2} - (x_i^* + \mu)\mathrm{II}_e(3) - u_i^*\mathrm{II}_e(4)$$

$$-\left(\frac{\mu}{1-\mu}\right)\left[(x_i^* + \mu - 1)\mathrm{II}_m(3) + u_i^*\mathrm{II}_m(4)\right]$$

$$x_3^* = -\frac{1}{6}\omega^{*3} v_i^* t^{*4} + \frac{1}{3}\omega^{*3} y_i^* t^{*3} - 2\omega^*\left[y_i^*\mathrm{III}_e(3) + v_i^*\mathrm{III}_e(4)\right.$$

$$\left. + \left(\frac{\mu}{1-\mu}\right) y_i^*\mathrm{III}_m(3) + \left(\frac{\mu}{1-\mu}\right) v_i^*\mathrm{III}_m(4)\right] - \omega^* v_i^*\mathrm{II}_e(5)$$

$$+ 3\omega^*\zeta_e^*\left[u_i^*\mathrm{II}_e(9) + (x_i^* + \mu)\mathrm{II}_e(8)\right] - \left(\frac{\mu}{1-\mu}\right)\omega^* v_i^*\mathrm{II}_m(5)$$

$$+ \left(\frac{\mu}{1-\mu}\right)3\omega^*\zeta_m^*\left[u_i^*\mathrm{II}_m(9) + (x_i^* + \mu)\mathrm{II}_m(8)\right] - \left(\frac{\mu}{1-\mu}\right)3\omega^*\zeta_m^*\mathrm{II}_m(8)$$

$$y_0^* = y_i^* + v_i^* t^*$$

$$y_1^* = -\omega^* u_i^* t^{*2}$$

[redacted]

$$y_2^* = -\frac{1}{2}\omega^{*2} v_i^* t^{*3} + \frac{1}{2}\omega^{*2} y_i^* t^{*2} - y_i^* \mathrm{II}_e(3) - v_i^* \mathrm{II}_e(4)$$
$$- \left(\frac{\mu}{1-\mu}\right)\left[y_i^* \mathrm{II}_m(3) + v_i^* \mathrm{II}_m(4)\right]$$
$$y_3^* = \frac{1}{6}\omega^{*3} u_i^* t^{*4} - \frac{1}{3}\omega^{*3} x_i^* t^{*3} + 2\omega^*\left[(x_i^* + \mu)\mathrm{III}_e(3) + u_i^* \mathrm{III}_e(4)\right]$$
$$+ 2\omega^*\left(\frac{\mu}{1-\mu}\right)\left[(x_i^* + \mu - 1)\mathrm{III}_m(3) + u_i^* \mathrm{III}_m(4)\right] + \omega^* u_i^* \mathrm{II}_e(5)$$
$$+ 3\omega^* \zeta_e^*\left[y_i^* \mathrm{II}_e(8) + v_i^* \mathrm{II}_e(9)\right] + \omega^* u_i^* \left(\frac{\mu}{1-\mu}\right)\mathrm{II}_m(5)$$
$$+ 3\omega^* \zeta_m^* \left(\frac{\mu}{1-\mu}\right)\left[v_i^* \mathrm{II}_m(9) + y_i^* \mathrm{II}_m(8)\right]$$

$$z_0^* = z_i^* + w_i^* t^*$$
$$z_1^* = 0$$
$$z_2^* = -z_i^* \mathrm{II}_e(3) - w_i^* \mathrm{II}_e(4) - \left(\frac{\mu}{1-\mu}\right)\left[z_i \mathrm{II}_m(3) + w_i^* \mathrm{II}_m(4)\right]$$
$$z_3^* = 3\omega^* \zeta_e^*\left[w_i^* \mathrm{II}_e(9) + z_i^* \mathrm{II}_e(8)\right] + 3\left(\frac{\mu}{1-\mu}\right)\omega^* \zeta_m^*\left[w_i^* \mathrm{II}_m(9)\right.$$
$$\left. + z_i^* \mathrm{II}_m(8)\right]$$

The series for the position and velocity components are:

$$x^* = x_0^* + \eta x_1^* + \eta^2 x_2^* + \eta^3 x_3^* + \cdots\cdots$$
$$y^* = y_0 + \eta y_1^* + \eta^2 y_2^* + \eta^3 y_3^* + \cdots\cdots$$
$$z^* = z_0^* + \eta^2 z_2^* + \eta^3 z_3^* + \cdots\cdots$$
$$u^* = u_0^* + \eta u_1^* + \eta^2 u_2^* + \eta^3 u_3^* + \cdots\cdots$$
$$v^* = v_0^* + \eta v_1^* + \eta^2 v_2^* + \eta^3 v_3^* + \cdots\cdots$$
$$w^* = w_0^* + \eta^2 w_2^* + \eta^3 w_3^* + \cdots\cdots$$

The integrals previously used are:

$$I(1) = \int_0^{t^*} \frac{dt^*}{X^{1/2}} = \frac{1}{a^{1/2}} \ln \left| \frac{2(aX)^{1/2} + 2at^* + b}{2(ac)^{1/2} + b} \right|$$

$$I(2) = \int_0^{t^*} \frac{t^* dt^*}{X^{1/2}} = \frac{X^{1/2}}{a} - \frac{c^{1/2}}{a} - \frac{b}{2a} I(1)$$

$$I(3) = \int_0^{t^*} \frac{dt^*}{X^{3/2}} = \frac{4at^* + 2b}{(4ac - b^2) X^{1/2}} - \frac{2b}{(4ac - b^2) c^{1/2}}$$

$$I(4) = \int_0^{t^*} \frac{t^* dt^*}{X^{3/2}} = - \frac{2bt^* + 4c}{(4ac - b^2) X^{1/2}} + \frac{4c^{1/2}}{(4ac - b^2)}$$

$$I(5) = \int_0^{t^*} \frac{t^{*2} dt^*}{X^{3/2}} = \frac{(2b^2 - 4ac)t^* + 2bc}{a(4ac - b^2) X^{1/2}} - \frac{2bc^{1/2}}{a(4ac - b^2)} + \frac{1}{a} I(1)$$

$$I(6) = \int_0^{t^*} \frac{dt^*}{X^{5/2}} = \frac{(4at^* + 2b)}{3(4ac - b^2) X^{3/2}} + \frac{8a(4at^* + 2b)}{3(4ac - b^2)^2 X^{1/2}}$$

$$- \frac{2b}{3(4ac - b^2) c^{3/2}} - \frac{16ab}{3(4ac - b^2)^2 c^{1/2}}$$

$$I(7) = \int_0^{t^*} \frac{t^* dt^*}{X^{5/2}} = - \frac{1}{3aX^{3/2}} + \frac{1}{3ac^{3/2}} - \frac{b}{2a} I(6)$$

$$I(8) = \int_0^{t^*} \frac{t^{*2}dt^*}{X^{5/2}} = -\frac{t^*}{2aX^{3/2}} - \frac{b}{4a} I(7) + \frac{c}{2a} I(6)$$

$$I(9) = \int_0^{t^*} \frac{t^{*3}dt^*}{X^{5/2}} = -\frac{t^{*2}}{aX^{3/2}} + \frac{b}{2a} I(8) + \frac{2c}{a} I(7)$$

$$II(1) = \frac{t^*}{a^{1/2}} \ln\left| \frac{2a^{1/2}X^{1/2}+2at^*+b}{2(ac)^{1/2}+b} \right| - I(2)$$

$$II(2) = \frac{2at^*+b}{4a^2} X^{1/2} - \frac{bc^{1/2}}{4a^2} - \frac{c^{1/2}}{a} t^*$$

$$+ \frac{(4ac-b^2)}{8a^2} I(1) - \frac{b}{2a} II(1)$$

$$II(3) = \frac{2b}{(4ac-b^2)} I(1) + \frac{4a}{(4ac-b^2)} I(2) - \frac{2bt^*}{(4ac-b^2)c^{1/2}}$$

$$II(4) = -\frac{2b}{(4ac-b^2)} I(2) - \frac{4c}{(4ac-b^2)} I(1) + \frac{4c^{1/2}t^*}{(4ac-b^2)}$$

$$II(5) = \frac{(2b^2-4ac)}{a(4ac-b^2)} I(2) + \frac{2bc}{a(4ac-b^2} I(1)$$

$$- \frac{2bc^{1/2}t^*}{a(4ac-b^2)} + \frac{1}{a} II(1)$$

$$II(6) = \frac{2}{3(4ac-b^2)}\left[2aI(4)+bI(3)\right] + \frac{16a}{3(4ac-b^2)}\left[2aI(2)\right.$$

$$\left.+bI(1)\right] - \frac{2b}{3(4ac-b^2)c^{1/2}}\left[\frac{t^*}{c} + 8at^*\right]$$

$$\mathrm{II}(7) = -\frac{1}{3a}\,\mathrm{I}(3) + \frac{t^*}{3ac^{3/2}} - \frac{b}{2a}\,\mathrm{II}(6)$$

$$\mathrm{II}(8) = -\frac{1}{2a}\,\mathrm{I}(4) - \frac{b}{4a}\,\mathrm{II}(7) + \frac{c}{2a}\,\mathrm{II}(6)$$

$$\mathrm{II}(9) = -\frac{1}{a}\,\mathrm{I}(5) + \frac{b}{2a}\,\mathrm{II}(8) + \frac{2c}{a}\,\mathrm{II}(7)$$

$$\mathrm{III}(3) = \frac{2b}{(4ac-b^2)}\,\mathrm{II}(1) + \frac{4a}{(4ac-b^2)}\,\mathrm{II}(2) - \frac{bt^{*2}}{(4ac-b^2)c^{1/2}}$$

$$\mathrm{III}(4) = -\frac{2b}{(4ac-b^2)}\,\mathrm{II}(2) - \frac{4c}{(4ac-b^2)}\,\mathrm{II}(1) + \frac{2c^{1/2}t^{*2}}{(4ac-b^2)}$$

The following table lists quantities used in integrals as a, b and c.

	I_e	I_m
a	$\left[u_i^{*2} + v_i^{*2} + w_i^{*2}\right]$	$\left[u_i^{*2} + v_i^{*2} + w_i^{*2}\right]$
b	$2\left[u_i^*(x_i^* + \mu) + v_i^* y_i^* + w_i^* z_i^*\right]$	$2\left[u_i^*(x_i^* + \mu - 1) + v_i^* y_i^* + w_i^* z\right]$
c	$\left[(x_i^* + \mu)^2 + y_i^{*2} + z_i^{*2}\right]$	$\left[(x_i^* + \mu - 1)^2 + y_i^{*2} + z_i^{*2}\right]$

SYMBOLS

I = first integration

II = second integration

III = third integration

$l_e^* = \left[(x_i^* + \mu) v_i^* - y_i^* u_i^* \right]$

$l_m^* = \left[(x_i^* + \mu - 1) v_i^* - y_i^* u_i^* \right]$

t = time

u, v, w = components of the vehicle's velocity vector in the instantaneous directions of x, y, z, respectively.

x, y, z = coordinates of the R. H. rotating coordinate system with the origin at the earth-moon center of mass, the x-axis passing through the moon's c.g. and the z-axis perpendicular to the moon's orbital plane.

SUBSCRIPTS

e = earth

i = initial

m = moon

APPENDIX C

MARTIN IBM 7090 PROGRAM FOR TRAJECTORY COMPUTATION

PREFACE

The proposed program assumes a universe consisting of the sun, earth, moon and a vehicle. It is assumed that the Sun is fixed in space. The sun's gravitational field affects the earth, moon, and vehicles; the earth's gravitational field affects the moon and vehicle; the Moon's gravitational field affects the earth and vehicle. The sun and moon are spheres; the earth is oblate according to specifications contained in NASA Project Apollo Working Paper No. 1004. (All astronomical constants used in the program conform to this reference; they may easily be changed to conform to later references should the occasion arise.) The vehicle is assumed to be an ideal point-mass. No forces are assumed other than the gravitational ones.

The program will definitely solve any one of the following three problems:

(1) Compute the trajectory of a vehicle starting in the vicinity of the earth and terminating in the vicinity of the moon

(2) Compute the trajectory of a vehicle starting in the vicinity of the moon and terminating in the vicinity of the earth

(3) Compute the trajectory of a vehicle starting in the vicinity of the earth, passing near the moon, and returning to the vicinity of the earth.

It was orginally intended to provide also for a fourth problem:

(4) Determine the trajectory for several (perhaps thirty) revolutions of a vehicle in orbit about the moon.

The assumption that the moon is spherical is made simply because there does not seem to be available any accurate data on the moon's exact shape. Since this exact shape is clearly a significant influence on the motion of a vehicle near the moon (particularly when several revolutions in lunar orbit are to be computed), it has been decided for the moment to ignore problems of type (4). If and when accurate lunar data become available, the issue will certainly be reconsidered, but no further mention of problems of type (4) will be made in the present report.

The eventual need for accurate trajectories by Project Apollo was the primary incentive for the developement of the subject program.

The present report will outline the theory and general arrangement of the computations involved in the program. How far work has progressed on the various phases will be indicated by remarks at appropriate times.

Minor assumptions in addition to those listed in this preface will also appear at appropriate places.

INPUT AND OUTPUT COORDINATE SYSTEMS

Input data (initial conditions) for any trajectory to be computed by the program will include the following items:

(1) The initial value of time, hereafter denoted by t_o

(2) The initial position vector and velocity vector of the earth with respect to the sun

(3) The initial position vector and relative velocity vector of the moon with respect to the earth

(4) The initial position vector and relative velocity vector of the vehicle with respect to the earth

(5) The initial position vector and relative velocity vector of the vehicle with respect to the moon.

It is clear that (4) and (5) are not independent; i. e., the data of either imply the data of the other. Presumably (4) will be used if at t_o the vehicle is near the earth and (5) will be used if at t_o the vehicle is near the moon. If (4) is given, the program will compute (5), and conversely.

Now what coordinate system or systems should be used in submitting input position and (relative) velocity vectors? There is no answer to this question which will meet universal approval. We therefore contemplate the preparation of a library of sub-programs permitting the submission of data in any of several standard coordinate systems depending on the preference of the particular submitter.

Nothing concrete has been done on this as yet. So far as the coordinate systems we will use in the computing part of our program, however, our minds have been made up for some time. When our library is made, there will be included instructions for converting the input data in all cases to the coordinate systems which we define below:

(1) An x, y, z Cartesian system fixed in space with origin at the center of the sun. The positive z axis will be parallel to the earth's North Pole. The system will be right-handed; i.e., if the fingers of the right hand curl in the direction from the positive x axis toward the

positive y axis, the extended right thumb will point roughly in the directon of the positive z axis. This system is clearly an inertial one.

(2) An x, y, z system with the origin always at the center of the earth. The directions of the axes will be respectively parallel to those of (1). This system is not an inertial one since the origin is being continuously accelerated.

(3) An x, y, z system with origin always at the center of the moon. The directions of the axes will be respectively parrallel to those of (1) and of (2). This system is not an inertial one.

We remark that we ignore variations in the direction of the earth's rotation axis (direction of North Pole).

Our notations are illustrated by the following: ExS, EyS, EzS denote the x, y, z coordinates respectively of the earth with respect to the system with origin at the center of the sun. MxE, MyE, MzE denote the x, y, z coordinates respectively of the moon with respect to the system with origin at the center of the earth. VxE and VxM denote the x coordinates of the vehicle with respect to the earth-origin and moon-origin systems, respectively. Dots over any x, y, z denote time derivatives; e.g.,

$$V\dot{x}E = \frac{d}{dt}(VxE) \qquad V\ddot{y}M = \frac{d^2}{dt^2}(VyM)$$

and so on.

Our program will be capable of calculating:

(1) An ephemeris of the earth with respect to the sun; i. e., a table of t, VxE, VyE, VzE, $V\dot{x}E$, $V\dot{y}E$, $V\dot{z}E$ with listings every six hours starting with $t = t_o$

(2) An ephemeris of the moon with respect to the earth; i. e., a table of t, MxE, MyE, MzE, $M\dot{x}E$, $M\dot{y}E$, $M\dot{z}E$ with listings every six hours starting at $t = t_o$

(3) An ephemeris of vehicle with respect to the earth; i. e., a table of t, VxE, VyE, VzE, $V\dot{x}E$, $V\dot{y}E$, $V\dot{z}E$. Time intervals will not here be constant; space-wise successive points will be closer together when vehicle is near earth or moon than during midcourse

[redacted]

(4) An ephemeris of vehicle with respect to moon; i. e., a table of t, VxM, VyM, VzM, $V\dot{x}M$, $V\dot{y}M$, $V\dot{z}M$. As with (3), time intervals will depend on relative positions.

A possible alternative to having the subject program compute (1) and (2) is the storing of E with respect to S and M with respect to E ephemerides which have been computed by some other source. This alternative is being investigated by Mr. Harvey Safren. Since no decisions are final on this, we shall proceed in the present memorandum on the assumption that our subject program will compute (1) and (2). It will in its final form certainly be capable of so doing, whether the possibility of storing data from some other source is allowable or not.

We shall also develop a library of sub-routines of converting output data (i. e., items (1), (2), (3), (4) just listed) to any of several standard coordinate systems at the whim of the submitter in any case. Nothing concrete has been done on this at the present time; the problem is being studied simultaneously with the problem of the input library mentioned earlier.

Henceforth, in the present memorandum we confine our attention to Cartesian coordinate systems. Our attention will also be confined to that part of the subject program which starts with the initial conditions (transformed to the Cartesian systems mentioned above) and computes the ephemerides listed. Roughly speaking, the status of this part of the work may be described as follows: Theoretical matters have been almost completely resolved (say about ninety-five percent) flow charting of the actual computational steps is three quarters complete and currently in the hands of a coder. This rough statement will be made more specific as we proceed.

THE DIFFERENTIAL EQUATIONS

By the distance between two bodies we shall always mean the distance between their centers of mass. We write d(S, E) for the distance between the sun and the earth, d(E, M) for the distance between the earth and the moon, and so on.

We have already noted that our sun-origin coordinate system is an inertial one. Then in this system $E\ddot{x}S$, $E\ddot{y}S$, $E\ddot{z}S$ are the acceleration components of the earth, and we have

$$E\ddot{x}S = \frac{-\mu_S(ExS)}{[d(S,E)]^3} + \frac{\mu_M(MxE)(1+q_{M_1})}{[d(E,M)]^3} \qquad (1)$$

[redacted]

$$\left.\begin{aligned} E\ddot{y}S &= \frac{-\mu_S(ExS)}{[d(S,E)]^3} + \frac{\mu_M(MyE)(1+q_{M1})}{[d(E,M)]^3} \\ E\ddot{z}S &= \frac{\mu_S(EzS)}{[d(S,E)]^3} + \frac{\mu_M(MzE)(1+q_{M1}+q_{M2})}{[d(E,M)]^3} \end{aligned}\right\} (1)$$

where

μ_S = product of sun's mass and universal gravitational constant G,

μ_M = product of moon's mass and universal gravitational constant G,

and q_{M1}, q_{M2} are quantities depending upon the earth's oblateness.

We shall not in this report give the precise formulas for computing q_{M1} and q_{M2}. They are functions of MxE, MyE, MzE and in calculating them we conform exactly to the specifications of NASA Project Apollo Working Paper No. 1004. Note, by the first terms on the right of equations (1), that no oblateness enters the calculations of the sun's gravitational influence on the earth, this omission being justified by the large magnitude of a(S,E) relative to the earth's dimensions.

We note incidentally that equations (1) simply set acceleration equal to force divided by mass. For if m_S and m_E are the respective masses of the sun and earth, the gravitational force with which they attract each other has magnitude

$$\frac{G\, m_S m_E}{[d(S,E)]^2}$$

[redacted]

and dividing by m_E gives

$$\frac{\mu_S}{[d(S,E)]^2}$$

as the magnitude of that part of the earth's acceleration due to the sun's influence.

The direction cosines of this contribution are clearly

$$-\frac{(ExS)}{d(S,E)}, \quad -\frac{(EyS)}{d(S,E)}, \quad -\frac{(EzS)}{d(S,E)}$$

in the x, y, z directions respectively. Thus

$$\text{Contribution to} \begin{pmatrix} E\ddot{x}S \\ E\ddot{y}S \\ E\ddot{z}S \end{pmatrix} \text{due to sun} = \begin{pmatrix} \frac{\mu_S (ExS)}{[d(S,E)]^3} \\ \frac{\mu_S (EyS)}{[d(S,E)]^3} \\ \frac{\mu_S (EzS)}{[d(S,E)]^3} \end{pmatrix}$$

Similarly considering the moon's influence on the earth (except for the contributions of q_{M1}, q_{M2}), we obtain the three terms on the right of equations (1).

We now desire formulas for $M\ddot{x}E$, $M\ddot{y}E$, $M\ddot{z}E$. We must bear in mind, however, that these are not components of the moon's acceleration since the earth-origin coordinate system is not an inertial one. Hence, we first (with reasoning similar to the above) write the equations for $M\ddot{x}S$, $M\ddot{y}S$, $M\ddot{z}S$, to wit:

$$M\ddot{x}S = \frac{-\mu_S (MxS)}{[d(S,M)]^3} - \frac{\mu_M (MxE)(1+q_{M1})}{d(E,M)} \qquad (2)$$

$$M\ddot{y}S = \frac{-\mu_S (MyS)}{[d(S,M)]^3} - \frac{\mu_M (MyE)(1+q_{M1})}{[d(E,M)]^3} \qquad (2)$$

$$M\ddot{z}S = \frac{-\mu_S (MzS)}{[d(S,M)]^3} - \frac{\mu_M (MzE)(1+q_{M1}+q_{M2})}{[d(E,M)]^3}$$

We now note (since all our x axes are parallel, etc.) the relations

$$(M\ddot{x}E) = (M\ddot{x}S) - (E\ddot{x}S)$$

$$(M\ddot{y}E) = (M\ddot{y}S) - (E\ddot{y}S)$$

$$(M\ddot{z}E) = (M\ddot{z}S) - (E\ddot{z}S)$$

Hence we obtain the formulas we desire by subtracting equations (1) from equations (2) in order. Defining μ_B by the equation

$$\mu_B = \mu_E + \mu_M$$

the results are

$$M\ddot{x}E = -\mu_S \left\{ \frac{MxS}{[d(S,M)]^3} - \frac{ExS}{[d(S,E)]^3} \right\} - \frac{\mu_B (MxE)(1+q_{M1})}{[d(E,M)]^3}$$

$$M\ddot{y}E = -\mu_S \left\{ \frac{MyS}{[d(S,M)]^3} - \frac{EyS}{[d(S,E)]^3} \right\} - \frac{\mu_B (MyE)(1+q_{M1})}{[d(E,M)]^3} \qquad (3)$$

$$M\ddot{z}E = -\mu_S \left\{ \frac{MzS}{[d(S,M)]^3} - \frac{EzS}{[d(S,E]^3} \right\} - \frac{\mu_B (MzE)(1+q_{M1}+q_{M2})}{[d(E,M)]^3}$$

We desire the differential equations for the motion of the vehicle in two forms:

(1) We desire $V\ddot{x}E$, $V\ddot{y}E$, $V\ddot{z}E$ for most of our computations;

(2) We desire $V\ddot{x}M$, $V\ddot{y}M$, $V\ddot{z}M$ for computations when the vehicle is near the moon.

None of the second derivatives just listed are true acceleration components since nether the earth-origin nor moon-origin system is an inertial one. We must therefore proceed in each case much as we did in obtaining equations (3). Since the details can hardly require explanation, we merely list the results. First, for $V\ddot{x}E$, $V\ddot{y}E$, $V\ddot{z}E$ we obtain

$$\begin{aligned}
V\ddot{x}E &= -\mu_S\left\{\frac{VxS}{[d(S,V)]^3}-\frac{ExS}{[d(S,E]^3}\right\}-\mu_E\frac{(VxE)(1+q_{v1})}{[d(E,V)]^3}\\
&\quad -\mu_M\frac{VxM}{[d(M,V)]^3}-\mu_M\frac{(MxE)(1+q_{M1})}{[d(E,V)]^3}\\
V\ddot{y}E &= -\mu_S\left\{\frac{VyS}{[d(S,V]^3}-\frac{EyS}{[d(S,E]^3}\right\}-\mu_E\frac{(VyE)(1+q_{v1})}{[d(E,V)]^3}\\
&\quad -\mu_M\frac{VyM}{[d(M,V)]^3}-\mu_M\frac{(MyE)(1+q_{M1})}{[d(E,V)]^3}\\
V\ddot{z}E &= -\mu_S\left\{\frac{VzS}{[d(S,V)]^3}-\frac{EzS}{[d(S,E)]^3}\right\}-\mu_E\frac{(VzE)(1+q_{v1}+q_{v2})}{[d(E,V)]^3}\\
&\quad -\mu_M\frac{VzM}{[d(M,V)]^3}-\mu_M\frac{(MzE)(1+q_{M1}+q_{M2})}{[d(E,V)]^3}
\end{aligned}\tag{4}$$

In the above q_{v1} and q_{v2} are factors depending on the oblateness of the earth, just as are q_{m1} and q_{m2}. But whereas q_{m1}, q_{m2} are functions of MxE, MyE, MzE as noted earlier, q_{v1} and q_{v2} are functions of VxE, VyE, VzE. Again we conform to the specifications of NASA Project Apollo Working Paper No. 1004 but shall not list the precise formulas here.

Finally we have

$$V\ddot{x}M = -\mu_M \frac{VxM}{[d(M,V]^3} - \mu_S \left\{ \frac{VxS}{[d(S,V)]^3} - \frac{MxS}{[d(S,M)]^3} \right\}$$

$$-\mu_E \left\{ \frac{(VxE)(1+q_{V1})}{[d(E,V)]^3} - \frac{(MxE)(1+q_{M1})}{[d(E,M)]^3} \right.$$

$$V\ddot{y}M = -\mu_M \frac{VyM}{[d(M,V)]^3} - \mu_S \left\{ \frac{VyS}{[d(S,V]^3} - \frac{MyS}{[d(S,M)]^3} \right\} \qquad (5)$$

$$-\mu_E \left\{ \frac{(VyE)(1+q_{V1})}{[d(E,V)]^3} - \frac{(MyE)(1+q_{M1})}{[d(E,M)]^3} \right.$$

$$V\ddot{z}M = -\mu_M \frac{VzM}{[d(M,V)]^3} - \mu_S \left\{ \frac{VzS}{[d(S,V)]^3} - \frac{MzS}{[d(S,M)]^3} \right\}$$

$$-\mu_E \left\{ \frac{(VzE)(1+q_{V1}+q_{+V2})}{[d(E,V)]^3} - \frac{(MzE)(1+q_{M1}+q_{M2})}{[d(E,M)]^3} \right.$$

where q_{m1}, q_{m2}, q_{v1}, q_{v2} are as before. We remark that the computations required by the earth's oblateness would be much more involved had we not specified that the z axis in each of our coordinate systems has the same direction as the earth's North Pole.

DIGRESSION: THE CLASSICAL "INVERSE SQUARE LAW" PROBLEM

Our problem is to compute ephemerides of the earth with respect to the sun and of the moon with respect to the earth by solving the sets of equations (1) and (3) of the preceding section, and then to determine the motion of the vehicle by solving the sets (4) and (5). We shall attend to these problems in succeeding sections.

In order to facilitate later discussion, however, we shall in the present section confine our attention to a much simpler problem, to wit:

Assume that we have a right-handed inertial x y z coordinate system and denote its origin by 0. Assume that a particle moves so that its coordinates satisfy the differential equations

$$\left.\begin{aligned} \ddot{x} &= -\frac{\mu x}{r^3} \\ \ddot{y} &= -\frac{\mu y}{r^3} \\ \ddot{z} &= -\frac{\mu z}{r^3} \end{aligned}\right\} \qquad (6)$$

where $r = (x^2+y^2+z^2)$ and μ is a positive constant. Denote initial valves of t, x, y, z, $\dot{x}$, $\dot{y}$, $\dot{z}$ by t_0, x_0, y_0, z_0, $\dot{x}_0$, $\dot{y}_0$, $\dot{z}_0$, respectively.

The solution to this is well known. Except in degenerate cases (where the initial position and velocity vectors have the same or exactly opposite directions) the path of the particle lies on a conic with a focus at 0 and the radius vector sweeps out area at a constant rate. We shall now outline a computational procedure for obtaining various points on the path and the corresponding times at which they are occupied by the particle.

We first reduce the problem to a two-dimensional one by defining a second coordinate system as follows: The origin of our new system is also at 0. We call the three axes $\bar{x}$, $\bar{y}$, $\bar{z}$ The positive direction of the $\bar{x}$-axis shall be the direction of the initial position vector of our particle. The $\bar{y}$ axis shall be so chosen that the initial velocity vector of our particle lies in the $\bar{x}$, $\bar{y}$ plane and has positive $\bar{x}$ and $\bar{y}$ components. (The path will then lie entirely in the $\bar{x}$, $\bar{y}$ plane.) The positive direction of the $\bar{z}$ axis shall be such that $\bar{x}$, $\bar{y}$, $\bar{z}$ is a right-handed system.

Let the direction cosines be denoted by C_{11}, C_{12}, etc., according to the following table:

	x	y	z
$\bar{x}$	C_{11}	C_{12}	C_{13}
$\bar{y}$	C_{21}	C_{22}	C_{23}
$\bar{z}$	C_{31}	C_{32}	C_{33}

Here each C_{ij} is the cosine of the angle between the axis appearing at its left and the one appearing above it; e. g., C_{23} is the cosine of the angle between the positive $\bar{y}$ direction and the positive z direction.

The elements of the cosine table may be obtained by doing the following computations in order:

$$r = (x_0^2 + y_0^2 + z_0^2)^{\frac{1}{2}}$$
$$C_{11} = \frac{x_0}{r_0}$$
$$C_{12} = \frac{y_0}{r_0}$$
$$C_{13} = \frac{z_0}{r_0}$$
$$d_1 = y_0 \dot{z}_0 - z_0 \dot{y}_0$$
$$d_2 = z_0 \dot{x}_0 - x_0 \dot{z}_0$$
$$d_3 = x_0 \dot{y}_0 - y_0 \dot{x}_0$$
$$d_0 = (d_1^2 + d_2^2 + d_3^2)^{\frac{1}{2}}$$
$$C_{31} = \frac{d_1}{d_0}$$
$$C_{32} = \frac{d_2}{d_0}$$
$$C_{33} = \frac{d_3}{d_0}$$
$$C_{21} = C_{32}C_{13} - C_{33}C_{12}$$
$$C_{22} = C_{33}C_{11} - C_{31}C_{13}$$
$$C_{23} = C_{31}C_{12} - C_{32}C_{11}$$

We next state that the initial position vector has components in the $\bar{x}\,\bar{y}\,\bar{z}$ system given by

$$\bar{x}_0 =$$
$$\bar{y}_0 = 0$$

and the initial velocity vector has components given by

$$\dot{\bar{x}}_0 = C_{11}\dot{x}_0 + C_{12}\dot{y}_0 + C_{13}\dot{z}_0$$
$$\dot{\bar{y}}_0 = C_{21}\dot{x}_0 + C_{22}\dot{y}_0 + C_{23}\dot{z}_0$$

Note that we have not listed $\bar{z}$ and $\dot{\bar{z}}$ since these are always zero whether we are speaking of initial or later values, since our path lies entirely in the $\bar{x}, \bar{y}$ plane.

Let $\dot{A}$ denote the rate at which the radius vector sweeps out area. We have

$$\dot{A} = \frac{1}{2}\left(\bar{x}\dot{\bar{y}} - \bar{y}\dot{\bar{x}}\right)$$

equal to a constant throughout the path; we may therefore compute it once and for all using the initial point and obtain

$$\dot{A} = \frac{1}{2}\,\bar{x}_0\dot{\bar{y}}_0$$

since $\bar{y}_0 = 0$.

Now any conic in the $\bar{x}$, $\bar{y}$ plane having a focus at 0 has an equation of the form

$$a\bar{x} + b\bar{y} + c = r = \left(\bar{x}^2 + \bar{y}^2\right)^{\frac{1}{2}}$$

where a, b, c are constants. To obtain a, b, c for the particular conic on which our particle travels, we perform the following computations in the order given:

$$c = \frac{\left(\bar{x}_0\dot{\bar{y}}_0\right)^2}{\mu}$$

$$a = \frac{\bar{x}_0 - \alpha}{\bar{x}_0}$$

$$b = \frac{\dot{\bar{x}}_0(1-a)}{\dot{\bar{y}}_0}$$

It will be noted that the substitution

$$\bar{x} = r\cos\theta$$

$$\bar{y} = r\sin\theta$$

converts $a\bar{x} + b\bar{y} + c = r$ to

$$r = \frac{c}{1 - a\cos\theta - b\sin\theta}$$

which is the standard polar form for a conic with focus at 0. (It is customary, however, to combine the two θ terms into one cosine term with a phase shift.) Sometimes it is simpler to use one form and sometimes the other.

In any event it is clear that once the constants a, b, c have been determined we may compute the $\bar{x}$, $\bar{y}$, coordinates of particular points on our conic. How the computations should be best arranged depends upon how we desire our computed points to be spaced along the path. (We use two distinct schemes for doing this in the subject program, one is obtaining the relative motions of the sun, earth, and moon and the second in determining the motion of the vehicle.)

Once the $\bar{x}$, $\bar{y}$, coordinates of any particular point on the path have been determined, the corresponding velocity components $\dot{\bar{x}}$, $\dot{\bar{y}}$ may be computed from the formulas

$$r = (\bar{x}^2 + \bar{y}^2)^{\frac{1}{2}}$$

$$\dot{\bar{x}} = \frac{2\dot{A}}{rc}(br - \bar{y})$$

$$\dot{\bar{y}} = \frac{2\dot{A}}{rc}(\bar{x} - ar)$$

The computation of the time t at which we are at each particular point depends essentially on determining the area swept out by the radius vector during the passage of our particle from the initial point to the particular point in question, dividing this area by $\dot{A}$, and adding the quotient to the initial time t_o. The best scheme for computing this area again depends on circumstances. Again the subject program uses two distinct schemes, one for conics of very low eccentricity (nearly circles) and one for conics whose eccentricity is unity (parabolas) or nearly so.

We end up with a tabulation of t, $\bar{x}$, $\bar{y}$, $\dot{\bar{x}}$, $\dot{\bar{y}}$ for each particular point chosen. Of course, the introduction of the $\bar{x}$, $\bar{y}$, $\bar{z}$ coordinate system is merely a gimmick to permit us to compute in two dimensions (all $\bar{z}$'s and $\dot{\bar{z}}$'s being zero). Our

[redacted]

final step then is to convert $\bar{x}$, $\bar{y}$, $\dot{\bar{x}}$, $\dot{\bar{y}}$ to x, y, z, $\dot{x}$, $\dot{y}$, $\dot{z}$, i.e., back to our original coordinate system. This is easily accomplished by referring to our direction cosine table; the formulas are:

$$x = C_{11}\bar{x} + C_{21}\bar{y}$$

$$y = C_{12}\bar{x} + C_{22}\bar{y}$$

$$z = C_{13}\bar{x} + C_{23}\bar{y}$$

$$\dot{x} = C_{11}\bar{x} + C_{21}\bar{y}$$

$$\dot{y} = C_{12}\bar{x} + C_{22}\bar{y}$$

$$\dot{z} = C_{13}\bar{x} + C_{23}\bar{y}$$

COMPUTATION OF EARTH RELATIVE TO SUN AND MOON RELATIVE TO EARTH EPHEMERIDES

Since the vehicle has negligible mass, we ignore it in the present section.

We mention at this point that one of the items each submitter will be required to furnish is an estimated total time of flight. One purpose of this is to provide for a program test which will prevent the computations from going on indefinitely in the event of an error in other input items. (Most of the testing is on relative distances.)

Let us now return to our differential equations for $E\ddot{x}S$, $E\ddot{y}S$, $E\ddot{z}S$ and $M\ddot{x}E$, $M\ddot{y}E$, $M\ddot{z}E$, given earlier as sets (1) and (3), and rewrite them with a slight rearrangement of terms in set (3). We shall also omit the items q_{M1}, q_{M2} solely for the purpose of simplifying our discussion. Of course we include these terms in the subject program itself, but our purpose in the present report is to outline our general theory, to an understanding of which a consideration of the terms q_{M1}, q_{M2} would contribute nothing essential. We have then

$$E\ddot{x}S = \frac{-\mu_S (ExS)}{[d(S,E)]^3} + \frac{\mu_M (MxE)}{[d(E,M)]^3} \qquad (1')$$

[redacted]

$$E\ddot{y}S = \frac{\mu_S(EyS)}{[d(S,E)]^3} + \frac{\mu_M(MyE)}{[d(E,M)]^3}$$

$$E\ddot{z}S = \frac{\mu_S(EzS)}{[d(S,E)]^3} + \frac{\mu_M(MzE)}{[d(E,M)]^3} \tag{1'}$$

$$M\ddot{x}E = \frac{\mu_B(MxE)}{[d(E,M)]^3} - \mu_S\left\{\frac{MxS}{[d(S,M)]^3} - \frac{ExS}{[d(S,E)]^3}\right.$$

$$M\ddot{y}E = \frac{\mu_B(MyE)}{[d(E,M)]^3} - \mu_S\left\{\frac{MyS}{[d(S,M)]^3} - \frac{EyS}{[d(S,E)]^3}\right. \tag{3'}$$

$$M\ddot{z}E = \frac{\mu_B(MzE)}{[d(E,M)]^3} - \mu_S\left\{\frac{MzS}{[d(S,M)]^3} - \frac{EzS}{[d(S,E)]^3}\right.$$

No purely analytical solution to these equations is possible. We therefore employ a "perturbation" procedure which is an adaptation of what is known to astronomers as "Encke's Method."

Looking first at equations (1'), we remark that the motion of E with respect to S is almost completely dominated by the three first terms; i. e., by the gravitational influence of the sun. (The ratio of the attractive forces of the sun and moon on the earth is roughly 180 to 1.) Moreover, if the μ_M terms on the far right of equations (1') were neglected, the remaining equations would, except for notation, be exactly the same as the differential equations (6) of the preceding section. The correspondence is simply

Notations of Eqs. (1')		Notations of Eqs. (6)
μ_S	⟷	μ
ExS	⟷	x
EyS	⟷	y
EzS	⟷	z
$d(S,E)$	⟷	r

If, then, we ignore the terms containing μ_M as a factor from equations (1'), we can obtain an analytical solution. We shall call this the "unperturbed solution" and denote the corresponding ("unperturbed") values of ExS, EyS, E **z** S by $(ExS)_u$, $(EyS)_u$, $(E\,z\,S)_u$ respectively. After following precisely the procedure of the preceding section, supplemented by some additional calculations which will not be described here, we obtain a table

t	$(ExS)_u$	$(EyS)_u$	$(EzS)_u$	$(E\dot{x}S)_u$	$(E\dot{y}S)_u$	$(E\dot{z}S)_u$
t_0	$[(ExS)]_0$	$[(EyS)]_0$	$[(EzS)]_0$	$[(E\dot{x}S)]_0$	$[(E\dot{y}S)]_0$	$[(E\dot{z}S)]_0$
t_0+6	$[(ExS)_u]_6$	$[(EyS)_u]_6$	$[(EzS)_u]_6$	$[(E\dot{x}S)_u]_6$	$[(E\dot{y}S)_u]_6$	$[(E\dot{z}S)_u]_6$
t_0+12	$[(ExS)_u]_{12}$	$[(EyS)_u]_{12}$	$[(EzS)_u]_{12}$	$[(E\dot{x}S)_u]_{12}$	$[(E\dot{y}S)_u]_{12}$	$[(E\dot{z}S)_u]_{12}$
⋮						⋮
t_0+120	$[(ExS)_u]_{120}$	$[(EyS)_u]_{120}$	$[(EzS)_u]_{120}$	$[(E\dot{x}S)_u]_{120}$	$[(E\dot{y}S)_u]_{120}$	$[(E\dot{z}S)_u]_{120}$

Our time unit is the hour and the table is intended to indicate that each row corresponds to a time six hours later than the time of the row above it. The total time span is 120 hours. Note that at time t_0 the items are simply the initial values, since there is at the start no difference between actual and unperturbed values.

We now look at equations (3'). Here the dominating terms are those containing μ_B as a factor. (Their contribution to the relative acceleration of M with respect to E is always at least 90 times the contribution of the terms containing μ_S as a factor, the exact ratio varying considerably with relative positions.) Here we write $(MxE)_u$, $(MyE)_u$, $(MzE)_u$ for "unperturbed" MxE, MyE, MzE respectively, with the understanding, analogous to the situation with equations (1') that $(MxE)_u$, $(MyE)_u$, $(MzE)_u$ are the values obtained by solving (3') with the terms on the far right omitted. Again the analysis of the preceding section can be applied and we eventually obtain a table with the headings

$$t \quad (MxE)_u \quad (MyE)_u \quad (MzE)_u \quad (M\dot{x}E)_u \quad (M\dot{y}E)_u \quad (M\dot{z}E)_u$$

similar to our table for t, $(ExS)_u$, etc. Again the times are t_o, $t_o + 6$, $t_o + 12$, ---, $t_o + 120$.

This is as far as we can go analytically. We must now account for the terms in our differential equations which we ignored in obtaining our unperturbed solutions.

We have in all six dependent variables (ExS, EyS, EzS, MxE, MyE, MzE), but it will be sufficient for immediate explanations to consider instead that we have but two, which we shall call x and y. Let the differential equations be represented by

$$\ddot{x} = D_1(x,y) + P_1(x,y)$$
$$\ddot{y} = D_2(x,y) + P_2(x,y)$$

where D_1, D_2, P_1, P_2 are functions of x, y. We have used the letters D and P to suggest the words "dominant" and "perturbative" respectively. Now let $x_u = x_u(t)$ and $y_u = y_u(t)$ denote the "unperturbed" solution; i. e., x_u and y_u satisfy exactly the differential equations

$$\ddot{x} = D_1(x_u, y_u)$$
$$\ddot{y} = D_2(x_u, y_u)$$

Furthermore let

$$\epsilon_x = \epsilon_x(t) = x - x_u$$

$$\epsilon_y = \epsilon_y(t) = y - y_u$$

In words, ϵ_x and ϵ_y are the "perturbations" which must be added to the unperturbed values x_u and y_u to obtain the actual x and y. Then

$$\ddot{\epsilon}_x = \ddot{x} - \ddot{x}_u$$

$$\ddot{\epsilon}_y = \ddot{y} - \ddot{y}_u$$

and substituting our differential equations for $\ddot{x}$, $\ddot{y}$, $\ddot{x}_u$, $\ddot{y}_u$ into these we obtain

$$\ddot{\epsilon}_x = \left\{ D_1(x,y) - D_1(x_u, y_u) \right\} + P_1(x,y)$$

$$\ddot{\epsilon}_y = \left\{ D_2(x,y) - D_2(x_u, y_u) \right\} + P_2(x,y)$$

as the differential equations for ϵ_x and ϵ_y

We now solve these by iteration method. We suppose (corresponding to our actual problem) that we have tabulated x_u, y_u, $\dot{x}_u$, $\dot{y}_u$ for every six hours from t_0 to $t_0 + 120$. We denote the "n^{th} iterated" values of x, y, $\dot{x}$, $\dot{y}$ by $(x)_n$, $(\dot{x})_n$, $(\dot{y})_n$ respectively and set our "0^{th} iterated" values equal to the unperturbed values. The process of stepping up from n^{th} to $(n+1)th$ values is this: For each point we obtain n^{th} values of ϵ_x, ϵ_y by the formulas

$$(\ddot{\epsilon}_x)_n = \left\{ D_1((x)_n, (y)_n) - D_1(x_u, y_u) \right\} + P_1((x)_n, (y)_n)$$

$$(\ddot{\epsilon}_y)_n = \left\{ D_2((y)_n, (y)_n) - D_2(x_u, y_u) \right\} + P_2((x)_n, (y)_n)$$

Having thus obtained $(\ddot{\epsilon}_x)_n$, $(\ddot{\epsilon}_y)_n$ for each point we integrate twice by a numerical procedure to obtain $(\dot{\epsilon}_x)_n$, $(\dot{\epsilon}_y)_n$, $(\epsilon_x)_n$, $(\epsilon_y)_n$; note here that at $t = t_0$ we have $\epsilon_x = \epsilon_y = \dot{\epsilon}_x = \dot{\epsilon}_y = 0$. Then

$$(x)_{n+1} = (x)_n + (\epsilon_y)_n$$

$$(y)_{n+1} = (y)_{n+1} + (\epsilon_y)_n$$

$$(\dot{x})_{n+1} = (\dot{x})_n + (\dot{\epsilon}_x)_n$$

$$(\dot{y})_{n+1} = (\dot{y})_n + (\dot{\epsilon}_y)_n$$

at each point. Three iterations are normally satisfactory.

Why not simply integrate the original equations for $\ddot{x}$, $\ddot{y}$ by a numerical procedure? The reason is that all numerical integrations schemes involve some slight error; let us say, for example, that the final answer can be out by a factor of 0.001. Our technique then (roughly speaking) means an error at most 0.001 times the perturbation values ϵ_x, ϵ_y in x and y instead of 0.001 times the main variables x and y.

Return now to our actual problem. Here we have six dependent variables and thus must have six perturbation variables. Otherwise the procedure is essentially the same as for the miniature case just described.

There are, it must be said, numerous programming pitfalls. It would not be appropriate to detail these here, but we shall call attention to one simply for illustrative purposes. In evaluating such an expression (see equations (3')) as

$$\frac{M_xS}{[d(S,M)]^3} - \frac{E_xS}{[d(S,M)]^3}$$

it must be borne in mind that each of the terms involved may have a very large value, although the difference between them is quite small. If then we were to evaluate each alone and then take the difference, we might have only one or two significant figure accuracy as every one with computing machine experience well knows. The difficulty is avoided by the following considerations.

Noting that MxS = (ExS) + (MxE), etc., the expression discussed can be written

$$\frac{(E_xS)+(M_xE)}{\left[\left\{(E_xS)+(M_xE)\right\}^2+\left\{(E_yS)+(M_yE)\right\}^2+\left\{(E_zS)+(M_zE)\right\}^2\right]^3} - \frac{(E_xS)}{\left[(E_xS)^2+(E_yS)^2+(E_zS)^2\right]}$$

This is of the form

$$f(x+\Delta x, y+\Delta y, z+\Delta z) - f(x, y, z)$$

which, to a first order approximation, is equal to

$$\frac{\partial f}{\partial x}\Delta x + \frac{\partial f}{\partial y}\Delta y + \frac{\partial f}{\partial z}\Delta z$$

This is an amply accurate approximation in our given case since d(E,M) is very small compared to d(S, E). The partial derivatives in this, and in other similar cases occurring in the program, can easily be evaluated.

Assume now that our iteration process has converged. We then have our ephemerides up to time $t = t_o + 120$. We may now do another 120 hours in the same way; this merely amounts to a re-labelling in which we take our last time as a new t_o for the next 120 hours. Theoretically we could continue indefinitely; actually, storage space in the subject program has been provided to continue until $t = t_o + 840$ (a span of 35 days) only. This is minimum; the process will normally be terminated earlier depending upon the estimated total flight time which, as noted earlier, must be an input item.

The flow charting corresponding to this section has been completed and is currently being coded.

COMPUTATION OF MOTION OF VEHICLE RELATIVE TO EARTH

Although we have hardly done more than sketch the general procedure adapted in the subject program for computing the earth-sun and moon-earth ephemerides, we shall give even less details in discussing the motion of the vehicle. The reason for this is our hope that the basic theory of our perturbation technique has been adequately covered in the two preceding sections.

We shall therefore limit ourselves to pointing out the most essential differences between the motion of the vehicle on the one hand and the motion of the earth and moon on the other.

We observe first that while certain terms could quite clearly be marked as dominating ones in the differential equations for earth relative to sun and for moon relative to earth, the situation is not so easily characterized in the case of the vehicle.

For definiteness let us limit ourselves to the case of a vehicle starting just outside the earth's atmosphere, proceeding to a point some 5,000 nautical miles from the moon, and then returning to the vicinity of the earth. In the early (and the very last) part of the trip it is quite clear that the gravitational attraction of the earth is the dominating influence. With some differences to be noted shortly, we can proceed essentially as before with our perturbation technique, taking as the differential equations of the unperturbed motion

$$\left.\begin{aligned}(V\ddot{x}E)_u &= \frac{\mu_E (VxE)_u}{[d(E,V)]^3}\\ (V\ddot{y}E)_u &= \frac{\mu_E (VyE)_u}{[d(E,V)]^3}\\ (V\ddot{z}E)_u &= \frac{\mu_E (VzE)_u}{[d(E,V)]^3}\end{aligned}\right\} \qquad (7)$$

where, as before, the subscript u denotes "unperturbed."

It will perhaps help to compare these equations with the actual equations, given earlier as set (4). Note that the effects of the earth's oblateness must be excluded from the unperturbed equations in order to permit an analytical solution. (The oblateness effects must then be included later in the perturbation equations.)

The first question to be settled is how far we can proceed toward the moon on the assumption that the unperturbed equations just listed actually dominate the motion. Here a considerable amount of computational work has been performed in order to determine a "safe" solution. We shall here simply state our decision. We shall proceed so long as the vehicle is no closer to the moon than 45,000 nautical miles. Schematically the situation is as follows:

[redacted]

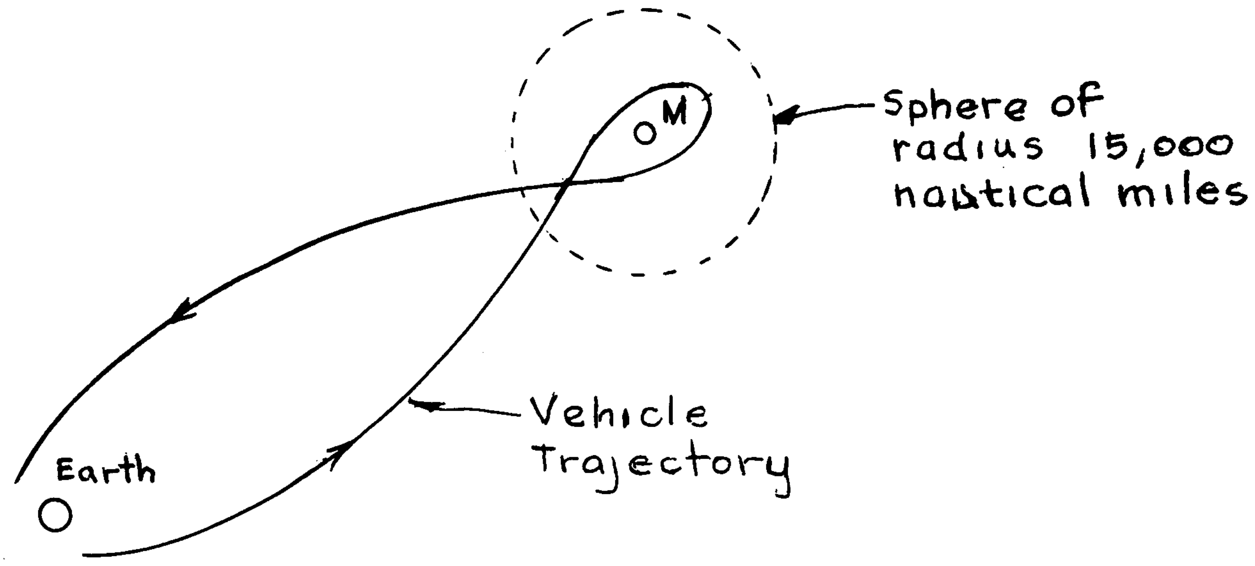

In the two parts of the trajectory (one leaving and the other returning to earth) for which we are greater than 45, 000 nautical miles from the Moon, we employ our adaptation of Encke's method with the unperturbed equations (7).

Now a brief mention of some further complications. Very near the Earth we need short intervals since the perturbative effect of the earth's oblateness is considerable here. As we leave the earth, our intervals may become longer for a while, but then must become shorter again because the moon's influence (a perturbative influence for us) becomes more and more significant.

We have thus devised an "interval function" depending on our distances. Roughly speaking this prescribes that successive points on our trajectory be about 100 nautical miles apart when the vehicle is very near the earth. The spacing increases gradually, reaching a maximum of 4000 nautical miles when d(E, V) = 120, 000 and decreasing thereafter as we approach the moon.

Varying the interval size in this way has made the computation of the "unperturbed" points and the numerical integration of the perturbation equations much more difficult than in the case of the earth relative to sun and moon relative to earth ephemerides. The basic theory involved is hardly different, however, and will not be expounded here. We will mention that the greatest distance over which we use one analytic solution to the unperturbed equations (7) is less than 32, 000 miles, being most of the way considerably less.

This part of the subject program has been completely flow-charted and is

[redacted]

currently being coded.

COMPUTATIONS OF MOTION OF VEHICLE RELATIVE TO MOON

There remains only the problem of what to do when the vehicle is within about 45,000 nautical miles of the moon. We state first that no detailed flow-charting of this part of the subject program is in final form. Decisions listed below are to be considered tentative.

Whatever computational scheme we finally adopt will use, as the basic differential equations, the set (5) given earlier; i. e., we will regard the moon-origin coordinate system as the basic one for computing purposes.

We feel that the difficulties of attempting to adapt Encke's method to this part of the program far outweighs the advantages. First of all, it is necessary to be considerably closer to the moon than 45,000 nautical miles before one can properly say that the moon's influence dominates the motion to such a large extent that other influences are merely perturbative. Moreover in attempting to obtain the analytic solutions to the unperturbed equations there is considerable risk of running into cases which are very nearly degenerate ones, in which case machine overflow or underflow could create havoc. Our present plan, therefore, is to proceed near the moon with a purely step integration procedure (such as Runge-Kutta). This will require smaller interval size, not any greater programming difficulty, and only slightly less accuracy. The latter can be tolerated, however, since in the vicinity of the moon some sort of guidance will be required in any case; in other words no practical vehicle could hold to a purely ballistic trajection all the way from the earth to the moon.

We conclude by reviewing the present work status:

(1) Nothing definite has been done on the "input" or "output" libraries.

(2) Flow-charting is complete on the earth relative to sun and moon relative to earth ephemerides and coding is under way.

(3) Flow-charting is complete on motion of vehicle relative to earth for portions of trajectory during which $d(M, V)$ 45,000 nautical miles. This includes both the case of vehicle leaving the earth and vehicle returning to earth.

(4) Nothing definite has been done on computations of vehicle motion when $d(M, V)$ 45,000 nautical miles. Present preference is to do this in steps as opposed to the use of a perturbation method.

We remark that the overall machine logic for passing from one phase of the program to another has been completed.

APPENDIX D

DERIVATION OF ERROR PARTIALS

A. NAVIGATION BY MEASUREMENT OF θ AND t AT FOUR TRAJECTORY POINTS

It is assumed that the trajectory can be represented as a limited two body problem and that all measurements are made in the trajectory plane so that it is also coplanar.

The ballistic time of flight (τ_n) from any position on the trajectory (r_n, θ_n) to perigee can be expressed as:

Equation I

$$\tau_n = t_n - T = f(p, e, \delta, \theta_n)$$

where

τ_n = Time of flight to perigee.

t_n = Measured time.

T = Reference perigee time.

p = Semi-latus rectum.

e = Eccentricity.

δ = Angle between the trajectory major axis and an inertial reference.

θ_n = Angle between local vertical and an inertial reference.

r_n = Range between the vehicle and the mass center of the earth.

μ = Universal gravitational constant.

The conventions are indicated in Fig D-1. Inasmuch as there are 4 unknowns (ρ, e, δ, T), 4 equations of the form of equation I will be required. This stipulates that readings of t_n and θ_n at four points along the trajectory must be made. It is assumed that time measurements can be made ideally such that $d\,t_n = 0$. Taking the total derivative of equation I:

Equation II

$$-dT = \frac{\partial \tau_n}{\partial p}dp + \frac{\partial \tau_n}{\partial e}de + \frac{\partial \tau_n}{\partial \delta}d\delta + \frac{\partial \tau_n}{\partial \theta}d\theta_n$$

The error equations for n = 4 can be written in Matrix form as:

Equation III

$$\begin{vmatrix} \frac{\partial T_1}{\partial p} & \frac{\partial T_1}{\partial \delta} & \frac{\partial T_1}{\partial e} & 1 \\ \frac{\partial T_2}{\partial p} & \frac{\partial T_2}{\partial \delta} & \frac{\partial T_2}{\partial e} & 1 \\ \frac{\partial T_3}{\partial p} & \frac{\partial T_3}{\partial \delta} & \frac{\partial T_3}{\partial e} & 1 \\ \frac{\partial T_4}{\partial p} & \frac{\partial T_4}{\partial \delta} & \frac{\partial T_4}{\partial e} & 1 \end{vmatrix} \begin{vmatrix} dp \\ d\delta \\ de \\ dT \end{vmatrix} = \begin{vmatrix} -\frac{\partial T_1}{\partial \theta} & 0 & 0 & 0 \\ 0 & -\frac{\partial T_2}{\partial \theta} & 0 & 0 \\ 0 & 0 & -\frac{\partial T_3}{\partial \theta} & 0 \\ 0 & 0 & 0 & -\frac{\partial T_4}{\partial \theta} \end{vmatrix} \begin{vmatrix} d\theta_1 \\ d\theta_2 \\ d\theta_3 \\ d\theta_4 \end{vmatrix}$$

The partials to be used are given in equations VI and VII. The solution of equation III to determine dp, de, $d\delta$ and dT as a function of $d\theta_1$, $d\theta_2$, $d\theta_3$, and $d\theta_4$, is conventional. The resultant error equations will be in the form of:

$$dp = \frac{\partial p}{\partial \theta_1} d\theta_1 + \frac{\partial p}{\partial \theta_2} d\theta_2 + \frac{\partial p}{\partial \theta_3} d\theta_3 + \frac{\partial p}{\partial \theta_4} d\theta_4$$

$$de = \frac{\partial e}{\partial \theta_1} d\theta_1 + \frac{\partial e}{\partial \theta_2} d\theta_2 + \frac{\partial e}{\partial \theta_3} d\theta_3 + \frac{\partial e}{\partial \theta_4} d\theta_4$$

etc.

The partials for equation III are derived for the case where e = 1 and $e < 1$. The time to perigee for $e < 1$ can be written as:

Equation IV

$$T_n = \frac{p^{\frac{3}{2}}}{(1-e^2)\sqrt{\mu}} \left[\frac{-e \sin(\theta_n - \delta)}{1 + e \cos(\theta_n - \delta)} + \frac{2}{\sqrt{1-e^2}} \tan^{-1}\left(\sqrt{\frac{1-e}{1+e}} \tan\left| \frac{\theta_n - \delta}{2} \right| \right) \right]$$

For the specific case where time to perigee in the vicinity of e = 1 is of interest, the time equation can be expanded in terms of 1-e around e = 1. Considering only the first term of the series:

Equation V

$$T_n = \left\{ \frac{1}{2}\left(\frac{p^3}{\mu}\right)^{\frac{1}{2}} \left[\tan\left|\frac{\theta_n-\delta}{2}\right| + \frac{1}{3}\tan^3\left|\frac{\theta_n-\delta}{2}\right| \right] \right\}$$

$$+ \left\{ \frac{1}{2}\left(\frac{p^3}{\mu}\right)^{\frac{1}{2}} \left[\tan\left|\frac{\theta_n-\delta}{2}\right| - \frac{1}{5}\tan^5\left|\frac{\theta_n-\delta}{2}\right| \right] \right\} (1-e)$$

Equation V is valid for:

$$\frac{1-e}{1+e} \tan^2\left|\frac{\theta_n-\delta}{2}\right| \ll 1$$

For an eccentricity of 0.97, the single term expansion can be used for ranges less than 45,000 naut mi. It is assumed that the inertial axis and the major axis of the trajectory are coincident so that $\delta = 0$.

The partials for equation V (i.e., e = 1) are:

Equation VI

$$\frac{\partial T_n}{\partial p} = \frac{3}{2p} T_{n_0}$$

$$-\frac{\partial T_n}{\partial \delta} = \frac{\partial T_n}{\partial \theta} = \frac{1}{p}\sqrt{\frac{p}{\mu}}\, r_n^2$$

$$\frac{\partial T_n}{\partial e} = -\frac{1}{2}\left(\frac{p^3}{\mu}\right)^{\frac{1}{2}} \left\{ \tan\frac{\theta_n}{2} - \frac{1}{5}\tan^5\frac{\theta_n}{2} \right\}$$

where $r_n = \frac{p}{1+\cos\theta_n}$

T_{n_0} is the the first term of equation V

The partials for equation IV (i.e., $e < 1$) are:

Equation VII

$$\frac{\partial \tau_n}{\partial p} = \frac{3}{2p}\tau_n$$

$$-\frac{\partial \tau_n}{\partial \delta} = \frac{\partial \tau_n}{\partial \theta} = \frac{1}{p}\sqrt{\frac{p}{\mu}}\, r_n^2$$

$$\frac{\partial \tau_n}{\partial e} = \frac{3et_n}{1-e^2} - \frac{p^2}{\sqrt{\mu p}\,(1-e^2)}\left\{\frac{r_n^2}{p^2}\sin\theta_n + \frac{r_n}{p}\sin\theta_n\right\}$$

where $r_n = \dfrac{p}{1+e\cos\theta_n}$

τ_n is defined by equation IV

B. NAVIGATION BY MEASUREMENT OF θ, r AND t AT TWO TRAJECTORY POINTS

It is assumed that the trajectory can be represented as a limited two body problem and that all measurements are made in the trajectory plane so that it is also coplanar.

The ballistic time of flight (τ_n) from any position on the trajectory (r_n, θ_n) to perigee can be expressed as:

Equation I

$$\tau_n = t_n - T = f(p, e, \delta, \theta_n)$$

Similarly, the corresponding range can be expressed as:

Equation VIII

$$r_n = f(p, e, \delta, \theta_n)$$

Inasmuch as there are 4 unknowns (p, e, δ, T), four equations are required such that equations I and VIII will be used at 2 points along the trajectory. This indicates that readings of θ_n, r_n and t_n must be made at these 2 points. Taking the total derivatives of equations I and VIII:

Equation II

$$-dT = \frac{\partial T_n}{\partial p} dp + \frac{\partial T_n}{\partial e} de + \frac{\partial T_n}{\partial \delta} d\delta + \frac{\partial T_n}{\partial \theta} d\theta_n$$

Equation IX

$$dr_n = \frac{\partial r_n}{\partial p} dp + \frac{\partial r_n}{\partial e} de + \frac{\partial r_n}{\partial \delta} d\delta + \frac{\partial r_n}{\partial \theta} d\theta_n$$

The error equations for n = 2 can be written in Matrix form as:

Equation X

$$\begin{vmatrix} \frac{\partial T_1}{\partial p} & \frac{\partial T_1}{\partial \delta} & \frac{\partial T_1}{\partial e} & 1 \\ \frac{\partial T_2}{\partial p} & \frac{\partial T_2}{\partial \delta} & \frac{\partial T_2}{\partial e} & 1 \\ \frac{\partial r_1}{\partial p} & \frac{\partial r_1}{\partial \delta} & \frac{\partial r_1}{\partial e} & 0 \\ \frac{\partial r_2}{\partial p} & \frac{\partial r_2}{\partial \delta} & \frac{\partial r_2}{\partial e} & 0 \end{vmatrix} \begin{vmatrix} dp \\ d\delta \\ de \\ dT \end{vmatrix} = \begin{vmatrix} -\frac{\partial T_1}{\partial \theta} & 0 & 0 & 0 \\ 0 & -\frac{\partial T_2}{\partial \theta} & 0 & 0 \\ -\frac{\partial r_1}{\partial \theta} & 0 & 1 & 0 \\ 0 & -\frac{\partial r_2}{\partial \theta} & 0 & 1 \end{vmatrix} \begin{vmatrix} d\theta_1 \\ d\theta_2 \\ dr_1 \\ dr_2 \end{vmatrix}$$

The partials to be used are given in equations VI and XII for e = 1 or VII and XII for $e < 1$. The solution to equation X to determine d_p, d_e, $d\delta$ and dT as a function of $d\theta_1$, $d\theta_2$, dr_1 and dr_2 is conventional. The resultant error equations will be in the form of:

$$dp = \frac{\partial p}{\partial \theta_1} d\theta_1 + \frac{\partial p}{\partial \theta_2} d\theta_2 + \frac{\partial p}{\partial r_1} dr_1 + \frac{\partial p}{\partial r_2} dr_2$$

$$de = \frac{\partial e}{\partial \theta_1} d\theta_1 + \frac{\partial e}{\partial \theta_2} d\theta_2 + \frac{\partial e}{\partial r_1} dr_1 + \frac{\partial e}{\partial r_2} dr_2 \text{, etc.}$$

The partials $\frac{\partial T_n}{\partial p}$, $\frac{\partial T_n}{\partial \delta}$ and $\frac{\partial T_n}{\partial e}$ are defined by equations VI and VII.

Range can be expressed as:

Equation XI

$$r_n = \frac{p}{1 + e\cos(\theta_n - \delta)}$$

The error partials are:

Equation XII

$$\frac{\partial r_n}{\partial p} = \frac{r_n}{p}$$

$$\frac{\partial r_n}{\partial e} = -\frac{r_n^2}{p}\cos\theta_n$$

$$\frac{\partial r_n}{\partial \theta} = \frac{r_n}{p} e\sin\theta_n$$

$$\frac{\partial r_n}{\partial \delta} = -\frac{r_n}{p} e\sin\theta_n$$

When it is assumed that $e = 1$:

$$r_n = \frac{p}{1 + \cos\theta_n}$$

C. DETERMINATION OF SYSTEM PARAMETERS

The error equations have been derived in terms of the trajectory parameters dp, de, $d\delta$ and dT. Of greater interest are the system parameters and their associated error partials which can be expressed in terms of the above. The system parameters will be determined at perigee for an eccentricity approximately equal to one so that $(\theta_p - \delta) = 0$, $\gamma_p = 0$, $2r_p = p$ and $V_p^2 = 2\mu/rp$ where:

r_p = Range from earth center at perigee.

v_p = Velocity at perigee.

γ_p = Flight path angle at perigee.

p = Semi latus rectum.

μ = Universal gravitational constant.

The system parameters are obtained by taking the total derivative of the desired function and then applying the constraints of eccentricity equal to one and location at perigee.

Range and range error are:

Equation XIII

$$r = \frac{p}{1 + e\cos(\theta - \delta)}$$

$$dr_p = \frac{1}{2}(dp - r_p\,de)$$

Velocity and velocity error can be expressed as:

Equation XIV

$$V^2 = \mu\left(\frac{2}{r} - \frac{1-e^2}{p}\right)$$

$$dV_p = \frac{V_p}{4r_p}\left(-dp + 2r_p\,de\right)$$

At perigee, equation II can be expressed as:

$$-dT = \frac{\partial T_n}{\partial \delta}\,d\delta + \frac{\partial T_n}{\partial \theta}\,d\theta$$

where $-\frac{\partial T_n}{\partial \delta} = \frac{\partial T_n}{\partial \theta} = \frac{1}{p}\sqrt{\frac{p}{\mu}}\,r_p^2 = r_p\sqrt{\frac{r_p}{2\mu}} = \frac{r_p}{V_p}$

[redacted]

Equation XV

$$d\theta_p = -dT\left(\frac{V_p}{r_p}\right) + d\delta$$

Equation XV represents the range angle error.

The flight path angle and flight path angle error are:

$$\tan\gamma = \frac{e\sin(\theta-\delta)}{1+e\cos(\theta-\delta)}$$

$$d\gamma_p = \frac{d\theta - d\delta}{2}$$

Substituting equation XV in the above yields:

Equation XVI

$$d\gamma_p = \frac{-dT\left(\frac{V_p}{r_p}\right)}{2}$$

By substituting the trajectory parameters dp, de, d δ and dT in equations XIII thru XVI, the system parameters and the associated system error partials are obtained. As an example, for the case where measurements of r, θ and t are made at two trajectory points, dr_p becomes:

$$dr_p = \frac{1}{2}\left(dp - r_p\,de\right)$$

$$dr_p = \frac{1}{2}\left(\frac{\partial p}{\partial\theta_1} - r_p\frac{\partial e}{\partial\theta_1}\right)d\theta_1 + \frac{1}{2}\left(\frac{\partial p}{\partial\theta_2} - r_p\frac{\partial e}{\partial\theta_2}\right)d\theta_2$$

$$+ \frac{1}{2}\left(\frac{\partial p}{\partial r_1} - r_p\frac{\partial e}{\partial r_1}\right)dr_1 + \frac{1}{2}\left(\frac{\partial p}{\partial r_2} - r_p\frac{\partial e}{\partial r_2}\right)dr_2$$

$$dr_p = \left(\frac{\partial r_p}{\partial\theta_1}\right)d\theta_1 + \left(\frac{\partial r_p}{\partial\theta_2}\right)d\theta_2 + \left(\frac{\partial r_p}{\partial r_1}\right)dr_1 + \left(\frac{\partial r_p}{\partial r_2}\right)dr_2$$

[redacted]

APPENDIX E

ASTRO-INERTIAL PLATFORM (LITTON)

The following information is extracted from Litton Industries Publication No. 1253 which is a technical description of the LN-5 Astro-Inertial Navigation System. The work was done for the United States Naval Aeronautics Facility under Contract N163-8433 to satisfy the requirements of the Facility's Technical Specification TS 820-14.

The Astro-Inertial Platform Assembly portion of the LN-5 System is designated the P-200S. This is a combination of a standard production version of the Litton P-200 Inertial Platform and a Kollsman Astrotracker modified to include an optical coupling link. The entire assembly weighs about 90 pounds. The unit is approximately 16 inches in diameter and 24-1/2 inches high. The electronic units required with the P-200S are:

(1) Platform Amplifier--This unit provides all the electronics and circuitry required to stabilize the platform and to close accelerometer control loops.

(2) Astrotracker Electronics Assembly--This unit provides all the electronic amplifiers and circuitry to stabilize the tracker gimbal system; to drive the telescope to track stars; and to resolve the error signals. It also contains the power supplies required by the astrotracker subsystem.

Figure N-1 is a block diagram of the Astro-Inertial Tracker portion of the LN-5 system.

A description of the P-200 is given first, followed by a discussion of the modifications incorporated in the P-200S. This is followed with a description of the astrotracker and the optical coupling link.

The basic platform is a four gimbal system which uses 2 two-degree-of-freedom gyros which are mounted in a dumbbell configuration. Three pendulous-type, torque balance, miniature accelerometers can be mounted between the gyros although only two are required in the LN-5 system. The gimbals are gear driven with a-c servo motors.

The gimbal axes configuration from inside out is:

Gimbal	Freedom
Azimuth	± 360°
Inner roll	± 20°
Pitch	± 360°
Outer roll	± 360°

Two Litton G-200 two-degree-of-freedom gyros are used on the platform. The significant gyro characteristics are indicated in the following tables:

Gyro Performance Data

Type of Error	RMS Error Magnitude
Bias torque uncertainty, each axis	0.01 °/hr
Error torque linear with respect to applied accelerations, each axis	0.08 °/hr/g
Error torque proportional to square of applied acceleration, most unfavorable orientation	0.04 °/hr/g

Gyro Mechanical Characteristics

Fully floated instrument	
Degrees of freedom	Two
Drift rate	0.01 °/hr
Angular momentum	1.5×10^6 gm-cm^2/sec
Maximum torquing rate	2000 °/hr
Size	3" dia x 4" L
Weight	2 pounds

These gyros provide the signals for angular stabilization of the pitch, roll, and azimuth platform axes. The use of two-degree-of-freedom rather than single-degree-of-freedom gyros results in a number of significant advantages in design and performance:

(1) The gyro dynamics do not affect the gimbal control loop dynamics, thus permitting higher stabilization gain and bandwidth to be obtained and eliminating the need for critical adjustments of the servo amplifiers.

(2) Interaxis coupling effects, which normally necessitate critical adjustments and additional complexity of the electronics circuitry for satisfactory operation, are completely negligible.

(3) Nonlinear coupling due to rotor precession, which introduces platform drifts in the presence of vibration or transient oscillations, is completely absent.

(4) A highly efficient dumbbell mounting configuration of the gyros can be employed, resulting in a very compact inner structure and consequently in a smaller weight and volume for the complete platform.

The accelerometers used in the P-200 inertial system are a floated pendulum, miniature, torque balance type, combining extreme simplicity, small size, and high precision. This type of design is rugged and has only one moving part which is limited in angular freedom to a few minutes of arc and which, under operating conditions, never deflects more than a few seconds of arc. The excellent intrinsic damping afforded by the floatation fluid prevents the build-up of any appreciable relative motion of the element with respect to the case even under severe environments. All parts are designed to have stiffness and strength of several orders of magnitude greater than that ordinarily needed to meet operational requirements. Careful attention has been given to alleviating excessively close tolerance parts and assemblies wherever possible.

The accelerometer is very similar to the Litton A-300 accelerometer used on the P-300G platform. This accelerometer is described in Chapter IV, E, 3, d. The specifications for the accelerometer used on the P-200 platform are listed below:

Accelerometer Specifications

Size	1.00 x 1.135 x 1.80 inches
Volume	2.04 cubic inches
Weight	7 ounces
Pickoff excitation	15 volts rms at 5000 cps
Pickoff power	1 watt
Torquer scale factor	2.7 ma/g
Maximum acceleration	In excess of 15 g
Threshold acceleration	Less than 10^{-5} g
Bias error	5×10^{-5} g
Scale factor and nonlinearity error	5×10^{-5} of applied acceleration
Combined orientation errors	3 seconds of arc

The P-200S inertial platform in the LN-5 is almost identical to the production P-200 platform. The only differences are in the housing and in the addition of a reflector for the optical link coupling the Astrotracker and the Inertial Platform.

The standard P-200 housing cover is being replaced in the P-200S by a cover whose dimensions are increased to provide for the mounting of the Astrotracker assembly within a common housing chamber. The resultant configuration is shown in Fig. N-2.

The optical link reflector is a simple mirror system. The mirror allows 6° of tilt between the Astrotracker and the Inertial Platform before the optical link is broken.

The addition of a mirror to the existing P-200 removes the full maneuverability capability of the platform because of a lack of sufficient clearance for the gimbal structure. This disadvantage could be overcome by a more complex reflector structure or by an increase in the platform gimbal size. Neither of these techniques were within the scope of the LN-5 test program.

ASTROTRACKER

The Astrotracker consists of the optics, pointing drives, stabilization devices, and means of detecting and tracking the celestial body. It is housed within the hermetically sealed inertial enclosure containing a quartz transparent dome. This housing also provides within it the rigidity required between the astro and inertial elements. The telescope is stabilized with respect to the inertial platform by synchro signals. Increased accuracy is obtained by use of the optical link.

The tracker monitors the azimuth and position of the platform by automatic photoelectric star tracking. The tracker-platform assembly plus the proper computer system will provide automatic azimuth and position corrections.

In operation, the telescope continuously scans a sky area of two minutes diameter about the command bearing. The light energy of any star of magnitude 2.0 or greater within the scan field actuates electronic circuits through a photoelectric detector. The resulting star presence signals are electronically correlated to the position of the center of the telescope field. The star signal data are further operated upon to obtain outputs of the position of the star in the field relative to the telescope command bearing. These outputs are nulled in a control loop within the Astrotracker to center the telescope on the star.

The Astrotracker will perform suitably with the following extremes in dynamic conditions.

Max roll velocity	0.75 rad/sec
Max roll acceleration	2.75 rad/sec^2
Max pitch velocity	0.20 rad/sec

Max pitch acceleration	0.60 rad/sec^2
Max yaw velocity	0.20 rad/sec
Max yaw acceleration	0.60 rad/sec^2

The telescope consists of an optical system gimballed in bearing and elevation and containing the necessary gimbal servo drives, scanning mechanism, and photomultiplier. The optics of the tracker will bring the sky area being viewed to a focus at the field stop plane. The scanning mechanism will examine this focused sky area. The photomultiplier outputs will indicate star presence and star position in the scan field.

The telescope is positioned in star elevation and true bearing by gimbals in response to data signals received from a computer. The true-bearing gimbal has unlimited freedom in the azimuth plane. The altitude gimbal has a range of rotation of 20 to 90 degrees of star altitude.

The optical system consists of the dome window, an objective lens, several folding mirrors, a motor-driven nutating mirror, a motor-driven shutter mirror, and the condensing lens system.

The optical dome, made of quartz to withstand extremes of environment permits starlight to enter the sealed package. The objective lens is 1.75 inches in diameter; it collects adequate light to detect stars of second magnitude and brighter and focuses the light in the plane of the shutter. The folding mirrors reduce the 12-inch focal length to about five inches.

The rotating mirrors are a part of the scanning mechanism as well as a part of the optics. They modulate the light so that the resulting error signals provide star presence and attitude information.

The condensing lens system relays the light onto a photodetector. A photomultiplier similar to the 1P21 is used as the photosensor. It provides, within a single envelope, an amplification of approximately two million.

OPTICAL TIE

The optics of the azimuth, pitch and roll optical tie between the tracker and platform are shown in Fig. N-3, the method is one of photoelectric autocollimation. The method employs a small photoelectric telescope in the Astrotracker and a relatively simple reflective surface in the stable platform. A continuous light path is provided by windows in the bottom of the tracker and the top of the platform. The optical system begins at the light source which illuminates a small aperture. The output of the aperture is collimated by the objective lens after being deflected by the beam splitter. After being reflected by the mirror, the returning illumination is refocused by the objective lens so that an image of the aperture is formed near the modulating shutter. The resultant output of the photoreceiver is modulated in accordance with the misalignment present.

The shutter is essentially a disc rotated about its own center. This disc is made up of a transmitting semicircle and an occulting semicircle. If the small image of the aperture lies uniformly distributed about the point of rotation of the shutter, a constant d-c photoreceiver output will be obtained. If the image center is displaced from the shutter center because of misalignment, then the photo receiver output will be amplitude-modulated at a frequency determined by the rotational velocity of the shutter. The position of the image on the field relative to some reference line can be detected by a phase comparison between the signal and a reference voltage which is synchronous with the shutter. This phase comparison will permit the resolution of any vertical error signal into its orthogonal components of pitch and roll or correction of an azimuth error. The radial error distance of the image from the center of the field can be determined from the amplitude of the error signal.

Using reasonable control of ambient light levels, this technique has demonstrated a static servo repeatability within 10 seconds of arc. Considering the constant motion present in airborne operation, a usable sensitivity of five seconds of arc is reasonable.

ACCURACY

Assuming errorless stabilization and star pointing commands, the accuracy of the equipment in each axis is 15 seconds of arc rms in establishing the line-of-sight to the body being tracked. The limiting factor in attaining this accuracy is the precision of the high-accuracy miniature inductosyn angle transducers used.

The major sources of Astrotracker error may be divided into three groups; optical errors, tracking errors, and transducer errors. Optical errors include all errors in optical elements and their alignment. It is estimated that viewing-window errors, lens-curvature, correction and alignment errors, and variation of these errors under environment have been restricted to eight seconds of arc rms.

Tracking errors include servo errors associated with each tracking axis, resolution of star error signals, phototube errors and other errors associated with the tracking process. It is estimated that these errors are six seconds of arc rms.

An allowance of 10 seconds rms was made for transducing telescope angles. This includes errors in the transducer and its alignment, as well as errors in orthogonality of axes. The rms of these major sources of error plus an extra five seconds of arc rms for miscellaneous sources is fifteen seconds of arc rms.

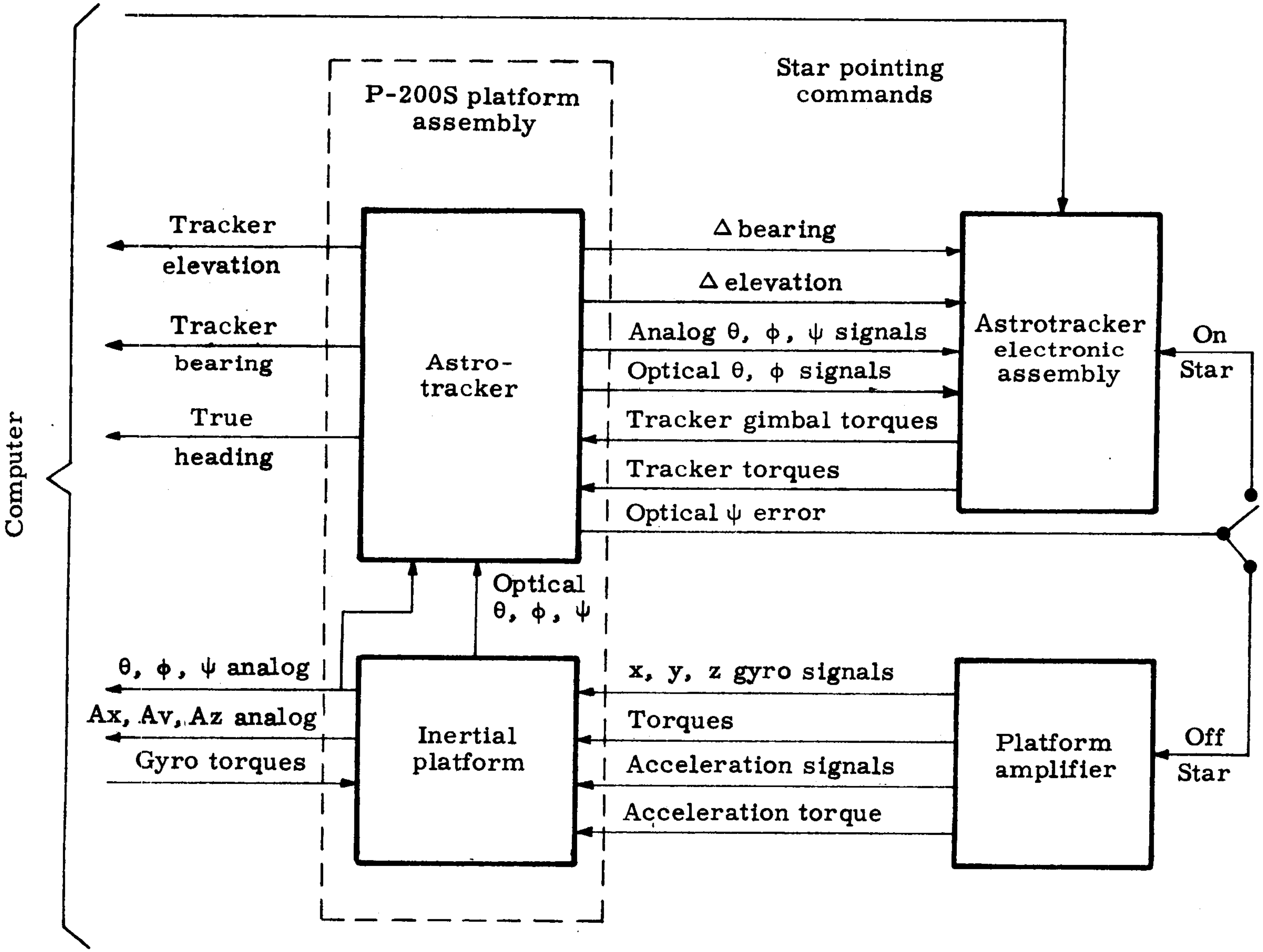
P-200S platform assembly
Star pointing commands
Tracker elevation
Tracker bearing
True heading
Computer
Astro-tracker
Δ bearing
Δ elevation
Analog θ, ϕ, ψ signals
Optical θ, ϕ signals
Tracker gimbal torques
Tracker torques
Optical ψ error
Astrotracker electronic assembly
On Star
Off Star
Optical θ, ϕ, ψ
θ, ϕ, ψ analog
Ax, Av, Az analog
Gyro torques
Inertial platform
x, y, z gyro signals
Torques
Acceleration signals
Acceleration torque
Platform amplifier

Fig. E-1. Block Diagram Astro-Inertial Tracker Configuration

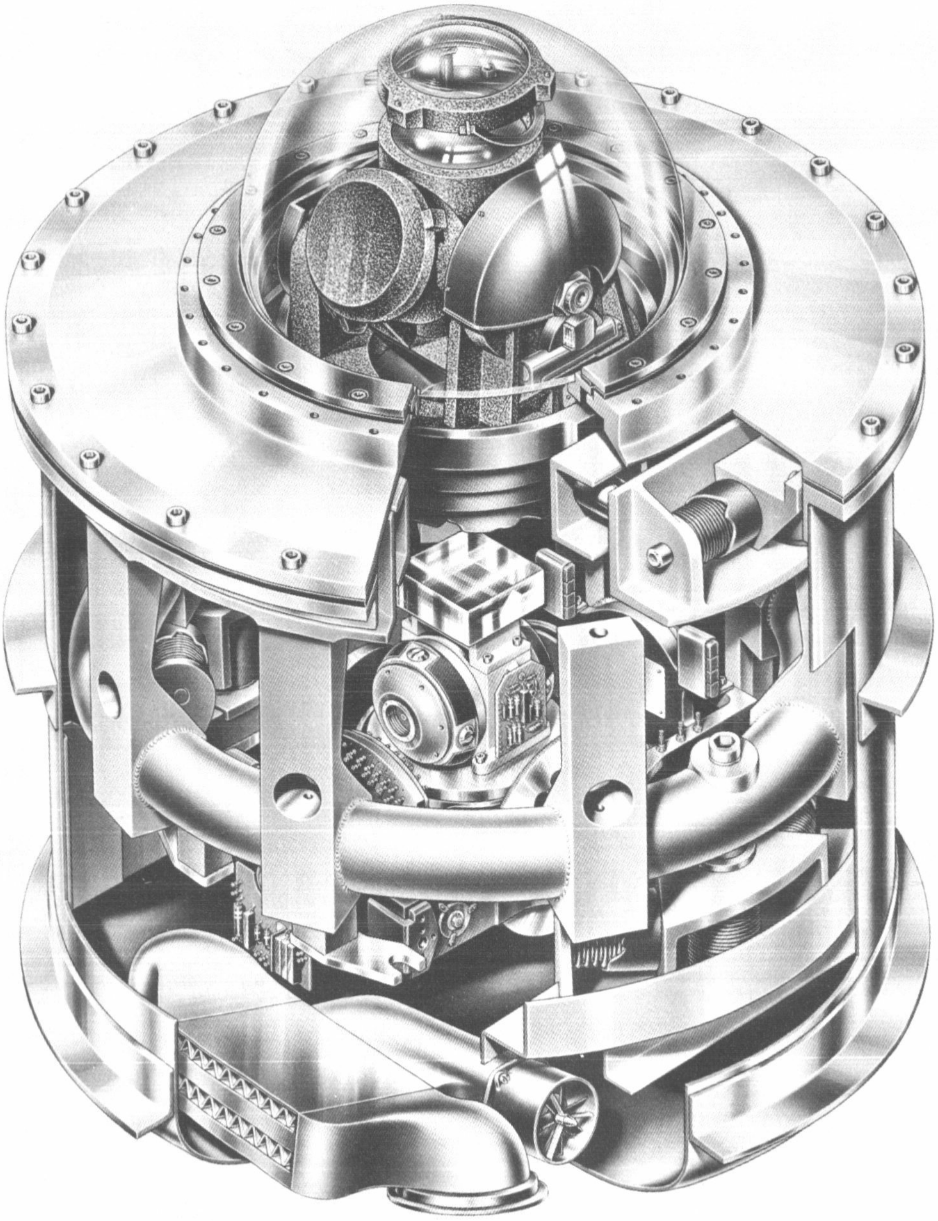

Fig. E-2. P-200S Inertial Platform

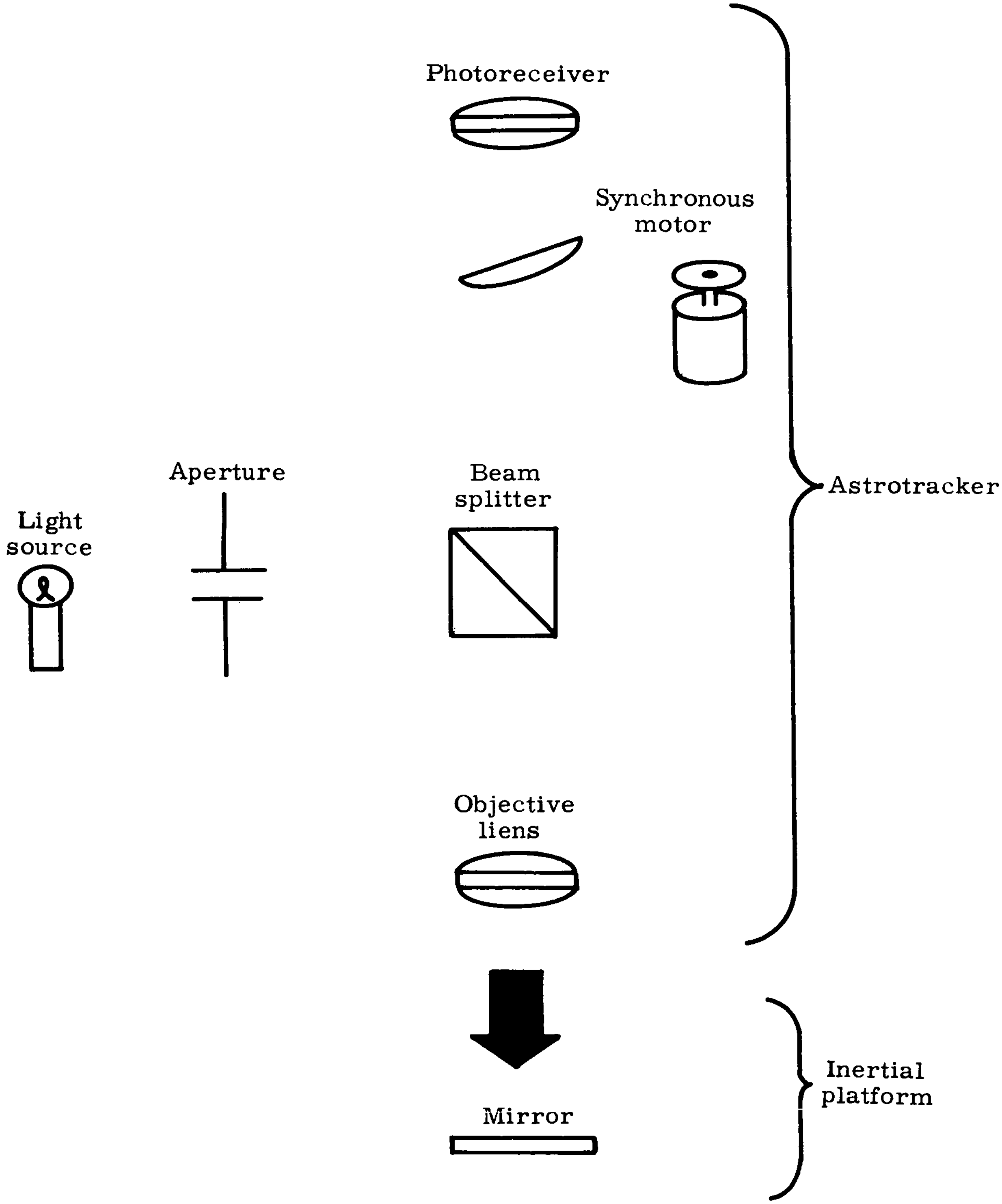
Photoreceiver
Synchronous motor
Astrotracker
Aperture
Beam splitter
Light source
Objective liens
Inertial platform
Mirror

Fig. E-3. Azimuth, Pitch and Roll (optical tie)

APPENDIX F

ASTRO-INERTIAL PLATFORM (NORTRONICS)

The astroinertial instrument consists of the stable platform assembly and a separately removable module, the astroinertial instrument electronics. Both are contained within a single, hermetically-sealed housing. Table F-1 presents the principal characteristics of the unit.

Stable platform assembly: The astronertial instrument utilizes a three-gimbal system which provides unrestricted normal operation of the vehicle, the required optical visibility for the celestial tracker, and direct azimuth readout relative to the platform reference coordinate system. In the Apollo application, a four gimbal version would be developed with an additional optical feature permitting it to track the rim of a partially illuminated body.

The azimuth gimbal, or stable element, mounts the following components:

(1) Three single-degree-of-freedom floated rate-integrating gyros

(2) One size 16 PIGA with input axis aligned in the nominal thrust direction

(3) Two size 16 pulse positioning servo accelerometers mounted with input axes orthogonal to the PIGA input axis and to each other

(4) Vidicon star tracker

(5) A two-axes horizontal leveling (bubble) accelerometer.

Table F-1 Astroinertial Instrument Characteristics

Volume	1.06 cu ft
Weight	63.5 lbs
Primary power	28 volts dc
Number of gimbals	Three
Tracker	Direct pointing Cassegrainian telescope with vidicon sensor
Window	Fused quartz
Gyros	Kearfott Model 2519 or equivalent
Accelerometers	One size 16 PIGA Two size 16 pulse positioning servo accelerometers

Leveling accelerometers	Nortronics two-axes bubble level
Temperature control	Liquid freon cooling system; individual inertial component heaters used for warm-up and precision control
Electronic packaging	Printed circuit plug-in units utilizing state-of-the-art components

The components will be mounted orthogonal to within three arc minutes. The non-orthogonality of the accelerometer triad will be determined optically and appropriate correction coefficients inserted into the digital computer so that a non-orthogonality correction can be made. The resulting uncertainty in axis alignment is seven arc seconds.

Signal preamplifiers, and other required stable element electronics will be mounted on the azimuth gimbal. Each gimbal axis contains a direct drive d-c torquer, a precision (two arc minute rms) pancake resolver (to transmit gimbal angle), and capsule slip rings.

The gimbaled assembly will be mounted within the hermetically-sealed housing and separated from the platform electronics section by a sealed bulkhead, to allow maintenance of either section of the astro-inertial instrument without disturbing the hermetic seal of the other assembly.

Table F-2 is a tabulation of the pertinent gimbal system characteristics.

Table F-2 Gimbal System Characteristics

Number	Three
Order	Azimuth, roll, pitch (inner to outer)
Degrees of freedom	No physical limitation
Pick-off	Two arc minute pancake resolver available from Kearfott or Clifton Precision Products
Torquers	On-axis d-c pancake torquer available from Inland Motors or Gianninni
Servo response	Five milliseconds equivalent first-order time constant (100 cps bandwidth)

(1) Tracker subsystem--A survey of photosensors has been completed under a WADD star tracker contract. This survey led to the conclusion that a vidicon sensor is best for the star tracker application since it is capable of a short acquisition time. Also, it eliminates a mechanical scanning mechanism, and leads to flexibility in system design. The latter means that tradeoffs can be made among frame speed, number of frames per search field, and signal-to-noise ratio in order to obtain the shortest acquisition time with high probability of acquisition.

The accuracy of the star tracker subsystem is determined principally by the accuracy of the angle pickoffs, the accuracy with which the telescope optical axis is known with respect to the pickoffs, and the accuracy with which the tracker determines the location of the star with respect to the optical axis of the telescope. By averaging the time of star signal when the beam first approaches the star image and when the beam leaves the star image the position of the star in the field of the telescope is determined. The tracker characteristics are listed in Table F-3.

Table F-3 Tracker Characteristics

Type	Vidicon, direct pointing
Tracker freedom	360° azimuth, 80° elevation
Accuracy	
(a) Vidicon readout	Three arc sec (rms)
(b) Telescope pickoff	Five arc sec (rms)
(c) Telescope boresight	Three arc sec (rms)
(d) Over-all environmental refraction	Seven arc sec (rms)
Total	10 arc sec (rms)
Search field size	120 arc min azimuth, 5 arc min elevation
Acquisition time	Five sec maximum
Acquisition probability	98 percent minimum
Telescope type	Modified Cassegrainian
Telescope pickoff	Precision multipole resolver
Theoretical minimum star brightness	3.5 magnitude in 30 foot-lambert background
Field and laboratory performance	Acquisition of 1.33 color corrected magnitude star in daylight; 4.7 magnitude at night

(2) Accelerometers--The accelerometer system employed in the astro-nertial instrument is as follows:

(a) One size 16 PIGA mounted with the input axis approximately parallel to the nominal thrust vector; the size 16 PIGA is currently being produced to MIT drawings by Minneapolis-Honeywell, Sperry and A. C. Spark Plug

(b) Two size 16 magnetic force, pulse-positioning servo accelerometers orthogonal to the PIGA axis and to each other

(c) A Nortronics two-axes leveling bubble to erect the platform, normal to the local vertical.

The size 16 pulse-positioning servo accelerometers were chosen because they provide satisfactory dynamic range and excellent accuracy at minimum cost. They are also easy to maintain.

The accelerometer characteristics are listed in Table F-4.

Table F-4 Accelerometer Characteristics

Accelerometer	Size 16 PIGA	Size 16 PPS
Readout	0.1 ft/sec	0.025 ft/sec
Range	20 g	15 g
Threshold	10^{-5} g	10^{-5} g
Linearity and scale factor	.003 percent	.005 percent
Null shift	10^{-4} g	10^{-4} g
Anisoelastic cross-coupling	5×10^{-6} g/g^2	5×10^{-6} g/g^2
Bias due to vibration rectification and cross-coupling	3×10^{-5} g/g^2	3×10^{-5} g/g^2

(3) Gyroscopes--The platform gyros chosen are Kearfott Model 2519 single-axis floated rate-integrating units. The gyros are mounted so that the output axes of all three are parallel to the trajectory plane, and the input axes form an orthogonal triad with the "X" and "Y" axes horizontal. This mounting configuration was chosen to minimize anisoelastic drift errors.

Table F-5 is a summary of the gyro characteristics.

Table F-5 Kearfott Model 2519 Gyro Characteristics

Type	Kearfott Model 2519
Fixed restraint drift	1.0 deg/hour
Nominal calibrated	0.033 deg/hour
Mass unbalance drift	1.0 deg/hour/g
Nominal calibrated	0.033 deg/hour/g
Anisoelastic drift	0.005 deg/hour/g^2
Random drift	0.02 deg/hour OAH 0.01 deg/hour OAV
Angular momentum	4 x 10^5 gm-cm^2/sec
Temperature control	Individual gyro temperature sensors and individual heaters

The stable platform has been so designed that other advanced gyros, such as the Minneapolis-Honeywell 8001 and GG-137, or Sperry SYG 1000, can be incorporated into the astro-inertial instrument at a later date with only minor modifications and no increase in size or weight. Tests on the Sperry SYG 1000 are currently in progress at Nortronics.

Gas bearing gyros are currently under development which offer longer life and can hold a calibration for a longer period of time. The most promising miniature gas bearing gyro is the Minneapolis-Honeywell GG-124. Development of the GG-124 has reached the stage where several units have been produced. Because this gyro shows considerable promise for use in later guidance system configurations, its features are listed in the following table:

Table F-6 Principal Features of the GG-124 Gyro Design

Feature	Effects
Beryllium gimbal	Material stability and stiffness
Gas spin motor bearing	Gyro motor stability, low wear
Paddle damping	Fast warmup
Gimbal suspension (pivot dithering)	Accuracy
Eutectic balance	Mass unbalance calibration
Permanent magnet torquer	Control reaction torques
Iron-free pickoff	Accuracy and control of reaction torques

(4) Precision pick-offs--Several available pick-offs can meet a five arc second accuracy; such as the multipole resolver, inductosyn, and single-cycle pancake resolver. The relative merits of each is discussed in the following paragraphs.

(a) Multipole resolver--This is an angle transducer which, from the standpoint of performance, resembles a geared-up synchro resolver. The gear ratio is obtained by a unique magnetic field configuration. Both the excitation windings and the output windings are on the stator; there are no sliding contacts. Both rotor and stator are laminated, and all the poles of the rotor and stator are involved in each cycle. Because of the averaging effects inherent in the design, the accuracy of the multipole resolver output exceeds the machining accuracy.

A standard 27-pole unit has been tested at Nortronics and has a proven repeatability within three arc seconds, an rms accuracy with proper calibration of 10 arc seconds, and peak errors of 30 arc seconds.

(b) Inductosyn--The inductosyn is another angle-sensing device which functionally resembles a geared-up synchro resolver. The rotor and stator of the inductosyn are glass plates with conductive patterns on one side. The glass plates are mounted so that the conductors are parallel, concentric and separated by about 0.005 inches. A 360-pole, three inch inductosyn is being tested at Nortronics and peak errors of ± 13 arc seconds in 360 degrees have been observed. These peak errors are expected to be reduced to less than 10 arc seconds by adjusting the concentricity of the mounts. The peak variations observed in each two-degree cycle are less than ± 2 arc seconds. These units, like the geared-up synchro resolvers they resemble, are capable of accurately determining the angular position within any cycle, but cannot indicate which cycle is being read. Therefore, a coarse angle pick-off is also required to provide nonambiguous angle readings. The coarse pick-off need only be accurate enough to determine which cycle is being used. A potentiometer type is adequate and can be designed to fit into the available space.

(c) Single-cycle pancake resolver--A somewhat different type of precision pick-off is the single-cycle pancake resolver which is shaped like an annular ring. This type of resolver does not require a coarse pick-off as in the case of the inductosyn. However, some difficulty is encountered in obtaining the angle information in digital form because the time between zero crossings of the output voltages must be resolved into very small increments. No such digitilization problem is encountered with the multipole resolver and the inductosyn.

Astro-inertial instrument electronics--Circuitry associated directly with the tracker or stable platform such as preamplifiers will be mounted within the gimbaled assembly. The following are included:

(1) Vidicon high voltage supply.

(2) Vidicon signal preamplifiers.

(3) Inertial component signal preamplifiers.

(4) Inertial component quadrature rejection circuitry.

(5) Inertial component temperature control bridge circuits and temperature compensation circuits.

(6) Torquer amplifier output stages.

(7) Gimbal transformation servo geared assembly.

All other platform and astro-inertial instrument electronics with associated power supplies will be mounted in the astro-inertial instrument electronics section (lower housing) and separated from the gimbaled assembly by a sealed bulkhead. This allows the platform electronics to be removed from the instrument assembly without disturbing the gimbaled assembly section. The electronics will be of the conventional printed circuit board type. Two circuit board assemblies will be mounted on opposite sides of a stiffening frame to form a plug-in module. This type of packaging has been selected because of its flexibility and reliability. The circuits to be packaged in the astro-inertial instrument electronics section include:

(1) Vidicon detection.

(2) Vidicon sweep generation.

(3) Telescope pointing servo.

(4) Telescope angle detection.

(5) Gyro pulsing.

(6) Accelerometer digitilization.

(7) Gimbal angle transformation servo.

(8) Temperature control amplifiers.

(9) Power supplies and frequency dividers.

[redacted]

[redacted]

APPENDIX G

ASTRO-INERTIAL PLATFORM (ARMA)

I. GENERAL REMARKS

The primary inertial platform proposed for the Apollo guidance system is based on Arma's six years of experience in managing the design, development, fabrication and field evaluation of operational and advanced inertial guidance platforms.

The principal units in Arma's inertial platform program are:

(1) The First Generation platform: in quantity production for Atlas missiles. Currently undergoing a highly successful flight test program at AMR.

(2) The Second Generation platform: developed under contract to BMD and currently undergoing sled tests at Holloman AFB.

(3) The Third Generation platform: an all-attitude unit currently under development, to be available December 1961; features inertial components developed in the Second Generation program, a simplified integral star tracker, and greatly improved packaging design.

The Third Generation platform is proposed by Arma as the astro-inertial platform for the primary Apollo guidance system.

From an equipment viewpoint, the inertial portion of Arma's Apollo Guidance System is composed of two parts: the astro-inertial platform and the digital computer. The digital computer determines the vehicle's velocity and position as a function of vehicular acceleration and also solves the vehicle's guidance problem. The astro-inertial platform is primarily designed to provide the navigation and guidance computer with vehicular acceleration data referenced to a regularized coordinate system. This is accomplished by mounting three mutually perpendicular accelerometers on a platform stabilized in inertial space by two gyros and four servo-driven base-motion-isolation gimbals. The second function of the inertial platform is to provide the guidance computer and/or the vehicle control system with vehicular attitude information. This is accomplished by noting the angles that the various isolation gimbals of the platform make with the vehicle and with each other. In some cases these gimbal angles are used directly, while in other cases they are transformed by the digital computer as a function of vehicular position into vehicular attitude with respect to a local spherical coordinate system.

The astro-inertial platform has been designed with the following features:

(1) Vibrating-String-Accelerometers: the astro-inertial platform utilizes three Arma miniature vibrating-string-accelerometers to measure the rectangular components of vehicular acceleration.

(2) Two-Degree-of-Freedom Gyros: the astro-inertial platform will utilize two Arma miniature two-degree-of-freedom gyros to stabilize the accelerometers in inertial space.

(3) Stellar Alignment Nulling Device (SAND): the astro-inertial platform will utilize one stellar alignment nulling device to align the astro-inertial platform when the Apollo vehicle is in space. This device is a simplified version of the SPI (Star Position Indicator) currently being incorporated in Arma's Third Generation platform.

(4) Inertially Fixed Coordinate System: the inertial navigation system will utilize a rectangular inertially-fixed coordinate system throughout. Therefore, the accelerometers and gyros will maintain a fixed angular orientation in inertial space. This coordinate system was chosen because it provides for the simplest and most accurate solution of the vehicle's equations of motion and, since the gyros do not have to be torqued, the requirements for a precision power supply and gyro torquing amplifiers are eliminated.

(5) Equatorial Azimuth Gimbal Bearing: the azimuth gimbal of the stable platform will be supported by a single equatorial bearing. This design feature has been tested on the Arma second generation platform. It is being used because it provides space savings, rigidity, and maximum accessibility to the major components for ease of assembly, test and maintenance. Its use is particularly desirable on an astro-inertial platform since it provides the stellar alignment nulling device with the maximum possible unrestricted viewing angle.

(6) All-Attitude Astro-Inertial Platform: the astro-inertial platform will utilize a four gimbal, all-attitude base-motion-isolation system. This will allow the Apollo vehicle complete maneuvering freedom.

(7) Computational Component Trimming: the inertial navigation system will utilize computational instead of mechanical methods to trim the inertial components. This will reduce the complexity of ground support and airborne equipment. It will also provide maximum system accuracy and flexibility.

II. DESCRIPTION AND FUNCTIONAL OPERATION OF ASTRO-INERTIAL PLATFORM

The astro-inertial platform can best be discussed by considering separately its main parts. The following sections will describe separately the G-8 two-degree-of-freedom gyro, the D4 vibrating-string-accelerometer, the stellar alignment nulling device and the four gimbal all-attitude stable platform that are proposed for use on the Apollo Program.

A. GYROS

1. General

The G-8 gyro is an advanced miniature two-degree-of-freedom floated gyro and is a design refinement of an Arma gyro currently in production for operational ICBM guidance systems. The G-8 gyro has been under development since mid-1957, and it has been extensively evaluated for over one and one-half years with tests including vibration and long term stability of drift parameters. The G-8 gyro is the latest model in a family of two-degree-of-freedom floated gyroscopes dating back over a decade. This family of gyroscopes has demonstrated accuracy and reliability under severe environmental conditions including:

(1) Atlas ICBM - Seven completely successful flights to date without any malfunctions. Gyro performance was well within required accuracy. (All Arma equipment has operated correctly on all 13 Atlas flights to date--including six flights that were terminated for a variety of reasons.)

(2) Rocket sled (1958) - Six Arma gyros were fired down the sled track at NOTS, China Lake, California, for 12 or more runs each, without any malfunction. (The G-8 gyros are now being sled tested at Holloman AFB.)

(3) Army vehicles and Naval vessels - Arma north-seeking gyrocompasses have demonstrated suitability in tanks, track vehicles, jeeps, Arctic snow vehicles (80° latitude Greenland) and naval vessels over the last 10 years.

Twelve G-8 gyros have been fully evaluated. Their outstanding performance characteristics include stability of non-acceleration sensitive drifts of less than 0.01°/hr for periods of one week, and 0.1°/hr for a one year period, including effects of vibration and shutdowns.

The G-8 gyro operates reliably in the ICBM environment (up to 30 g's) because of special design features, e. g., the gimbal construction, the proven flotation suspension system, and the precision bearing preload. The center of mass shift is minimized because of the simple symmetrical construction of the gyro.

2. Description of the G-8 Gyro

As shown in Figs. G-1, -2, -3, the gyro includes two floated gimbals. The inner gimbal is a hermetically sealed beryllium sphere which contains the spinning wheel supported on precision ball bearings. The outer gimbal is a beryllium ring surrounding, but not touching, the inner gimbal. Two degrees of freedom are supplied by thin elastic centering filaments. One set of filaments connects the floated sphere with the gimbal ring. A second set connects the gimbal ring with the outer housing. The centering filaments provide two axes of rotation, orthogonal to each other and the spin axis. Pickoffs detect rotation of the gyro housing relative to the inner gimbal and torquers precess the gyro about each of the two stabilization axes during tests and initial system alignment.

The gyro has the following design features:

Size	3-1/2 inch diameter (0.013 cu. ft.)
Weight	2. 3 pounds
Suspension	Wire centered, no pivot friction, high shock capability of fluid suspension.
Pickoffs	Negligible magnetic reaction torque, no iron on secondary coils.
Torquers	Negligible hysteresis due to no secondary iron. Linear due to long air path in magnetic circuit.
Beryllium Float	A 2-1/2 inch sphere supported in a static fluorolube flotation system. Preloaded isoelastic bearing pair. Outer race rotation of 12,000 rpm. Bearing shaft is a strut which ties the float halves together. Magnet housing serve as shaft nuts.
Power Leads	None required. Centering filaments conduct power to float.
Configuration	Two-degree-of-freedom results in minimum of forced precession due to angular inputs and allows low levels of viscous coupling from housing to float.
Producibility	Simple construction with large fluid gaps. Centering filament subassembly permits rapid "plug-in" assembly without adjustment. Number of parts sizeably reduced from earlier Arma gyros.

Long Life	15,000 hours minimum (based on G-8 bearing life test units - no failures to date).
Reliability	Few parts, reliability has been demonstrated during ten years of development and production of this type of gyro.

Figures G-2 and G-3 illustrate the design features of the G-8 Gyro.

3. Gyro Performance

The significant performance parameters of the G-8 gyro, as applied to the Apollo Program, are:

	For 2 Days	For 30 days
Non-acceleration sensitive drift rate	0.001°/hr	0.02°/hr
Drift rates due to mass unbalance of:		
inner gimbal along spin axis	0.02°/hr/g	0.15°/hr/g
inner gimbal along outer wire axis	0.01°/hr/g	0.05°/hr/g
inner gimbal plus outer gimbal along inner wire	0.01°/hr/g	0.05°/hr/g
outer gimbal along spin axis	0.01°/hr/g	0.01°/hr/g
Drift rate due to:		
Unequal compliance along spin axis and radial axis	0.05°/hr/g^2	0.05°/hr/g^2
Drift rate due to non-neutral buoyancy are:		
displacement of inner suspension wires along spin axis	0.04°/hr/g/°C	0.04°/hr/g/°C
displacement of inner suspension wires along outer wire axis	0.06°/hr/g°C	0.06°/hr/g/°C
displacement of outer suspension wires along spin axis	0.1°/hr/g/°C	0.1°/hr/g/°C
displacement of outer suspension wires along inner wire axis	0.1°/hr/g/°C	0.1°/hr/g/°C
Gyro angular displacement due to non-orthogonality of suspension wires with respect to spin axis and % change in power supply frequency	0.001°/%	0.001°/%

[redacted]

The above 48 hour performance is based on calibration without shutdown prior to launch of the non-acceleration sensitive drift and the mass unbalance drift parameters. The 30-day performance assumes intervening shutdowns. No calibration is required for the compliance effects, buoyancy unbalance, and non-orthogonality parameters.

The above gyro performance data is a conservative extrapolation, based upon Arma's continuing G-8 gyro development program, of the presently available experimental data. The validity of this extrapolation can be demonstrated by noting that the actual Atlas flight tests have yielded an average impact error on all flights to date, of less than one quarter of the original contractual requirement.

4. Gyro Summary

The G-8 gyro meets all the reliability, performance, environmental and schedule requirements of the Apollo Program. Prototypes have been fabricated and tested and clearly indicate a high level of performance. The gyro is an Arma designed and manufactured unit. This permits optimum integration of this important system component into the platform and system. The production test equipment required for the efficient manufacture of this component is very similar to existing items and in most cases presently available equipment can be utilized with only minor modifications.

B. ACCELEROMETER

1. General

The D4 miniature vibrating-string-accelerometer is a design refinement of an Arma accelerometer that has been outstandingly successful in the guidance of 7 Atlas ICBM test flights. It represents the knowledge and experience that has been gained during five years of design, development and production of over 500 vibrating-string-accelerometers. Among the many refinements that have been incorporated into the miniature accelerometer are: a major reduction in size, a three-to-one reduction in non-linearity, and a significant reduction in sensitivity to both transient and steady state temperature changes. The miniature vibrating-string-accelerometer has been develcped for over two years and its improvements have been verified on over ten units.

2. Description of Accelerometer System

Three single-axis accelerometers are rigidly mounted, orthogonally to each other, on the azimuth gimbal of the stable platform via a mounting fixture so as to measure the three rectangular components of its vehicle's thrust acceleration. They are mounted on the accelerometer mounting fixture via ceramic insulators that are ground and polished to obtain the correct alignment. The individual

~~CONFIDENTIAL~~

accelerometers may be easily replaced inasmuch as the accelerometer mounting feet define a surface that is perpendicular to the sensitive axis within two seconds of arc and the fixture mounting surfaces are perpendicular to each other to within two seconds of arc. The assembly will then be coated with foamed plastic in order to reduce the effects of temperature transients and acoustic noise. This entire structure will be assembled as a separate unit so as to achieve the ultimate in stability and accuracy of alignment of the critical components. It will then be rigidly attached to the azimuth gimbal of the stable platform. The arrangement of the accelerometers on the mounting fixture can be seen in Fig. G-4.

A high density oscillator-amplifier package is utilized to drive the vibrating strings of the accelerometers. This package contains six oscillator-amplifiers and a power supply and is also mounted on the platform's azimuth gimbal.

3. Description of D4 Accelerometer Sensing Unit

The accelerometer system is made up of three Arma D4 vibrating-string-accelerometers. The D4 accelerometer, which is shown in Fig. G-5 is approximately 1-1/4 inch in diameter and 2-3/8 inches long and weighs approximately 5.7 ounces.

Each accelerometer of the accelerometer system is designed to accurately measure the component of acceleration that lies along a precisely determined line called the sensitive axis. This is accomplished by measuring the reaction to the acceleration force acting on a constrained weight (proof mass). The proof mass is supported within the accelerometer by longitudinal strings and transverse cross supports.

The cross supports prevent motion on the proof mass in a plane perpendicular to the sensitive axis. The component of acceleration force along the sensitive axis changes the tension of the longitudinal vibrating strings; one string increasing in tension and the other decreasing. These changes in tension are measured by noting the changes in the resonant frequencies of the vibrating strings.

The strings are vibrated at their resonant frequency by placing them in permanent magnet fields and passing alternating current through them. This current is supplied at the string resonant frequency by a small transistorized oscillator-amplifier. The magnitude of the current is controlled so as to maintain a constant string driving force.

An analysis of the dynamics of the vibrating strings in their respective magnetic fields reveals properties that are analogous to those of a parallel-resonant electrical circuit. This feature permits the design of a controlled feedback oscillator-amplifier which maintains a constant current drive at the natural frequency. The strings and their associated frame are designed to make the vibrating string very sharply resonant. The electromechanical figure of merit (Q) is 2,500. The amplifier phase shift is accurately controlled over wide frequency and temperature ranges by self-contained negative feedback. The equation for string frequency (f) as a function of tension (T) for an ideal string is given by:

$$f = K\sqrt{T} \qquad (1)$$

To reduce non-linearities and to avoid compression in the strings, the two strings are maintained under an initial tension (T_0) which is large compared to the acceleration force. If the initial tension in each string is identical and their frequency vs. tension characteristics are matched then:

$$f_1 - f_2 \approx K_1 a + K_3 a^3 \qquad (2)$$

where

$f_1 - f_2$ = difference between the two string frequencies

K_1 = scale factor

K_3 = third order coefficient

a = acceleration in g's

Figure G-6 shows the actual accelerometer construction schematically. The proof mass is divided into two proof masses of equal weight (M) that are connected by a relatively soft center spring. This reduces the variation of the preset tension T_0 as a result of differential expansion or creep in the accelerometer structure and has the added advantages of greatly reducing vibration coupling between the two strings, permitting steady state scale factor temperature control by controlling the spring stiffness, and permitting individual string scale factor control. With a single mass the string tension changes would be equal only if the axial stiffness of the strings were precisely equal.

In effect, the accelerometer becomes two single-string accelerometers mounted back to back and connected by the soft center spring to maintain constant and equal initial tensions in the strings. Each string mass system is essentially independent of the other permitting individual trimming of scale factors to reduce inaccuracies resulting from mismatch of the strings. The decoupling between the two strings is enhanced by employing flattened cross-sectional strings (tapes) which vibrate in perpendicular planes. To minimize the effects of temperature on accuracy the internal sensitive structure is thermally insulated from the outer shell and mounting feet. This thermal isolation has also made possible true hermetic sealing (solder seals) of the outer shell.

4. Description of Accelerometer Electronics

The electronics portion of the accelerometer system consists of six identical oscillator-amplifiers and a power supply. The accelerometer electronics are all-transistorized, utilize high density packaging techniques and are mounted on the azimuth gimbal of the stable platform.

All the components and subassemblies used in this electronics group are existing items under the present Arma ICBM guidance program.

Each accelerometer sensing string is connected to an oscillator-amplifier circuit so as to form a variable frequency oscillator whose frequency is controlled by the resonant characteristics of the vibrating string. The string, in its magnetic field, behaves as a high "Q" electrical resonator and oscillator action is very similar to a quartz crystal resonator.

Each oscillator-amplifier is made up of three functional sections.

(1) An oscillator gain section using a direct coupled feedback amplifier which supplies the energy to maintain the sensing string vibrating at its resonant frequency.

(2) A regulator section which maintains a constant current driving force to the sensing string and consists of: a diode limiter network, an output current limiting resistor and a temperature correction thermistor network.

(3) An output amplifier consisting of a one transistor gain stage driving an output transformer. This section raises the string frequency signal to a moderate power level for external use while isolating the oscillator loop from external loads.

The electronics package power supply utilizes single phase, 115v, 400 cps power which is converted into the various dc voltages required. All critical dc voltages are zener diode regulated to permit a variation of ±10% in the input ac power.

5. Accelerometer Output Equations

The simplified string equation ($f = K \sqrt{T}$), given in equation 1, is correct only for an ideal string. Since the real strings have finite stiffness, the frequencies computed using this equation do not agree with measured data. Analysis, verified by measurement, has shown that the following formula describes the relationship between frequency and tensions for the real string to an accuracy within the limits of present measurement techniques.

$$f = A\sqrt{T+h} + K \qquad (3)$$

where

	Nominal Value	Units
$A = 1/2\sqrt{Lm}$	9737	$sec^{-1}\ lb^{-1/2}$
$h = 2.47 EI/L^2$	.0399	lbs
$K = 1/L\sqrt{EI/Lm}$	740	cps
L = length of vibrating string	.375	inches
m = mass of vibrating string	$.00723 \times 10^{-6}$	$lb\ sec^2\ in^{-1}$
E = Young's Modulus (BeCu)	19×10^6	$lb\ in^{-2}$
I = moment of inertia of string cross sectional area	2.63×10^{-11}	in^4
T = tension in string	(variable)	lb

In a complete accelerometer the two string tensions T_1 and T_2 are given by:

$$T_1 = T_o + M_1 a, \quad T_2 = T_o - M_2 a \qquad (4)$$

where

T_o = initial tension (0.75 lb)

M_1, M_2 = weight of each proof mass (0.0063 lb)

a = acceleration in g

Letting subscripts denote string number and letting

$P = T_o + h$ formula (3) becomes

$$f_1 = A_1 (P_1 + M_1 a)^{\frac{1}{2}} + K_1 \qquad (5)$$

and

$$f_2 = A_2 (P_2 - M_2 a)^{\frac{1}{2}} + K_2 \qquad (6)$$

The two above equations may then be expanded and combined to provide the following relationship:

$$\begin{aligned} f_1 - f_2 = {} & (K_1 - K_2 + A_1\sqrt{P_1} - A_2\sqrt{P_2}) + \qquad (7) \\ & a(A_1 M_1/2\sqrt{P_1} + A_2 M_2/2\sqrt{P_2}) \\ & + a^2(A_2 M_2^2/8P_2\sqrt{P_2} - A_1 M_1^2/8P_1\sqrt{P_1}) \\ & + a^3(A_1 M_1^3/16P_1^2\sqrt{P_1} + A_2 M_2^3/16P_2^2\sqrt{P_2}) \end{aligned}$$

NOTE: All terms of higher than third order have negligible value and have been eliminated.

Nominal values of the above terms, for the D4 accelerometer, are as follows:

K = 740 cps

A P = 8650 cps

$AM/2$ P = 32.16 cps/g (local value of g-ft/sec^2)

$AM^2/8P$ P = 0.69 cps/g^2

$AM^3/16P^2$ P = .00027 cps/g^3

With matched strings, masses, and initial tensions this reduces to:

$$f_1 - f_2 = a(AM/\sqrt{P}) + a^3(AM^3/8P^2\sqrt{P}) \qquad (8)$$

or

[redacted]

$$a = \frac{f_1 - f_2}{AM\sqrt{P}\,(1 + a^2M^2/8P^2)} \qquad (\;)$$

where $a^2M^2/8P^2$ is small compared to one and is corrected for in the computer.

The fixed term $(K_1 - K_2 + A_1\sqrt{P_1} - A_2\sqrt{P_2})$ is generally made equal to 1 cps to avoid the small string vibration coupling which occurs when the two string frequencies are nearly equal.

6. Accelerometer Performance

The D4 accelerometer is designed to operate accurately in the presence of input accelerations within the range of ±20 g's. It is highly insensitive to cross accelerations and has exceptional long term stability. The longitudinal frequency response of the D4 accelerometer to input accelerations is approximately 1400 cps. Its acceleration resolution is well below 10^{-6}g and is only limited by noise in the readout system.

Since the Apollo computer will take into account changes in accelerometer scale and zero based on pre-launch measurements, string creep presents no limitation on accelerometer storage life prior to use. The instrument contains no moving parts other than the sensing strings which vibrate at a minute amplitude. Total internal power dissipation is approximately 0.5 microwatts which generates no thermal stresses internally. The above factors combined with the reliability of the simple all transistor electronic circuitry insures extremely long accelerometer life. The mean time between failures of a sensing unit and its electronics is expected to be at least 40,000 hours. This estimate is based on the extremely reliable performance of the present Atlas ICBM units which have had no mechanical failures to date.

The one sigma scale factor drift at the operating temperature of 32°C is less than 0.1×10^{-6} g/g for a 24-hour period. Similarly the one sigma zero drift will be less than 0.7×10^{-6} g. The steady state temperature will have a one sigma variation of less than 0.15°C. This will induce an accelerometer scale change of 1×10^{-6} g/g. Since the thermal mismatch between the strings will be less than 1%, the above temperature change will induce an accelerometer zero shift of less than 3×10^{-6} g.

The accelerometer has no anisoelastic constant in the usual sense. However, the accelerometer does have a precisely definable second and third order nonlinearity with respect to input acceleration. The third order nonlinearity

[redacted]

(K_3) is nominally 9 x 10^{-6}g/g^3 and will be known within 0.3 x 10^{-6}g/g^3 while the second order nonlinearity term will have nominal value of 5 x 10^{-6}g/g^2 and will be known within 3 x 10^{-6}g/g^2.

The sensing units have an rms cross acceleration scale factor change of less than 10^{-5}g/g per cross g. Only the uncertainty in the cross acceleration scale factor change introduces errors since the digital computer will trim for the nominal value. This sensitivity is measured to better than 10^{-6}g/g/cross g for each individual accelerometer. The sensing units have an rms cross acceleration zero error of less than 6 x 10^{-6}g per cross g.

Vibrational accelerations cause an acceleration error as a result of the rectification caused by higher order terms in the accelerometer's equation (7). However, it is anticipated that the platform's vibration isolation system, in conjunction with the internal mass dampers, will reduce the vibrations seen by the accelerometers to such a level as to cause negligible rectification errors.

Therefore, the significant performance parameters of the D4 vibrating-string-accelerometer, as it will be utilized on the Apollo Program, are:

Zero determination uncertainity	3 x 10^{-6}g
Zero drift	0.7 x 10^{-6}g (1 day)
Temperature sensitive zero shift	3 x 10^{-6}g (for ±0.15°C)
Cross acceleration zero shift	6 x 10^{-6}g/cr-g
Power Supply frequency zero shift	3 x 10^{-6}g (for 1%)
Scale determination uncertainty	6 x 10^{-6}g/g
Scale drift	0.1 x 10^{-6}g/g (1 day)
Scale drift	3 x 10^{-6}g/g (30 days)
Temperature sensitive scale shift	1.0 x 10^{-6}g/g (for ±0.15°C)
Cross acceleration scale uncertainty	1 x 10^{-6}g/g/cr-g
Second order uncertainty	3 x 10^{-6}g/g^2
Third order uncertainty	3 x 10^{-6} g/g^3

[redacted]

The Apollo operational conditions for the above performance include:

1. (1) Operating temperature of 32°C.
2. (2) Calibration of accelerometer scale and zero within 24 hours of orbital injection.
3. (3) Calibration of accelerometer zero before atmospheric re-entry.
4. (4) Accurate determination of higher order effects at the factory.
5. (5) Computational trimming of the accelerometer within the airborne digital computer.

The above accelerometer performance data is based upon a conservative extrapolation of the presently available experimental data shown in D4 Vibrating String Accelerometer Performance Summary (Fig. G-13). The validity of this extrapolation can be demonstrated by noting that the Air Force has decided to retrofit the Arma Vibrating String Accelerometer into the inertial guidance system of an advanced ICBM having accuracy requirements more stringent than Atlas. Further confidence in the attainment of the specified Apollo performance can be gained from the fact that the Air Force is contractually supporting the continuing refinement of the Arma D4 Vibrating String Accelerometer.

7. Summary

The D4 acclerometer can meet all the requirements of the Apollo Program. Detailed designs are available and the major program effort will be fabrication and integration of the units. The accelerometer is designed and fabricated by Arma, hence, early and efficient integration of this key component into the platform can be accomplished. The production test equipment required for efficient manufacture of this component is very similar to existing items and in many cases presently available equipment can be utilized with only minor modifications.

C. STELLAR ALIGNMENT NULLING DEVICE

1. General

Arma is currently developing an astro-inertial platform of which the first model will be available by December 1961. This platform incorporates a Stellar Position Indicator (SPI) which is being developed jointly by Arma and Perkin-Elmer. The Stellar Alignment Nulling Device (SAND) proposed for Apollo is a simplified version of the SPI. The SAND and SPI units are completely interchangeable on the Arma astro-inertial platform. The simplicity of the SAND as compared with the SPI arises because the SAND is simply a stellar nulling device, whereas the SPI requires a highly accurate linear readout of star positions off the optical axis as well.

The astro-inertial platform can be aligned on the ground, prior to flight, by means of pendulums and an optical line. It can also be aligned during flight, whenever the vehicle is above the sensible atmosphere, by means of a Stellar Alignment Nulling Device. It has been determined that the airborne alignment can be efficiently accomplished using only stars of second magnitude or brighter that are angularly separated by at least 5° from stars brighter than 4th magnitude. This coupled with the fact that background atmospheric radiation problem will be eliminated by the high operating altitude, allows the use of a rather conventional nulling type telescope for the airborne alignment. More important, it allows the use of a reasonable telescopic field of view (±1/4°). This moderate field of view allows the required stars to be acquired manually without the use of complicated computer correlation techniques.

The airborne alignment of the astro-inertial platform is accomplished by controlling the angular orientation of the stable platform with respect to the orientation of two predetermined stars. In particular, the platform's Z axis is directed towards one predetermined star (Star #1) and the Y axis is directed such that a second predetermined star (Star #2) is contained in the Y-Z plane. These two conditions, and right ascension and declination data for the two stars, are sufficient to completely define the orientation of the astro-inertial platform. This airborne alignment is accomplished through the use of a manually operated "off-mount" telescope and an on-mount automatic Stellar Alignment Nulling Device (SAND).

This section will discuss only the design of the Stellar Alignment Nulling Device.

2. Description of Stellar Alignment Nulling Device Telescope

From a mechanical viewpoint, the Stellar Alignment Nulling Device consists of an automatic nulling telescope and a gimballing system. This section will discuss the design and operation of the automatic nulling telescope.

The telescope is a solid Cassegrain with 13.75 inches focal length, f/6.1 relative aperture and a 1/2° field of view. This telescope is folded so as to deviate the optical axis through an angle of 90°. This deviation is accomplished by a plane surface where light rays are twice reflected; however, this is a total internal reflection and no energy losses are involved. The solid telescope design provides a highly stable optical system under severe environmental conditions. Telescopes of this type are manufactured at present by the Perkin-Elmer Corporation.

The arrangement of the optical, electronic and electromechanical components is shown in Fig. G-7. The telescope, rotating prism, stationary reticle and phototube with pre-amplifier are mounted together and can be rotated about a horizontal axis. The whole package is contained in a 6-inch diameter sphere.

The star image on the stationary reticle is nutated by means of a double-isosceles prism in place of the more conventional optical wedge. While the mass of the former is larger than the latter, there are two definite advantages. The first is that the reticle can be placed closer to the optical system. The second advantage is that the air-to-glass surfaces are normal to the optical axis and the prism is equivalent to a plane-parallel piece of glass where all the aberrations can be corrected. The deviating prism or optical wedge is afflicted with coma that deteriorates the image and cannot possible be corrected when placed in a converging beam of light.

The light falling on the stationary reticle is spread over the photocathode of the 1P21 tube by means of a field lens. The photomultiplier is shielded and a pre-amplifier is built within the shield. A 1P21 photomultiplier will be used as a sensing detector because of its high sensitivity and peak spectral response characteristics in the 5000°A region. An FM/PM modulation technique is accomplished through the use of a rotating prism and stationary spoke reticle. A carrier frequency in the region of 400 to 1000 cps is adequate for the information requirements of this system. The block diagram of the system is shown in Fig. G-8. The system incorporates a pre-amplifier-limiter followed by pre-detection filtering and discriminator demodulation. Resolution of the dual coordinate error signals are achieved in a phase demodulator, using a reference signal generated by a magnetic pick off integral with the rotating prism. The phase demodulator output has the form of a d-c off-set in each of the two channels, proportional to the angular deviation of the star image from field center as resolved by the demodulators. Low pass filter networks for smoothing as well as rate or derivative action are employed in the signal channels to the gyros.

3. Description of Stellar Alignment Nulling Device Gimballing

The telescope of the Stellar Alignment Nulling Device is physically attached to the azimuth gimbal of the astro-inertial platform with a single degree of rotational freedom, as shown in Fig. G-11. This rotational freedom allows the telescope and its optical axis to rotate about a precisely defined axis that is parallel to the platform's X axis. The telescope is actually rotated, with respect to the stable platform, by dual push-pull servomotors and its angular orientation is measured by a single speed resolver. In addition to the single speed resolver, an angular null detector is used to accurately align the telescope's optical axis with the platform's Z axis. This angular null detector is of the same design as the angular pick-offs used in the Arma gyros and will allow alignment of the telescope to the Z axis with an rms error of less than two seconds of arc.

4. Functional Operation of the Stellar Alignment Nulling Device

The airborne alignment of the astro-inertial platform is accomplished by orienting the stable platform so that its Z axis points towards a predetermined star (Star #1) and so that its Y-Z plane contains a second predetermined star (Star #2). However, the functional operation of the Stellar Alignment Nulling Device will be discussed below.

The platform's Z axis is directed towards Star #1 in the following manner:

(1) The optical axis of the telescope is aligned with the Z axis of the platform. This is accomplished by servoing the telescope in elevation so as to null the output of the angular null detector.

(2) The platform is oriented so that Star #1 appears in the field of view of the telescope. This is accomplished by servoing the platform's roll and pitch gimbals to the angular data generated by the manually operated "off-mount" telescope.

(3) The platform is oriented to null the output of the Stellar Alignment Nulling Device. This is accomplished by torquing the platform stabilization gyros to drive the platform roll and pitch gimbals in accordance with the output signals of the SAND. When these signals have been nulled, they are decoupled, and the platform is gyro stabilized about the roll and pitch axes, with the Z-axis pointed accurately at Star #2. The platform's Y axis is directed so that the platform's Y-Z plane contains Star #2. This is accomplished in the following manner.

(4) The platform is rotated in azimuth so that the Y-Z plane is within 1/4° of Star #2. This is accomplished by servoing the platform's azimuth to the angular data generated by the manually operated "off-mount" telescope.

(5) The SAND is rotated in elevation until Star #2 appears in its field of view. This is also accomplished by servoing in accordance with the angular data generated by the "off-mount" telescope.

(6) The SAND telescope is rotated so as to eliminate the vertical component of the error between the optical axis and Star #2. This is accomplished by driving the telescope elevation servo so as to null the vertical component of the SAND's error signal.

(7) The platform is rotated in azimuth so as to eliminate the horizontal component of the error between the optical axis and Star #2. This is accomplished by precessing the stabilization gyros in azimuth so as to null the horizontal components of the SAND error signal. When this signal has been nulled, it is decoupled and the platform is completely gyro-stabilized and properly aligned.

5. Performance of the Stellar Alignment Nulling Device

It is intended that the Stellar Alignment Nulling Device will be used operationally under free fall flight conditions at altitudes in excess of 400,000 ft. Therefore, its accuracy will not be decreased by acceleration, vibration or background radiation. Under these conditions the null or optical axis of the Stellar Alignment Nulling Device will be within 6 seconds of arc (rms) of a previously defined boresight line. In addition, the accuracy of the telescope mechanical gimballing and the angular null detector will allow the telescope boresight line to be aligned within 2 seconds of arc (rms) with the platform's Z axis. For use in the Star #2 mode, the deviation of the boresight line from the Y-Z plane will be calibrated as a function of the elevation angle to within 2 seconds of arc (rms).

For the purposes of this study it has been assumed that the RMS line-of-sight shift due to the vehicle viewing window can be limited to less than 3 seconds of arc.

Therefore, it is concluded that the astro-inertial platform can be aligned inflight--under the conditions stated--to within 7.6 seconds of arc (rms) about each axis. It should be stressed that the SAND unit is used only for aligning the platform in inertial space, and is completely unrelated to the midcourse navigation of the vehicle by optical sighting techniques. Midcourse navigation optical data is taken with equipment which is not mounted on the platform. On a typical re-entry trajectory on which the platform is aligned using SAND prior to re-entry, the errors in platform alignment (7.6 seconds rms) result in the accelerometers being slightly misaligned, and this in turn results in the following navigational errors at the landing site:

Down Range:	0.40 naut mi
Cross Range:	0.04 naut mi

6. Stellar Alignment Nulling Device Summary

The Stellar Alignment Nulling Device discussed herein represents a simple and effective solution to the Apollo inflight alignment problem. It utilizes the man to solve the star acquisition problem and it utilizes nulling techniques to eliminate the accurate angular data pick-off problem that is usually associated with astro-inertial platforms. The device utilizes well established techniques and equipment and represents a simplification of an existing company development program.

D. STABLE PLATFORM

1. General

The stable platform is a four-gimbal configuration providing all-attitude inertial stabilization of the acceleration sensing system. It is an integrated assembly of: the gimballed inertial components, all inertail component electronics, the Stellar Alignment Nulling Device, modes control electronics, and the vibration isolation system. The platform reflects refined design concepts evolved from the Arma ICBM platform currently in production and successfully flight tested in Atlas, and from the Arma lightweight ICBM platform now undergoing a rocket sled test program at Holloman AFB.

The stable platform is approximately 15 inches in diameter and 16.4 inches long, and weighs approximately 48 lbs. The general outline of the Apollo platform is shown in Figs. G-9, -10.

2. Functional Operation of Stable Platform

In order to be compatible with the proposed inertial navigation equations, the sensitive axes of the system's three accelerometers are maintained collinear with the axes of a rectangular coordinate system that has a known, fixed orientation in inertial space. This is accomplished by rigidly mounting the three accelerometers orthogonally on the azimuth gimbal of the stable platform. The azimuth gimbal is then stabilized in inertial space by two two-degree-of-freedom gyros and four servo-driven isolation gimbals. The functional operation of this isolation system can be described by referring to Fig. G-10.

The velocity and acceleration lags are readily limited to negligible values by designing for high servo gain and high torque-to-inertia ratio respectively. Also, the integrated effect of the dynamic servo errors during the flight will be negligible.

Extensive investigations of average servo errors have been conducted by Arma during the 107A Program. It has been determined that, with the exception of the random servo errors at the time of inertial-reference axis alignment, all causes of the average error are adequately minimized by careful design of the mechanical structure and electrical circuitry of the servos. The method that is utilized to eliminate the random servo error at the time of inertial-reference axis alignment is named the "zero lag" method.

Essentially the "zero lag" circuitry adds the scaled gyro pick-off voltage to the output of the alignment transducer. This not only eliminates the effects of the random servo error that existed at the instant of inertial-reference axis alignment, but it also removes the characteristics of the gimbal servo from the alignment loop. Physically the "zero lag" system consists of a small, proportional amplifier in the ground support equipment.

a. Vibration isolation

A compact, rubber composition vibration mount isolates the platform from vehicle translational and rotational high frequency vibration in order to optimize accelerometer performance and assist in stabilization of the platform. Arma' s approach to isolator design, as reflected in production and developmental platforms, incorporates tunable masses in the elastic elements. The natural frequency of such systems is in the 20 to 22 cps range. The transmissibility is altered at 200 cps by means of the tunable mass to provide attenuation of 0.0001 at frequencies from 1000 to 1400 cps.

b. Gimbal angle readouts

Incremental digital pick-offs are employed to measure the rotation of each of the platform's isolation gimbals. This angular data is utilized during the system's automatic ground calibration and alignment procedures. It is also used during flight to provide the guidance system with vehicular attitude information. Work on the Arma advanced platform has resulted in the availability of a fully developed component (similar to the optisyn) measuring 1-3/8" and weighing 1.6 oz. Resolution is 1024 counts per revolution or approximately twenty (20) minutes of arc without benefit of count multiplication by computer logic or gearing. Resolution of five (5) minutes of arc will be accomplished by precision gearing between the pick-offs and gimbals.

c. Gimbal resolvers

The resolvers used on the platform are the miniature size 8 type measuring 3/4" in diameter and 1-1/4" long. The accuracy of the units is within 5 minutes.

Two resolvers are used on the platform's azimuth gimbal. One resolver is used on each of the other axes. One azimuth unit is used to transform the gyro pick-off signals for proper transmission to the inner roll and pitch gimbal servos. The inner roll unit is used to drive the outer roll gimbal servo so as to maintain the pitch gimbal in the plane of the inner roll gimbal and thus prevent gimbal lock. The pitch and outer roll units are used to transform vehicular attitude control information from the inertial navigation coordinate system into the required airframe control coordinate system. The second azimuth resolver and the outer roll and pitch gimbal resolvers are also used to slave the optical axis of the Stellar Alignment Nulling Device to the line-of-sight of the off-mount telescope during the star acquisition procedures.

d. Gimbal slip rings

Precision slip rings are used on the azimuth, pitch and outer roll axes to transmit electrical signals. Since the inner roll has a limited motion of ±45 degrees, a cable flex is used on this axis. The azimuth axis uses a single 70 ring unit mounted at the top of the azimuth gimbal. It is 5/8" in diameter and is 2-3/4" long. The pitch and outer roll axes each use two 32 ring units, one mounted at each end of the gimbal. These units are 3/8" in diameter and are 1-1/2" long.

These units are the minature cartridge type with self-contained bearings. Friction torque is below 1 oz. in. Continuity is assured by using double brushes on each ring.

The most important electrical characteristic of the slip ring assembly is the noise generated by the rubbing action between the ring and the brushes. Proper selection of the materials, surface finish, brush pressure and configuration maintains the noise level below 5 microvolts rms per ma. of current. This level does not interfere with the proper operation of the critical platform elements, namely, the gyros, accelerometers and pendulums.

The azimuth gimbal is made of a dimensionally stable aluminum alloy which insures long term mechanical relationships to better than 0.4 seconds of arc per 'g' load. The azimuth gimbal mounts at its equatorial plane to the inner race of a large bearing, whose outer race is integral with the inner roll gimbal. The inner roll gimbal rigidity is therefore comparable to that of the azimuth gimbal since the four point contact preloaded azimuth bearing provides a low friction rigid link. The pitch and outer roll gimbals are of hollow welded sheet aluminum construction to provide maximum rigidity and space for mounting electronic assemblies.

Analytical design techniques have been evolved by Arma which assure that the dynamic response of the complex mass spring gimballing system will result in very low energy levels being transmitted to components from vibration acoustic energy inputs.

The housing which supports the gimballing system, the electronics unit, the optical viewing window, and the vibration isolation system is designed primarily to insure that the pressure seal of the platform is maintained and that its heat transfer characteristics are compatible with the requirements of the thermal control system.

e. Gimbal servos

The gimbal servos are required to position the four isolation gimbals of the inertial platform in such a manner as to stabilize the azimuth gimbal in inertial space. This is accomplished by slaving each servo to appropriate angular pick-off. The gimbal servos utilize two-phase 400-cycle induction type motors specially made for high performance and high temperature operation. Two motors are used on each axis mounted in a push-pull geared type arrangement. Since the azimuth axis employs an equatorial bearing, with its slightly higher friction, size 11 motors are used on this axis. The other axes use size 8 motors. The size 11 motor has a no load speed of 6,000 rpms, a stall torque of 1 oz. in. and a maximum power rating of 12 watts. It measures 1-1/6" in diameter and is 1-3/4" long. The size 8 motor has a no load speed of 7,300 rpm, a stall torque of 0.4 oz. in., and has a maximum power rating of 8 watts. It measures 3/4" in diameter and is 1-1/4" long. This type of servo reduces both average and dynamic angular errors to acceptable values with minimum weight, space and power penalties. The selection of this type of geared a-c motor rather than a d-c torquer is based upon the tests and analyses made by Arma during the 107A (Atlas) Program. Arma built, evaluated, and compared various gimbal servo drives employing both geared a-c and d-c torquer motors. The conclusion obtained from this program was that the geared a-c motor drive is preferable. This is based upon the following advantages of the a-c motor drive:

(1) The all a-c amplifiers and circuitry provide for a lighter, smaller, and a more reliable system.

(2) Higher torque capacity is obtained so that no design compromises are required for slip rings or gimbal bearings in order to lower the gimbal friction level. Similarly, factory attention to assembly or gimbal balancing techniques is negligible.

(3) The variable gear ratio permits the selection of the optimum load torque-to-inertia ratio for a fixed motor size.

With careful selection of the gear ratio, a perfectly adequate rotational transmissibility is obtained.

The Arma two-degree-of-freedom gyros and vibrating string accelerometers suffer from no significant rotational-vibration rectification or anisoelastic effects when integrated with a platform employing the geared gimbal servo drives. This has been frequently demonstrated during in-plant vibration tests and further substantiated by the accurate Atlas flights which were guided by the 107A Inertial Guidance System.

Each gimbal servo will be stabilized with shaping network feedback around the servo amplifier. In addition, backlash will be removed by operating two biased servo motors in a push-pull fashion for each axis. These are essentially the methods employed in the 107A platforms where it has been shown that these high gain servos can be manufactured with large stability margins on a production line basis.

The rotational transmissibilities for all axes will be such that at all frequencies, including the primary resonances, the gimbal motions will be only a fraction of the missile vibrations. This is readily accomplished by the proper selection of the critical servo parameters of gear ratio, isolation system

[redacted]

stiffness, and gear train compliance.

The two gyro housings and the three accelerometers are rigidly attached to the azimuth gimbal or stable table. The gyro housings are oriented such that, when the gyro pickoffs are nulled, the gyro spin axes will have the following orientations. The spin axis of the pitch gyro (Gyro #1) will be in the X-Z plane of the platform and makes an angle of approximately 50° with the X axis. The spin axis of the azimuth roll gyro (Gyro #2) will be parallel to the Y axis of the platform.

The stable table is suspended from the missile by four gimbals (azimuth, inner roll, pitch and outer roll) that provide the table three degrees of rotational freedom with respect to the missile. The gyro spin axes are driven to the desired orientation in inertial space during the alignment procedures. Then the gyros are cast free in inertial space and the table is slaved to the orientation of the gyros. This is accomplished by driving the gimbal servos in accordance with the proper gyro pick-off signals. Whenever the table becomes misaligned with respect to the gyro spin axes, the gyro pick-off signals are sent to the proper servo which then drives the gimbals until the gyro housings are aligned with their respective gyro spin axes. This action causes the stable table and the three accelerometers to maintain the desired fixed orientation in inertial space.

The azimuth, pitch, and outer roll gimbals have unlimited angular freedom and the inner roll has approximately ± 45° of angular freedom. The outer roll gimbal is driven so as to keep the inner roll gimbal parallel to the pitch gimbal. This is accomplished by nulling the output of the inner roll gimbal resolver. This gimbal system avoids the problem of gimbal lock and thus provides the Apollo vehicle with unlimited maneuvering freedom.

The major platform design requirements are primarily predicated upon providing the proper environment and operating conditions for the acceleration sensing system. Therefore, the stable platform is provided with the following capabilities:

(1) Internal ambient air temperature control at 32°C ± 0.15°C (rms)

(2) Initial ground azimuth alignment of the accelerometer coordinate system within 7.0 sec of arc (rms)

(3) Initial ground vertical alignment of the accelerometer coordinate system within 4.0 sec of arc(rms)

(4) Airborne alignment of the accelerometer coordinate system within 7.0 sec of arc (rms)

(5) Alignment of accelerometer sensitive axis to accelerometer coordinate system to within 3 sec of arc (rms)

(6) Stabilization against vehicle roll, pitch and yaw rates up to approximately 570 deg/sec with errors not exceeding 4.0 sec of arc (rms)

(7) Stabilization against all possible combinations of vehicular roll, pitch, and yaw motion

(8) Gimbal servo stiffness of 1 sec of arc/g

(9) Isolation from vehicle vibration to assure maximum attenuation of critical disturbing frequencies with minimum effect on platform orientation relative to vehicle

(10) Provide gimbal angle data to an accuracy of five minutes of arc for generation of vehicle attitude information

(11) Exceptional mechanical stiffness and dimensional stability

3. Stable Platform Design

The stable platform consists of stabilization gimbals, gimbal servos, gimbal pick-offs, vibration isolation system, electronics and a housing. The system's two two-degree-of-freedom gyros, three vibrating-string-accelerometers, two single-degree-of-freedom pendulums, one azimuth alignment prism, and one Stellar Alignment Nulling Device are mounted on the platform's azimuth gimbal which is supported by a single equatorial bearing.

The gimbal servo amplifiers, accelerometer oscillator-amplifiers, and gimbal pick-off preamps are gimbal mounted where possible for maximum space utilization. This approach minimizes slip ring sizes, external connector sizes and the number of interconnecting cables. Remaining units such as the proportional temperature control amplifier, power supply and modes control devices are in the electronics unit mounted on the platform housing

The following paragraphs will discuss separately the design of the major functional areas of the stable platform.

(1) Gimbaling and housing

The gimbal system is made up of azimuth, inner roll, pitch and outer roll gimbals which provide the angular freedom shown in Fig. G-11.

(2) The other electrical characteristics, such as current carrying capacity, dielectric resistance between circuits, contact resistance, etc., are within the specified requirements.

(3) Thermal stabilization system

The platform operates at an internal ambient temperature of 32°C. This low temperature is employed to insure long life and high reliability for all of the astro-inertial platform components. The thermal stabilization system is an adaptation of the system used on the Atlas platform and consists of the following elements:

(1) Temperature sensor-A 1/4" diameter stainless steel tube containing both a platinum sensing element and a precision bridge circuit adjusted to yield a null at 32°C ±0.1°C (rms).

(2) Temperature control amplifier (TCA)-A solid-state device which provides proportional control of heater power between 0 and 80 watts. The amplifier, in conjunction with the sensor is very insensitive to line voltage variations. A variation of ±5% on the 115v, 400 cps/sec excitation results in a maximum overall control point shift of only 0.02°C. The unit is vacuum impregnated with epoxy resin for protection against environmental extremes. Size of the TCA is 3" x 1-1/2" x 1" and its weight is 7 ounces. A power gain of approximately 10^{10} insures negligible bridge loading. The overall one sigma temperature variation from null will be less than 0.1°C.

(3) Heaters-Strip heaters are suitably deployed both on the azimuth casting and in the air stream so as to minimize termperature gradients and hot spots.

(4) Fans-The platform contains three fans: one situated on lower half of the azimuth gimbal, which is enclosed by the azimuth cover, and two on the top cover which direct a vigorous flow of air between the roll cover and the outer housing.

From a temperature stabilization viewpoint, the Apollo platform has been designed with a great deal of flexibility. The platform can be operated with its outermost covers removed or it can be operated with either an air cooled or a fluid cooled outermost cover in place. If the outermost covers are removed, the platform can be operated for extended periods of time in an ambient of 70°F. If the outermost covers are in place, extended platform operation requires the use of either 300 cfm of cooling air at less than 50°F or cooling fluid at less than 60°F. It should also be noted that the platform can, with all covers in place, tolerate significant external ambient temperature rises for periods in excess of 5 minutes. Therefore, it can be seen that the overall temperature stabilization problem of the Apollo astro-inertial platform can be solved in a number of different ways. The optimum cooling system will therefore be chosen after joint consideration of the problem by Arma, NASA, and the prime contractor.

4. Power Requirements

The platform is designed to operate from the three phase 400-cps and 28-v dc airborne power supplies. Total maximum input power is approximately 295 watts and the breakdown is as follows:

3 400 cps:	290 va at 0.8 p f
28-v dc:	63 watts

Total average power is approximately 235 watts.

Most of the a-c power is usable in square wave form. Therefore, high efficiency may be attained in the power supply inverter by using transistors in a switching mode. The remaining small portion of the a-c power requires the harmonic distortion to be less than 10%. This power can be obtained by filtering the static inverters square wave output.

5. Astro-Inertial Platform Weight and Balance

A program to control weight, balance, and inertia of the inertial platform has been instituted from the inception of the platform design. The institution of this program insures the following:

(1) Minimum equipment weight which results in improved figure of merit for the operational vehicle. Proper deployment of components results in minimum dead weight.

(2) Maximum balance about load axis of gimbal system for improved servo performance under dynamic environments.

(3) Accurate knowledge of gimbal load inertias for determination of servo performance.

(4) Accurate location of equipment c. g. and inertias about primary mounting axes which permit effective designs for the vibration isolation system and mounting equipment in operational vehicle.

The present design indicates that the overall astro-inertial platform for Apollo will weigh approximately 48 pounds.

6. Summary

The stable platform proposed for use on the Apollo program is a design refinement of the stable platform currently in production for the Atlas ICBM and the Arma lightweight platform that has been developed under Air Force contract. The type of production test equipment required for the efficient manufacture of this component is presently available.

III ASTRO-INERTIAL PLATFORM PREFLIGHT ALIGNMENT AND CALIBRATION

A. INITIAL ALIGNMENT

The inertial navigation system that is proposed for use on the Apollo Program utilizes a rectangular XYZ navigational coordinate system that is fixed in inertial space. For reasons of convenience and maximum system accuracy the navigational coordinate system will initially be oriented such that the Z axis of the system is collinear with the local (plumb-bob) vertical at the time and place of launch. The X axis, which is perpendicular to the Z axis, is directed down range such that the thrust acceleration of the nominal missile will be in the X-Z plane. The Y axis which is orthogonal to both the X and Z axis is directed so as to form a right-handed XYZ coordinate system. In order to be compatible with the instrumentation of the inertial navigational system, the sensitive axes of the three accelerometers must be maintained collinear with the respective axes of the navigational coordinate system. The problem of aligning the accelerometers to the navigational coordinate system reduces to the problem of obtaining the correct initial orientation of the two gyro spin axes. This is accomplished by the system's ground support equipment prior to missile launch. The initial alignment of the inertial components can be divided into two parts: verticality alignment and azimuth alignment. The verticality alignment procedure aligns the Z axis of the platform with the local vertical. This is accomplished via two single-degree-of-freedom pendulums. These pendulums consist of: a bob that tends to align itself with the local gravity vector, an outer case that is rigidly attached to the stable platform, and a pick-off that detects the misorientation between the bob and the case. The case of the pendulum is oriented such that the platforms Z axis will be collinear with the pendulum bob whenever the pick-off signal is nulled. Verticality alignment is thus accomplished by precessing the two gyros about two orthogonal horizontal axes until the two pendulum pick-off signals are nulled. The circuitry that accomplishes this is physically located in the ground support equipment. The azimuth alignment directs the platform's X axis to a precise azimuth angle that is approximately down-range. This is accomplished via the optical alignment link. An optical prism is accurately attached to the stable platform such that it can be seen from a ground alignment station. The platform's gyros are then precessed about the vertical axis until the face of the prism is precisely perpendicular to the line-of-sight from the ground alignment station to the platform mounted prism. The prism is positioned on the azimuth gimbal so that the system's X axis will then have the desired azimuth orientation. The positioning of the prism on the platform will be accomplished in the hangar maintenance area before the system is installed in the vehicle.

The above alignment procedure is that used during prelaunch countdown. Alignment of the platform while in space is accomplished via the Stellar Alignment Nulling Device which was described in Section I-C.

[redacted]

B. INERTIAL COMPONENT CALIBRATION

The inertial navigation accuracy requirements for the Apollo Program are such that certain of the inertial component performance parameters must be calibrated and trimmed before vehicle launch. The performance parameters that must be so calibrated are the scale and zero of the accelerometers and the spring torques and mass unbalances of the gyros. These calibrations will be performed automatically by the ground support equipment while the navigation system is in the Apollo vehicle. The remainder of the inertial component performance parameters will be calibrated at the factory at the time of manufacture. The zero of the accelerometers and the spring torques of the gyros will be recalibrated during the transearth portion of the Apollo trajectory, just prior to atmospheric re-entry.

C. TRIMMING OF INERTIAL COMPONENTS

Inertial navigation of the accuracy desired for the Apollo Program requires the use of extremely accurate gyros and accelerometers. In many areas the required component performance is greater than realistic production tolerances or material stability can provide. In these areas the required accuracy is obtained via component calibration and trimming. The actual component trimming may be accomplished mechanically or computationally.

Mechanical component trimming has several operational disadvantages. Namely, the component may be relatively inaccessible during the "countdown," the component parameter may not be readily adjustable, the mechanical trimming may require considerable equipment, or the "screw driver" adjustment of one parameter may disturb the values of other parameters. In any event, it would usually be necessary to recalibrate the component in order to check the adequacy of the mechanical trimming. In fact, the entire procedure may have to be repeated several times before the component performance is satisfactory. All of these difficulties can be avoided by utilizing computational component trimming. The computational trimming procedure is a technique of measuring, and storing in the digital computer, the constants describing the performance of the various components. For example, the equation of the X axis vibrating-string-accelerometer is of the form:

$$\Delta F_x = C_0 + C_1 A_x + C_2 A_x^2 + C_3 A_x^3 + C_4 A_x A_z + C_5 A_x A_y \qquad (10)$$

where

ΔF_x = the difference frequency of the X axis accelerometer

C_o = zero offset

C_1 = scale factor

C_2 = second order effect

C_3 = third order effect

C_4 = cross acceleration scale change due to Z axis acceleration

C_5 = cross acceleration scale change due to Y axis acceleration

A_x = X component of thrust acceleration

A_y = Y component of thrust acceleration

A_z = Z component of thrust acceleration

Most of the above constants or parameters will be determined in the factory but the scale and zero will be determined during the system's countdown procedure. In any event, the above equation will be inverted so as to define the input acceleration as a function of the accelerometer's difference frequency output. That is:

$$A_x = K_0 + K_1 \Delta F_x + K_2 (\Delta F_x)^2 + K_3 (\Delta F_x)^3 + K_4 \Delta F_x \Delta F_y + K_5 \Delta F_x \Delta F_z \qquad (11)$$

where the above "K's" are functions of the C's appearing in equation (10).

This equation is then instrumented in the navigational digital computer so as to computationally trim the X axis accelerometer. The Y and Z axis accelerometers will of course be trimmed in a similar manner. Ideally the system's two-degree-of-freedom gyros should maintain a fixed angular orientation in inertial space and thus keep the three orthogonal accelerometers aligned with the axes of the navigational coordinate system. If the gyros should drift, the accelerometers will become misoriented and the vehicle's accelerations will be sensed in a rectangular coordinate system that is not collinear with the navigational coordinate system. Normally this would cause navigation errors; however, if the gyro drift angles are known, the sensed acceleration can be transformed into the navigational coordinate system. Since the magnitude of the gyro drift angles is very small, the standard small angle approximations can be utilized and the transformation can be simplified to:

$$A_x = A_x' - A_y \epsilon_z + A_z \epsilon_y$$

$$A_y = A_y' + A_x \epsilon_z - A_z \epsilon_x$$

$$A_z = A_z' - A_x \epsilon_y + A_y \epsilon_x$$

where

A_x, A_y, A_z = rectangular components of vehicle acceleration as seen in the navigational coordinate system

A_x', A_y', A_z' = rectangular components of vehicle acceleration as seen in the platform coordinate system

ϵ_x, ϵ_y, ϵ_z = angles, about each axis, by which platform coordinate system is misaligned from navigational coordinate system

The above misalignment angles are functions of the various gyro parameters and the various rectangular components of the vehicular thrust acceleration impressed on the gyros. Therefore, the above misalignment angles can be computed in the airborne navigation computer and can then be used to provide computational trimming for the gyros. The inertial component trimming equations that are required for the Apollo inertial navigation system have been determined by means of system's performance analyses.

The various K's in the referenced equations are functions of the physical characteristics of the individual gyros and accelerometers in the given inertial navigation system and are determined either in the factory or during the system's prelaunch countdown. In any event the numerical values of the above K's are read into the system's digital computer so that the accelerometer output data can be transformed into the navigational coordinate system components of vehicular thrust acceleration.

[redacted]

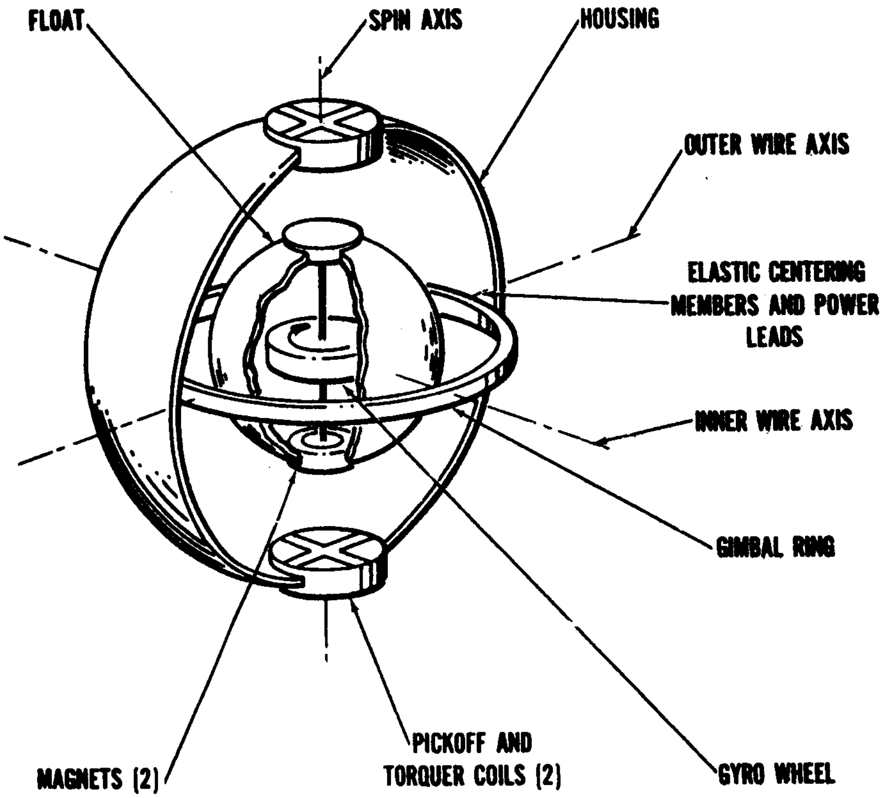
FLOAT
SPIN AXIS
HOUSING
OUTER WIRE AXIS
ELASTIC CENTERING MEMBERS AND POWER LEADS
INNER WIRE AXIS
GIMBAL RING
MAGNETS (2)
PICKOFF AND TORQUER COILS (2)
GYRO WHEEL

Fig. G-1. Functional Construction of G8 Gyro

[redacted]

[redacted]

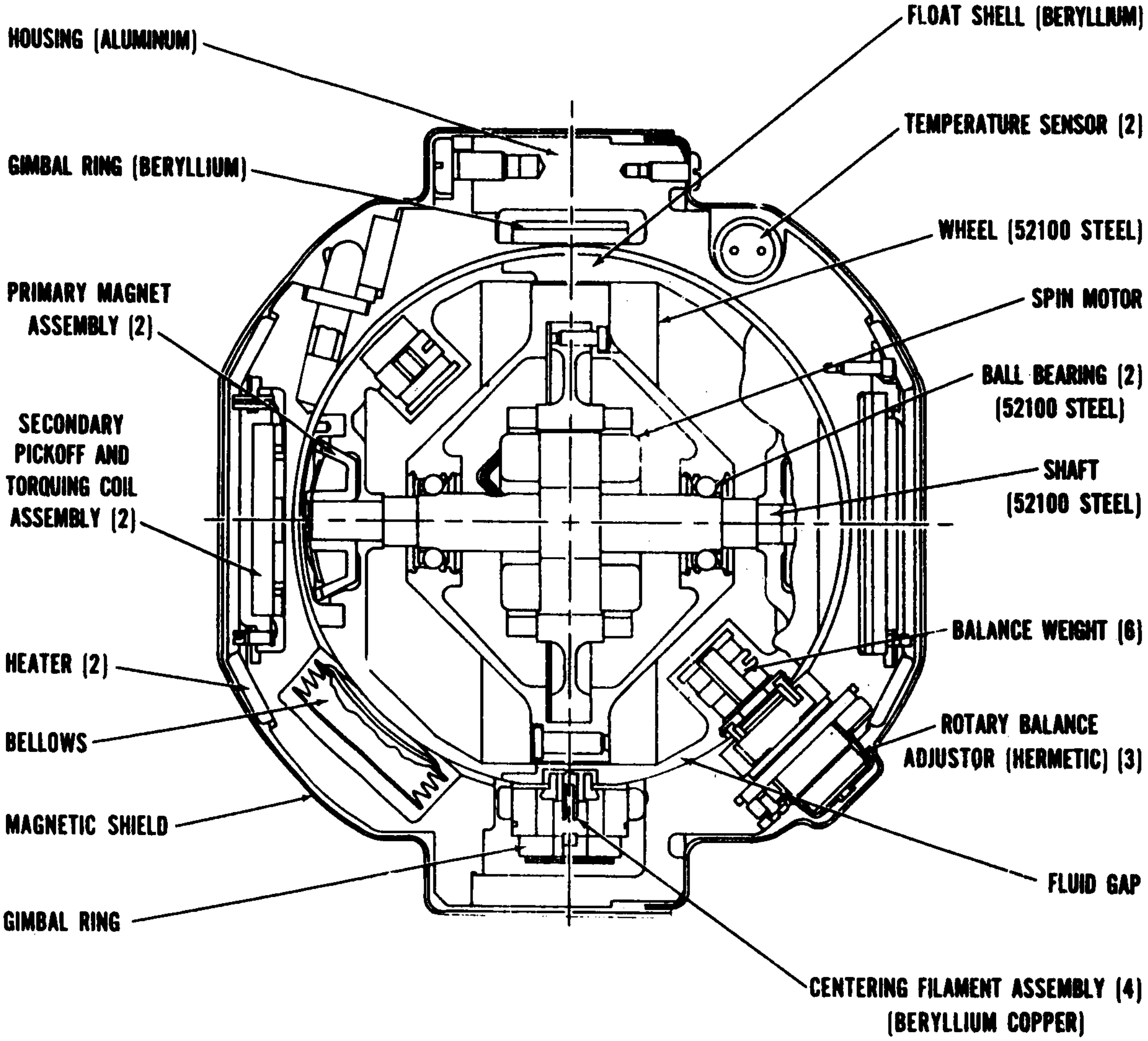
HOUSING (ALUMINUM)
GIMBAL RING (BERYLLIUM)
PRIMARY MAGNET ASSEMBLY (2)
SECONDARY PICKOFF AND TORQUING COIL ASSEMBLY (2)
HEATER (2)
BELLOWS
MAGNETIC SHIELD
GIMBAL RING
FLOAT SHELL (BERYLLIUM)
TEMPERATURE SENSOR (2)
WHEEL (52100 STEEL)
SPIN MOTOR
BALL BEARING (2) (52100 STEEL)
SHAFT (52100 STEEL)
BALANCE WEIGHT (6)
ROTARY BALANCE ADJUSTOR (HERMETIC) (3)
FLUID GAP
CENTERING FILAMENT ASSEMBLY (4) (BERYLLIUM COPPER)

Fig. G-2. Cross Section of G8 Gyro

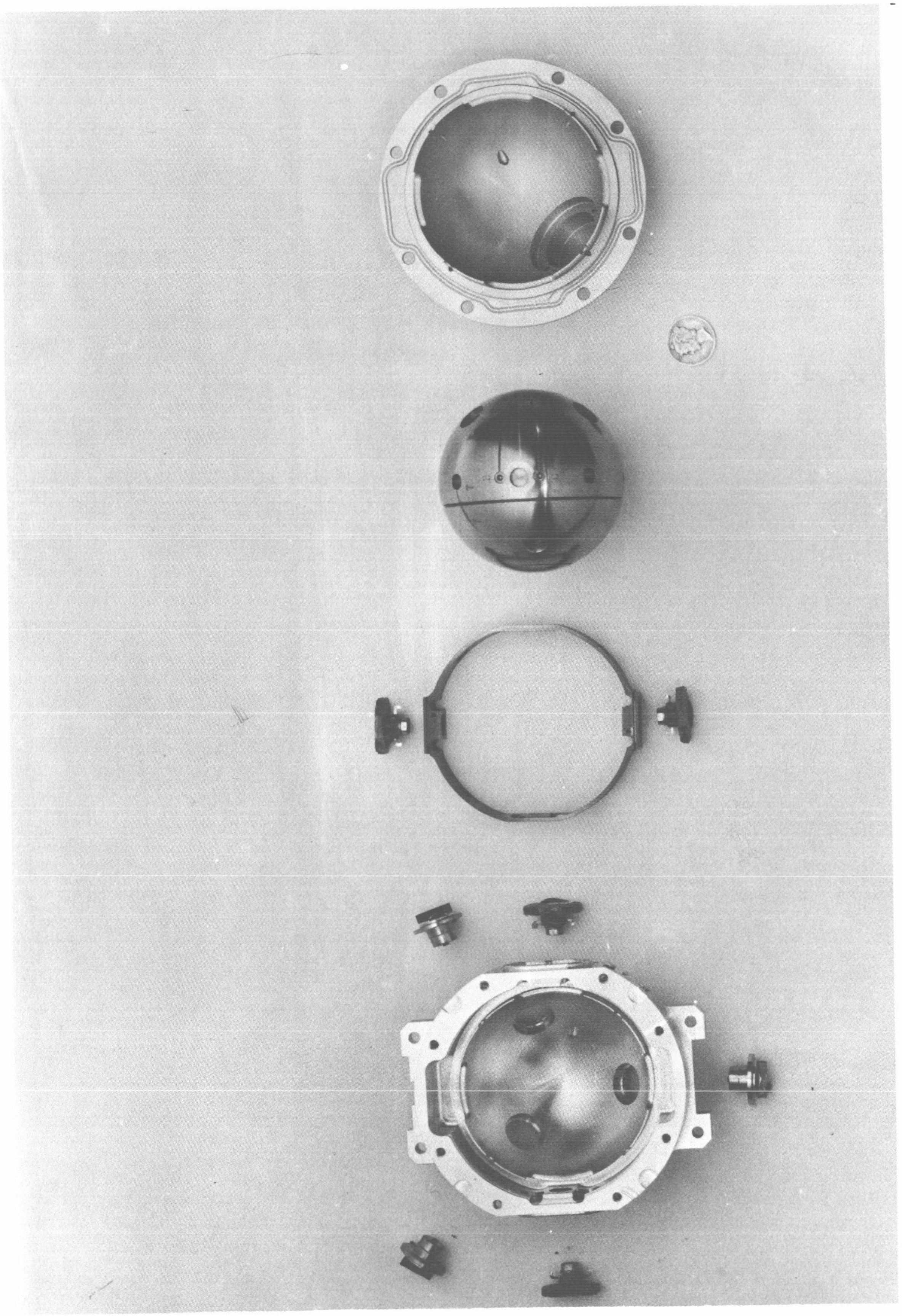

Fig. G-3. G8 Gyro Assembly Layout

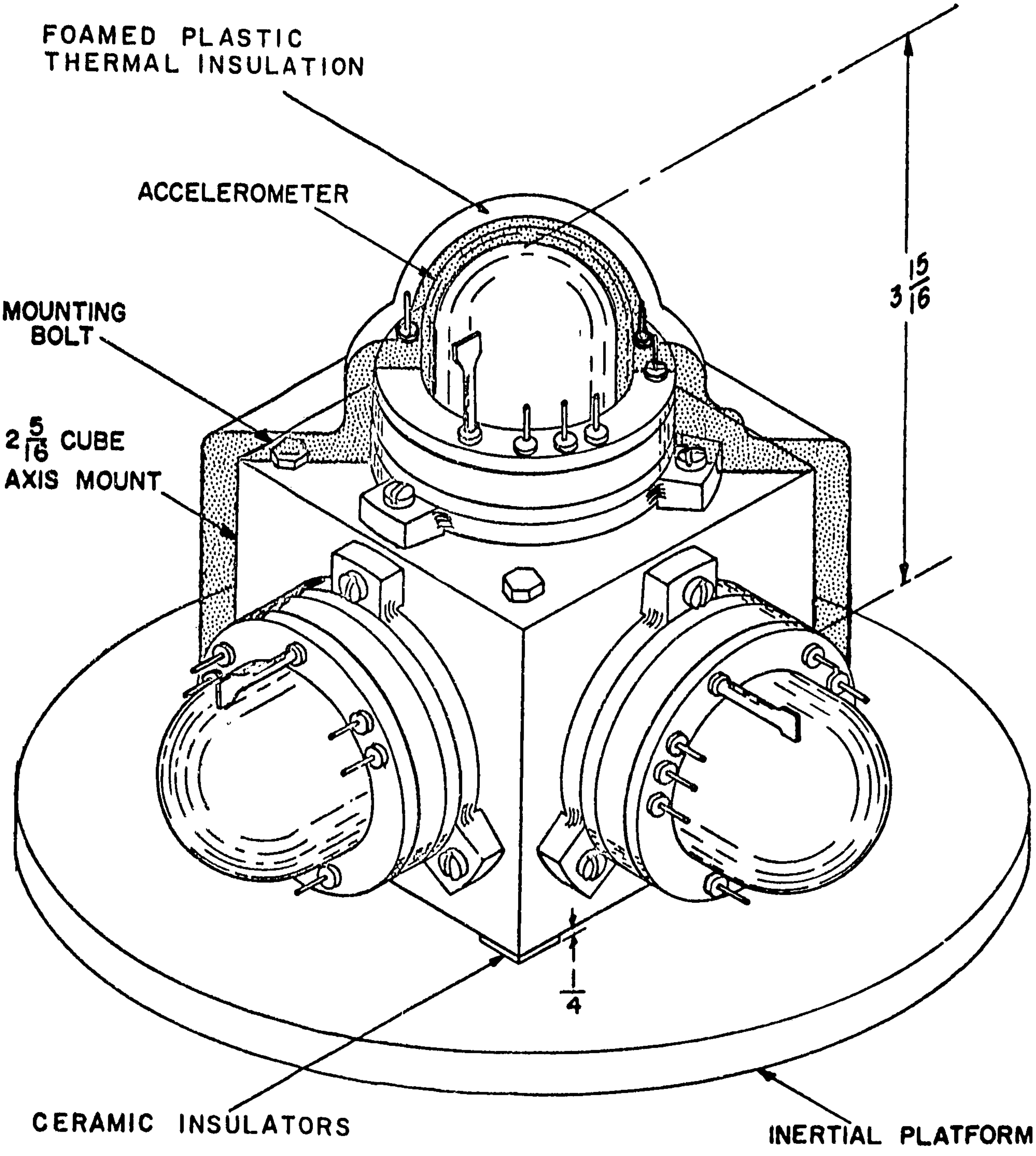
FOAMED PLASTIC THERMAL INSULATION
ACCELEROMETER
MOUNTING BOLT
$2\frac{5}{16}$ CUBE 3 AXIS MOUNT
$3\frac{15}{16}$
$\frac{1}{4}$
CERAMIC INSULATORS
INERTIAL PLATFORM

Fig. G-4. Accelerometer Mounting Fixture

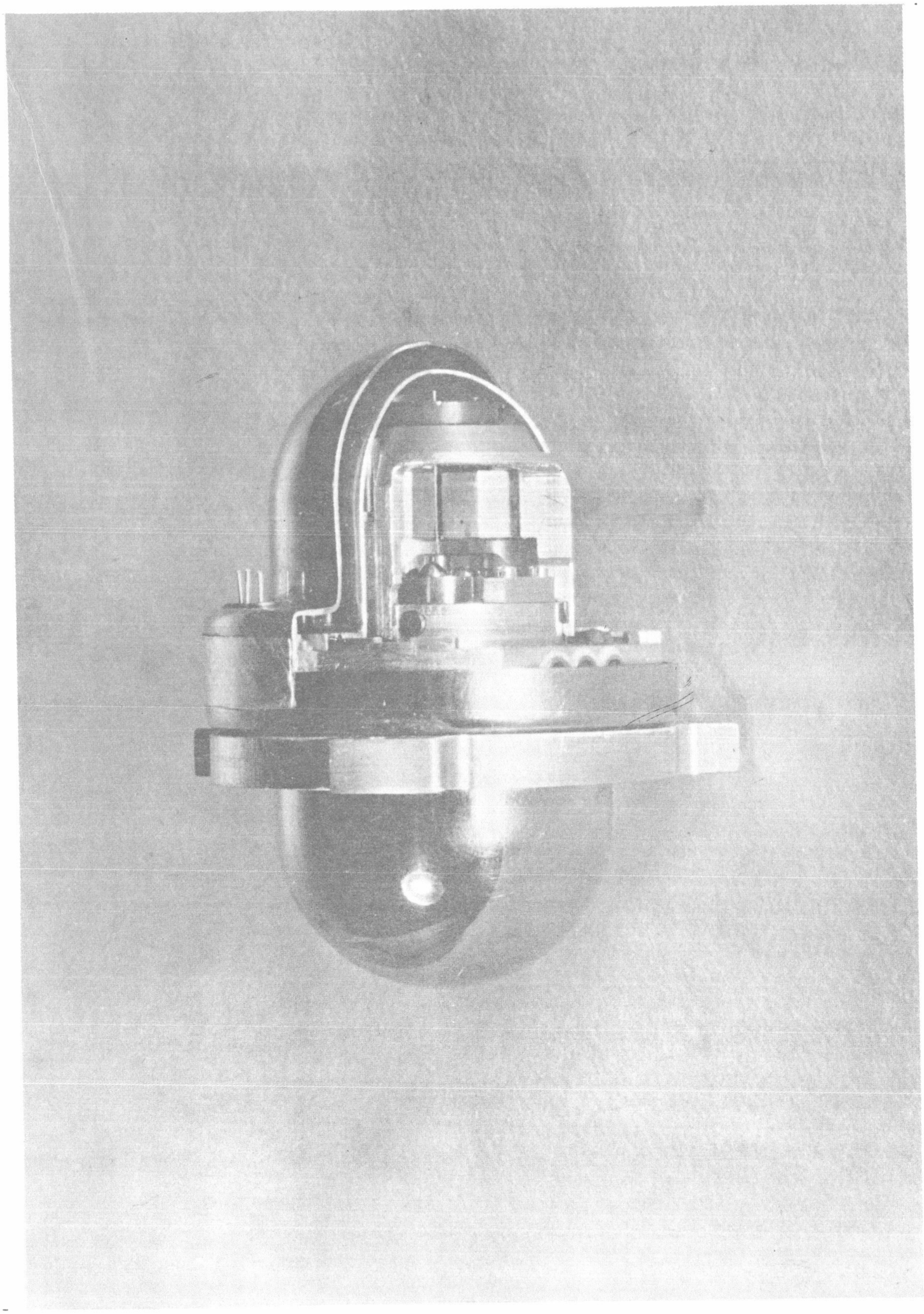

Fig. G-5. Cutaway of D4 Vibrating String Accelerometer

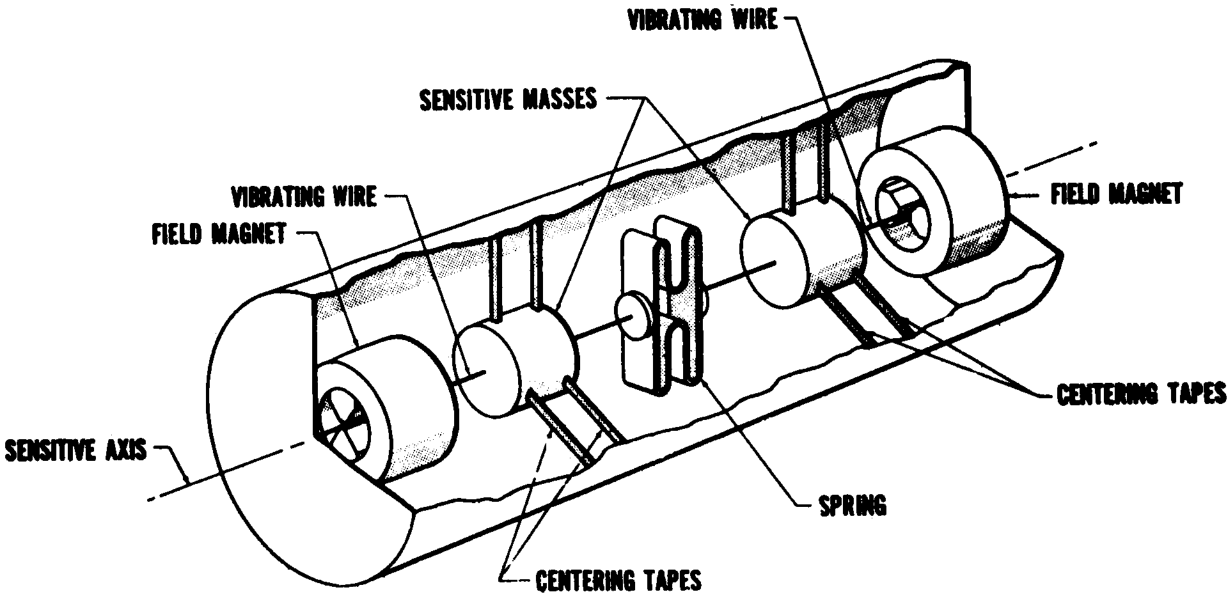
VIBRATING WIRE
SENSITIVE MASSES
VIBRATING WIRE
FIELD MAGNET
FIELD MAGNET
CENTERING TAPES
SENSITIVE AXIS
SPRING
CENTERING TAPES

Fig. G-6. Schematic of Vibrating String Accelerometer

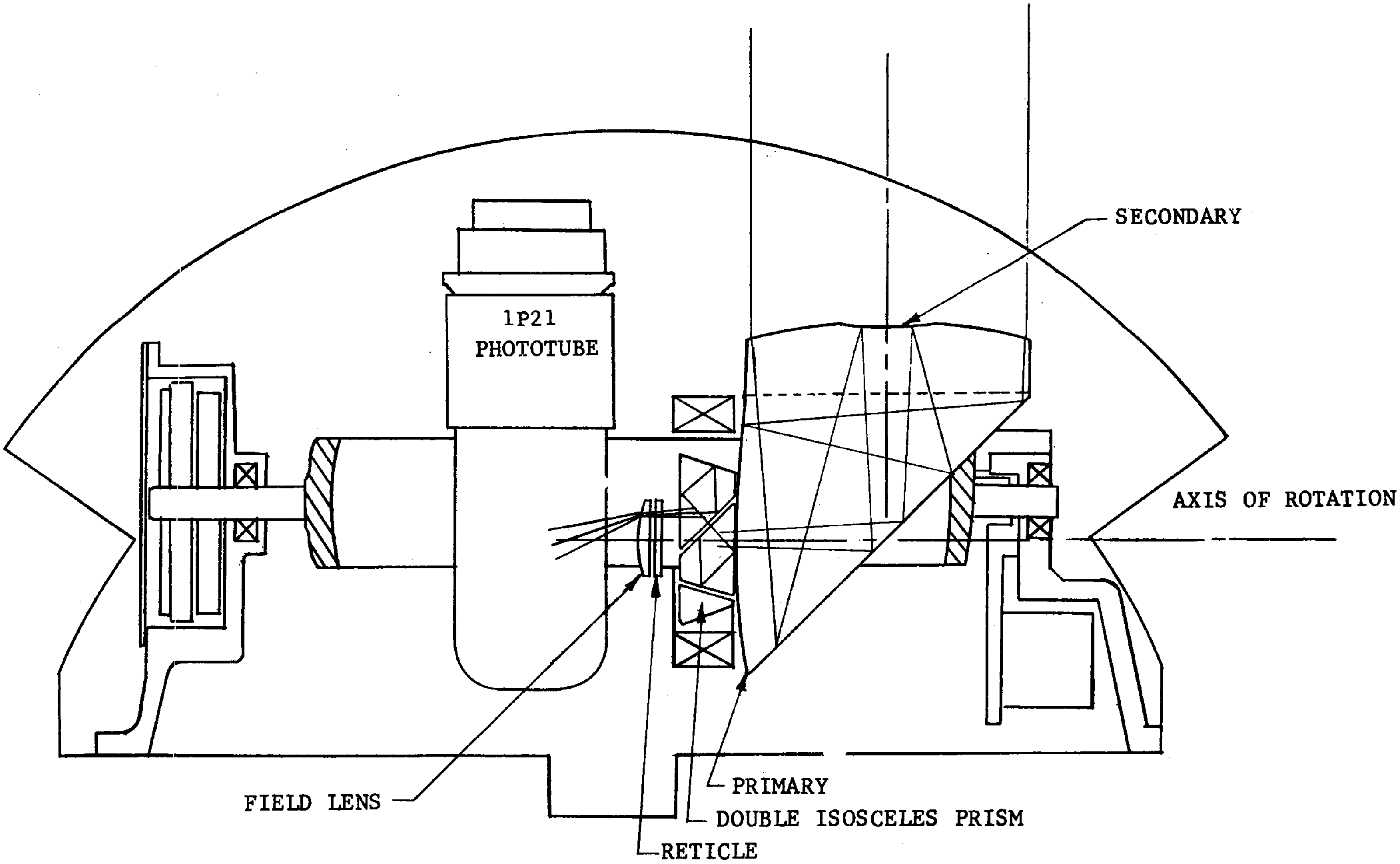
SECONDARY
1P21
PHOTOTUBE
AXIS OF ROTATION
FIELD LENS
PRIMARY
DOUBLE ISOSCELES PRISM
RETICLE

Fig. G-7. Stellar Alignment Nulling Device Telescope

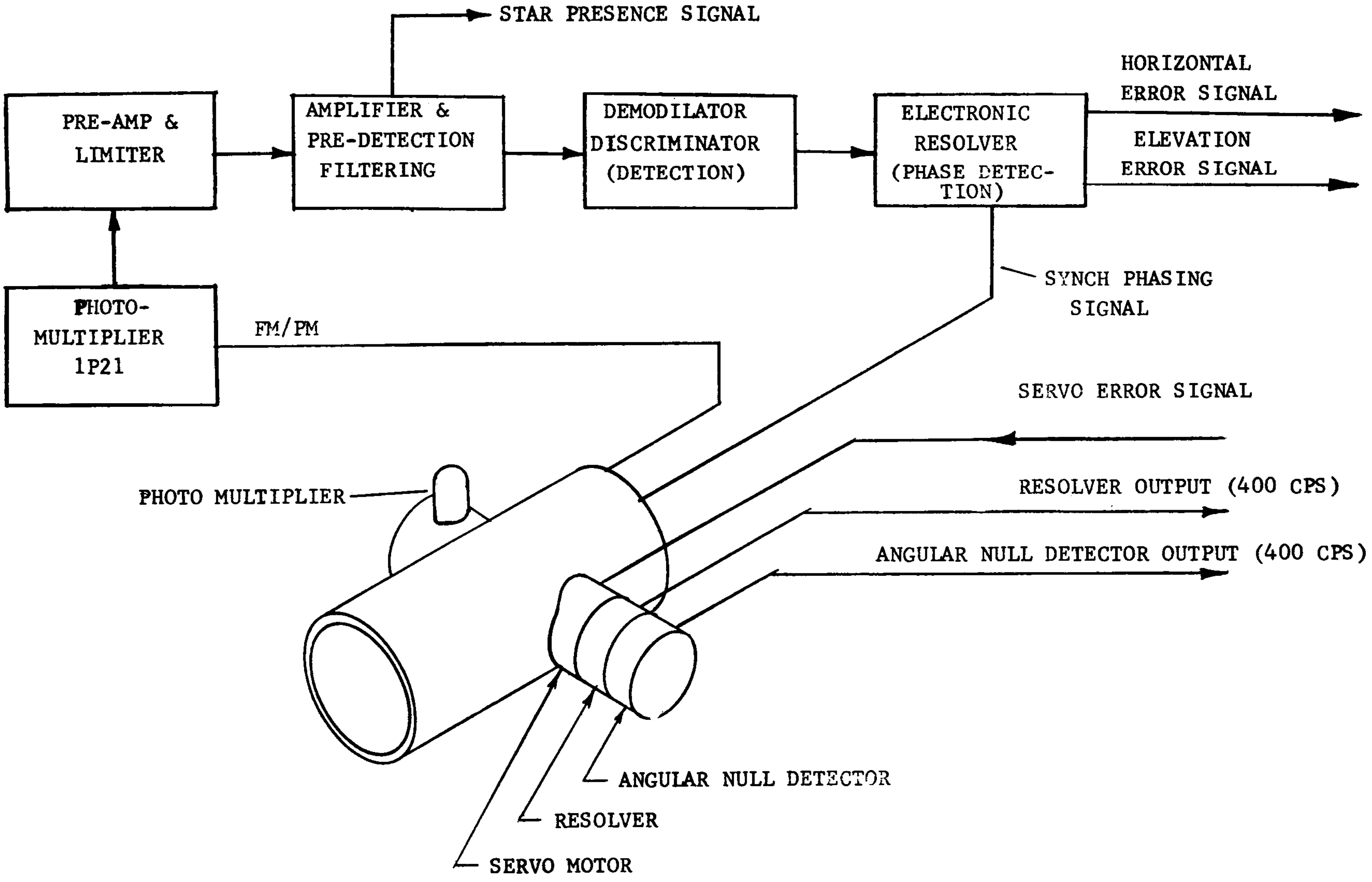
STAR PRESENCE SIGNAL
PRE-AMP & LIMITER
AMPLIFIER & PRE-DETECTION FILTERING
DEMODILATOR DISCRIMINATOR (DETECTION)
ELECTRONIC RESOLVER (PHASE DETECTION)
HORIZONTAL ERROR SIGNAL
ELEVATION ERROR SIGNAL
PHOTO-MULTIPLIER 1P21
FM/PM
SYNCH PHASING SIGNAL
SERVO ERROR SIGNAL
RESOLVER OUTPUT (400 CPS)
ANGULAR NULL DETECTOR OUTPUT (400 CPS)
PHOTO MULTIPLIER
ANGULAR NULL DETECTOR
RESOLVER
SERVO MOTOR

Fig. G-8. Stellar Alignment Nulling Device Block Diagram

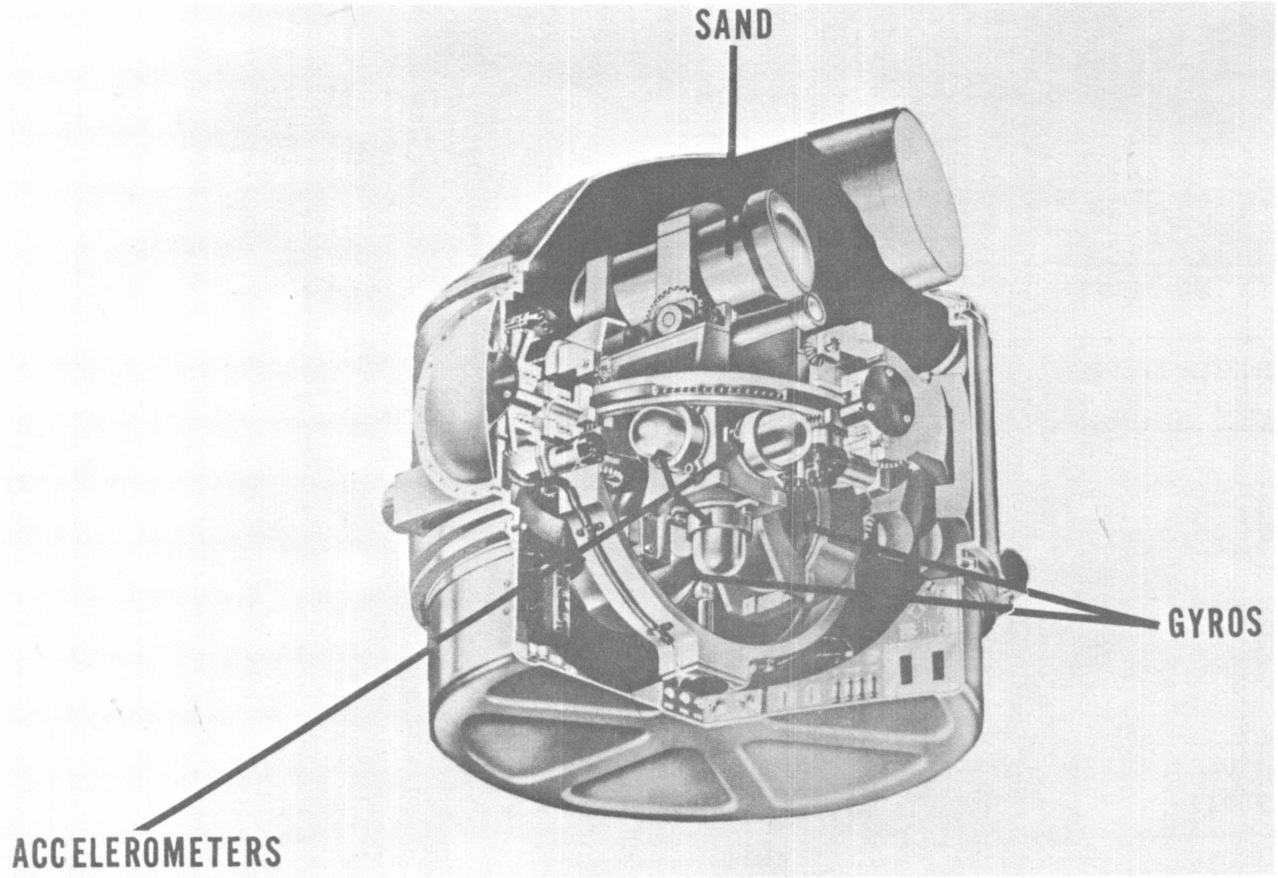
SAND
GYROS
ACCELEROMETERS

Fig. G-9. Primary Inertial Platform With Stellar Alignment Nulling Device (SAND)

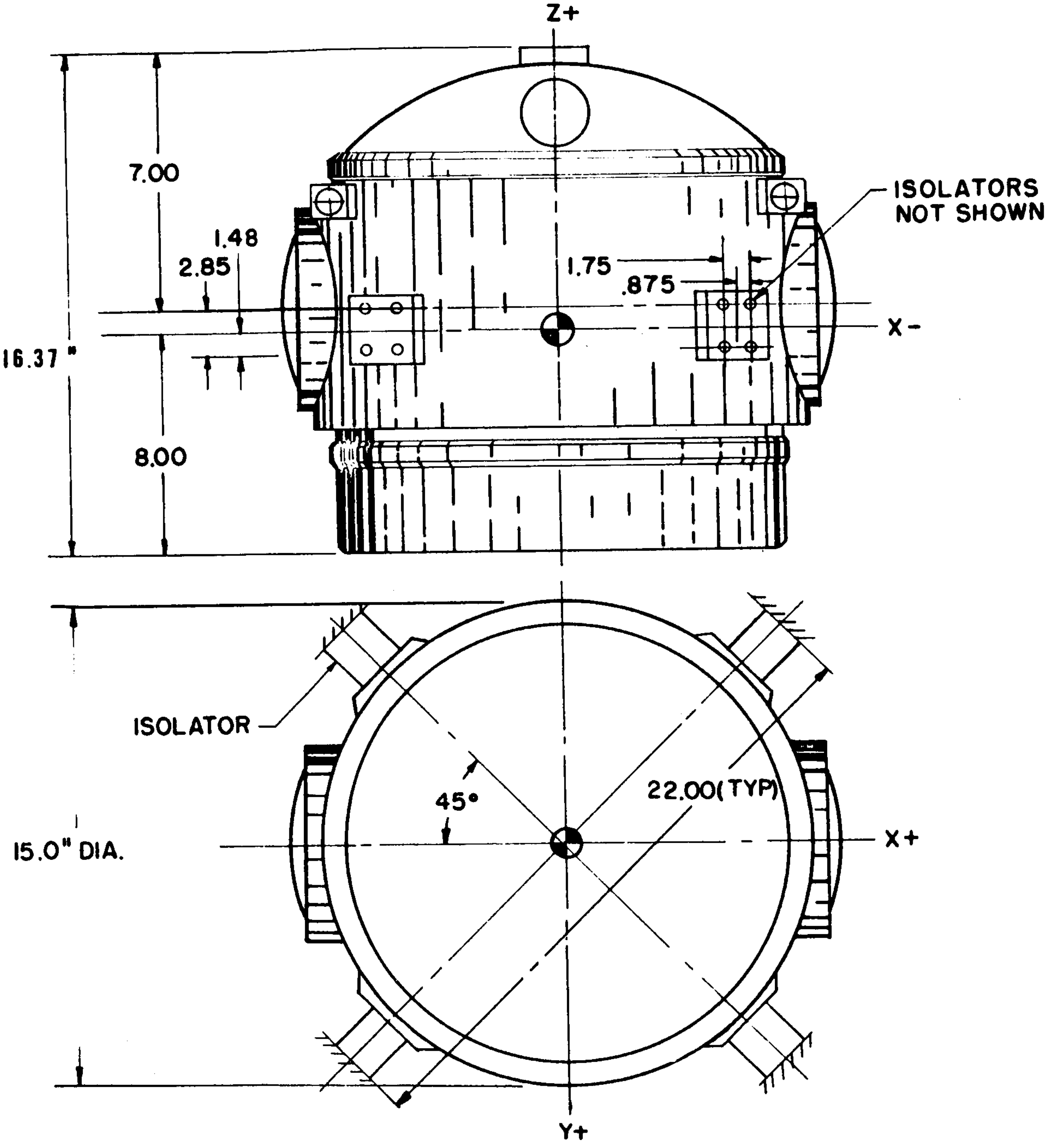
Z+
7.00
1.48
2.85
16.37"
8.00
1.75
.875
ISOLATORS NOT SHOWN
X-
ISOLATOR
45°
22.00(TYP)
15.0" DIA.
X+
Y+

Fig. G-10. General Outline of Apollo Platform Configuration

[redacted]

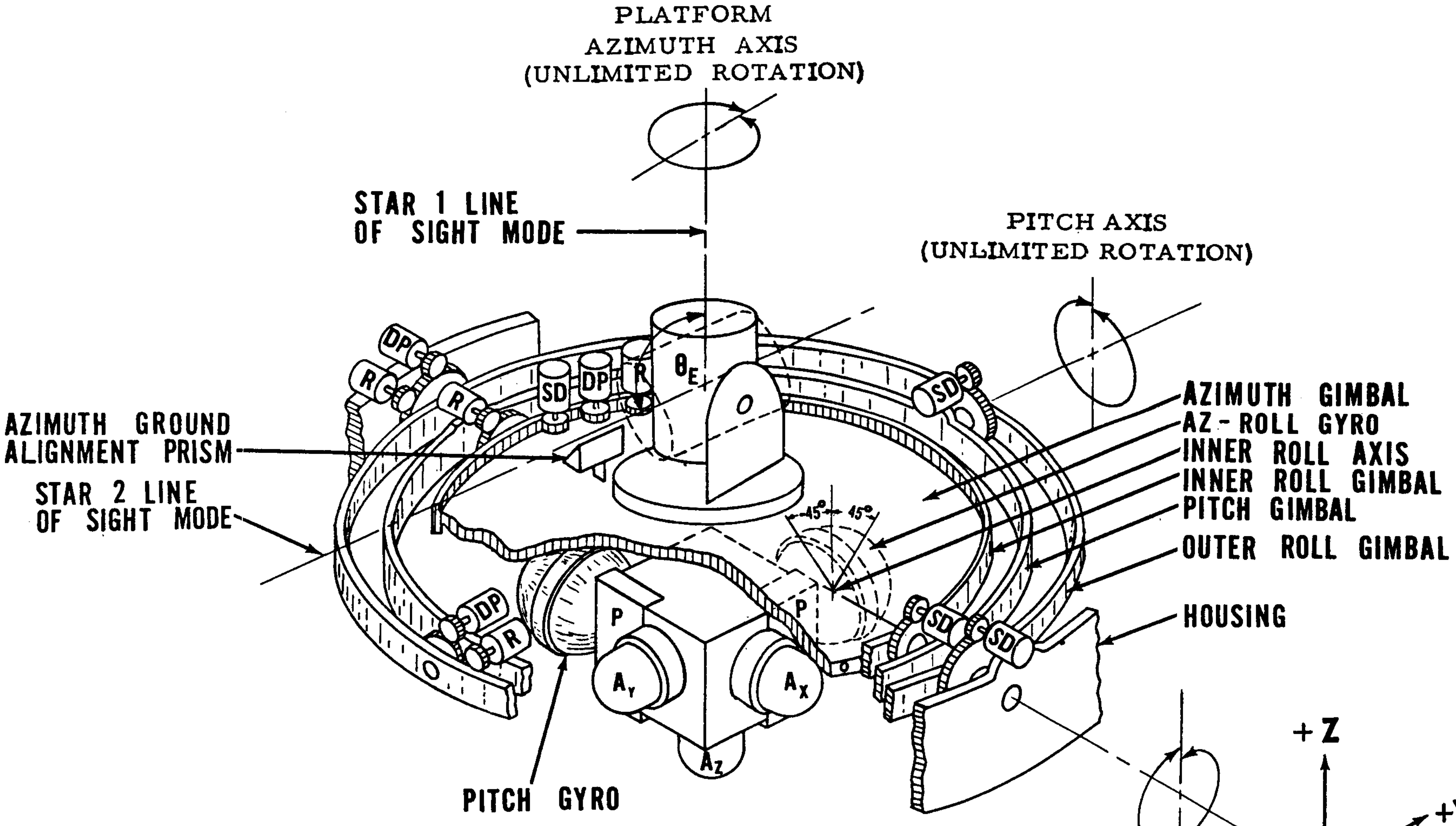
PLATFORM
AZIMUTH AXIS
(UNLIMITED ROTATION)
STAR 1 LINE OF SIGHT MODE
PITCH AXIS
(UNLIMITED ROTATION)
AZIMUTH GROUND ALIGNMENT PRISM
STAR 2 LINE OF SIGHT MODE
AZIMUTH GIMBAL
AZ - ROLL GYRO
INNER ROLL AXIS
INNER ROLL GIMBAL
PITCH GIMBAL
OUTER ROLL GIMBAL
HOUSING
PITCH GYRO
OUTER ROLL AXIS
(UNLIMITED ROTATION)
+Z
+Y
+X
θE
45°
45°
DP
R
SD
P
A_X
A_Y
A_Z

LEGEND

P - PENDULUM
R - RESOLVER
A - ACCELEROMETER
DP - DIGITAL PICKOFF
SD - SERVO DRIVE

Fig. G-11. Schematic of Apollo Inertial Platform

[redacted]

APPENDIX H

ALTERNATE PLATFORM (KEARFOTT)

Kearfott is developing several inertial guidance platforms which might meet the requirements for the miniature platform in Apollo's guidance system. The characteristics of two such platforms given below are taken from Kearfott brochure No. GTO 115A.

I. SMALL INERTIAL GUIDANCE PLATFORM

Type number: C70 2603 002

Size: 12.5" length; 10" diameter

Weight: 30 pounds

Gimbal configuration: 3-gimbal, #85° pitch, 360° roll, 360° yaw.

Also available as a 4-gimbal all-attitude inertial reference

Gimbal Outputs	Azimuth	Pitch	Outer Roll
Quantity	1	1	1
Type	Synchro cx	Synchro cx	Synchro cx resolver
Scale factor	208 mv/deg	208 mv/deg	208 mv/deg
Accuracy	3 min	10 min	10 min
Gimbal torques	Gear drive	Gear drive	Gear drive
Type	R124-5	R124-5	R119
Stall torque	0.30 in-oz	0. 30 in-oz	0.60 in-oz
Gear ratio	50:1	50:1	70:1

All Axes

Accelerometer type	force balance
Range	#20g
Scale factor	5 ma/g
Linearity	0.01%

[redacted]

Gyroscope Type	2066326 (Kearfott)
Drift Rate	
Short Term	0.15°/hr
Day to Day	1°/hr maximum
Torquer	83°/ hr/ma

II. MINIATURE INERTIAL GUIDANCE PLATFORM

Type number: C70 2611 001

Size: 10.6" L, 8.25" H, 8.25" W

Weight: 18/pounds

Gimbal configuration: 3-gimbal, #85° azimuth, 360° roll, 360° pitch.

Also available as a small 4-gimbal all-attitude inertial platform.

Gimbal Outputs	Azimuth	Pitch	Outer Roll	
Quantity	1	1	1	1
Type	Synchro cx	Synchro cx	Synchro cx	resolver
Scale factor	200 mv/°	200 mv/°	200 mv/°	454 mv/°
Accuracy	5 min	5 min	5 min	5 min
Gimbal torques	Gear drive	Gear drive	Gear drive	
Type	R124	R124	R110	
Stall torque	0.28 in-oz	0.28 in-oz	1.53 in-oz	
Gear ratio	50:1	50:1	50:1	

All Axes

Accelerometer type	force balance
Range	#20g
Scale factor	5 ma/g
Linearity	0.01%

[redacted]

Gyroscope Type	(C702516001 Kearfott)
Drift rate	
short term	0.05 °/hr
day-to-day	0.2 °/hr
Torquer (ac)	$2\ ^\circ/\text{hr/ma}^2$

APPENDIX I

MINIATURE PLATFORM MINNEAPOLIS-HONEYWELL

The following information is extracted from MH Aero Document R-ED 28050.

The GG 8025 is a miniaturized version of the MH Miniature Platform currently in production at Honeywell. In the design of the platform electronics, advanced circuitry and packaging techniques are combined to produce an assembly a fraction of the size of conventional units. This extreme miniaturization has been achieved without sacrifice in performance or versatility as evidenced by the following features:

(1) Compact and light weight - - Platform is eight inches in diameter by 10-1/2 inches long and weighs 16 pounds. The platform electronics occupies 100 cubic inches and weighs less than five pounds.

(2) Choice of inertial components - - Platform can accommodate advanced gyro and accelerometer designs.

(3) Suitable for use in both digital and analog system - - Inertial components can be proportional-current or pulse-torqued.

(4) Low operating power requirements - - Less than 100 watts is required by the platform and associated electronics during normal operation.

(5) High level reliability - - Utilizes the features proven in the production MH Miniature Platform.

(6) Adaptability to specific applications - - The gimbal arrangement can be modified to provide either a three or four gimbal unit. The platform can be either a two or three accelerometer version.

Design details and performance characteristics are discussed in the following paragraphs. The unit employs the MH GG 8001 Miniature Integrating Gyro and the MH GG177 Miniature Hinged Pendulum accelerometer.

Gimbal System. The platform is a four-gimbal device which permits all-attitude operation. The gimbal structure design is based on results of the Miniature Inertial Platform production program. The gimbals are identified as follows (from inside out to case).

Gimbal	Freedom
Azimuth	360 degrees
Inner roll	± 20 degrees
Pitch	360 degrees
Outer roll	360 degrees

High strength and light weight have been achieved by use of magnesium alloy castings. Compared with aluminum, this provides a significant reduction in vibration transmissibility. Preloaded bearing pairs are used in each gimbal axis trunnion. During assembly, the interface dimension of the bearing pairs is adjusted by shimming and the bearing preload is set to negate axial play along any gimbal axis.

Component complement. Listed below are the components mounted on each gimbal in a normal four-gimbal configuration.

Azimuth Gimbal

Three	GG8001 miniature integrating gyros
Three	GG117 miniature accelerometers
Three	gryo preamplifiers
Three	accelerometer preamplifiers
Three	gyro temperature control amplifiers
One	pancake d-c torque motor (10 in. -oz)
One	double-stacked pancake gimbal angle pickoff- - one unit of this stack resolves north and east gyro torquing signals; the second unit provides synchro or resolver azimuth gimbal angle readout
One	optical prism for azimuth alignment

Inner Roll Gimbal

One	pancake d-c torque motor (10 in. -oz)
One	pancake synchro (provides angular input to drive outer roll gimbal)

Pitch Gimbal

One pancake d-c torque motor (10 in.-oz)

One pancake gimbal angle pickoff for pitch angle readout

Outer Roll Gimbal

One pancake d-c torque motor (30 in.-oz)

One pancake gimbal angle pickoff for roll angle readout

Gimbal drive motors. The advantages of the use of d-c pancake motors for gimbal drive devices have been proven in the production miniature platform. Compared with gear driven systems, the direct drive is subject only to the small errors introduced by the low level friction contributions of the commutator and the slip ring assembly. The direct drive technique eliminates the acceleration error and high friction contribution present in a geared-drive system.

Temperature control. The gyro temperatures are maintained by heaters which are integral with the gyro. Each gyro contains its own heat sensor. Heat is supplied individually to each gyro by a temperature control amplifier mounted adjacent to it on the inner gimbal casting. The accelerometers do not require individual temperature control. For operation above 110° F ambient, the platform is supplied with a finned case. When cooling air is required, an insulated shroud is provided to conduct coolant over the case.

Platform electronics. The platform electronics includes the gimbal servos, accelerometer servos, and power transformers. The circuit modules may be mounted around the platform end bells. This requires the platform length to be increased to 12 inches. Power amplifier efficiency is kept high by the use of silicon controlled rectifiers in the output stages. This eliminates the need for extensive heat sinks required with the more conventional transistor power circuits and permits the use of highly miniaturized welded module packaging. The gyro and accelerometer signal preamplifiers are welded modules potted in a threaded form. The units are installed by screwing into threaded holes adjacent to the accelerometers on the stable element casting.

Inertial components. The platform has been designed to accept any of a number of inertial components now in production or under development. The MH GG8001 gyro and the MH GG177 accelerometer have been selected for description in this document.

[redacted]

GG8001 PHYSICAL AND PERFORMANCE CHARACTERISTICS

Dimensions	1.830 dia. x 2.817 long
Weight	0.68 pound
Operating temperature	180°F
Gyro angular momentum	1×10^5 CGS units
Random drift (short term)	
OA vertical	0.01 deg/hr (1 sigma)
OA horizontal	0.02 deg/hr (1 sigma)
Anisoelastic coefficient (O- 500 cps)	0.02 deg/hr/g^2 rms (max)
Acceleration sensitive drift	0.2 deg/hr/g (max untrimmed)
Shift after storage at + 50° F	0.6 deg/hr/g (3 sigma)
Acceleration insensitive drift	2.5 deg/hr (max untrimmed)
Shift after storage at + 50° F	0.3 deg/hr (3 sigma)
Torquer linearity	0.01 percent of full scale (3 sigma)

GG177 PHYSICAL AND PERFORMANCE CHARACTERISTICS

Threshold	less than 10^{-6}g
Range	± 60 g
Scale factor	1.5 milliamperes/g
Null torque	less than 10^{-4}g
Null torque stability	8×10^{-5}g (3 sigma)
Null angle stability	5×10^{-5}g (3 sigma)
Zero stability	2×10^{-5} radians (3 sigma)
Scale factor stability	+0.005 percent

[redacted]

Linearity	10×10^{-5}g to one g, +0.01 percent above on g - (3 sigma)
Null uncertainty	$\pm 2 \times 10^{-5}$ g maximum
Size	1.45 dia. x 1.83 long
Weight	5 ounces

Platform characteristics. The following data reflect the ability of the platform to remain stable and aligned.

Vehicle angular acceleration limit	essentially none
Vehicle angular velocity limit	100 rad/sec
Velocity error coefficient	0.002 mr/rad/sec
Static friction threshold	0.01 mr
Static stiffness	50 in. -oz/mr

[redacted]

[redacted]

APPENDIX J

ASTRONAUT'S SEXTANT (AUTONETICS)

An artist's rendition of the sextant is shown in Fig. J-1.

The sextant serves three nonsimultaneous functions:

(1) It provides a gimbaled base from which the astronaut can orient his sextant.

(2) It can serve as a manual device with which the astronaut can orient the inertial platform.

(3) It can serve as a star-tracker for automatically updating of the inertial platform attitude.

The best accuracy is obtained when the instrument is used as a sextant; and the sextant reading can be obtained manually to a few sec. Autonetics readings are to code wheel accuracy without interpolation (40 sec or 80 sec).

When used as a sextant, (optics shown schematically in Fig. J-2) the astronaut overrides the servo drives. The code wheel gimbal angle readout provides the computer with information to check the astronaut's star selection.

Four limited-freedom gimbals are provided; this is the number required to define the lines-of-sight to two stars. Two of these gimbals can be used to servo the telescope optical axis to a star within the telescope field of view. The other two provide manual rotation of the telescope about its optical axis and rotation of the sextant prism.

When operating as a star-tracker, the computer provides slew information which points the telescope generally towards the selected star. Once rough orientation has been obtained, control is transferred to an optical sensor, similar to one of Autonetic's current autocollimator sensors, and a servo centers the telescope on the star.

In the optical system chosen, a rotating dove prism serves to rotate the line-of-sight from a star down to the lunar edge, or put opposite lunar diameters in apparent superpositions. The astronaut puts the star in coincidence with the lunar edge. The angle between the star and the lunar edge is then determined by this dove prism rotation; the astronaut can read-out information through an auxiliary optical relay system, in much the same way that one reads a modern theodolite. In order that the line-of-sight to the moon has the same number of reversals in the optical system, the moon is viewed through a fixed dove prism. Three mirrors are incorporated in the optical path as shown in Fig. J-2; these mirrors invert the image, and fold the optical system.

Finally, a portion of the light is split off to be used for automatic scanning while the remainder goes through the eyepiece to the astronaut. To further assist the astronaut in making precision settings, a complimentary color filter is provided. This filter can be removed manually, its operation causes an apparent color change as the star is brought in coincidence with the edge of the moon. Consider, for instance, that the optical path to the star passes green light, whereas the filter which allows sighting of the moon passes light with green deleted. It is then apparent that the superposition of the two images would cause a color change. Another possibility is a red filter for the moon and a cyan for the star. By this means, it is expected that the setting accuracy can be obtained someplace between the 1.5-minute resolving actuity of the human eye and the 12-second vernier actuity using perhaps 60 seconds as an estimate. Other considerations imposed a minimum focal length eyepiece at half an inch. A setting-precision approximating 2 seconds, dictates a 30-power system which, taking 1.5-inch diameter objective as a reasonable figure, gives a 15-inch focal length objective.

During the course of this study, it became apparent that the astronaut could be forced to rely entirely upon his sextant and velocity meter to exit from a lunar orbit. A considerable propulsion savings for subsequent corrections could be obtained with a precise alignment of the thrust axis to the stars. For this purpose, there is merit in having a bubble level within the field of view. Naturally, a bubble level only functions during acceleration; but this is precisely when it is required. Incorporation of a bubble level into the sextant should be investigated as part of the hardware program.

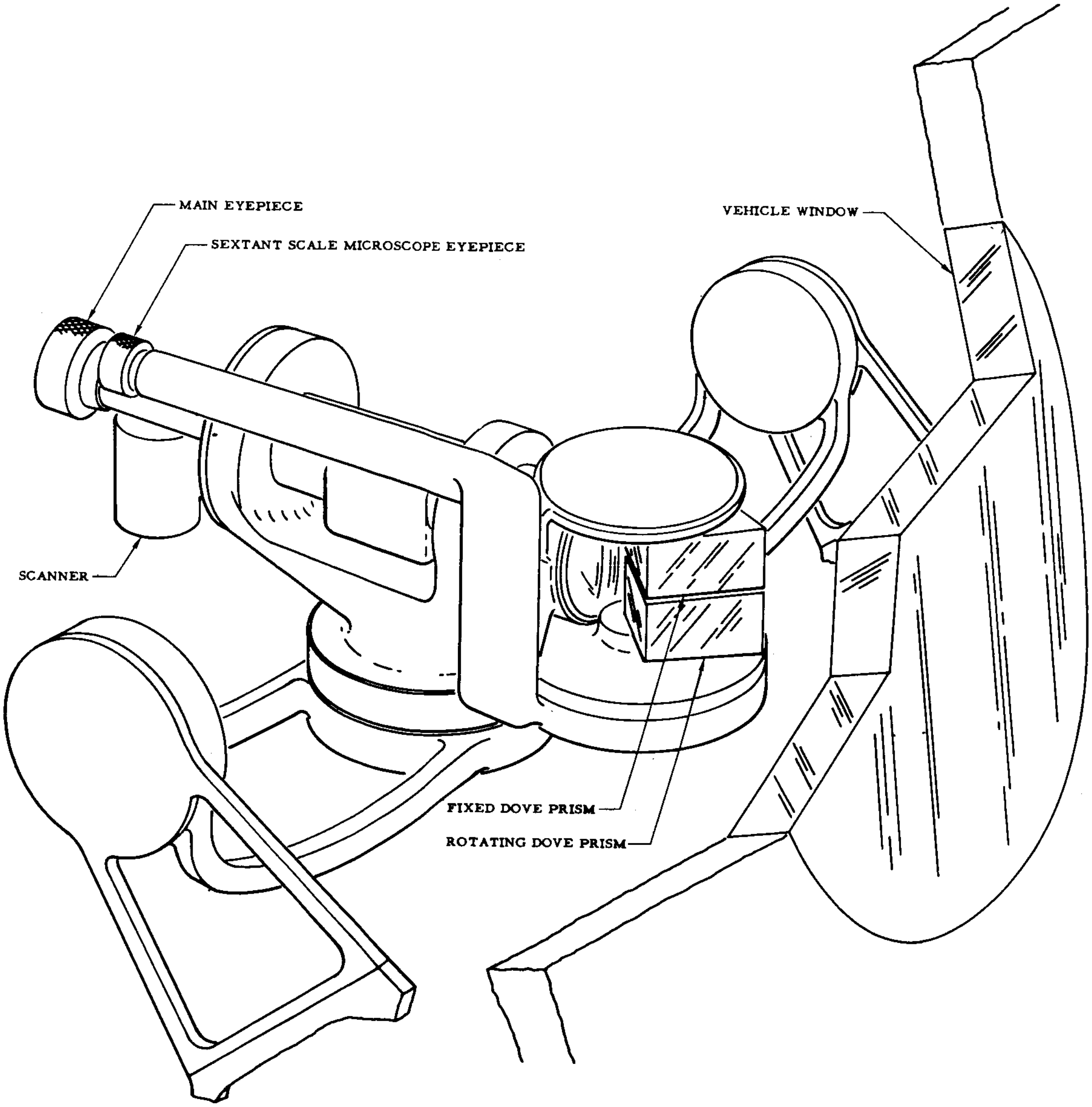
MAIN EYEPIECE
SEXTANT SCALE MICROSCOPE EYEPIECE
VEHICLE WINDOW
SCANNER
FIXED DOVE PRISM
ROTATING DOVE PRISM

Fig. J-1. Artist's Concept of Astronaut's Sextant

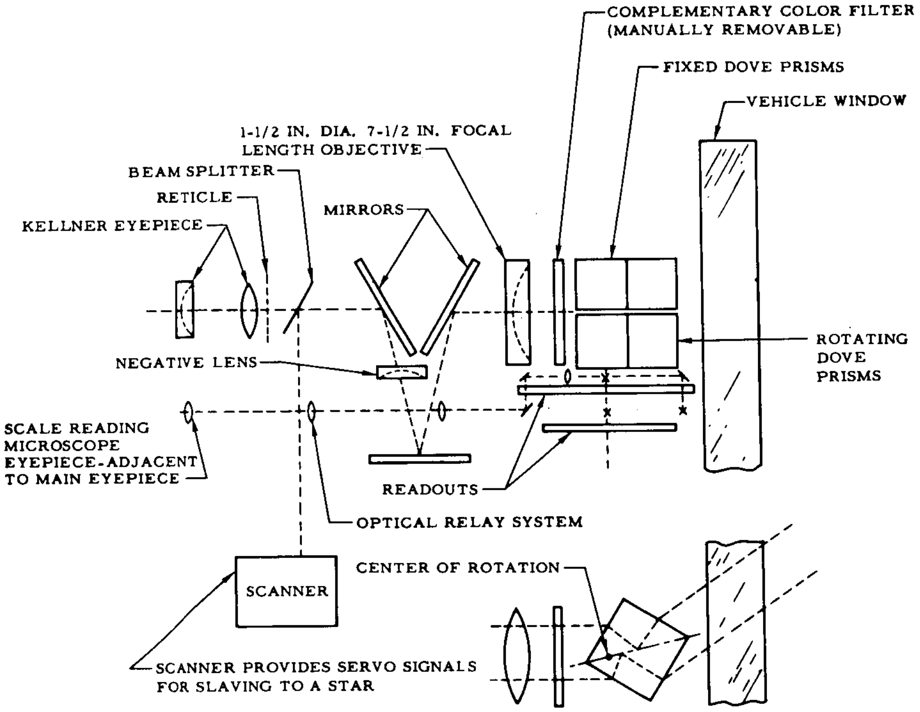
COMPLEMENTARY COLOR FILTER (MANUALLY REMOVABLE)
FIXED DOVE PRISMS
VEHICLE WINDOW
1-1/2 IN. DIA. 7-1/2 IN. FOCAL LENGTH OBJECTIVE
BEAM SPLITTER
RETICLE
MIRRORS
KELLNER EYEPIECE
ROTATING DOVE PRISMS
NEGATIVE LENS
SCALE READING MICROSCOPE EYEPIECE-ADJACENT TO MAIN EYEPIECE
READOUTS
OPTICAL RELAY SYSTEM
CENTER OF ROTATION
SCANNER
SCANNER PROVIDES SERVO SIGNALS FOR SLAVING TO A STAR

Fig. J-2. Schematic of Astronaut's Sextant Optics

APPENDIX K

ASTRO-SEXTANT (ARMA)

I. GENERAL

The astro-sextant is a device for optically measuring the angle subtended by two points in space. It differs from a conventional navigational sextant only in that it enjoys meticulous precision of manufacture and therefore entails greater accuracy in the angle reading device.

In determining an approach to ensure the utmost reliability in executing the midcourse portion of the Apollo mission, it was agreed that maximum utilization of the man and his integration with the overall guidance system should be effected. In employing this concept, both the functional and operational simplicity of manually operated equipment were considered of primary importance.

After evaluating various possible methods of obtaining midcourse navigational data, it was decided that the astro-sextant configuration would use identified stars and recognized lunar and terrestrial landmarks; this method offers the greatest potential in attaining initial goals of simplicity and reliability consistent with specified accuracy.

In selecting a company to participate in Arma's study to provide the technical information for this report it was decided, based upon the relatively limited time allotted to performance of this study, to contact one company whose background was of sufficient depth to be considered representative of the precision optical angle measuring instrumentation field. Kueffel and Esser has, for a number of decades, supplied standard theodolite components identical to those which would be used in the proposed astro-sextant. A description of this equipment is given below.

II. FUNCTIONAL DESCRIPTION

The instrument proposed measures the angle subtended at the observer's position by a known star and a known lunar or terrestial landmark to an absolute accuracy involving only 3-arc seconds overall error.

This instrument consists primarily of a precisely graduated arc and reading system, a star acquisition mirror, an image-combining prism, and a variable power telescope; these components are joined mechanically in a manner similar to the conventional navigator's sextant, with the entire assembly supported on a ball-socket joint. See Figure K-1.

III. PRINCIPLE OF OPERATION

It is an optical principle that, when a ray of light is reflected by two mirrors, it changes direction by twice the angle between the mirror surfaces. This change in direction is measured by the trace of the ray in a plane mutually perpendicular to the mirrors. Since the change in direction of the ray is affected only by the angle between the mirrors, simultaneous rotation of both mirrors in the plane perpendicular to them will not affect the change in the direction of the ray.

Figure K-2 shows the principle of the sextant. The aimer's eye is at (E). He sees the moon crater L through beam-splitter (H). In the beamsplitter (H) he also sees the star image (R) after two reflections. He adjusts the indexing mechanism (T) until the star acquisition mirror (P) is at the proper angle to make (R) and (L) both appear coincident, rotating the instrument about its optical axis until this coincidence occurs. When coincidence does occur, a time marker is transmitted by the observer to the computer. Before the next observation is made, the arc observer (M) records the arc angle. The sighting and time marking can be done by only one observer.

The actual angle between (R) and (L) is (Z). Angle (X) between the mirrors is equal to 1/2 (Z). Therefore, the graduated arc is numbered in values equal to twice the actual angle (X), so that the value of (Z) is read directly.

IV. QUANTITATIVE PERFORMANCE DATA

The sextant is graduated in arcs which can be read directly to 1-arc second. The aiming telescope will have maximum resolving power of 3-arc seconds, and variable power in steps of 5 x -10 x - 30 x. All reflecting surfaces will be flat to 1/4-wavelength. Filters will be provided in the optical system as required.

While the system will be capable of rendering an absolute accuracy of 3-arc seconds for a single observation; substantially better accuracies can be obtained by averaging several observations. The maximum value obtainable for angle (Z) will be 70°.

V. PHYSICAL CHARACTERISTICS

Weight:	Approximately 15 pounds.
Volume:	Contained within a cubic envelope measuring 10 inches on a side.
Power:	6 volts, 0.20 amperes, 1.2 watts.

VI. RELIABILITY INFORMATION

The instrument proposed is based upon a proven theodolite design currently used for making precision geodetic surveys throughout the world. It is expected that the mean-time between equipment failures would be measured in years.

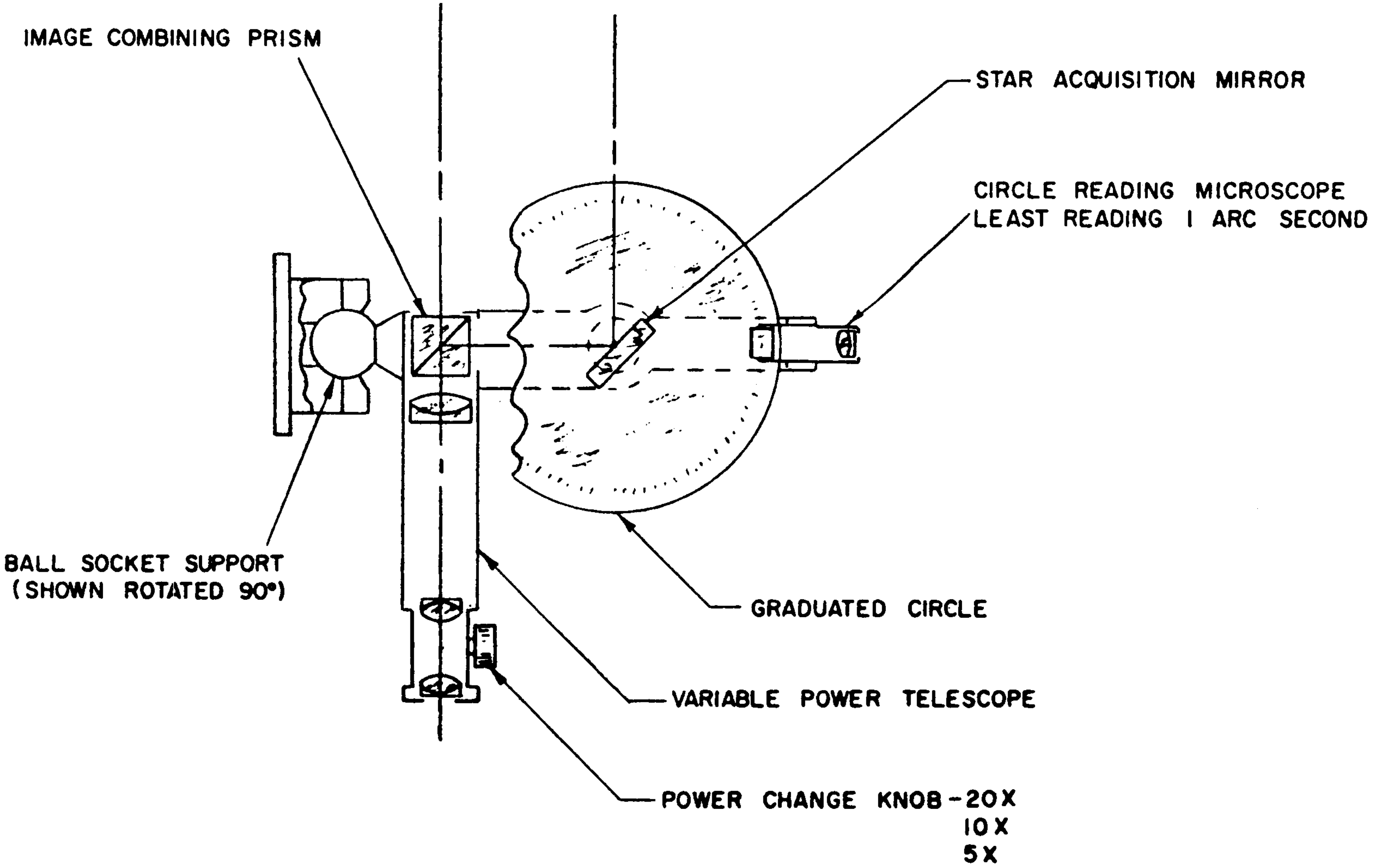
IMAGE COMBINING PRISM
STAR ACQUISITION MIRROR
CIRCLE READING MICROSCOPE
LEAST READING I ARC SECOND
BALL SOCKET SUPPORT
(SHOWN ROTATED 90°)
GRADUATED CIRCLE
VARIABLE POWER TELESCOPE
POWER CHANGE KNOB -20X
10X
5X

Fig. K-1. Astro-Sextant Assembly

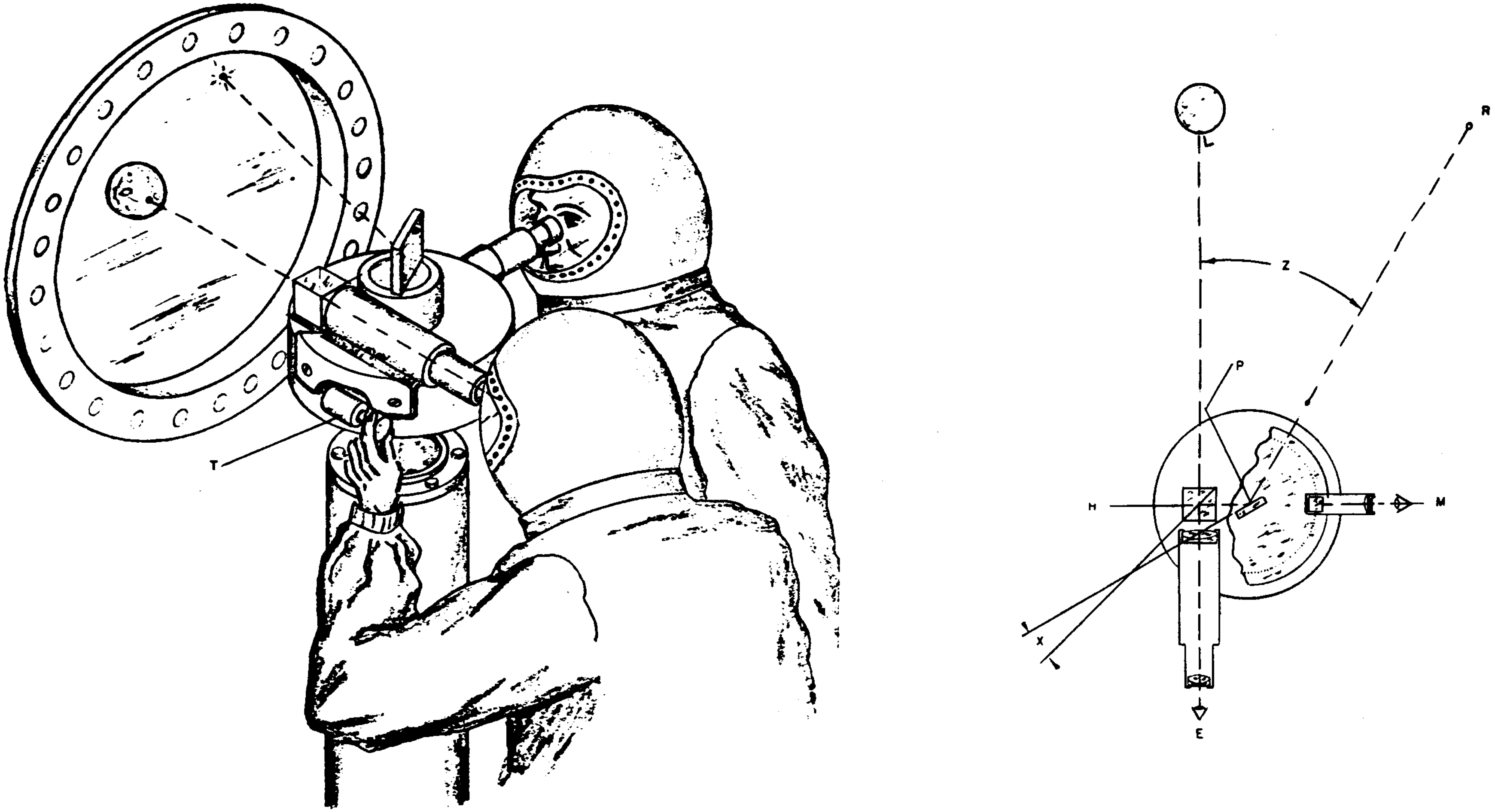
Q
T
L
R
Z
P
H
M
X
E

Fig. K-2. Principle of Astro-Sextant

APPENDIX L

DIGITAL COMPUTER (TEXAS INSTRUMENTS)

I. INTRODUCTION

The prolonged missions planned for Apollo place severe requirements on all parts of the system, and notably the guidance subsystem. This document describes an approach recommended by Texas Instruments toward the solution of the Apollo digital flight control problem. Basically, this approach requires the design of a digital system which 1) has the computational capabilities required by the various missions assigned to Apollo, 2) provides a significantly higher reliability level than currently existing systems, 3) is compact and consumes little power, and 4) may be produced at reasonable cost.

Texas Instruments believes that it has a unique concept for a system meeting these requirements.

This concept is based upon the solid circuit semiconductor network; this is comprised of functional electronic blocks developed and manufactured by Texas Instruments. In essence, these devices perform the functions of entire circuits, such as flip-flops, logic gates and amplifiers. Each device is constructed from a single small silicon wafer by a multistep process of diffusion, alloying, deposition and etching. When one compares the semiconductor network with a conventional component circuit, it is noted that the total number of manufacturing process steps involved is much smaller in the solid circuit semiconductor network. This factor, together with others named in this proposal, implies both higher reliability and lower ultimate cost in the case of solid circuit semiconductor networks.

A. ORGANIZATION AND FUNCTIONAL DESCRIPTION

To meet the requirements of the digital flight controller for Apollo, Texas Instruments proposes a high-speed, general-purpose digital computer having computational speeds greater than those of the IBM 704, 7090, and the Bendix G-20 computers. The Apollo digital flight controller will be a parallel machine, with an 18-bit word, operating asynchronously at an effective clock rate of 10 mc.

The following compares the basic Apollo digital flight controller cycle times with the corresponding cycle times of similar computers.

Comparison of:	Apollo (μ sec)	7090 (μ sec)	704 (μ sec)
Memory cycle	2.0	2.4	12.0
Add time	2.0	4.2	24.0
Multiply time	13.0	36.0	240.0
Divide time	15.0	41.0	265.0

So that a quick appraisal may be made regarding the running time of any given problem in the digital flight controller, consider that a fixed point instruction, including accesses, averages three microseconds. To be more specific, all instructions requiring operands (except multiply and divide) require the three microseconds; all instructions not requiring operands require about 1.5 microseconds; multiply and divide instructions require 13 to 15 microseconds. Obviously, certain routines needing many multiplies and divides would increase the overall running time. Actual experience has shown, however, that only a few routines of this nature will be required for Apollo; hence they are not considered in this proposal.

To indicate properly the rapid calculating ability of the proposed controller, the following comparisons are given (Table L-1). The front two categories (convolution and cross correlation) are listed to show the capability of the controller to perform integrations rapidly. The computers chosen were picked because of their reputation and are considered to be favorably representative of computing facilities.

One feature of the proposed digital flight controller is its ability to do high-speed integrations. To perform the three-velocity integration at a rate of 800 points per second throughout the flight will require approximately 12 locations in the working memory and will take about 60 milliseconds from each second of computing time available. Since this total time requirement represents six percent of the time available, it is felt that enough time is left for other needed calculations. Based on this high-speed integration feature, digital differential analyzer sections will not be required for Apollo.

An analysis of the Apollo guidance equations supplied by The Martin Company has been made and the running time of each of the subroutines computed. These times are given below. It is not clear to Texas Instruments what the exact linkages are between these subroutines and so we have not attempted to tie them together. It is believed that the computational speeds of the proposed controller will exceed the requirements of Apollo.

TABLE L-1

Comparison of Calculating Speeds of Apollo Controller and Other Computers (in Minutes)

Description of Problem	Apollo 2K*	IBM 704 8K	IBM 704 32K	IBM 7090 32K	BENDIX G-20 8K	BENDIX G-20 32K
Convolution of 8000 points of data						
250-point operator	1.7	19.0	19.0	3.8	10.6	10.6
700-point operator	3.9	52.8	52.8	10.6	31.0	31.0
5000-point operator	43.0	379.0	379.0	75.4	222.0	222.0
Cross correlation of 8000 points of data						
200-point delay	1.85	15.2	15.2	3.04	8.9	8.9
500-point delay	3.30	37.9	37.9	7.61	22.2	22.2
Simultaneous equations**						
200 x 300 floating point	65.0	133.0	120.0	24.0	78.0	70.0
300 x 300 fixed point	65.0	374.0	350.0	70.0	219.0	205.0

* Memory size (K = 1000 words)

** The time to do an equivalent size matrix inversion is very near the same.

Subroutines	Time in microseconds (N = number of times through the subroutines)
A	990N + 250
B	410N + 250
C	760N + 250
D	86N
E	578N + 840N (λ= 1,F)
F	594N
G	332N
H	80N

These running times will be slightly increased to accomodate the integrations as described in the paragraph above.

B. MEMORY

The working memory of the digital flight controller will contain 2048 18-bit storage locations. Of these, approximately 12 locations will be needed for the continual routine. The remaining 2036 locations will be used during each of the eight stages of flight. Transfer from bulk memory to main memory will be under program control and can be done more than once per phase.

Bulk memory will be provided for storing subroutines and other programming material. Based on the information supplied by The Martin Company, 8192 words of this memory will be required. Study of equations supplied by NASA indicates that 16,384 words are required for this bulk memory to meet their requirements.

So that integrations will be carried on at intervals spaced equally during each second, priority processing of the integration routine will be incorporated. This will allow for interruption of other routines when it is time for another set of integrations to take place. The 8192-word bulk memory will be a read-only memory which will be loaded prior to flight.

C. INPUT-OUTPUT

The Apollo digital flight controller must perform many arithmetic operations on data from several signal sources. Output information is generated by the digital flight controller and must be transferred from it to the appropriate signal sink, or output transducer. The requirements exist, therefore, for input buffering and format control so that the input data will be presented to the digital flight controller in a format suitable for the required operations. Format control must also be exercised between the digital flight controller and the output transducers. This is particularly true in the output data being supplied to the display subsystem.

1. Input Buffers

The approach that will be taken is one of assembling the input data into an input buffer unit which, upon command from the central controller, will dump the contents of the buffer into the working memory of the central controller. This process is quite similar to the execution of a read tape command in a computer system that used magnetic tape units. Figure L-1 is a block diagram of the digital flight controller with input and output buffer units attached. Input unit No. 1 assembles and places in proper format the clock signals, the X, Y and Z gimbal angles, the X, Y and Z accelerometer outputs, and the output from the data link. If analog-to-digital conversion is required for any of these signals, it will be performed in the input unit prior to assembly into format.

It is assumed that two data link words of 18 bits each will be read at each interrogation of the input unit. Also, the format of the words from the clock consists of three 18-bit words. Interrogation of input unit No. 1 will result in the transfer of 12 words into the working memory of the digital flight controller. This transfer will require approximately 300 microseconds and can be considered a simultaneous reading of all input data.

Input unit No. 2 is similar in operation to input unit No. 1. It differs only in the data it handles. It is assumed that 10 words of information will be read from the booster computer for abort monitoring, two words from the star tracker, and two words from the planet tracker, making a total of 14 words read on each interrogation of input unit No. 2. After the booster computer drops off, only four words of data will be read by input unit No. 2.

A third input unit is provided for scanning the contents of the keyboard for introduction of data into the central controller. This unit can scan the keyboard periodically and can transfer data present for introduction directly into the working memory.

2. Output Buffers

Output unit No. 1 provides the buffering between the central controller and the YES-NO outputs and the X, Y, and Z gyros. This unit receives from the central controller a block of data in a form analogous to a write tape command. The words are decoded and the appropriate relay energized if a YES-NO output is required, or the word is converted into a pulse rate for pulsing the gyros.

The function of output unit No. 2 is to buffer, in a fashion similar to output unit No. 1, the data from the central controller, the telemetry system and the output display subsystem. This output unit will also receive a block of information and do the necessary format conversion for output to telemetry or display.

D. ANALOG-TO-DIGITAL AND DIGITAL-TO-ANALOG CONVERTERS

1. Analog-to-Digital Converters

Two types of analog-to-digital converters are considered, voltage analog inputs and pulse-rate inputs. The voltage analog converter will make the analog-to-digital conversion by the successive approximation technique commonly used in this type of converter. Work at Texas Instruments indicates that the design and fabrication of such a converter utilizing semiconductor networks is entirely feasible. Converters that convert to an accuracy of 12 binary bits will probably be used. The complete converter will be of semiconductor networks, except for the precision resistors required to provide the comparison analog. The pulse rate analog converters will be essentially events-per-unit-time counters. An accurate time base will be established from the masterclock. This time base will be used for gating the input pulse train to a counter. This type of converter is also feasible using semiconductor networks.

2. Digital-to-Analog Converters

Two types of digital-to-analog converters probably will be required. These are digital-to-voltage converters and digital-to-pulse-rate converters. The digital-to-voltage-analog converter will be similar in function to the analog-voltage-to-digital converter described in the paragraph above. The design and fabrication of such a converter is a straightforward engineering problem. The digital-to-pulse-rate converter will be designed around the technique of using a binary word to set up the frequency of an oscillator. This technique is completely digital and is commonly used in digital programmers designed and built by Texas Instruments.

II. TIMING SYSTEM

The timing system for the Apollo digital flight controller is shown in the block diagram of Fig. L-2.

The oscillator is a crystal controlled type with the following characteristics:

Stability: 0.5×10^{-6} cycle per second per 14 days

Outputs: 10 megacycles and 100 cycles per second

Size: 5 inches by 5 inches by 3 inches

Weight: 2.1 pounds

Stability

10 percent change in input voltage: $0.5\text{x}10^{-7}$ cycle per sec

Ambient temperature change 25° C: $0.5\text{x}10^{-7}$ cycle per sec

10-g shock: $0.5\text{x}10^{-7}$ cycle per sec

Temperature: 0 to 55°C

Vibration: 10-g random and sine from 5 cycles per second to 2 kilocycles

The 10-megacycle output will be used for the digital flight controller timing signal, while the 100 cycles per second will be used to update the two time registers and the day register. The oscillator circuits will be of conventional components, while the countdown and the time registers will be semiconductor networks.

Twenty stages are required in the countdown to reduce the 10 megacycles to the 100-cycles-per-second signal used to update the time register.

The time register is divided into three separate registers for convenient entry of time data into the digital flight controller. The 10 millisecond pulses will be accumulated into time register No. 1, which consists of 12 bits. Overflow of this register will update time register No. 2 which is also 12 bits.

A game-on time register No. 1 and No. 2 will update the day register, since midnight does not correspond to full-time register.

A signal from the countdown gating will control time data entry into the digital flight controller.

Equipment necessary for synchronizing and loading Greenwich mean time into the timing section must be provided as part of the ground equipment.

Timing system specifications are as follows:

Size:	5 inches by 5 inches by 4 inches
Weight:	2.8 pounds
Ouputs:	10 megacycles stable to 0.5 in 10^{-6} cycle per second per 14 days Greenwich mean time in parallel binary form to 10 milliseconds ± 20 microseconds Readout control signal
Shock:	10-g
Vibration:	10-g random and sine from 5 cycles to 20 kilocycles
Temperature:	0 to 55° C

III. PACKAGING CONSIDERATIONS

Two critical factors that must be considered in packaging the Apollo digital flight controller are the protection of the semiconductor network and other circuit elements from shock and vibration and the removal of internally generated heat. Since the Apollo digital flight controller will generate only 0.056 watt per cubic inch of internal heat, heat removal will present no problem.

The following listing gives the volume-weight-power breakdown for the digital flight controller:

Volume	Weight	Power
1020 cu. in.	30.0 lbs	56 watts

The packaging of the rope memory presents a unique problem. The 128 tape-wound cores will be packaged in plug-in modules, 64 of which will make up the 8192 word memory. Each module is a slim cylinder. The cylinders are joined along their length by structural adhesive to form a rugged honeycomb assembly.

No effort will be made at this time to describe a form factor for the Apollo digital flight controller. It is felt that any form factor which does not require breaking the digital flight controller into more than three separate packages can be accomplished without an increase in volume over that listed. A desirable form would be a single rectangular box.

The weight, volume and power requirements of the keyboard and display subsystems have not been considered in making the volume, weight and power analysis. The shock and vibration requirements given for the timing system are expected to be the requirements for the entire digital flight controller.

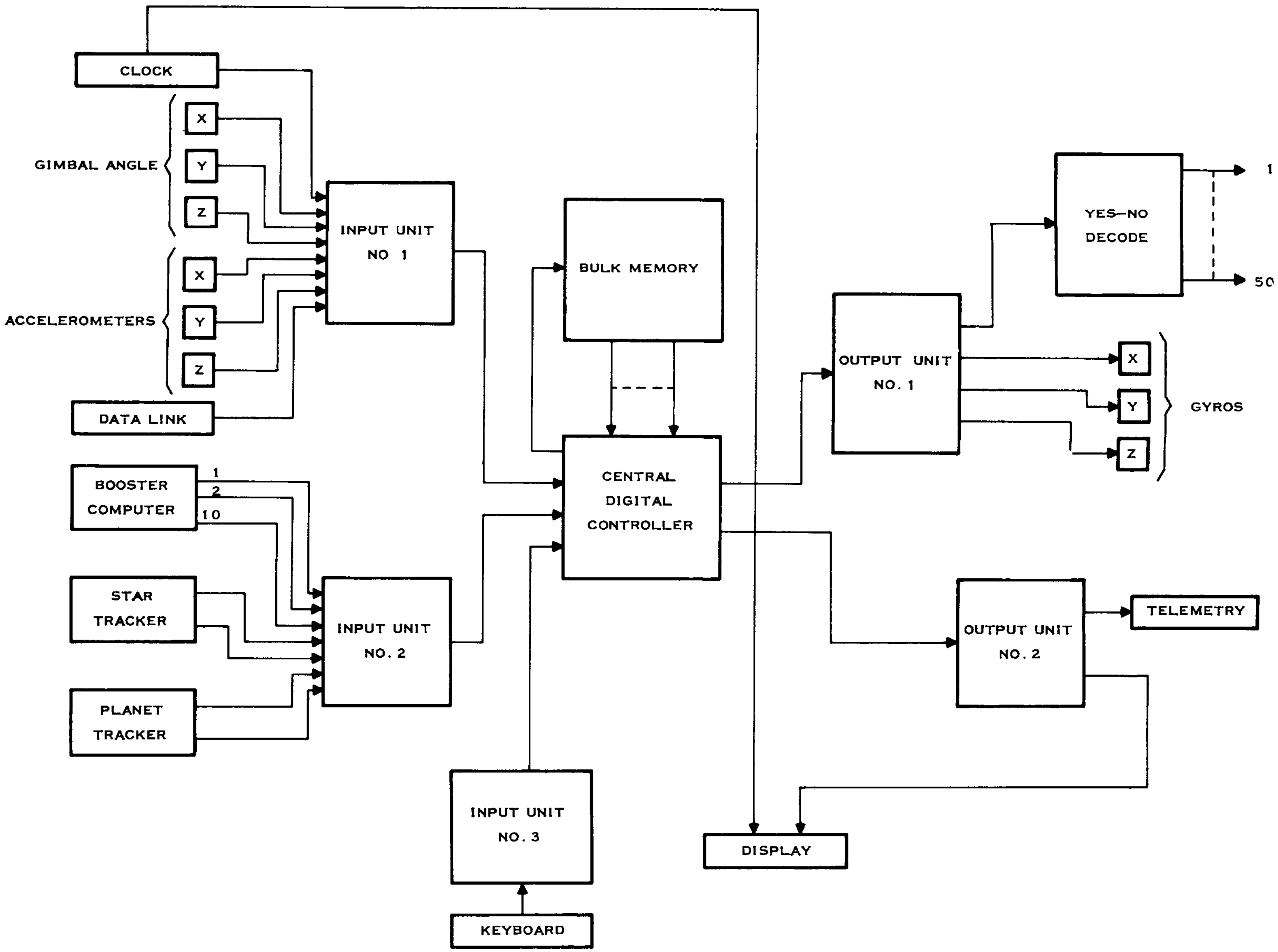
CLOCK
GIMBAL ANGLE
X
Y
Z
ACCELEROMETERS
X
Y
Z
DATA LINK
BOOSTER COMPUTER
1
2
10
STAR TRACKER
PLANET TRACKER
INPUT UNIT NO 1
INPUT UNIT NO. 2
INPUT UNIT NO. 3
KEYBOARD
BULK MEMORY
CENTRAL DIGITAL CONTROLLER
OUTPUT UNIT NO. 1
OUTPUT UNIT NO. 2
YES–NO DECODE
1
50
X
Y
Z
GYROS
TELEMETRY
DISPLAY

Fig. L-1. Apollo Digital Flight Controller Block Diagram

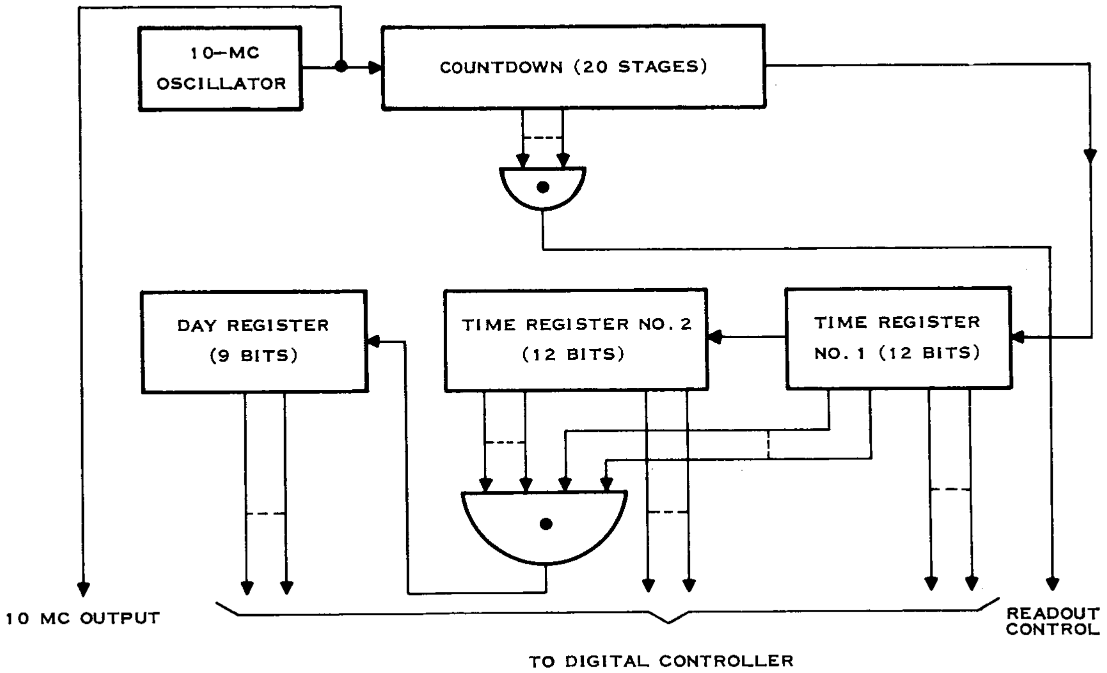
10-MC OSCILLATOR
COUNTDOWN (20 STAGES)
DAY REGISTER (9 BITS)
TIME REGISTER NO. 2 (12 BITS)
TIME REGISTER NO. 1 (12 BITS)
10 MC OUTPUT
READOUT CONTROL
TO DIGITAL CONTROLLER

Fig. L-2. Timing System for Digital Flight Controller

APPENDIX M

DIGITAL COMPUTER (LITTON)

A. STATEMENT OF THE PROBLEM

The Apollo vehicle is designed to provide for manned space flights with flight paths which orbit the earth, make single passes around the moon, or orbit the moon, and then return to the earth. Mission times may range from a minimum of hours to a maximum of 14 days. The computer must be capable of operating in a space environment.

The establishment of computer parameters has been investigated by Martin with respect to the guidance area only. Guidance techniques depend upon the computations of explicit guidance equations resulting from the establishment of two-body determined orbits which meet various geometric constraints. These orbit computations, for the various phases of the flight, are based on the execution of a proper combination of pre-established subroutines. The latter have been developed by Martin in some detail and served as the principal computer evaluation tool for this proposal. Litton has established the validity of the computer's capability for the Apollo application to provide ample margins of computing speed and storage capacity to cope with requirements of the various orbit computations involving these subroutines.

Present position during various phases of the flight is determined from a number of different types of input information. During thrust portions of the flight, either inertial or ground-based sensor information may be used. During nonthrust, or midcourse phases, observed residuals from stadiametric, occulation, or sextant measurements may be used to improve accuracy of orbit parameters. Presumably, reliable ground track residuals would also be used whenever these were available. All the available residual information is combined in a weighted, least-squares determination of corrections to an assumed Kepler orbit. In the terminal phases of flight, distance and velocity measurements determined by radar and/or optical tracking devices would be used for accurate position determination and velocity control. The computer is required to maintain an accurate star catalog and be capable of accurately positioning a star tracker so that useful occulation and sextant measurements may be made. The result of these calculations is the determination of a desired thrust vector and the establishment and control of vehicle attitude and thrust initiation, and duration to provide the required velocity and position correction.

As will be shown in the following sections, the most rapid calculations (those for boost, re-entry, and midcourse thrusting) are performed with more than adequate speed. Since the number and positions of midcourse corrections are not known, it is difficult to assess the accuracy of computation required to terminate thrust periods. However, the boost calculations, which certainly require more computation speed and accuracy than midcourse thrust termination, are performed at a rate of 10 complete calculations per sec. With quadratic extrapolation, this provides an accuracy of 0.015 ft per sec per calculation, or 0.4 ft per sec at cutoff. The time of initiation of engine cutoff is controllable to 100 μ sec. These accuracies are more than ample in view of the presence of midcourse guidance.

Two other major factors have been considered in the analysis of the Apollo problem, although these have not been specifically covered in information received from Martin. Litton, under a contract with WADD, is presently constructing a prototype of an integrated air-data sensor, inertial guidance system to effect the re-entry of an advanced Dyna-Soar type vehicle into the earth's atmosphere. This program has clearly shown the necessity for steering during re-entry to control dynamic pressure, temperature, L/D, angle of attack, angle of side-slip or other aerodynamic parameters to ensure survival of the vehicle and proper control over its landing point. These considerations have been taken into account in the design of the proposed computer to assure that it will possess the capability to perform these aerodynamic calculations.

B. COMPUTER SYSTEM DESIGN

1. General

As a result of analyses based on the considerations described in the previous sections, a computer configuration considered optimum for the Apollo Program has been developed. The basic design characteristics of this machine have been under active consideration at Litton during the past year. As a result, the computer organization has been undergoing development for a considerable period of time prior to the receipt of the Apollo requirements. A good deal of design time, therefore, has gone into the development of a computer with capabilities which are ideal for the mechanization of guidance and control tasks of the class required by Apollo.

The computer described in the following sections is a specially designed, high speed, serial, general-purpose machine which utilizes a large capacity magnetic drum memory and incorporates a versatile and programmable input-output system possessing an independent computing capability of its own. The characteristics of this computer and details of its organization are presented as follows:

2. Summary of Computer Characteristics

Construction Technique:	Welded wire
Volume	0.45 cu ft
Weight	35 lb

Power Consumption:	114 watts
Word Length	25 bits.
	23 bits plus sign plus parity.
Memory Structure:	8000 rpm magnetic drum.
	Two 1-word accumulator registers.
	Two 2-word, high speed, recirculating registers.
	One 4-word recirculating register.
	One 16-word recirculating register. With read heads at the 8 and 16-word points.
	Two 640-word recirculating registers for input-output.
	One 128-word track for input-output addressing, programming and control.
	Four 128-word tracks which may be loaded from an external source during computation.
	Four 128-word tracks with read/write provision during computation (to act as a scratch pad memory).
	Forty five 128-word permanent memory tracks with read provision only.
	Total addressable storage is 6,808 words.
Word Time:	58.6 μ sec.
Instruction Type:	One and one-half address. Command contains address of operand and sector or track address of next command.

Arithmetic Rates:

Add	117μ sec--8533 additions per sec.
Multiply	996μ sec--1004 multiplications per sec.
Divide	1641μ sec--610 divisions per sec.
Square Root	1641μ sec--610 square roots per sec.
Average of 4 Additions and One Multiply	293μ sec/per operations. Average command executive rate with this ratio of additions to multiplications is 3413 commands per sec.

Input Capability:

Discretes	Arbitrary number of discrete inputs. Each discrete input is stored as a one-bit in a word of the input line.
Fill During Compute	Four channels, each containing 128 words, are available for this purpose. These channels become permanent once the system is airborne. They can be filled only under ground control.
Information Flow During Compute	Sixty four input word buffer track. The words of these 2 tracks operate under control of an input-output program track. They may accept incremental input, whole-number input or discrete signal input. They may operate together to perform extrapolation operations for polynominal-type function generation during the output process. Two 2-word loops, each recirculating 8533 times per sec, provide accumulating and storage capability for input of digitized accelerometer signals and for the external frequency standard signals. The time-storage word of one loop is used for the countdown process required for accurate thrust cutoff.

Output Capability:	Sixty four words devoted to servos for whole-number type shaft encoders, incremental outputs and DDA-type extrapolations.
Reliability Estimate:	2200 hr mean time between failures.

C. COMPUTER EQUIPMENT DESIGN

1. Design Approach

The electronic and mechanical design of this computer is oriented toward the unique requirements of aerospace environments. Primary emphasis is placed on the achievement of high reliability although typical objectives of more conventional airborne designs, such as minimum size, weight, and power consumption, are also important considerations. However, in order to meet the requirements for aerospace reliability, it may be necessary to make some compromises in the latter objectives. For example, although the vehicle's use of solar cells may place a premium on power requirements, reliability considerations may dictate the use of other than minimal power consumption electronic techniques. Similarly, realistic analysis of cooling requirements may indicate the necessity for thermal devices which increase both size and weight.

The availability of previously developed systems provides a realistic basis for meeting the development and fabricating schedule requirements of one Phase I computer. Well-established electronic and packaging techniques will ensure that the first computer will have the inherent reliability required for applications of this type.

2. Computer Configuration

The mechanical design of this computer is oriented toward the unique requirement of aerospace environments. Primary emphasis is placed upon the construction of adequately cooled equipment which will provide the highest reliability with a minimum of size and weight. Serviceability features are provided, but they have not been expanded at the expense of reliability or size.

The proposed Apollo Computer will consist of welded wire circuit modules, laminated wire harnesses, a magnetic memory drum, heat dissipation and a round sheet metal outside cover. The assembly of these units is shown in Fig. M-1. Note that two layers of welded wire modules are separated by a heat conductor latch plate. The modules attach to the plate through a hook and latch arrangement. The modules are each constructed with a flange-type hook. The latch plate is a pair of scissor-action grates which serve to latch the module hooks (refer to Fig. M-1 for details). The module circuit pins are soldered to laminated wire harnesses at the outside top and bottom. For servicing, the latch can be opened and the whole layer of modules removed at one time. When assembled, the modules at one end are held firmly in place by the latch connection and at the other end by the soldered connections.

The drum memory occupies the lower half of the package. The drum, in addition to performing its memory function, also serves as a heat conductor and main structural member. The bottom plate provides the interface to a cold plate heat sink. The heat generated by the circuit modules is conducted to the latch plate which, in turn, carries the heat to the shroud end; hence, to the cold plate. The drum beat carries directly to the shroud and to the cold plate.

The outer cover fastens down with an hermetic seal to protect the electronics from contamination and also to entrap the air utilized by the floating magnetic drum heads.

3. Size, Weight and Power Requirements

The physical components are listed in Table M-1. The size of the welded wire circuit modules is expressed in terms of "running inches" rather than the number of modules. This is an expression peculiar to the welded wire technique and reflects the repeatability of the process. The total weight indicated is 35 lb, and the volume is 0.45 cu ft. The power requirements are 76 watts dc, and 38 watts ac.

4. Cooling

The primary mode of heat dissipation from the computer is conduction. Very little heat is dissipated by radiation because of the relatively low temperature and small temperature differentials which exist within the computer. Heat dissipation by natural convection is considered negligible. It is assumed that the computer unit will dissipate its heat to a cold plate (infinite heat sink) which is maintained at a constant temperature within the normal operating range specified for such devices in present spacecraft designs.

Heat generated in the components of the welded wire modules is transferred (by conduction) through their leads and the encapsulating material surrounding them to the module shell. This heat is then transferred to the conduction plate upon which the modules are mounted. The drum shroud acts as the thermal path along which this heat is transferred from the conduction plate to the drum base plate. The drum base plate, in intimate contact with the cold plate, dissipates all the heat generated within the computer to this cold plate. Heat generated within the drum is transferred through its structure to the cold plate.

There is always the possibility that the computer cover may absorb heat from other equipment and/or from a high external environmental temperature condition. Heat absorbed from either or both of these sources will be transferred to the cold plate directly from the cover. To ensure this condition, the

TABLE M-1

Electronic Complement and Physical Dimensions

Circuit or Assembly	Number of Circuits	Power (watts)	Running Inches of Module	Volume (cu in)	Weight (lb)
1. Circuits:					
Flip-flop	67	22.1	41.9		
Read amplifier	20	6.2	15.0		
Write amplifier	11	10.2	4.1		
Write head switch	9	1.7	1.1		
Master clock Generator	1	1.4	1.0		
Logical pulse Amplifier	7	3.1	7.0		
Inverting amplifier	16	2.1	4.0		
Noninverting Amplifier	54	4.9	13.5		
Read head switch	53	1.3	6.7		
Logic	2000 diodes	10.0	100.0		
Subtotal		63.0	194.3x(0.9375)*=182		$\frac{194.3}{1728}(90)^{**}=9.5$
2. Regulator:		13		16	1.5
Latch plate				18	2.0
Laminates (7)				28	2.0
Connectors and misc.				50	3.0
Subtotal		13		112	8.5
3. Drum:		38(ac)			
Shroud and base plate					
Subtotal		38(ac)		295	15
4. Cover				191	2
Total		114(38ac + 76dc)		780	35

*0.9375 = Cross-sectional area of the Litton standard welded module config.

**90 = Pounds per cubic feet of welded modules.

cover is isolated as much as possible from other computer structures except the drum base plate. Heat transfer by radiation from the cover to other structures is minimized by the use of a low emissivity surface finish on the inside surfaces of the cover.

A preliminary thermal analysis of the computer indicates that all components will be maintained at reliable operating temperatures by dissipating the heat generated along the conduction paths described above.

5. Welded Wire Modules

The welded module construction which is to be used in the Apollo Computer has been chosen as the optimum choise considering weight, reliability and established technology. The spot-welding technique eliminates the majority of solder connections and also minimizes the amount of heat applied to components during fabrication. A major advantage of welded modules is that optimum miniaturization can be obtained with standard size components. This means that circuit redesign is not required in order to accommodate special or limited circuit element parameters peculiar to the packaging technique. Furthermore, welded-module production techniques are currently available. Litton is presently incorporating welded circuit modules into a military drum memory subsystem. Hence, in addition to the various mechnical and fabrication advantages, welded construction offers the quickest and least expensive method of obtaining proven miniaturization.

6. Typical Circuits

A complete set of silicon circuits is available for application to the proposed computer. Representative of these circuits are the flip-flop, clock generator and drum circuitry.

The flip-flop shown in Fig. M-2 is designed to operate at clock rates up to 1 mc over an ambient temperature range of -55°C to +100°C. Characteristics include a fan-in of 20 OR gates plus 10 AND gates. The output is capable of driving 12 gates plus 200 $\mu\mu f$ of stray capacitance. The circuit utilizes high frequency transistors and features a two-capacitor delay network at the base of the amplifier transistors to provide precise control of time delay (which prevents double triggering) without consuming excess propagation time. Recently developed epitaxial transistors are used for the output amplifiers. These transistors offer significant improvements in saturation voltage and switching speed at higher current levels.

The clock generator circuit shown in Fig. M-3 provides the basic timing signal for the entire computer. The pulse width is 0.2 μ sec with the maximum repitition rate being 650 kc over an ambient temperature range of -55°C to + 100°C. Pulse amplitude is 4 volts, and typical rise and fall times are 0.025 μ sec. A delay line is the basic element in determining pulse width. This circuit is capable of driving a 100-ma load that consists of repeater amplifiers distributed throughout the computer.

The read amplifier shown in Fig. M-4 is typical of the memory circuitry. This circuit is designed to amplify and shape the signal obtained from a contact type drum read head. Using Ferranti recording, the bit rate may be in the range of 200 to 500 kc. Under worst case conditions, the magnitude of the input signal is between 0.1 and 0.8 volt. When fully loaded, the output signal is symmetric within 5%, and the maximum phase shift of 0.75 μ sec.

D. RELIABILITY OF THE COMPUTER

An estimate of the inherent reliability index attainable for the computer is approximately 2200 hr mean time between failures. This estimate is based on the failure rates shown in Table M-2. It should be noted that these failure rates are not the ones which are being experienced for parts in the field today. They are based on the following assumptions:

(1) Internal environment of the computer will be designed such as to minimize catastrophic failure rates.

(2) Semiconductors will all be silicon.

(3) Semiconductors will be those which can be bought in the 1963 to 1965 era, and will exhibit catastrophic failure rates equivalent to the goals of present component part reliability programs, such as the program on Minuteman.

(4) All failures which can result from drift or parameters of parts due to environment, life, manufacture and assembly will be designed through the use of sufficiently wide safety margins in the design of circuits.

(5) There will be only digital circuits in the computer. In addition, the computer failure rate is calculated on a series basis; that is, a failure of any part causes computer failure. By the reduction of part failure rates to the minimum catastrophic failure level, the predicted computer mean time to failure of 2200 hr can be achieved, see Table M-3.

TABLE M-2

Part Failure Rates Used for Apollo Computer Reliability Estimate

Part Time	Predicted Catastrophic Failure Rate (parts/10^6 hr
Transistors	0.1
Diodes	0.02
Capacitors	0.02
Resistors	0.001
Drum and heads	200
Wire and weld failure rate	0.05/component part

NOTE: Other components are not included in this estimate, because their total failure rate would account for less than 0.5% of the total estimated computer failure rate.

TABLE M-3

Apollo Computer Reliability Estimate

Circuit Reliability

Circuit	Transistors	Diodes	Capacitors	Resistors	Gross Failure Rate (parts/ 10^6 hr
Flip-flop	4	6	2	12	0.57
Dual inverting amplifier	2	8	0	7	0.37
Noninverting amplifier	2	5	0	5	0.31
Logical pulse amplifier	1	3	1	4	0.19
Clock generator	6	18	7	21	1.12

TABLE M-3 (cont)

Circuit Reliability (cont)

Circuit	Transistors	Diodes	Capacitors	Resistors	Gross Failure Rate (parts/ 10^6 hr
Read amplifier	5	12	5	12	0.85
Write amplifier	2	2	5	10	0.35

Computer Reliability

Circuit or Assembly	Number Used	Circuits or Ass'y Failure Rate	Gross Failure Rate (parts/10^6 hr
Flip-flop	65	0.57	37.1
Dual inverting amplifier	30	0.37	10.1
Noninverting amplifier	35	0.31	10.9
Logical pulse amplifier	2	0.19	0.4
Clock generator	1	1.12	1.1
Read amplifier	7	0.85	6.0
Write amplifier	6	0.35	2.1
2000 Logic diodes		0.02	40.0
Drum and heads	1	200	200.0
Wire-weld failure rate			145.6

Total Computer Failure Rate: 453 parts/10^6 hr MTBF ≈ 2200 hr

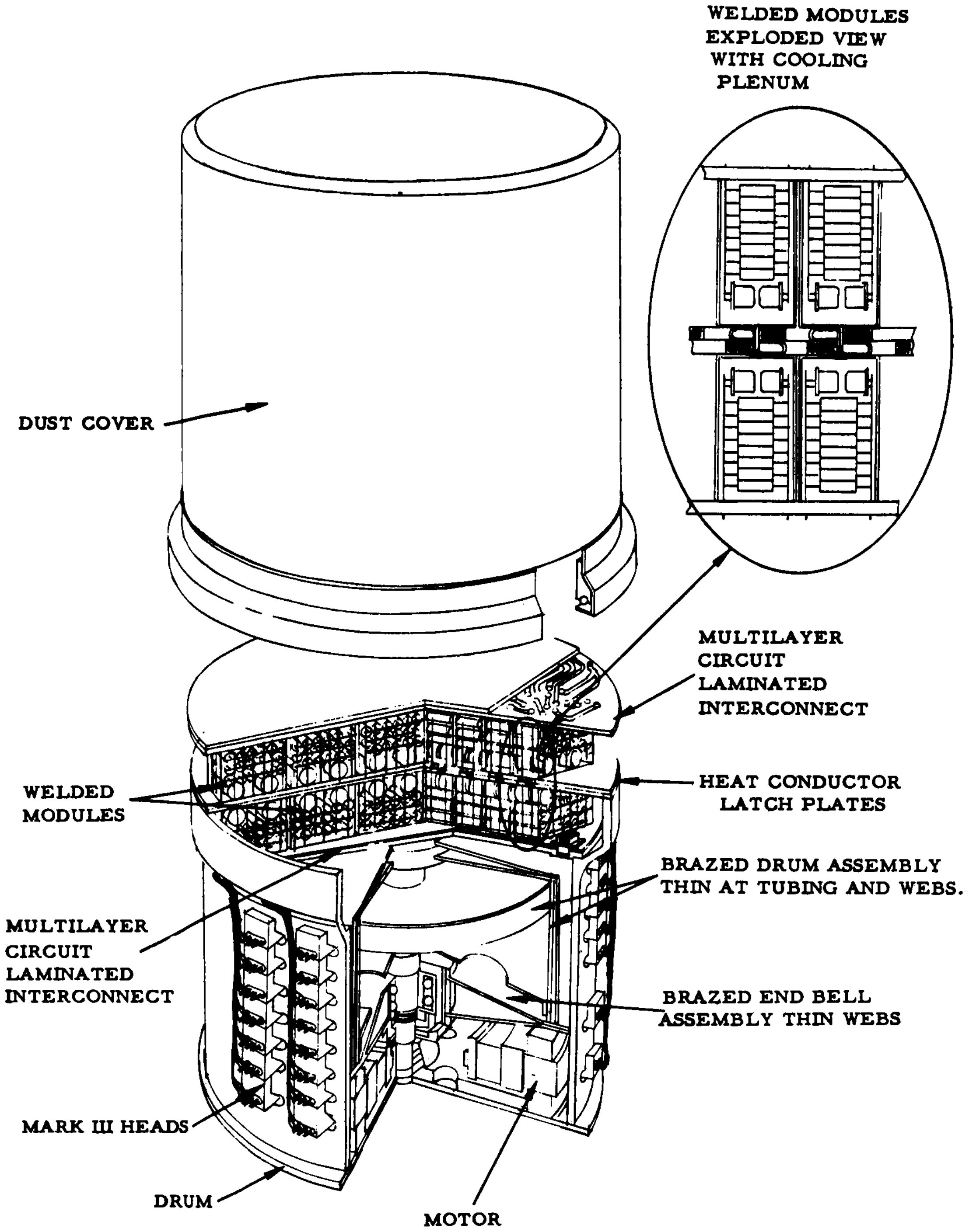
WELDED MODULES EXPLODED VIEW WITH COOLING PLENUM
DUST COVER
MULTILAYER CIRCUIT LAMINATED INTERCONNECT
WELDED MODULES
HEAT CONDUCTOR LATCH PLATES
BRAZED DRUM ASSEMBLY THIN AT TUBING AND WEBS.
MULTILAYER CIRCUIT LAMINATED INTERCONNECT
BRAZED END BELL ASSEMBLY THIN WEBS
MARK III HEADS
DRUM
MOTOR

Fig. M-1. Apollo Computer Packaging Configuration

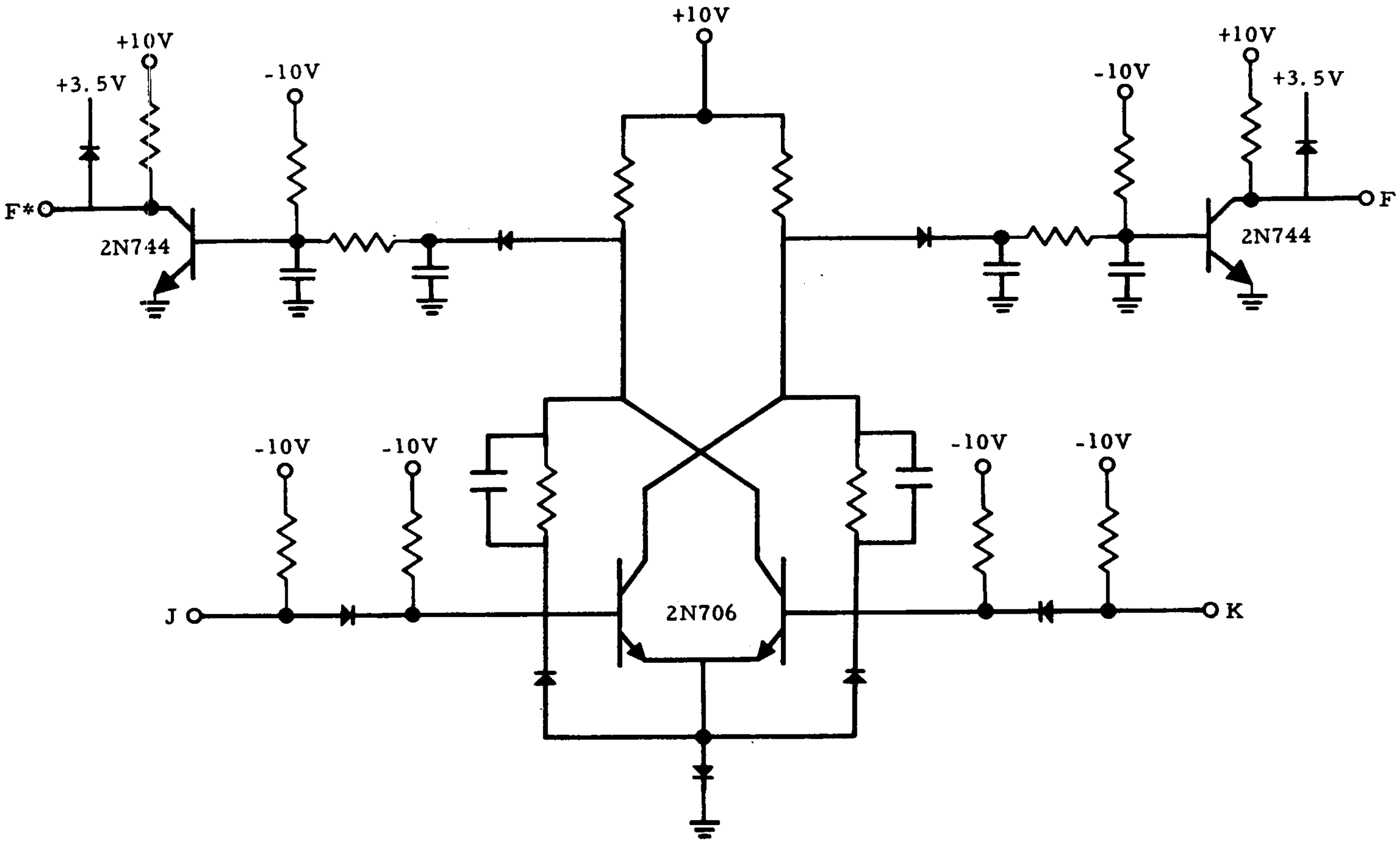
+10V
+3.5V
+10V
-10V
F*
2N744
-10V
-10V
-10V
J
2N706
-10V
-10V
K
-10V
+10V
+3.5V
F
2N744

Fig. M-2. Flip-Flop Circuit Schematic

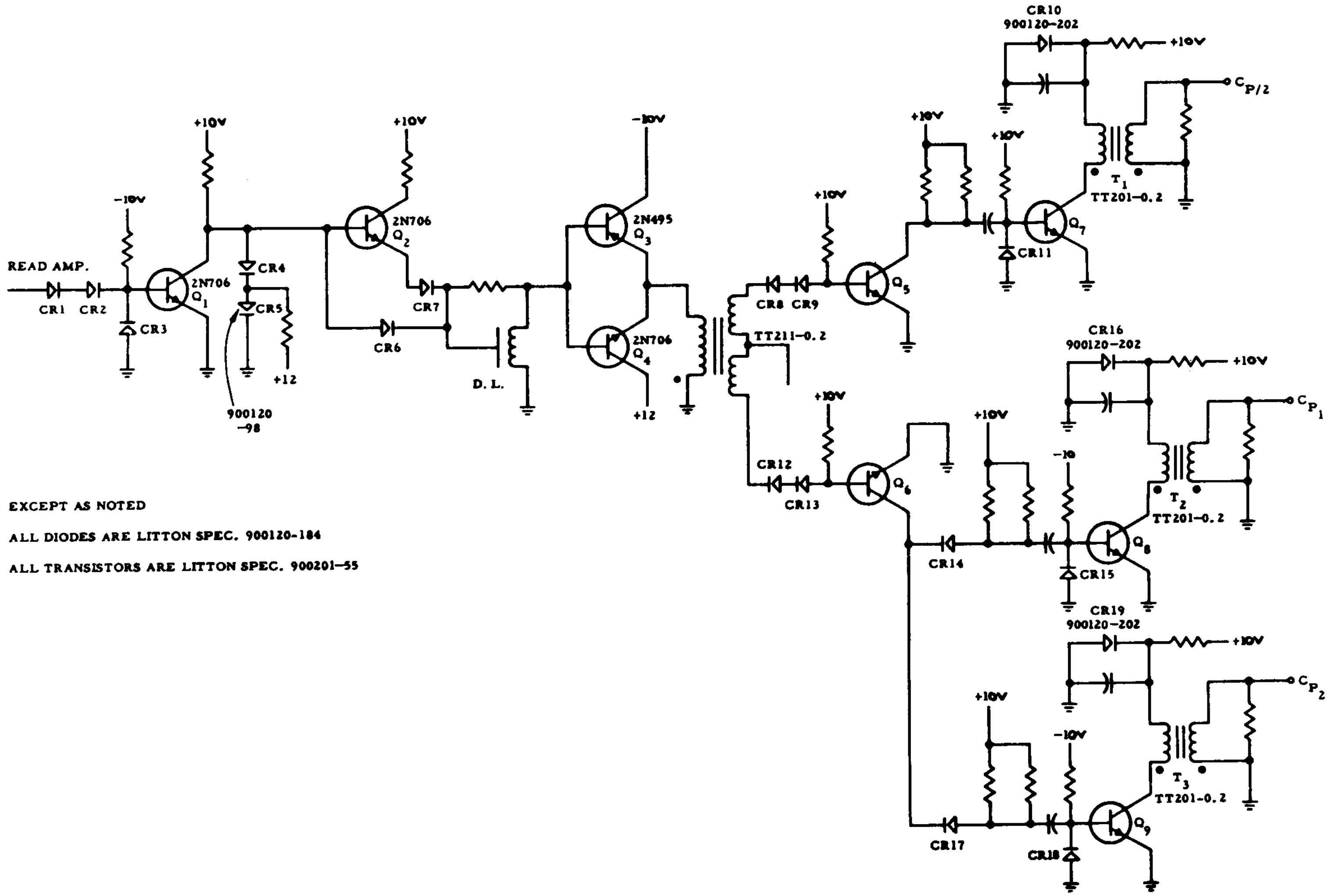
READ AMP.
CR1
CR2
CR3
-10V
+10V
2N706
Q_1
CR4
CR5
900120
-98
+12
+10V
2N706
Q_2
CR7
CR6
D. L.
-10V
2N495
Q_3
2N706
Q_4
+12
TT211-0.2
CR8
CR9
CR12
CR13
+10V
+10V
Q_5
Q_6
+10V
+10V
+10V
CR11
Q_7
CR10
900120-202
+10V
T_1
TT201-0.2
$C_{P/2}$
+10V
CR14
-10
CR15
Q_8
CR16
900120-202
+10V
T_2
TT201-0.2
C_{P_1}
+10V
CR17
-10V
CR18
Q_9
CR19
900120-202
+10V
T_3
TT201-0.2
C_{P_2}

EXCEPT AS NOTED

ALL DIODES ARE LITTON SPEC. 900120-184

ALL TRANSISTORS ARE LITTON SPEC. 900201-55

Fig. M-3. Clock Generator Circuit

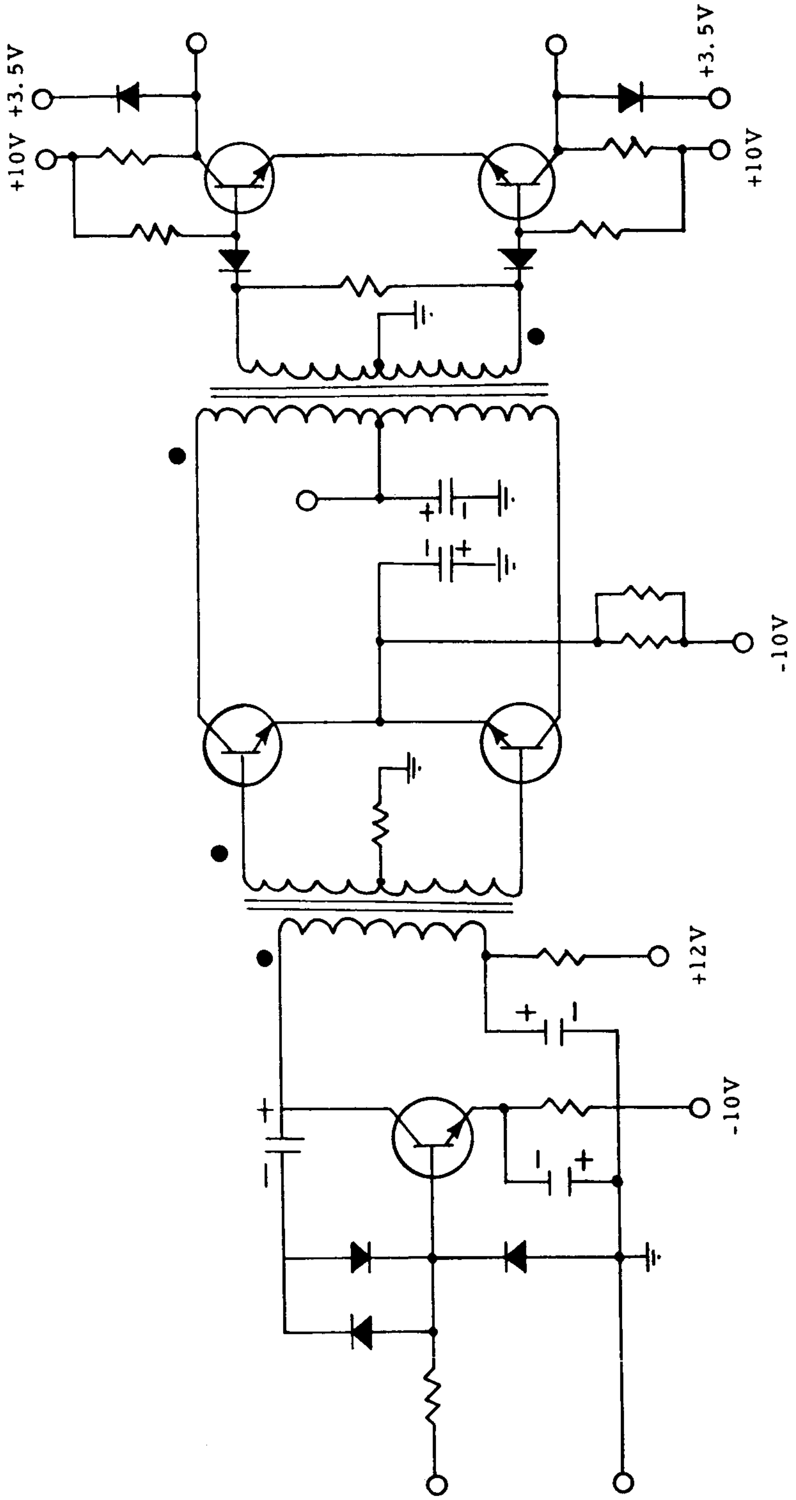
+10V
+3.5V
+3.5V
+10V
-10V
+12V
-10V

Fig. M-4. Read Amp Circuit

APPENDIX N

DIGITAL COMPUTER (IBM)

A. INTRODUCTION

A computer for the specific purpose of the Apollo mission must be capable of solving all the guidance problems for:

(1) Boost guidance

(2) Cislunar navigation

(3) Lunar approach

(4) Injection guidance for moon orbit

(5) Return trip navigation

(6) Earth approach

(7) Re-entry steering

The variety and magnitude of these problems generally defines the computer system which is required. The COMPASS III computer possesses these characteristics.

B. COMPUTER DESCRIPTION

1. Computer Organization

COMPASS III is a serial, complete-value, stored program digital computer. It employs a random access, non-destructive memory and a serial arithmetic element which operates on 2 bits in parallel. The basic timing period is 2.0 μsec. The computer logic is based on a 4 clock system, with each clock pulse being 0.5 μsec in duration.

All input-output is handled directly by the computer on a sub-routine basis. All I/0 data is stored in the non-destructive computer memory. Special input-output instructions will expedite processing of the I/0 data.

The random access, non-destructive memory will be organized in a sectored arrangement so that the memory size can be increased by adding additional sectors.

The computer is organized in a configuration which is readily adaptable to the use of redundancy techniques. Some form of redundancy will be required to meet the extreme reliability requirements of advanced space systems.

TABLE N-1

Summary of COMPASS III
Characteristics

Type:	Stored Program Serial, Binary, Fractional
Memory:	Size variable for sectors of 768 words - Proposed size is 4 sectors with addressing for 8 sectors. Memory word length - 28 bits Random access, Nondestructive read-out 4 bits at a time 2 instructions per word Read-write cycle - 4 μ sec
Arithmetic:	Serial by 2 bits parallel Add-Subt. Time - 54 μ sec Mult. time - 286 μ sec Divide time - 1026 μ sec Sq. Root time - 990 μ sec Shift time - 54 μ sec (20 places maximum) (Operation times given, include instruction access time.)
Accuracy:	27 bits plus sign

Physical Characteristics: TMR Computer

Power;	75 watts
Weight;	60 lbs
Volume;	1.1 cu ft

2. COMPASS III Timing And Control

The basic computer cycle is composed of 9 bit times. Each 2-μ sec bit time is divided into 4 clock times. A multiple clock system is used to facilitate time-shared logic.

A computer instruction syllable consists of the following bits: $0_1\ 0_2\ 0_3\ 0_4$ $A_1\ A_2\ A_3\ A_4\ A_5\ A_6\ A_7\ A_8\ A_9\ A_{10}$. Memory addressing is completed by the sector code which is stored in latches and remains the same until changed by a specific instruction.

Two instruction syllables are stored in each memory location. The memory location of the next instruction is determined by the instruction counter and the sector code. The syllable to be chosen is determined by a syllable latch (S) whose state remains fixed and can only be changed by instruction.

3. COMPASS III Control Cycles

There are 3 types of computer cycles. Each cycle is a multiple of the basic 9 bit word time (18 μ sec).

a. Instruction cycle

The instruction cycle is an 18 μ sec interval that provides selection and decoding of the next instruction.

b. Logic cycle

The logic cycle is an 18 μ sec interval that is used primarily for decision and instruction address modification.

c. Arithmetic cycle

The arithmetic cycle is a variable length cycle that varies in steps of 18 μ sec. This cycle is used to perform the arithmetic operations.

4. Arithmetic Processing

The computer has 2 serial arithmetic processing units consisting of an adder-subtracter and accumulating register. These dual units perform arithmetic 2 bits at a time. All arithmetic is performed in 2's complement form. Figure N-1 illustrates the data flow within the computer.

To achieve the multiplication speed required by this application, a 4 parallel by serial arrangement will be used. The recursion formula used provides for multiplication of two serial numbers where negatives are stored in complement module two form.

Divide and Square Root will be performed by a standard, nonrestoring serial divide-square root procedure.

Shifting right or left up to 20 places can be accomplished by one instruction.

The input/output instructions provide for reading into or out of the accumulator. These I/0 words can vary in length up to 28 bits maximum.

An input/output instruction allows a binary number from the addressed input location (device) to be subtracted from a number stored in the similarly addressed memory location. The number representing the binary difference will be made available as an output to the addressed device. This number is suitable for driving digital hydraulic devices or for conversion to an analog voltage.

5. Memory Organization

The memory is organized to give economical instruction storage. This is realized by dividing the memory into a number of sectors. The addressing capability is limited to a single sector, thereby reducing the number of address bits required in the instruction. A special operation can select any point in any sector for the next instruction. The sectors of COMPASS III contain 768 words each. The computer is able to address 8 sectors, but is planned to consist of 4 sectors in the suggested size.

An additional memory block called the residual memory is provided for communication of data generated in one sector and used in another. The residual memory is common to all sectors and is randomly addressable from all sectors. The residual memory size for COMPASS III will be 256 words.

Each instruction must be capable of addressing all the words in a sector plus the residual memory; i.e., 768 + 256 words or a total of 1024 words. This requires 10 bits of addressing capability. Since 4 bits will be used for operation code, each instruction will contain a total of 14 bits. With the data word for COMPASS III set a 28 bits, two instructions can be contained in each memory address. Information pertaining to the sector or syllable of the next instruction is not included in the standard instruction. This information is contained in registers and can only be changed by the special instruction as mentioned above. (The first or second syllable defines which of the two instructions of a given memory word is to be used.)

6. Physical Characteristics

The physical characteristics for the COMPASS III computer which are given in table N-2 are representative of a completely TMR computer (memory and arithmetic). The characteristics of a non-redundant computer can be approximated by taking 1/3 of the TMR values.

The volume of the computer plus the frame will be approximately 1.1 cu ft. The dimensions of a typical frame to house the computer and memory would be 19 in. x 15 in. x 6 1/2 in.

TABLE N-2

Weight Estimates

Potted cores	25.0 lb
Memory electronics	3.1 lb
Arithmetic electronics	6.3 lb
Harness and connectors	3.0 lb
Frame and misc.	13.5 lb
Input/output	9.1 lb
Total weights	60.1 lb

C. INPUT/OUTPUT CHARACTERISTICS

A cursory study of the input/output requirements for the Apollo space guidance system indicates that a variety of input/output devices will be necessary. This requirement is compounded by the displays and controls which must be provided for the passengers in the capsule. The redundancies in the system, required to achieve the high system reliability, also contribute their part toward requiring additional inputs.

1. Inertial and Stellar

To provide input data to the computer during the boost phases of the mission, some type of inertia measuring unit (IMU) will be required. Sensitive measuring instruments, mounted on a gyro stabilized platform, will sense acceleration of the vehicle and send this information to the computer. The position of the platform is continually monitored by the computer. Motion of the platform itself is interpreted by reading disc encoders or optical devices called optisyns, or both. The computer can furnish pulses to the platform to restore it to its initial reference position.

The IMU is very accurate for measurements of altitude and acceleration over short intervals of time. For long periods of time, however, some alternate method for determining vehicle motion and position may be desirable. Another gyro-stabilized platform, containing a telescope or other optical tracking device, will be considered. The tracking device is pointed by signals from the computer and then tracks the star (or other body) automatically. The telescope position is read out through a disc encoder or optisyn so the computer can monitor the star's position. The tracker is programmed by this computer to monitor the first star, slew to another star and monitor it. The number of stars to be tracked depends on the accuracy required and nature of the navigation scheme.

For additional system stability and input, a sighting platform is to be provided for manipulation by the passengers. This platform will contain a telescope, sextant, or other optical devices which can be operated by the crew. Pointing angles of the telescope will be read in to the computer from disc encoders.

The data from the stable platforms will be presented to the computer in a variety of forms. Consequently, each input will require some buffering or interpreting to make it compatible for entry into the computer.

The accelerometers will have a pulse rate output which will require a counter for each parameter entered. Each counter will be read into the computer on demand. After read in, the counter will be reset and counting will continue until the next read-in time. The rate at which the I/O subroutine is performed will govern the physical size and capacities of the counter.

The gimbal angle incremental read out will come from 2 bit optisyns. This information must be converted from Gray code to a two-digit binary number. These increments are accumulated in a register until read-in to the computer as explained above.

The torquing pulses will be generated as a function of the I/O subroutine. Pulses can be emitted at rates dependent on the number of times the I/O subroutine is performed during the computation cycle.

The pointing angles of optical tracking or fix-taking devices will be obtained from a disc encoder. This data will be decoded and utilized by the computer as programmed. An error signal is generated by subtracting the decoded disc value from the desired value stored in the computer. The error signal must be be converted from a digital number to an analog signal and used to drive the optical device to the desired position.

The sighting platform will be slaved to one of the above platforms and therefore will not require communication with the computer for stabilization.

2. Chronometer

Solution of the guidance equations will require an extremely accurate time source. A crystal oscillator accurate to one part in 10^{10} will be required. The oscillator pulses will be counted in a binary register and read into the computer as programmed by the I/O subroutine. Through selection of the chronometer frequency, it will be possible to generate the 500 kc computer clock and memory timing pulses from the same source.

3. Plot Board

A graphical display can be provided to visually depict the position of the vehicle throughout the mission. Instrumentation will depend on the complexity of the display. A crude system could utilize stepping motors and discrete outputs. A more sophisticated system could employ servo loops with disc encoders for tight control by the computer I/O subroutine.

4. Displays

Several types of visual displays will be required for the benefit of the vehicle passengers. Typical displays which could be provided include position coordinates, time, time-to-go, velocity, etc. Discrete outputs could be used to provide visual information such as mode, warnings, malfunction information, etc. The above displays would be operated directly from the computer. Octal coding of the real time values would represent the minimum amount of hardware.

5. Keyboard

A manual keyboard will be necessary to permit operator to insert star tables and other parameters. A decimal keyboard with visual verification of data to be inserted represents a sizable equipment penalty. Data inserted and verified octally would represent a minimal approach. Several switches for discrete inputs will also be provided to request specific quantities to be displayed or to insert mode and control information.

6. Steering Commands

The computer will generate steering commands for the vehicle during all phases of the mission. Digital hydraulic mechanisms are ideally suited for this purpose since the output of a binary register can directly drive the control elements. Digital-to-analog converters can be provided, however, if analog signals are required.

7. Analog Voltage Inputs and Outputs

In any integrated computer guidance system there usually exists a requirement to monitor or have access to numerous, miscellaneous analog signals. Typical analog voltage inputs could come from temperature sensors, rate gyros, etc. Figure N-2 illustrates a scheme for multiplexing a single input channel and analog-to-digital converter. Figure N-3 illustrates a scheme for multiplexing a single output channel and digital-to-analog converter. These schemes reduce the total hardware requirements, since each input or output device does not require its own conversion element and I/O channel.

D. RELIABILITY

The extremely long mean-time-to-failure needed for the guidance system in the Apollo space capsule is a difficult requirement which can be met only by use of inherently reliable component parts applied in a manner which will minimize the effects of component part failures on the over-all system reliability. This may be accomplished by first determining what stress induces component part catastrophic failure, how stresses influence component part degradation and how the component parts fail (e.g., open, short). The system is then designed to minimize the stresses or their effects, and make use of redundant elements on various levels to compensate for the inherent weaknesses of the component parts.

The COMPASS III Computer demonstrates how The Space Guidance Center organizes a system which will achieve a high level of reliability. Circuits and packaging have been designed to minimize component part failure rates by minimizing the stresses to which the parts will be subjected. The system has been organized to minimize component part usage, thereby reducing not only system failure rates but also power consumption, size and weight. For instance, the number of registers required is reduced by using memory locations for the multiplier and multiplicand registers. The arithmetic section contains only a simple adder-subtractor which is multiplexed to perform all the arithmetic operations (add, subtract, multiply, divide, and square root). The memory has been organized in a manner such that instruction length is reduced.

Furthermore, COMPASS III is a microminiature computer. Microminiaturization provides savings in weight, volume, and power which may be used for inclusion of redundancy features to achieve the required level of reliability.

APPENDIX O

ANALOG SIMULATION EQUATIONS

Guidance Law #2

$$\tan \gamma_d = \frac{B \pm \sqrt{B^2 - AC}}{A}$$

A, B, and C - Rectangular Coordinates

$$A = x\,(x_T - x) - K$$

$$B = -\left[\frac{2xz - zx_T - xz_T}{2}\right]$$

$$C = z\,(z_T - z) - K$$

$$K = \frac{\mu}{rV^2}\,(zz_T - rr_T + xx_T)$$

and in Polar Coordinates:

$$A = V_m \sin \Phi_m (R_E \sin \Phi_T - V_m \sin \Phi_m) - \frac{\mu R_E}{V^2}\left[\cos(\Phi_m - \Phi_T) - 1\right]$$

$$B = -\left[\frac{2(r_m \sin \Phi_m)(V_m \cos \Phi_m) - V_m \cos \Phi_m R_E \sin \Phi_T - r_m \sin \Phi_m R_E \cos \Phi_T}{2}\right]$$

$$C = r_m \cos \Phi_m (R_E \cos \Phi_T - r_m \cos \Phi_m) - \frac{\mu R_E}{V^2}\left[\cos(\Phi_m - \Phi_T) - 1\right]$$

where:

$r_m = R_E + h_m$

Φ_T = Central Angle to Target

$X_m = V_m \sin \Phi_m$ and x_T, z_T = Const. -(Non Rotating Earth)

$Z_m = V_m \cos \Phi_m$

Note:

$\bar{\gamma}_{actual} = \gamma - \Phi$ $\qquad C_{L_1} = K\bar{\gamma}_e$

$\bar{\gamma}_e = \bar{\gamma}_{act.} - \bar{\gamma}_d$

Equations of Motion

$$\dot{V} = -\left(\frac{A}{m}\right) q\, C_D - g_{SL}\left(1-\frac{2h}{R_E}\right) \sin\gamma$$

$$\dot{\gamma} = -g_{SL}\left(1-\frac{2h}{R_E}\right)\frac{\cos\gamma}{V} + \dot{\Phi}_m + \left(\frac{A}{m}\right)\frac{q}{V}\, C_L \cos\Phi_m$$

$$\dot{\Psi}_{aero} = \left(\frac{A}{m}\right)\frac{q}{V}\, C_L \sin\Phi_m$$

$$\dot{h} = V \sin\gamma$$

$$\dot{\Phi}_m = \frac{1}{R_E}\left(1-\frac{h}{R_E}\right) V\cos\gamma$$

ρ = function generator (ARDC 1959 Model Atmosphere)

$$q = \frac{1}{2} e V^2$$

C_L = Reference Guidance Law

$$C_D = f(C_L)$$

$$\bar{q}_c = \left(\frac{1}{e_0 R_N}\right)^{1/2} e^{1/2}\left(\frac{V}{1000}\right)^3$$

$$\bar{q}_R = \frac{.003\, R_N}{e_0^{1.78}}\, e^{1.78}\left(\frac{V}{10,000}\right)^{19.5}$$

$$Q_{c+R} = \int_0^t \left(\bar{q}_c + \bar{q}_R\right) dt$$

$$\eta = \left(\frac{A}{m}\right)\frac{1}{g_{SL}}\, q\, C_D \sqrt{1+\left(\frac{C_L}{C_D}\right)^2}$$

$$\Phi_m = \int_0^t \dot{\Phi}_m\, dt$$

$$\Delta\Psi = \frac{V\cos\gamma\cos\Psi_m \sin\lambda_m}{r\cos\lambda_m}$$

$$\mathring{\psi}_m = \dot{\psi}_{aero} + \Delta\dot{\psi}$$

$$\Phi_m = \Phi_o + \mathring{\Phi}_m \qquad \text{where } \mathring{\Phi}_m = \frac{V\cos\gamma\cos\psi_m}{r\cos\lambda_m}$$

$$\lambda_m = \lambda_o + \mathring{\lambda}_m \qquad \text{where } \lambda_m = \frac{V\cos\gamma\sin\psi_m}{r}$$

GUIDANCE LAW #1

$$\tan\gamma_d = \frac{B \pm \sqrt{B^2 - AC}}{A} \qquad (\tan\gamma_d = +\text{always})$$

$$A = -r_c\left(\frac{2r_c}{r} - \frac{r_c V^2}{\mu} - 2\right)$$

$$B = 0$$

$$C = A - \frac{r^2V^2}{\mu}$$

then

$$\tan\gamma_d = \pm\sqrt{-\frac{C}{A}}$$ use positive sign value

$$\frac{C}{A} = 1 + \frac{r^2V^2}{r_c\mu\left(\frac{2r_c}{r} - \frac{r_cV^2}{\mu} - 2\right)} \qquad r_c = 150{,}000\,\text{ft.} + R_E$$

Note:

① use only real values of $\sqrt{-\frac{C}{A}}$
② values A, B, C to be computed continuously
③ A, B, and C expressions will be modified during the study
④ r_c(variable) to be changed for various runs during the study

$$\tan\gamma_d - \tan\gamma_a = (\tan\gamma)_e$$

$$C_L \quad K\tan\gamma_e$$

REENTRY RANGE PREDICTION STEERING EQUATIONS

$$\bar{u}\,\frac{d^2 z}{d\bar{u}^2} - \left(\frac{dz}{d\bar{u}} - \frac{z}{\bar{u}}\right) = \frac{1-\bar{u}^2}{\bar{u}z}\,\mathrm{Cos}^4\gamma - \sqrt{\beta r}\,\frac{L}{D}\,\mathrm{Cos}^3\gamma$$

$$z = \frac{\bar{u}\rho}{2\left(\frac{M}{C_D A}\right)}\sqrt{\frac{r}{\beta}} = \frac{K A u}{\sqrt{\beta r}\,\bar{u}}$$

$$\bar{u} = \frac{u}{\sqrt{g r}}$$

$$\frac{\Delta s}{r} = \frac{1}{\sqrt{\beta r}}\int_{\bar{u}_2}^{\bar{u}_1} \frac{\mathrm{Cos}\,\gamma\, d\bar{u}}{z}$$

$$z' = \frac{dz}{d\bar{u}} = \sqrt{\beta r}\ \mathrm{Sin}\,\gamma + \frac{z}{\bar{u}}$$

$$t = \frac{1}{\sqrt{\beta g}}\int_{\bar{u}_2}^{\bar{u}_1} \frac{\mathrm{Cos}\,\gamma\, d\bar{u}}{\bar{u} z}$$

$$a = \frac{g\sqrt{\beta r}\ \bar{u} z}{\mathrm{Cos}\,\gamma}\sqrt{1+\left(\tan\gamma - \frac{L}{D}\right)^2}$$

$$q_s = 590\sqrt{\frac{M}{C_D A R}}\ \bar{q}$$

$$\bar{q} = \bar{u}^{5/2}\, z^{1/2}$$

$$\frac{Q_s}{S} = 15{,}900 \sqrt{\frac{M}{C_D AR}}\ \bar{Q}$$

$$\bar{Q} = \int_{\bar{u}_2}^{\bar{u}_1} \frac{\bar{u}^{3/2}\, d\bar{u}}{z^{1/2}}$$

$$R_y = y_1 + y_2$$

$$y_1 = L/D\ (3438)\ \ln \bar{u}\ \sin \phi_B \sin \phi_C$$

$$y_2 = 620\ (L/D)^{1.78}\ \sin 2\phi_B$$

$$\gamma_a = \gamma \left[\frac{\bar{u}_e^{\,2}}{1 - \left[1 - \bar{u}_e^{\,2} \left(\frac{\bar{u}_e^{\,2}}{\cos^2 \gamma_e} \right) \right]^{1/2}} \right]$$

Lateral Guidance

$$\cos \Gamma_1 = \cos \Delta \Phi \cos \lambda_T + \sin \Delta \Phi \sin \lambda_T \cos 90^\circ = \cos \Delta \Phi \cos \lambda_T$$

$$\sin i_{mT} = \frac{\sin \lambda_T}{\sin \Gamma_1}$$

$$\cos \Gamma_2 = \cos \lambda_m \cos \Gamma_1 + \sin \lambda_m \sin \Gamma_1 \sin i_{mT}$$

$$= \cos \lambda_m \cos \Delta \Phi \cos \lambda_T + \sin \lambda_m \sin \lambda_T$$

$$\cos \Psi_{mT} = \cos i_{mT} - \frac{\sin \Gamma_1}{\sin \Gamma_2}$$

$$\Psi_m - \Psi_{mT} = \Psi_e$$

Constants

$g_{SL} = 32.19$ ft/sec^2

$R_E = 2.0926 \times 10^7$ ft.

$\rho_0 = .0027$ slugs/ft^2

$\mu = 1.40765 \times 10^{16}$ ft^3/sec^2

ratios of the respective heating terms at angle-of-attack to their values at zero angle-of-attack. The constraint Equation (25), (26) and (27) represent the acceleration, altitude and dynamic pressure endurance limits respectively. The quantities $\mathcal{T}_a$, $\mathcal{T}_h$ and $\mathcal{T}_q$ are the maximum endurance times at which the vehicle can operate at the instantaneous value of acceleration, (a), altitude, (h), and dynamic pressure, (q), respectively. The values of $\mathcal{T}_a$, $\mathcal{T}_h$ and $\mathcal{T}_q$ versus a, h and q will be inputs to the program. By imposing final boundary conditions that ψ_f, ϕ_f and θ_f be less than or equal to unity we require that at no time during re-entry does the vehicle operate at an a, h or q for a period of time which exceeds the maximum specified by the endurance limits.

The system of equation adjoint to the small pertubation equations given previously by Equations (13) are:

$$\dot{\lambda}_v = g_{vv}\lambda_v + g_{v\gamma}\lambda_\gamma + g_{vx}\lambda_x + g_{vh}\lambda_h + g_{vQ}\lambda_Q + g_{v\psi}\lambda_\psi + g_{v\theta}\lambda_\theta \tag{28}$$

$$\dot{\lambda}_\gamma = g_{\gamma v}\lambda_v + g_{\gamma\gamma}\lambda_\gamma + g_{\gamma x}\lambda_x + g_{\gamma h}\lambda_h \tag{29}$$

$$\dot{\lambda}_x = 0 \tag{30}$$

$$\dot{\lambda}_h = g_{hv}\lambda_v + g_{h\gamma}\lambda_\gamma + g_{hx}\lambda_x + g_{hQ}\lambda_Q + g_{h\psi}\lambda_\psi + g_{h\phi}\lambda_\phi + g_{h\theta}\lambda_\theta \tag{31}$$

$$\lambda_Q = 0 \tag{32}$$

$$\dot{\lambda}_\psi = 0 \tag{33}$$

$$\dot{\lambda}_\phi = 0 \tag{34}$$

$$\dot{\lambda}_\theta = 0 \tag{35}$$

where

$$g_{vv} = \frac{2D}{mv}$$

$$g_{v\gamma} = -\frac{\cos\gamma}{R+h} - \frac{L}{mv^2} - \frac{g \cos}{v^2}$$

$$g_{vx} = -\frac{R\cos\gamma}{R+h}$$

$$g_{vh} = -\operatorname{Sin}\gamma$$

$$g_{vQ} = -3.15\, C_1 \rho^{1/2} V^{2.15} G_{avg} A(\alpha) - \frac{2H}{2V} B(\alpha)$$

$$g_{v\psi} = -\frac{2a}{v} \frac{d}{da} \left(\frac{1}{\tau_a}\right)$$

$$g_{v\theta} = -\frac{2q}{v} \frac{d}{d_q} \left(\frac{1}{\tau_q}\right)$$

$$g_{\gamma v} = g \operatorname{Cos}\gamma$$

$$g_{\gamma\gamma} = V\frac{\operatorname{Sin}\gamma}{R+h} - \frac{g\operatorname{Sin}\gamma}{v}$$

$$g_{\gamma x} = \frac{Rv \operatorname{Sin}\gamma}{R+h} \qquad (36)$$

$$g_{\gamma h} = -V\operatorname{Cos}\gamma$$

$$g_{hv} = -\frac{2 g \operatorname{Sin}}{R+h} + \frac{D}{\rho m} \frac{d\rho}{dh}$$

$$g_{h\gamma} = \frac{V\operatorname{Cos}\gamma}{(R+h)^2} - \frac{L}{\rho mv} \frac{d\rho}{dh} - \frac{2g\cos\gamma}{v(R+h)}$$

$$g_{hx} = \frac{RV\cos\gamma}{(R+h)^2}$$

$$g_{hq} = -\frac{1}{2} C_1 \rho^{-1/2} V^{3.15} G_{avg} \frac{d\rho}{dh} A(\alpha) - \frac{2H}{2h} B(\alpha)$$

$$g_{h\psi} = -\frac{a}{\rho} \frac{d\rho}{dh} \frac{d}{da} \left(\frac{1}{\tau_a}\right)$$

$$g_{h\phi} = -\frac{d}{dh} \left(\frac{1}{\tau_h}\right)$$

$$g_{h\theta} = -\frac{q}{\rho} \frac{d\rho}{dh} \frac{d}{dq} \left(\frac{1}{\tau_q}\right)$$

The equation for λ_α corresponding to Equation (17) is

$$\lambda_\alpha^{(i)} = g_{\alpha v} \lambda_v^{(i)} + g_{\alpha\gamma} \lambda_\gamma^{(i)} + g_{\alpha\psi} \lambda_\psi^{(i)} + g_{\alpha Q} \lambda_Q^{(i)} \qquad (37)$$

where

$$g_{\alpha V} = -\frac{D}{C_D m} \quad \frac{d\,C_D}{d\,\alpha}$$

$$g_{\alpha\gamma} = \frac{D}{C_D\,mv} \quad \frac{dC}{d\alpha}$$

$$g_{\alpha\psi} = \frac{D\left(\frac{C_L}{C_D}\ \frac{dC_L}{d\alpha} + \frac{dC_D}{d\alpha}\right)}{\sqrt{C_L^{\,2} + C_D^{\,2}}} \tag{38}$$

$$g_{\alpha Q} = \frac{dA}{d\alpha} C_1 \rho^{1/2} V^{3.15} G_{avg} + \frac{\partial B}{d\alpha} H(h,V)\ R_N$$

D. Methods of Solution

Having developed the necessary equations and presented their counterparts for the optimun re-entry problem, we now proceed to determine the desired correction $\delta\alpha(t)$ to the driving function. First, we recognize that the quantity which we are minimizing, Q_f, is dependent on the re-entry trajectory. The re-entry trajectory, in turn, is dependent upon the driving function $\alpha(t)$ assuming initial conditions are specified. Therefore, Q_f is dependent on the function $\alpha(t)$. **By the method of steepest descent the correction to** $\alpha(t)$ is determined by

$$\delta\alpha = -K \text{ grad } Q_f \tag{39}$$

where

$$\text{grad } Q_f = \frac{\partial Q_f}{\partial\alpha} \tag{40}$$

Thus, we wish to determine, $\frac{\partial Q_f}{\partial\alpha}$, the influence function which tells how a small change in α effects Q_f.

By defining

$$\lambda_i^{(Q)}(T) = \left[\frac{\partial Q}{\partial y_i}\right]_T \tag{41}$$

where y_i are the problem variables, then

$$\left[\sum_{i=1}^{n} \lambda_i^{(Q)} dy_i\right]_T = \left[\frac{\partial Q}{\partial y_1} dy_1 + \frac{\partial Q}{\partial y_2} dy_2 + \dots + \frac{\partial Q}{\partial y_n} dy_n\right]_T = \left[dQ\right]_T \tag{42}$$

and Equation (19) can be written for this case

$$\left[dQ\right]_T = J_Q\, dT + \int_{t_o}^{T} \lambda_\alpha^{(Q)} \delta\alpha \; dt + \left[\sum_{i=1}^{n} \lambda_i^{(Q)} \delta y_i\right]_{t_o} \tag{43}$$

where

$$J_Q = \left[\sum_{i=1}^{n} \lambda_i^{(Q)} f_i\right]_T \tag{44}$$

Note that $\lambda_\alpha^{(Q)}$ in Equation (43) is the influence function desired in Equation (40). Therefore, we can write

$$\delta\alpha = -K \; \lambda_\alpha^{(Q)} \tag{45}$$

for the desired correction. The values of $\lambda_\alpha^{(Q)}$ in Equation (45) are determined from Equation (37) where the λ_i in Equation (37) are solutions to the adjoint system Equations (28) - (35) with boundary conditions given by Equation (41). Since the boundary conditions are given at final time T, the adjoint equations are integrated backwards.

Equation (45) does not assure satisfaction of other problem requirements, namely specified range and final boundary conditions ψ, ϕ and θ. To simultaneously satisfy these requirements additional influence functions can be generated which tell how small changes in α effect their respective values. For instance define

$$\lambda_i^{(h)}(T) = \left[\frac{\partial h}{\partial y_i}\right]_T \qquad (46)$$

then Equation (19) becomes

$$\left[dh\right]_T = J_n\, dT + \int \lambda_\alpha^{(h)} \delta\alpha\, dt + \left[\sum \lambda_i^{(h)} \delta y_i\right]_{t_o} \qquad (47)$$

Similarly let

$$\lambda_i^{(x)}(T) = \left[\frac{\partial x}{\partial y_i}\right]_T \qquad (48)$$

then

$$\left[dx\right]_T = J_x\, dT + \int \lambda_\alpha^{(x)} \delta\alpha\, dt + \left[\sum \lambda_i^{(x)} \delta y_i\right]_{t_o} \qquad (49)$$

$$\lambda_i^{(\psi)}(T) = \left[\frac{\partial \psi}{\partial y_i}\right]_T \qquad (50)$$

then

$$\left[d\psi\right]_T = J_\psi\, dT + \int \lambda_\alpha^{(\psi)} \delta\alpha\, dt + \left[\sum \lambda_i^{(\psi)} \delta y_i\right]_{t_o} \qquad (51)$$

$$\lambda_i^{(\phi)}(T) = \left[\frac{2\phi}{2y_i}\right]_T \qquad (52)$$

then

$$\left[d\phi\right]_T = J_\phi\, dT + \int \lambda_\alpha^{(\phi)}\, dt + \left[\sum \lambda_i^{(\phi)} \delta y_i\right]_{t_o} \qquad (53)$$

$$\lambda_i^{(\theta)}(T) = \left[\frac{2\theta}{2y_i}\right]_T \qquad (54)$$

then

$$\left[d\theta\right]_T = J_\theta\, dT + \int \lambda_\alpha^{(\theta)} \delta\alpha\, dt + \left[\sum \lambda_i^{(\theta)} \delta y_i\right]_{t_o} \qquad (55)$$

The ultimate goal is to determine $\delta\alpha$ which simultaneously minimize Q_f and causes $(dh)_T$, $(dx)_T$, $(d\psi)_T$, $(d\phi)_T$ and $(d\theta)_T$ to vanish. Since initial conditions for the re-entry problem are specified the last term in Equations (43), (47), (49), (51), (53) and (55) is zero. If we extend our steepest descent form for $\delta\alpha$ to include the other boundary requirements we have

$$\delta\alpha = K_Q \lambda_\alpha^{(Q)} + K_x \lambda_\alpha^{(x)} + K_\psi \lambda_\alpha^{(\psi)} + K_\phi \lambda_\alpha^{(\phi)} + K_\theta \lambda_\alpha^{(\theta)} \qquad (56)$$

where K_p, K_x ... K_θ are unknown step sizes to be determined. Substituting (56) into (43, (47), (49), (51), (53) and (55) we obtain the following abbreviated system

$$\begin{pmatrix} dT \\ K_Q \\ K_x \\ K_\psi \\ K_\phi \\ K_\theta \end{pmatrix} = \left[A\right]^{-1} \begin{pmatrix} dh_f \\ dQ_f \\ dx_f \\ d\psi_f \\ d\phi_f \\ d\theta_f \end{pmatrix} \text{ where } \left[A\right] = \begin{bmatrix} J_h & I_{Qh} & I_{xh} & I_{\psi n} & I_{\phi h} & I_{\theta h} \\ J_Q & I_{QQ} & I_{xQ} & I_{\psi Q} & I_{\phi Q} & I_{\theta Q} \\ J_x & I_{Qx} & I_{xx} & I_{\psi x} & I_{\phi x} & I_{\theta x} \\ J_\psi & I_{Q\psi} & I_{x\psi} & I_{\psi\psi} & I_{\phi\psi} & I_{\theta\psi} \\ J_\phi & I_{Q\phi} & I_{x\phi} & I_{\psi\phi} & I_{\phi\phi} & I_{\theta\phi} \\ J_\theta & I_{Q\theta} & I_{x\theta} & I_{\psi\theta} & I_{\phi\theta} & I_{\theta\theta} \end{bmatrix} \qquad (57)$$

where

$$J_\beta = \left[\sum_{i=1}^{n} \lambda_i^{(\beta)} f_i \right]_T \qquad (58)$$

and

$$I_{\beta\delta} = \int_{t_0}^{T} \lambda_\alpha^{(\beta)} \lambda_\alpha^{(\delta)} \, dt \qquad (59)$$

From Equations (57) values of dT, K_Q ... K_θ are determined which in conjunction with the λ_α's yield the correction $\delta\alpha$ to be applied to the nominal driving function $\alpha(t)$. The corrected driving function is then used to determine a new nominal trajectory and the procedure is repeated until the optinium trajectory is determined.

At the optinium, the value of $\lambda_{\alpha}^{(Q)}(t)$ goes to zero.

When numerically integrating the constraint equations on a computer, the stopping condition is normally altitude,i.e. when a specified altitude is reached the integration stops. Therefore, $\left[dh\right]_f$ in Equation (47) vanishes. Solving (47) for dT gives

$$dT = \frac{1}{J_h} \int_{t_o}^{T} \lambda_{\alpha}^{(h)} \delta\alpha \, dt \tag{60}$$

Substituting (60) into (43), (49), (51), (53) and (55) we can reduce the order by one. The resulting equations after simplification are

$$\left[dQ\right]_T = \int_{t_o}^{T} \lambda_{\alpha}^{(Qh)} \delta\alpha \, dt + \left[\sum_{i=1}^{n} \lambda_i^{(Qh)} \delta y_i\right]_{t_o} \tag{61}$$

$$\left[dx\right]_T = \int_{t_o}^{T} \lambda_{\alpha}^{(x,h)} \delta\alpha \, dt + \left[\sum_{i=1}^{n} \lambda_i^{(x,h)} \delta y_i\right]_{t_o} \tag{62}$$

$$\left[d\psi\right]_T = \int_{t_o}^{T} \lambda_{\alpha}^{(\psi h)} \delta\alpha \, dt + \left[\sum_{i=1}^{n} \lambda_i^{(\psi,h)} \delta y_i\right]_{t_o} \tag{63}$$

$$\left[d\phi\right]_T = \int_{t_o}^{T} \lambda_{\alpha}^{(\phi h)} \, dt + \left[\sum_{i=1}^{n} \lambda_i^{(\phi h)} \delta y_i\right]_{t_o} \tag{64}$$

$$\left[d\theta\right]_T = \int_{t_o}^{T} \lambda_{\alpha}^{(\theta h)} \delta\alpha \, dt + \left[\sum_{i=1}^{n} \lambda_i^{(\theta h)} \delta y_i\right]_{t_o} \tag{65}$$

where

$$\lambda_i^{(\beta,h)}(T) = \left[\frac{\partial\beta}{\partial y_i} - \frac{J_\beta}{J_h} \frac{\partial h}{\partial y_i}\right]_{t = T} \tag{66}$$

and

$$J_\beta = \left[\sum_{i=1}^{n} \lambda_i^{(\beta)} f_i\right]_T = \left[\sum_{i=1}^{n} \frac{\partial\beta}{\partial y_i} f_i\right]_T \tag{67}$$

The λ_α's in Equations (61) - (65) correspond to solutions of the adjoint system, λ_i, obtained for the boundary conditions given by Equation (66). Substituting Equation (56) into (61) - (65) yields the following for $K_Q \dots K_\theta$

$$\begin{bmatrix} K_Q \\ K_x \\ K_\psi \\ K_\phi \\ K_\theta \end{bmatrix} = \left[A\right]^{-1} \begin{bmatrix} d_Q \\ d_x \\ d\psi \\ d\phi \\ d\theta \end{bmatrix} \text{ where } \left[A\right] = \begin{bmatrix} I_{QQ} & I_{Qx} & I_{Q\psi} & I_{Q\phi} & I_{Q\theta} \\ I_{xQ} & I_{xx} & I_{x\psi} & I_{x\phi} & I_{x\theta} \\ I_{\psi Q} & I_{\psi x} & I_{\psi\psi} & I_{\psi\phi} & I_{\psi\theta} \\ I_{\phi Q} & I_{\phi x} & I_{\phi\psi} & I_{\phi\phi} & I_{\phi\theta} \\ I_{\theta Q} & I_{\theta x} & I_{\theta\psi} & I_{\theta\phi} & I_{\theta\theta} \end{bmatrix} \qquad (68)$$

where

$$I_{\beta\delta} = \int_{t_o}^{T} \lambda_\alpha^{(\beta h)} \lambda_\alpha^{(\delta h)} \, dt \qquad (69)$$

Thus, by defining $\lambda_i(T)$ by Equation (66) we need only determine five sets of solutions to the adjoint equations.

Since the ultimate goal of the method is to determine the function $\alpha(t)$ which minimizes Q_f and causes dx_f, $d\psi_f$, $d\phi_f$ and $d\theta_f$ to vanish we will next define a scalar function to be

$$F = W_1 \, Q_f^2 + W_2 \, dx_f^2 + W_3 \, d\psi_f^2 + W_4 \, d\phi_f^2 + W_5 \, d\theta_f^2 \qquad (70)$$

Where $W_1 \; W_2 \dots W_5$ are arbitrary constant weighting functions selected to suit the needs of the problem. Minimizing Q_f and causing dx_f, $d\psi_f$, $d\phi_f$ and $d\theta_f$ to vanish is tantamount to minimizing F.

Therefore, let us define

$$\lambda_i^{(F)}(T) = \left[\frac{2F}{2y_i} \right]_T \qquad (71)$$

then Equation (19) becomes

$$\left[dF\right]_T = J_F \, dT + \int_{t_o}^{T} \lambda_{\alpha}^{(F)} \, \delta\alpha \, dt \tag{72}$$

where

$$J_F = \left[\sum_{i=1}^{n} \lambda_i^{(F)} \, f_i \right]_T \tag{73}$$

Once again the initial conditions on the problem variables are assumed known and their influence is eliminated from Equation(72). Let us also define

$$\lambda_i^{(h)}(T) = \left[\frac{\partial h}{\partial y_i}\right]_T \tag{74}$$

so that

$$\left[dh\right]_T = 0 = J_h \, dT + \int_{t_o}^{T} \lambda_{\alpha}^{(h)} \, \delta\alpha \, dt \tag{75}$$

Solving Equation (75) for dT and substituting the results into Equation (72) gives

$$\left[dF\right]_T = \int_{o}^{T} \lambda_{\alpha}^{(F,h)} \quad dt \tag{76}$$

where

$$\lambda_i^{(Fh)}(T) = \left[\lambda_i^{(F)} - \frac{J_F}{J_h} \lambda_i^{(h)}\right]_T = \left[\frac{\partial F}{\partial y_i} - \frac{J_F}{J_h} \frac{\partial h}{\partial y_i}\right]_T \tag{77}$$

Letting

$$\delta\alpha = K \, \lambda_{\alpha}^{(Fh)} \tag{78}$$

and substituting (78) into (76) we obtain for K

$$K = \frac{\left[dF\right]_T}{\int_{t_o}^{T} \lambda_{\alpha}^{(Fh)} \, \lambda_{\alpha}^{(Fh)} \, dt} \tag{79}$$

The boundary conditions for the single set of solutions to the adjoint equations are given by Equation (77).

The optimum solution is obtained by initially specifying desired changes in $(dF)_T$ and obtaining the corrections corresponding to these specified changes. After several iterations a curve can be fit to $(F)_T$ and the value of $(dF)_T$ selected so as to cause $(F)_T$ to be minimum.

NOMENCLATURE

A	Abbreviation of matrix in Equation (68)
a	Acceleration ~ g's
C_1	Coefficient in heating Equation (24) $\cong \frac{17600}{R_N \quad V_c^{5.15}}$
C_2	Lift Coefficient ~ L/qS_{REF}
C_D	Drag Coefficient ~ D/qS_{REF}
D	Aerodynamic Drag ~ lbs
f_i	Abbreviation in Constraint Equations (1)
F	Abbreviation of quantity given by Eq. (70)
g	Acceleration of gravity at Altitude
g_o	Acceleration of gravity at Sea Level
g_{ij}	Coefficients in Adjoint Equations (28)-(35) $= \frac{\partial f_j}{\partial y_i}$
G_{AVG}	Parameter in heating Equation (10) to account for wall temperatures variations.
h	Altitude - ft
$H(h_o V)$	Gas Cap Radiation Term in heating Equation (24)
I_{BS}	Abbreviation of Integral given by Eq. (59)
J	Abbreviation defined in Eq. (58)
L	Lift - lbs
m	Vehicle mass ~ Slugs
Q	Heat Transfer ~ BTU/ft^2
q	Dynamic Pressure ~ $1/2\ \rho V^2$
R	Mean Earth Radius = 2.09029×10^7 ft

R_N	Body Nose Radius ~ ft
T	Time at Termination of flight
t	Time
t_o	Time at initiation of flight
V	Velocity relative to earths surface
x	Range along earth s surface
y_i	Abbreviationof Dependent Variables in Equation (1)
α	Angle of Attack
β	Dummy Index in Equations (58) & (59)
γ	Flight Path angle, positive up from local horizon in Equation (20)-(27)
θ	Parameters Intrudocued in Equation (27)
λ	Adjoint variables Equation (13) (Influence coefficients)
ρ	Atmospheric Density
ϕ	Parameter Introduced by Equation (26)
ψ	Parameter Introduced by Equation (25)
V_c	Circular Satellite Velocity - $\sqrt{2\ r}$ 26,000 fps.

References

a. Bryson, A.E., Denham, W. F., Carroll, F. J. and Mikami, K.: "Determination of the Lift or Drag Program that Minimized Re-Entry Heating with Acceleration or Range Constraints Using a Steepest Descent Computation Procedure", Institute of the Aeronautical Sciences Paper No. 61-6, 1961.

b. Kelley, H. J.; "Gradient Theory of Optimal Flight Paths", American Rocket Society Preprint 1230-60, 1960.

c. Goodman, T. R. and Lance, G. N.; "The Numerical Integration of Two Point Boundary Value Problems", Mathematical Tables and Other Aids to Computation, Vol. 10, No. 54, April 1956.

Appendix P

Linear Perturbation Equations for the Analysis of the Hit-Point Steering System

Equations of Motion

$$\mathring{v} = -\frac{A}{M}\frac{\rho}{2}v^2 C_D - g_{s.L.}\left[1-\frac{2h}{r_e}\right]\sin\gamma$$

$$\mathring{\gamma} = -g_{s.L.}\left[1-\frac{2h}{r_e}\right]\frac{\cos\gamma}{v} + \mathring{\phi} + \frac{A}{2M}\rho v C_L$$

$$\mathring{h} = v\sin\gamma \qquad\qquad C_D = K_1 + K_2 C_L^2$$

$$\mathring{\phi} = \frac{1}{r_e}\left[1-\frac{h}{r_e}\right]v\cos\gamma$$

Guidance equations

$$\tan\gamma_d = \frac{B-\sqrt{B^2-CE}}{E}$$

$$E = \frac{\mu r_T}{v_0^2}\left[1-\cos(\phi_T-\phi)\right]$$

$$B = \frac{r_T(h+r_e)}{2}\sin(\phi_T-\phi)$$

$$C = r_T(h+r_e)\cos(\phi_T-\phi)-(h+r_e)^2+\frac{\mu r}{v_0^2}+\left[1-\cos(\phi_T-\phi)\right]$$

For purposes of linearization the above equation may be put in the form:

$$\mathring{v} = F_1(v, \gamma, h, C_L)$$

$$\mathring{\gamma} = F_2(v, \gamma, h, \mathring{\phi}, C_L)$$

$$\mathring{h} = F_3(v, \gamma)$$

$$\mathring{\phi} = F_4(v, \gamma, h)$$

The linearized equations are:

$$\mathring{v} = -a_{11} v - a_{12}\gamma - a_{13} h$$

$$\mathring{\gamma} = -a_{21} v - a_{22}\gamma - a_{23} h - a_{24}\dot{\phi} + b_2 C_L$$

$$\mathring{h} = -a_{31} v - a_{32}\gamma$$

$$\dot{\phi} = -a_{41} v - a_{42}\gamma - a_{43} h$$

where

$$-a_{11} = \frac{\partial F_1}{\partial v} = -\frac{A}{M}\rho v_0 C_{D_0}$$

$$-a_{12} = \frac{\partial F_1}{\partial \gamma} = -g_{s.l.}\left[1-\frac{2h_0}{r_e}\right]\cos\gamma_0$$

$$-a_{13} = \frac{\partial F_1}{\partial h} = 2g_{s.l.}\frac{\sin\gamma_0}{r_e}$$

$$-a_{21} = \frac{\partial F_2}{\partial v} = g_{s.l.}\left[1-\frac{2h_0}{r_e}\right]\frac{\cos\gamma_0}{v_0^2} + \frac{A}{\partial M}\rho C_{L_0}$$

$$-a_{22} = \frac{\partial F_2}{\partial \gamma} = g_{s.l.}\left[1-\frac{2h_0}{r_e}\right]\frac{\sin\gamma_0}{v_0}$$

$$-a_{23} = \frac{\partial F_2}{\partial h} = 2g_{s.l.}\frac{\cos\gamma_0}{r_e v_0}$$

$$-a_{24} = \frac{\partial F_2}{\partial \phi} = 1$$

$$-a_{31} = \frac{\partial F_3}{\partial v} = \sin\gamma_0$$

$$-a_{32} = \frac{\partial F_3}{\partial \gamma} = v_0\cos\gamma_0$$

$$-a_{41} = \frac{\partial F_4}{\partial v} = \frac{1}{r_e}\left(1-\frac{h_0}{r_e}\right)\cos\gamma_0$$

$$-a_{42} = \frac{\partial F_4}{\partial \gamma} = -\frac{1}{r_e}\left(1-\frac{h_0}{r_e}\right)v_0\sin\gamma_0$$

$$-a_{43} = \frac{\partial F_4}{\partial h} = -\frac{v_0^2\cos\gamma_0}{r_e^2}$$

$$b_1 = \frac{\partial F_1}{\partial C_1} = -\frac{A}{M}\rho v_0^2 K_2 C_{L_0}$$

$$b_2 = \frac{\partial F_2}{\partial C_L} = \frac{A}{\partial M}\rho v_0$$

Vehicle Transfer Functions

$$D = \begin{vmatrix} s+a_{11} & a_{12} & a_{13} & 0 \\ a_{21} & s+a_{22} & a_{23} & -s \\ a_{31} & a_{32} & s & 0 \\ a_{41} & a_{42} & a_{43} & s \end{vmatrix} =$$

$$(s+a_{11}) \begin{vmatrix} s+a_{22} & a_{23} & -s \\ a_{32} & s & 0 \\ a_{42} & a_{43} & s \end{vmatrix} - a_{12} \begin{vmatrix} a_{21} & a_{23} & -s \\ a_{31} & s & 0 \\ a_{41} & a_{43} & s \end{vmatrix} + a_{13} \begin{vmatrix} a_{21} & s+a_{22} & -s \\ a_{31} & a_{32} & 0 \\ a_{41} & a_{42} & s \end{vmatrix}$$

$$= (s+a_{11}) \Big[s^3 + a_{22} s^2 - a_{23} a_{32} s + a_{42} s^2 - a_{43} a_{32} s \Big] - a_{12} \Big[a_{21} s^2 - a_{23} a_{31} s$$

$$+ a_{41} s^2 - a_{43} a_{31} s \Big] + a_{13} \Big[a_{32} a_{21} s - a_{31} s^2 - a_{31} a_{22} s - a_{31} a_{42} s + a_{32} a_{41} s \Big]$$

$$= s^4 + (a_{11} + a_{22} + a_{42}) s^3 + \Big(a_{11} a_{22} + a_{11} a_{42} - a_{23} a_{32} - a_{43} a_{32} - a_{12} a_{21} - a_{12} a_{41} - a_{13} a_{31} \Big) s^2$$

$$+ \Big(- a_{11} a_{23} a_{32} - a_{43} a_{32} a_{11} + a_{12} a_{23} a_{31} + a_{43} a_{31} a_{12} + a_{13} a_{32} a_{21} - a_{13} a_{31} a_{22}$$

$$- a_{13} a_{31} a_{42} + a_{13} a_{32} a_{41} \Big) s$$

$$D_1 = \begin{vmatrix} b_1 & a_{12} & a_{13} & 0 \\ b_2 & s+a_{22} & a_{23} & -s \\ 0 & a_{32} & s & 0 \\ 0 & a_{42} & a_{43} & s \end{vmatrix} = b_1 \begin{vmatrix} s+a_{22} & a_{23} & -s \\ a_{32} & s & 0 \\ a_{42} & a_{43} & s \end{vmatrix} - a_{12} \begin{vmatrix} b_2 & a_{23} & -s \\ 0 & s & 0 \\ 0 & a_{43} & s \end{vmatrix} + a_{13} \begin{vmatrix} b_2 & s+a_{22} & -s \\ 0 & a_{32} & 0 \\ 0 & a_{42} & s \end{vmatrix}$$

$$= b_1\left[s^3 + a_{22}s^2 - a_{23}a_{32}s + a_{42}s^2 - a_{43}a_{32}s\right] - a_{12}\left[b_2 s^2\right] + a_{13}\left[b_2 a_{32} s\right]$$

$$= b_1 s^3 + \left(b_1 a_{22} + b_1 a_{42} - b_2 a_{12}\right)s^2 + \left(b_2 a_{13} a_{32} - b_1 a_{23} a_{32} - b_1 a_{43} a_{32}\right)s$$

$$D_2 = \begin{vmatrix} s+a_{11} & b_1 & a_{13} & 0 \\ a_{21} & b_2 & a_{23} & -s \\ a_{31} & 0 & s & 0 \\ a_{41} & 0 & a_{43} & s \end{vmatrix} = (s+a_{11}) \begin{vmatrix} b_2 & a_{23} & -s \\ 0 & s & 0 \\ 0 & a_{43} & s \end{vmatrix} - b_1 \begin{vmatrix} a_{21} & a_{23} & -s \\ a_{31} & s & 0 \\ a_{41} & a_{43} & s \end{vmatrix} + a_{13} \begin{vmatrix} a_{21} & b_2 & -s \\ a_{31} & 0 & 0 \\ a_{41} & 0 & s \end{vmatrix}$$

$$= (s+a_{11})\left[b_2 s^2\right] - b_1\left[a_{21}s^2 - a_{23}a_{31}s + a_{41}s^2 - a_{43}a_{31}s\right] + a_{13}\left[-b_2 a_{31} s\right]$$

$$= b_2 s^3 + \left(b_2 a_{11} - b_1 a_{21} - b_1 a_{41}\right)s^2 + \left(b_1 a_{23} a_{31} + b_1 a_{43} a_{31} - b_2 a_{13} a_{31}\right)s$$

$$D_3 = \begin{vmatrix} s+a_{11} & a_{12} & b_1 & 0 \\ a_{21} & s+a_{22} & b_2 & -s \\ a_{31} & a_{32} & 0 & 0 \\ a_{41} & a_{42} & 0 & s \end{vmatrix} = (s+a_{11}) \begin{vmatrix} s+a_{22} & b_2 & -s \\ a_{32} & 0 & 0 \\ a_{42} & 0 & s \end{vmatrix} - a_{12} \begin{vmatrix} a_{21} & b_2 & -s \\ a_{31} & 0 & 0 \\ a_{41} & 0 & s \end{vmatrix} + b_1 \begin{vmatrix} a_{21} & s+a_{22} & -s \\ a_{31} & a_{32} & 0 \\ a_{41} & a_{42} & s \end{vmatrix}$$

$$= (s+a_{11})\left[-b_2 a_{32} s\right] - a_{13}\left[-a_{31} s\right] + b_1\left[a_{32}a_{21}s - a_{31}a_{42}s + a_{41}a_{32}s - a_{31}s^2 - a_{31}a_{22}s\right]$$

$$= -(b_2 a_{32} + b_1 a_{31})s^2 + (a_{13}a_{31} - b_2 a_{11} a_{31} + b_1 a_{32} a_{21} - b_1 a_{31} a_{42} + b_1 a_{41} a_{32} - b_1 a_{31} a_{22})s$$

$$D_4 = \begin{vmatrix} s+a_{11} & a_{12} & a_{13} & b_1 \\ a_{21} & s+a_{22} & a_{23} & b_2 \\ a_{31} & a_{32} & s & 0 \\ a_{41} & a_{42} & a_{43} & 0 \end{vmatrix} = -b_1 \begin{vmatrix} a_{21} & s+a_{22} & a_{23} \\ a_{31} & a_{32} & s \\ a_{41} & a_{42} & a_{43} \end{vmatrix} + b_2 \begin{vmatrix} s+a_{11} & a_{12} & a_{13} \\ a_{31} & a_{32} & s \\ a_{41} & a_{42} & a_{43} \end{vmatrix}$$

$$= -b_1\left[a_{21}a_{32}a_{43} + a_{11}s^2 + a_{41}a_{22}s + a_{23}a_{31}a_{42} - a_{41}a_{32}a_{23} - a_{42}a_{21}s - a_{43}a_{31}s - a_{43}a_{31}a_{22}\right]$$

$$+ b_2\left[a_{43}a_{32}s + a_{11}a_{32}a_{43} + a_{12}a_{41}s + a_{13}a_{31}a_{42} - a_{41}a_{32}a_{13} - a_{42}s^2 - a_{42}a_{11}s - a_{43}a_{31}a_{12}\right]$$

$$= -(b_1 a_{41} + b_2 a_{42})s^2 + \left[b_1(a_{42}a_{21} + a_{43}a_{31} - a_{41}a_{22}) + b_2(a_{43}a_{32} + a_{12}a_{41} - a_{42}a_{11})\right]s$$

$$\frac{v}{C_L} = \frac{D_1}{D} = \frac{B_1 S^3 + B_2 S^2 + B_3 S}{S^4 + A_1 S^3 + A_2 S^2 + A_3 S}$$

$$\frac{\gamma}{C_L} = \frac{D_2}{D} = \frac{B_4 S^3 + B_5 S^2 + B_6 S}{S^4 + A_1 S^3 + A_2 S^2 + A_3 S}$$

$$\frac{h}{C_L} = \frac{D_3}{D} = \frac{B_7 S^2 + B_8 S}{S^4 + A_1 S^3 + A_2 S^2 + A_3 S}$$

$$\frac{\phi}{C_L} = \frac{D_4}{D} = \frac{B_9 S^2 + B_{10} S + B_{11}}{S^4 + A_1 S^3 + A_2 S^2 + A_3 S}$$

$$A_1 = a_{11} + a_{22} + a_{42}$$

$$A_2 = a_{11}(a_{22} + a_{42}) - a_{32}(a_{23} + a_{43}) - a_{12}(a_{21} + a_{41}) - a_{13}a_{31}$$

$$A_3 = -a_{11}(a_{23}a_{32} + a_{43}a_{32}) + a_{12}(a_{23}a_{31} + a_{43}a_{31}) + a_{13}a_{32}(a_{21} + a_{41}) - a_{13}a_{31}(a_{22} + a_{42})$$

$$B_1 = b_1, \qquad B_2 = b_1(a_{22} + a_{42}) - b_2 a_{12}$$

$$B_3 = b_2(a_{13}a_{32}) - b_1(a_{23}a_{32} + a_{43}a_{32})$$

$$B_4 = b_2, \qquad B_5 = b_2 a_{11} - b_1(a_{21} + a_{41})$$

$$B_6 = b_1 a_{31}(a_{23} + a_{43}) - b_2 a_{13} a_{31}$$

$$B_7 = -b_2 a_{32} - b_1 a_{31}$$

$$B_8 = -b_2 a_{31} a_{11} + b_1 a_{32}(a_{21} + a_{41}) - b_1 a_{31}(a_{22} + a_{42}) + a_{13} a_{31}$$

$$B_9 = -b_1 a_{41} - b_2 a_{42}$$

$$B_{10} = b_1(a_{42}a_{21} + a_{43}a_{31} - a_{41}a_{22}) + b_2(a_{43}a_{32} + a_{41}a_{12} - a_{11}a_{42})$$

$$B_{11} = b_1\left[a_{43}a_{32}a_{21} + a_{42}a_{23}a_{31} - a_{22}a_{13}a_{31} - a_{23}a_{32}a_{11}\right]$$

$$+ b_2\left[a_{11}a_{43}a_{32} + a_{13}a_{31}a_{42} - a_{41}a_{13}a_{32} - a_{43}a_{31}a_{12}\right]$$

Guidance pertubation equation

$$\varepsilon = C_1 v + C_2 \gamma + C_3 h + C_4 \varphi$$

$$C_1 = \frac{\partial \varepsilon}{\partial B}\frac{\partial B}{\partial v} + \frac{\partial \varepsilon}{\partial C}\frac{\partial C}{\partial v} + \frac{\partial \varepsilon}{\partial E}\frac{\partial E}{\partial v}$$

$$C_2 = -\sec^2 \gamma_0$$

$$C_3 = \frac{\partial \varepsilon}{\partial B}\frac{\partial B}{\partial h} + \frac{\partial \varepsilon}{\partial C}\frac{\partial C}{\partial h} + \frac{\partial \varepsilon}{\partial E}\frac{\partial E}{\partial h}$$

$$C_4 = \frac{\partial \varepsilon}{\partial B}\frac{\partial B}{\partial \varphi} + \frac{\partial \varepsilon}{\partial C}\frac{\partial C}{\partial \varphi} + \frac{\partial \varepsilon}{\partial E}\frac{\partial E}{\partial \varphi}$$

$$\frac{\partial \varepsilon}{\partial B} = \frac{1}{E} - \frac{B}{E\sqrt{B^2-CE}} \qquad \frac{\partial \varepsilon}{\partial C} = \frac{1}{\sqrt{B^2-CE}}$$

$$\frac{\partial \varepsilon}{\partial E} = \frac{\sqrt{B^2-CE}-B}{E^2} + \frac{C}{E\sqrt{B^2-CE}} \qquad \frac{\partial B}{\partial v} = 0$$

$$\frac{\partial C}{\partial v} = -\frac{2\mu r_T}{v_0^{\,3}}\left[1-\cos(\varphi_T-\varphi_0)\right]$$

$$\frac{\partial E}{\partial v} = -\frac{2\mu r_T}{v_0^{\,3}}\left[1-\cos(\varphi_T-\varphi_0)\right] \qquad \frac{\partial E}{\partial h} = 0$$

$$\frac{\partial E}{\partial \varphi} = -\frac{\mu R_T}{v_0^2}\sin(\varphi_T-\varphi_0)$$

$$\frac{\partial B}{\partial \varphi} = -r_T\frac{(h_0+r_e)}{2}\cos(\varphi_T-\varphi_0)$$

$$\frac{\partial B}{\partial h} = \frac{r_T}{2}\sin(\varphi_T-\varphi_0)$$

$$\frac{\partial C}{\partial h} = r_T\cos(\varphi_T-\varphi_0) - 2(h_0+r_e)$$

$$\frac{\partial C}{\partial \varphi} = r_T(h_0+r_e)\sin(\varphi_T-\varphi_0) - \frac{\mu r_T}{v_0^2}\sin(\varphi_T-\varphi_0)$$

APPENDIX Q
OPTIMUM TRAJECTORY PROGRAM

A. Introduction

During re-entry of the Apollo vehicle into the Earth's atmosphere on return from its space mission it is of extreme importance that the vehicle and its crew be protected from the tremendous heat energy generated during re-entry. To accomplish this task the vehicle must be guided through the atmosphere so as to minimize the amount of heat transferred to the vehicle. In addition the acceleration levels at which the vehicle operates must be restricted to tolerable levels. To determine the re-entry trajectories which satisfy the above requirements, an optimum trajectory study has been initiated. The primary goal of this study is to develop a method for determining and studying the re-entry trajectory,i.e., the angle of attack time history -- which minimizes the heat input to the vehicle while simultaneously satisfying the following requirements:

(1) The acceleration levels must be maintained within specified endurance limits, (2) The re-entry trajectory must terminate at a specified location on the surface of the earth, (3) The re-entry trajectory must be restrained from skipping back out of the atmosphere to altitudes at which radiation hazards exist. This is accomplished by imposing an altitude endurance limit on the trajectory, (4) To assure aerodynamic control of the vehicle a dynamic pressure endurance limit is being considered during the initial phases of the study. If this particular constraint does not appear restrictive, it will later be eliminated.

For the initial phase of the study, a two dimensional optimum rajectory technique has been formulated and is presently being programmed at Martin for calculation on the IBM 7090. A secondary goal of the study is to refine and if possible, simplify the digital program in order to determine the optimum re-entry trajectory in as little computer time and equipment as possible thus enabling feasible on-board computation with the vehicles airborne computer.

Several methods for trajectory optimization were initially considered, namely, the indirect method of variational calculus, specifically the Mayer problem; direct variational methods; dynamic programming techniques and approximate optimization methods. Because of the accuracy and short computation time desired a direct variational method similar to those of References (a) and (b) were deemed most feasible for application to the problem.

A discussion of the methods presently being programmed is given in the following sections.

B. Derivation of Method

The equations of motion which determine the trajectory, the equation representing the heat transferred to the vehicle and the equations which constrain the accelerations, altitude and dynamic pressure can be represented by the following system of non-linear differential equations

$$\frac{dyi}{dt} = fi\ (y, \alpha, t)\ i = 1,2, \ldots n \tag{1}$$

Let $\bar{y}_i(t)$ be values of the dependent variables which satisfy the constraining equation (1) for a specified driving function $\bar{\alpha}(t)$. The values of $\bar{y}_i(t)$ and $\bar{\alpha}(t)$ represent the nominal trajectory which in general is non-optimum. Let $y_i(t)$ and $\alpha(t)$ be neighboring values related to the nominal values as follows

$$y_i(t) = \bar{y}_i(t) + \delta y_i(t)$$
$$\alpha(t) = \bar{\alpha}(t) + \delta\alpha(t) \qquad (2)$$

where $\delta y_i(t)$ and $\delta\alpha(t)$ are small pertubations about the nominal trajectory. Performing a Taylor Expansion about the nominal we see that if second order terms are neglected the small pertubations are related by the following equation

$$\frac{d}{dt}(\delta y_i) = \sum_{j=1}^{n} \frac{\partial f_i}{\partial y_i} \; y_j + \frac{\partial f_i}{\partial \alpha}\,\delta\alpha \qquad (3)$$

$$i = 1, 2, \ldots n$$

Equations (3) are a system of linear differential equations with variable coefficients and are more amenable to mathematical analysis than the non-linear equations (1). The values of the variable coefficients in Equation (3) are known along the nominal trajectory.

Consider the homogeneous part of Equations (3) written in matrix notation as follows

$$\delta\dot{\mathbf{y}} = A\,\delta y \qquad (4)$$

where δy is an n-element column matrix and A is an nxn matrix of coefficients. Let δY be a fundamental solution to (4), then

$$\delta Y = A \; \delta Y \qquad (5)$$

and

$$\delta Y \; \delta Y^{-1} = A \qquad (6)$$

also

$$\delta Y^{-1}\,\delta Y = I \qquad (7)$$

where I is the identity matrix. Differentiating gives

$$\delta Y^{-1} \delta \dot{Y} - \delta \dot{Y}^{-1} \delta Y = 0$$

or

$$\delta \dot{Y}^{-1} = - \delta Y^{-1} \delta \dot{Y} \ \delta Y^{-1} \qquad (8)$$

Substituting (6) into (8) gives

$$\delta \dot{Y}^{-1} = - \delta Y^{-1} A \qquad (9)$$

Transposing both sides

$$\delta \dot{Y}^{*-1} = -A^{*} \ \delta Y^{*-1} \qquad (10)$$

Therefore δY^{*-1} is the fundamental solution to the homogeneous linear system

$$\dot{\lambda} = -A^{*} \lambda \qquad (11)$$

Equations (11) are adjoint to (14), the two having their fundamental solutions related by

$$\Lambda = \delta Y^{*-1} \qquad (12)$$

Rewriting the adjoint system in summation notation we get

$$\frac{d}{dt} \lambda i = - \sum_{j=1}^{n} \frac{\partial f_j}{\partial y_i} \lambda j \qquad (13)$$

Next multiply the small pertubation equations (3) by λi, the adjoint equations (13) by δy_i and add

$$\lambda i \frac{d}{dt} (\delta y_i) + \delta y_i \frac{d}{d_t} \lambda i = \sum_{j=1}^{n} \frac{\partial f_i}{\partial y_j} \delta y_j \lambda i - \sum_{y=1}^{n} \frac{\partial f_j}{\partial y_i} \delta y_i \lambda j +$$

$$\frac{\partial f_i}{\partial \alpha} d\delta\alpha \delta y_i \qquad (14)$$

Summing on i yields

$$\sum_{i=1}^{n} \frac{d}{dt} (\lambda i \, \delta y_i) = \sum_{i=1}^{n} \sum_{y=1}^{n} \frac{\partial f_i}{\partial y_j} \delta y_j \lambda i - \sum_{i=1}^{n} \sum_{y=1}^{n} \frac{\partial f_j}{\partial y_i} \delta y_i \ \lambda j +$$

$$\sum_{i=1}^{n} \frac{\partial f_i}{\partial \alpha} \delta\alpha \, \delta y_i \qquad (15)$$

The second and third terms in Equation (15) are equal but of opposite sign and therefore cancel each other. Integrating the remaining terms from $t = t_o$ to $t = T$, the initial and final time of the nominal trajectory we obtain

$$\left[\sum_{i=1}^{n} \lambda_i \, \delta y_i \right]_{t_o}^{T} = \int_{t_o}^{T} \lambda_\alpha \, \delta\alpha \, dt \qquad (16)$$

where

$$\lambda_\alpha = \sum_{i=1}^{n} \frac{\partial f_i}{\partial \alpha} \, \delta y_i \qquad (17)$$

Equation (16) is a one dimensional form of Green's Theorem. The method employed in the proceeding development is identical to those of Reference (a), (b) and (c).

In Equation(16), the upper limit of integration or "stopping condition" on the problem is assumed to be the final time, T. Frequently stopping conditions other than final time are desired for which case we can write

$$dy_i = \delta y_i + \dot{y}_i \, dT \qquad (18)$$

for small changes, dT, in final time. Substituting equation (18) into (16) and replacing y_i by f_i gives

$$\left[\sum_{i=1}^{n} \lambda_i \, dy_i \right]_{T} = \left[\sum_{i=1}^{n} \lambda_i \, f_i \right]_{T} dT + \int_{t_o}^{T} \lambda_\alpha \, \delta\alpha \, dt + \qquad (19)$$

$$\left[\sum_{i=1}^{n} \lambda_i \, \delta y_i \right]_{t_o}$$

The usefulness of Equations (17) and (19) in determining the correction, $\delta\alpha(t)$, to be applied to the nominal value of the driving function will become apparent in the following paragraphs.

C. Application of Method

Applying the equations discussed above to the optimum re-entry problem, we have for the constraint equations (1) the following system of differential equations.

$$\dot{V} = f_v \quad \text{where} \quad f_v = -g \sin\gamma - \frac{D(h,v,\alpha)}{m} \tag{20}$$

$$\dot{\gamma} = f_\gamma \qquad f_\gamma = \frac{V\cos\gamma}{R+h} - \frac{g\cos\gamma}{V} + \frac{L(h,V,\alpha)}{mV} \tag{21}$$

$$\dot{x} = f_x \qquad f_x = \frac{R}{R+h} V\cos\gamma \tag{22}$$

$$\dot{h} = f_h \qquad f_n = V\sin\gamma \tag{23}$$

$$\dot{Q} = f_q \qquad f_q = C_1 \rho^{1/2} V^{3.15} G_{avg} A(\alpha) + H(h,V)R_n B(\alpha) \tag{24}$$

$$\dot{\psi} = f_\psi \qquad f_\psi = 1/\tau_a \tag{25}$$

$$\dot{\phi} = f_\phi \qquad f_\phi = 1/\tau_h \tag{26}$$

$$\dot{\theta} = f_\theta \qquad f_\theta = 1/\tau g \tag{27}$$

Equations (20) and (21) are the dynamic equations of motion for a non-thrusting, constant mass vehicle about a spherical, non-rotating earth. Equations (22) and (23) are the kinematic equations of motion. Equation (24) is the heat transfer equation. In the first term on the right $C_1\rho^{1/2} V^{3.15} G_{avg}$ is the stagnation point convective heat transfer at zero angle-of-attack. In the second term on the right $H(h,V) R_n$ is the heat radiated to the stagnation point at zero angle of attack. The functions $A(\alpha)$ and $B(\alpha)$ represent the

APPENDIX R
DEVELOPMENT OF APPROXIMATION FOR EXPLICIT TANGENT STEERING

REFERENCE CHAPTER III SECTIONS B AND F

(1) $\tan \gamma_d - \tan \gamma_a = \tan \gamma_e$

(2) $C_L = K \tan \gamma_e$

(3) where $\tan \gamma_d = \dfrac{B \pm \sqrt{B^2 - AC}}{A}$

(4) $A - r_c \left[\dfrac{2 r_c}{r} - \dfrac{r_c V^2}{\mu} - 2 \right]$

using $r_c = r_e + h_c$

$r = r_e + h_c + \Delta h$

$V_c^2 = \dfrac{r_c}{\mu}$

then

(5) $\dfrac{2 r_c}{r} \approx 2 \left[1 - \dfrac{\Delta h}{r_e + h_c} \right]$

and

(6) $\dfrac{r_c V^2}{\mu} = V^2 V_c^2$

Then (4) becomes

$$A \approx -r_c \left[2 - \frac{2 \Delta h}{r_c} - V^2 V_c^2 - 2 \right]$$

$$A \approx 2 \Delta h + V^2 V_c^2 r_c$$

(7) $A \approx 2 \Delta h + \dfrac{V^2 r_c^2}{\mu}$

[redacted]

[redacted]

(8) For this case $B = 0$

(9) **Since** $C = A - \frac{r^2 V^2}{\mu}$

$$C/A \approx - \frac{\frac{r^2 V^2}{\mu}}{2 \Delta h + \frac{V^2 r_c^2}{\mu}}$$

(10) $$C/A \approx - \frac{2 \Delta h \mu}{V^2 r_c^2}$$

(11) **Then** $\tan \gamma_d = \pm \sqrt{- C/A}$

(12) $$\tan \gamma_d \approx \sqrt{\frac{2 \Delta h \mu}{V^2 r_c^2}}$$

Definition of Terms

r_c = Target orbit radius ft.

h_c = Target orbit altitude ft.

r = Radius of vehicle at any time (t) ft.

r_e = Radius of earth ft.

V = Velocity of vehicle at any time (t) ft./sec.

V_c = Circular satellite velocity at target orbit altitude.

μ = Universal gravitational constant.

$\Delta h = r - r_c$

~~CONFIDENTIAL~~

γ_d = Flight path angle desired.

γ_a = Actual flight path angle.

γ_e = Flight path angle error.

K = Control Law gain.

C_L = Vehicle Lift Coefficient.

~~CONFIDENTIAL~~

NOMENCLATURE

A, S	Reference area for drag and lift
A_u	Horizontal deceleration
a	Resultant deceleration
C_D	Drag coefficient
C_L	Lift coefficient
D	Drag force
h	Altitude
K	Control law gain
L	Lift force
M	Mass of vehicle
P	Perigee
q_{c+R}	Total heat at stagnation point (convective + radiative)
q	Dynamic pressure
$\bar{q}_c$	Convective heating rate
$\bar{q}_r$	Radiative heating rate
$\bar{q}$	Approximate convective heating rate parameter
R_n	Reynolds number

[redacted]

R_x	Longitudinal range
R_y	Lateral range
r	Radial distance from center of the earth
t	Time
u	Circumferential velocity normal to radius vector
$\bar{u}$	Normalized velocity
u_c	Circular orbital velocity
u_T	Approach velocity
V	Velocity along the flight path
X, Z	Position of vehicle in guidance plane
$\dot{X}, \dot{Z}$	Velocity of vehicle in guidance plane
X_T, Z_T	Destination position in guidance plane - constant for non-rotating earth
Z	Dimensionless function of $\bar{u}$ determined by equation and appropriate boundary conditions
γ	Local flight path angle (relative to local horizontal)
α	Angle of attack
β	Atmospheric decay parameter
ρ	Atmospheric density

[redacted]

ϕ	Vehicle roll angle
$\Delta \Phi$	Longitude from vehicle to destination
Φ_m	Longitude of venicle
Φ_T	Central angle to destination
Ψ_m	Angle from due east to velocity vector
Ψ_{mt}	Angle from due east to line of sight between vehicle and destination
λ_m	Latitude of vehicle
η	Load factor

Subscripts

$1, 0, i$	Initial condition
m	Missile (vehicle)
e	Exit condition or parameter error
T	Target
d	Desired parameter value
$S.L.$	Conditions with respect to sea level
c	Convective
R	Radiative

[redacted]

S	Stagnation point
a	Actual parameter value

Superscripts

$\bar{\ }$	Inertial axis reference
$\dot{\ }$	Rate of change with respect to time

APPENDIX S

APOLLO LANDING SIMULATION DISPLAY AND CONTROL

The scope display shown in Fig. III-2 will be used by the pilot for direct control of the vehicle employing the range prediction information obtained from the prediction computer. The destination dot will be presented on the display in relation to the predicted range capabilities and will not be directly related to projected latitude and longitude on the earth. The destination dot on the scope will have the coordinates:

$$Y_{SCOPE} = \left[\frac{R_{xtg} - R_{xMIN}}{R_{xMAX} - R_{xMIN}}\right] K_1$$

$$X_{SCOPE} = \left[\frac{R_{ytg}}{R_{yMAX}}\right] K_2$$

R_{xtg} = longitudinal range to go

R_{xmax} = max predicted longitudinal range

R_{xmin} = min predicted longitudinal range

R_{ytg} = lateral range to go

R_{ymax} = maximum predicted lateral range

The fixed profile of the display indicates the locus of end points, with respect to the desired destination, at which the vehicle would land if a constant L/D and roll angle were held for the remainder of the flight. Several profiles to cover various flight performance boundaries are prepared as plastic overlays and will be changed as flight conditions dictate. Figure III-2 shows a terminal condition profile. It is felt that the effect of discrepancies in the shape of the profile, in addition to the computing errors due to computer switching, etc., should not create a pilot control problem. The pilot should be able to adjust for these conditions by counteracting the apparent drift motion of the destination dot by choosing a new trim condition. When the destination appears in the center of the displayed control capability, i.e., (11° AOA; .4 L/D; 13° AOA, .5 L/D), the pilot will have a ± 50% control correction capability. Two limits will be displayed on the scope to establish the flight envelope limits. One, a 6 g limit, will be displayed as a bar on the scope positioned at a specified minimum L/D ratio that the pilot can maintain at that moment without exceeding the 6 g load, and moved as a function of predicted g's. The bar additionally indicates that lift modulation will be required to attain a range below that line. As the flight progresses, the line is moved with a slight lead on the actual predicted g's to allow the pilot time to maneuver, and thus avoid exceeding 6 g loads. A second limit, the skip out limit, will be displayed as a bar positioned at an L/D ratio which would indicate flight conditions causing the vehicle to skip beyond the 400 naut mi. The bar will be positioned and moved as follows:

$$Y_{SCOPE} = \left[\frac{(L/D)\,(K_x)\,(\bar{u}_{e\ ref.})}{\bar{u}_{e\ MAX}} \right] K_S$$

Other flight envelope condition limitations, i.e., heating etc. will be furnished to the pilot on "red lined" meters.

The pilot will use the display and control the flight path by trimming to the combination of angle of attack and roll angle that is indicated. By holding these conditions constant, it is assumed that he would be able to reach the desired destination. However, since these conditions would change during the trajectory, the pilot would match the new requirements and continue to maneuver to avoid exceeding the skip or g limits. Roll angle will generally be held out to a point beyond the destination, moving the destination dot to the center of the display and giving a maximum maneuver capability to provide for prediction variations.

Simulation

The flight simulator will consist of a fixed control center in conjunction with 6 REAC C400 Analog Computer Consoles. The pilot will be given the following information for vehicle control:

Console

Velocity
Altitude
Rate of climb
Range to go
Acceleration
Angle of attack
Bank angle
Predicted heating limit

Guidance Display (TV Monitor)

Maximum maneuver capability
Destination

Flight boundaries

Trim angle of attack $(aoa)_{trim}$.

Roll angle

The pilot control will be applied through a control stick mounted on the console. The Analog Computer will accept scaled voltages from the control console for vehicle bank angle and angle of attack. A block diagram of the analog simulation is shown in Fig. S-1. The equations programmed in the analog simulation can be found in Appendix O.

The guidance display to be used in this simulation is a 21-inch scope with an engraved Lucite overlay. This overlay will be changed as dictated by given flight conditions (See Fig. III-46 through III-49 Re-entry Ground Traces).

The destination dot and the g and skip boundaries are presented as moving bars on the scope. Vehicle attitude and other control information is available to the pilot on the control console.

The display to be used will be somewhat limited, due to analog equipment availability in that only one limit line will be available at any given time. The pilot may select the limit presentation desired by a switch on the control console. Several additions to the display are indicated:

(1) Modify console to provide completely integrated control unit.

(2) Use "flight type" instrumentation, i.e., bank angle indicator, roll indicator etc.

(3) Display limits simultaneously for g's and skip out limits (different scope and switches integrated into flight panel).

(4) Use of a Lissajous figure (small diameter circle) to indicate on scope the current AOA and roll angle and move it to encircle the proposed destination. This type of presentation would allow the pilot to more easily control to the flight limits and destination.

[redacted]

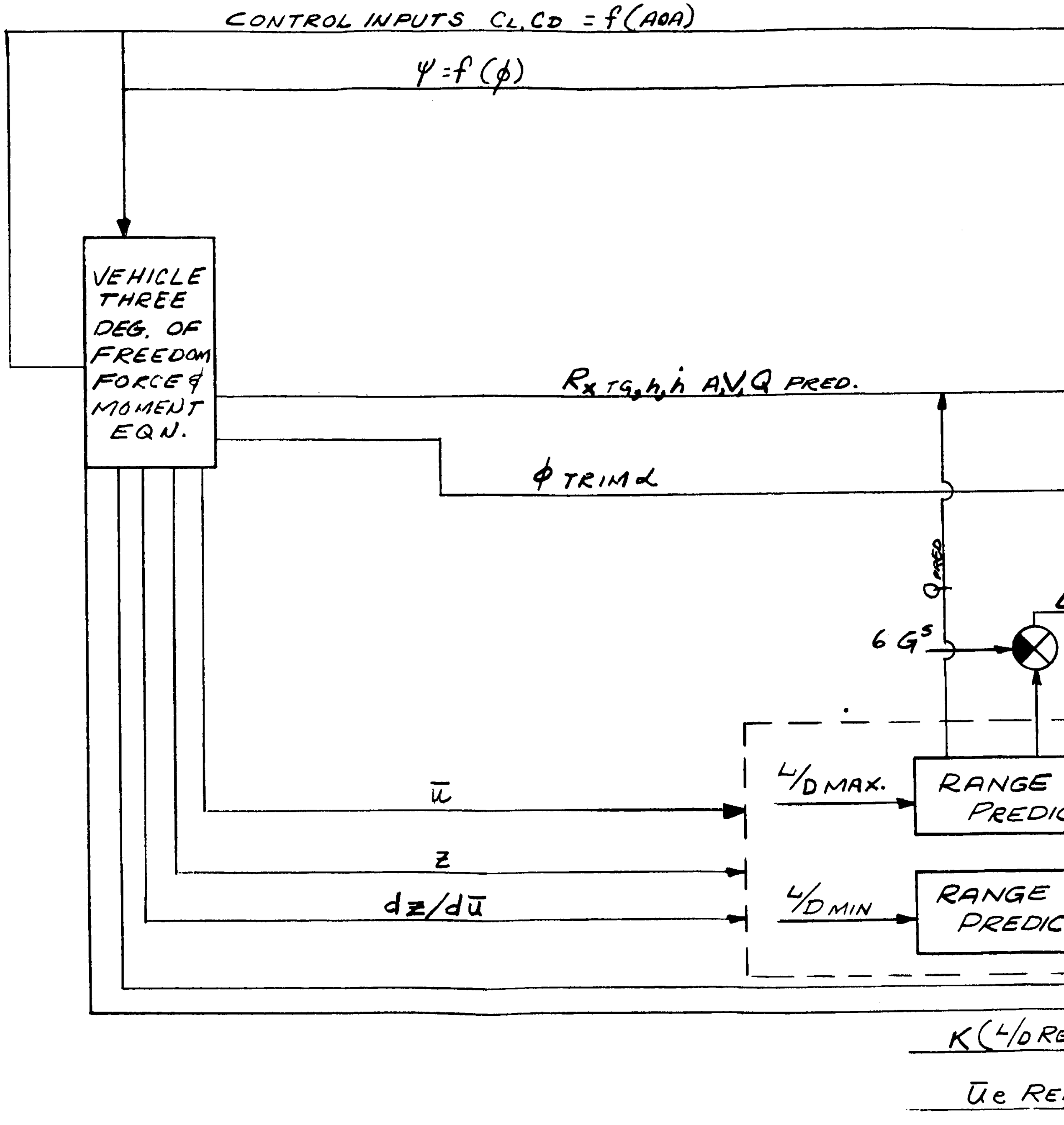
CONTROL INPUTS CL, CD = f(AOA)
ψ = f(φ)
VEHICLE THREE DEG. OF FREEDOM FORCE & MOMENT EQN.
Rx TG, h, ḣ A, V, Q PRED.
φ TRIM α
Q PRED
6 G^S
L/D MAX.
RANGE PREDIC
u̅
z
dz/du̅
L/D MIN
RANGE PREDIC
K(L/D RE
U̅e RE

[redacted]

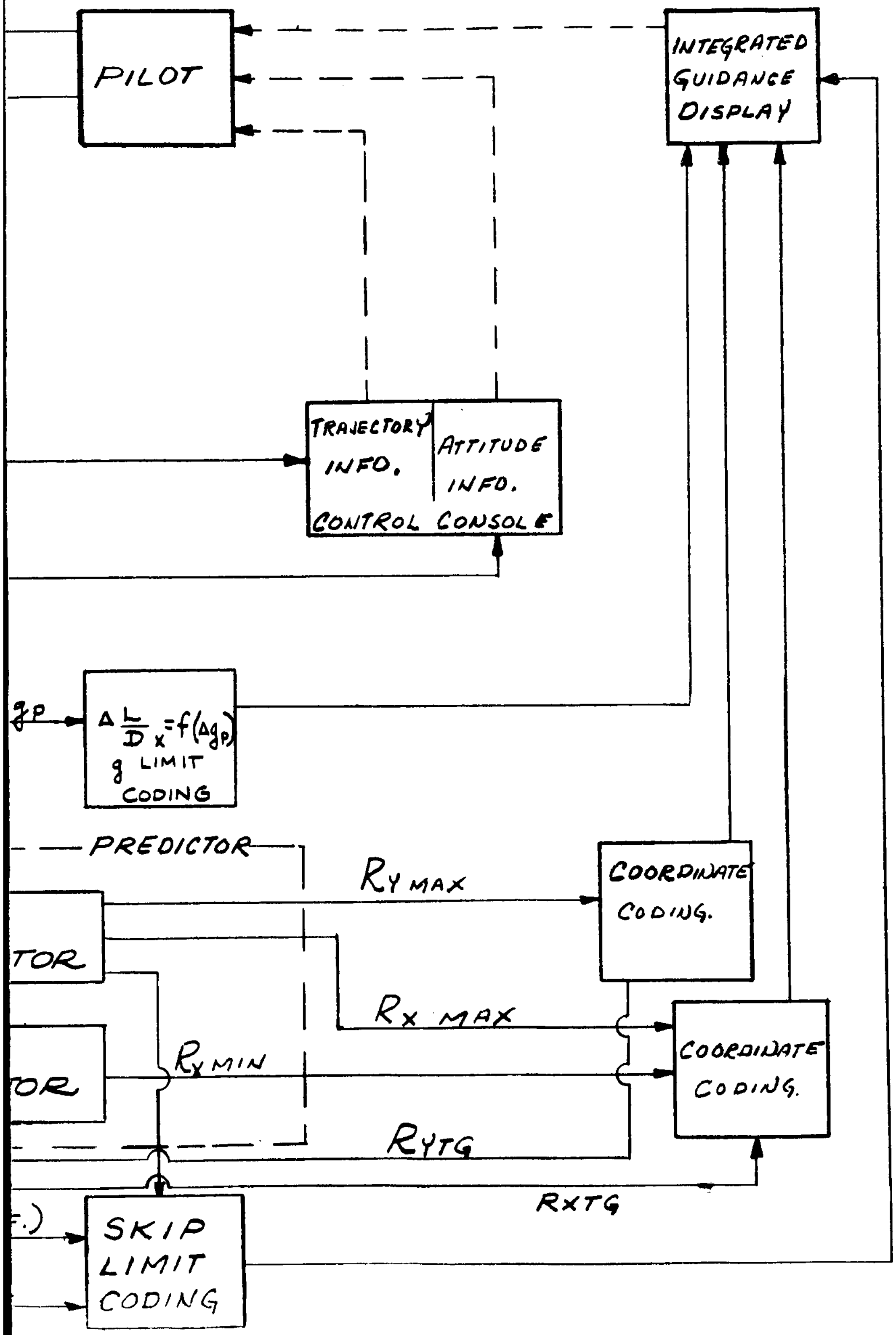
PILOT
INTEGRATED GUIDANCE DISPLAY
TRAJECTORY INFO.
ATTITUDE INFO.
CONTROL CONSOLE
gp
$\Delta \frac{L}{D}_x = f(\Delta g_p)$
g LIMIT
CODING
PREDICTOR
$R_{Y\,MAX}$
COORDINATE CODING.
TOR
$R_{X\,MAX}$
$R_{Y\,MIN}$
OR
COORDINATE CODING.
R_{YTG}
RXTG
F.)
SKIP LIMIT CODING

Fig. S-1. Simulation Block Diagram

APPENDIX T

MINIMIZING REACTION MASS EXPENDITURE DURING LIMIT CYCLING IN A SPACE VEHICLE ON-OFF ATTITUDE CONTROL SYSTEM

Introduction

The on-off reaction system with a dead spot is one of the simpler ways to control the attitude of a space vehicle. It is lighter than a proportional system and, unlike flywheel and gyroscopic systems, is not prone to velocity saturation. Providing that the limit cycle oscillation inherent to this method is tolerable, its chief weakness is its use of irreplaceable reaction mass. This report is chiefly devoted to the effect of various parameters in the expenditure of reaction mass in two simple but typical configurations.

Figure T-1 shows a system with displacement and rate signals available and is the easiest to analyze. Later in this report it will be compared with a system with only displacement signals available which utilizes a lead circuit. (Fig. T-2).

The phase plane analysis technique, as outlined by Mr. Josef Pistiner* in an ARS Technical Note, is a simple and accurate method of determining the performance of such systems and was used in this investigation. It permits both graphical and analytical solutions, allowing pictorial insight and precision.

Parameters

The parameters involved in the design of a configuration as shown in Fig. T-1 are:

(a) Moment of inertia of vehicle (I)

(b) Thrust of control jets (Th)

(c) Moment of control jets ($M_{cont.}$)

(d) Deadspot (θ_p) - one half the total deadspot angle

(e) Hysteresis - (r), where r is the drop-out signal to pull-in signal ratio.

(f) Ratio of rate to displacement gain (m) = $K_{\dot{\theta}}/K_{\theta}$

---

*Pistiner, J. S. "On-Off Control System for Attitude Stabilization of a Space Vehicle", ARS Journal, April 1959

(g) Time delay (T_D) - The time lag between a "jet-on" signal and actual "thrust-on" due to relay and solenoid action, transportation delays, thrust buildup, etc.

(h) Specific impulse of reaction mass (I_{sp})

The expenditure of reaction mass over a period of time is a function of thrust, specific impulse and ratio of "thrust-on" time (T_{on}) to total time (T_{total}) as follows:

(1) $$(\text{lbs. reaction mass}) = \frac{T_h}{I_{sp}} \left(\frac{T_{on}}{T_{total}} \right) \quad (\text{Time in seconds})$$

It is clear that for a given thrust level Th, the ratio $\frac{T_{on}}{T_{total}}$ must be made as small as possible to conserve reaction mass. This ratio is determined by the maneuvering requirements, disturbance conditions and the limit cycle oscillations which are a consequence of the on-off operation. The effect of the limit cycle only is investigated here since the other factors are unique to each application. It should be recognized, however, that these factors may make it impractical to optimize a system on the basis of the limit cycle alone.

Phase plane

A non-dimensional phase plane of the limit cycle will be used to obtain an expression for T_{on}/T_{total} in terms of the system parameters. If we consider only one axis, the attitude equation of motion of a space vehicle under the influence of control moment and initial rate and attitude conditions may be written as:

(2) $$\theta = \theta_0 + \dot{\theta}_0 t \pm (1/2)(\alpha_c t^2)$$

where

(3) $$\pm \alpha_c = \pm \frac{M_{CONT.}}{I} \quad Rad/Sec^2$$

and

(4) $$\dot{\theta} = \dot{\theta}_0 \pm \alpha_c t$$

If we eliminate time between equations (2) and (4) we obtain:

(5) $$\theta = \pm \frac{\dot{\theta}^2}{2\alpha_c} \pm \frac{\dot{\theta}_o}{2\alpha_c} + \theta_o$$

The following identities are used to non-dimensionalize equation (5)

(6) $$T = t/t_b$$

where t = real time and t_b = 1 second, an arbitrary time base.

(7) $$\ddot{\Omega} = \ddot{\theta}/\alpha_c = 1 \text{ or } 0$$

since $\ddot{\theta} = \alpha$ with control on and $\ddot{\theta} = 0$ with control off

(8) $$\ddot{\Omega} = \dot{\theta}/\alpha_c t_b = \dot{\theta}/\alpha_c$$

since $t_b = 1$

(9) $$\Omega = \theta/\alpha_c t_b^2 = \theta/\alpha_c$$

The non-dimensional form of equation (5) is then:

(10) $$\Omega = \pm \dot{\Omega}^2/2 \pm \dot{\Omega}_o^2/2 + \Omega_o$$

The advantages of using a non-dimensional phase plane include:

(a) The opportunity to use standard parabolic templates to describe the phase plane path of the vehicle while under control moment (since $\ddot{\Omega}$ has been made equal to unity) and,

(b) The time required to move from one point to another on the phase plane may be determined by a simple calculation using one of the following relations:

(11)	$\Delta T = \frac{\Delta \Omega}{\Omega} = \left| \Delta t \right|$	Constant velocity movement
(12)	$\Delta T = \Delta \mathring{\Omega} = \left| \Delta t \right|$	Movement under control moment
(13)	$\Delta T = \Delta \dot{\Omega} \left(\frac{M_{CONT}}{M_{ERROR}} \right) = \left| \Delta t \right|$	Movement under error moment
(14)	$\Delta T = \Delta \mathring{\Omega} \left(\frac{M_{CONT}}{M_{CONT} + M_{ERROR}} \right) = \left| \Delta t \right|$	Movement under control and error moment

Figure T-3 is the non-dimensional phase plane plot of a typical limit cycle. Section VI of this Appendix details the derivations of the expressions shown in the figure and the method for obtaining the terms for the times required by each part of the limit cycle.

Briefly, however, it can be seen that the "pull-on" and "drop-out" signal lines differ because of the hysteresis (r) and that their slope is the negative of the reciprocal of the gain ratio (m). The "jet-on" and the "jet-off" lines differ from their respective "pull-on" and "drop-out" signal lines because of the time delay (T_D) in the system. (In this study, the delay between "pull-on" and "jet-on" is considered equal to the delay between "drop-out" and "jet-off".)

Minimizing T_{on}/T_{off}

The relationships of Fig. T-3 may be used in equations (11) and (12) to show Section VI that the ratio of "jet-on" time to "jet-off" time during the limit cycle is:

$$(15) \qquad \frac{T_{on}}{T_{off}} = \frac{\left[\Omega_p (1-r) + m T_D - \frac{T_D^2}{2} \right]}{2(m-T_D)^2 \left[\Omega_p (1+r) - m T_D + T_D^2/2 \right]}$$

T_{on}/T_{off} is related to T_{on}/T_{total} as follows:

$$(16) \quad \frac{T_{ON}}{T_{TOTAL}} = \frac{T_{ON}/T_{OFF}}{1 + T_{ON}/T_{OFF}}$$

Since minimizing T_{on}/T_{off} will minimize T_{on}/T_{total}, we will investigate equation (15) and apply it to equation (16) as needed.

The ratio of rate channel to displacement channel gain (m) is the easiest parameter to change in equation (15). The others are either determined by system requirement (Ω_p) or by hardware considerations (r and T_D). By differentiating T_{on}/T_{off} with respect to m, it is found that the positive value of m making T_{on}/T_{total} a minimum is:

$$(17) \quad m = \frac{-(T_D^2 + 3b) + \left\{(T_D^2 + 3b)^2 + 4\left[(2a+b)T_D^2 + 2ab\right]\right\}^{1/2}}{2T_D}$$

where

$$(18) \quad a = \Omega_p(1+r) + \frac{T_D^2}{2}$$

and

$$(19) \quad b = \Omega_p(1-r) - \frac{T_D^2}{2}$$

Figure T-4 shows how the optimum m varies with Ω_p, and Fig. T-5 shows how it varies with T_D.

Equation (17) enables selection of the m giving the minimum T_{on}/T_{total} allowed by the other parameters. Since, however, the control system must maintain stability, it is appropriate to see if zeal for a low T_{on}/T_{total} could lead to instability. It can be seen from Fig. T-3 that there will be a limit cycle and consequently stable operation if the following conditions are met:

(a) The "jet-on" and "jet-off" lines have a negative slope $\left(\frac{-1}{m - T_D}\right)$ less than infinity, meaning that there is some effective lead or:

$$m - T_D > 0 \tag{20}$$

(b) The "jet-off" lines must be located so that only one jet will be on at any one time, or

$$\Omega_p (1 - r) + m T_D - T_D^2/2 < 2\,\Omega_p \tag{21}$$

from which

$$m < \Omega_p/T_D\,(r+1) + T_D/2 \tag{22}$$

When the limiting values of either equations (20) or (22) are reached the T_{on}/T_{off} ratio is infinite (making T_{on}/T_{total} equal to unity) indicating that one jet or the other is on at all times. We may therefore conclude that any m giving a value of T_{on}/T_{total} less than one insures stability.

When the value of m of equation (17) is substituted in equation (15) we get an expression for T_{on}/T_{off} minimum which automatically uses the optimum m for the other parameters. After slight manipulation and use of equation (16) we obtain:

$$\left(\frac{T_{on}}{T_{total}}\right)_{MIN.} = \frac{T_D^2\,(B^{1/2} - A)^2}{(B^{1/2} - 3A)^2(4\Omega_p + A - B^{1/2}) + T_D^2(B^{1/2} - A)^2}$$

where

$$(24) \qquad A = \Omega_p (1-r) + T_D^2/2$$

and

$$(25) \qquad B = (17-18r+r^2) + (9-r) T_D^2 \Omega_p + T_D^4/4$$

Equation (23) is awkward, making it laborious to use and difficult to determine the relative effects of Ω_p, r and T_D or the minimum T_{on}/T_{total} possible. It was noticed in plotting T_{on}/T_{total} min versus $1/\Omega_p$ for various T_D's and r's, however, that the variation was fairly linear between certain limits for all of these parameters. By plotting calculated values of T_{on}/T_{total} min against each of these parameters on log-log paper and measuring the slopes and intercepts, the following empirical relationship is obtained:

$$(26) \qquad \left(\frac{T_{on}}{T_{total}}\right)_{min.} \approx \frac{0.65 \, T_D^{2.5}}{\Omega_p^{1.28} \, r^3} \approx \frac{0.65 \, T_D^{2.5} \alpha_c^{1.28}}{\theta_p^{1.28} \, r^3}$$

for approximately:

$$0.05 < T_D < 0.2$$

$$0.02 < \Omega_p < 0.4$$

$$0.80 < r < 1.0$$

Equation (26) shows the importance of keeping the time delay (T_D) and the hysteresis (considered as 1 - r) as small as possible. Figure T-4 shows this graphically. The importance of a large deadspot and as small a control acceleration as possible is also indicated. If the acceleration (α_c), and consequently $1/\Omega_p$ is decreased by lessening the thrust of the control jets (Th), the fuel expenditure will be decreased by better than the square of the thrust, since the fuel expenditure is a function of both T_{on}/T_{total} and the thrust.

Because of their exponential effect on fuel expenditure, the control thrust, time delay, and hysteresis offer the most effective avenues of improvement. In many applications, however, the control thrust must be large enough to counteract moments from translation jet asymmetries or turbine decelerations, etc., and must therefore be greater than desired for limit cycle control alone The time delay (T_D) is an inherent characteristic of the configuration selected and is difficult to improve without changing components.

Equation (17) allows calculation of the optimum m for any combination of Ω_p, r, and T_D. (See Fig. T-4) In many applications, however, Ω_p will change as reaction mass is expended causing the moment of inertia (I) to decrease and the control acceleration (α_c) to increase. It is therefore interesting to investigate how reaction mass expenditure varies with non-optimum gain ratios (m), in order to decide whether m or the control thrust (Th) should be programmed.

Curves of T_{on}/T_{total} versus m for various Ω_p's and typical values of T_D and r are plotted in Fig. T-6. This shows that for larger values of Ω_p (Ω_p 0.1), the gain ratio (m) is not critical. As Ω_p is decreased, however, the range of m giving approximate (T_{on}/T_{total}) min is curtailed, and the penalty for using a non-optimum m is increased. It is apparent, however, that for many applications there will be little lost if m is selected for the smallest $_p$ anticipated, since for the large values of $_p$ the fuel expenditure is not so dependent on m.

Figure T-6 also illustrates that the T_{on}/T_{total} curves rise sharply toward unity as m approaches the limiting values of equations (20) and (21). System instability occurs when m exceeds these values.

Another interesting item arises from the observation that as Ω_p decreases, T_{on}/T_{total} min increases until at some point T_{on}/T_{total} min equals unity and m equals the limits of both equations (20) and (21) simultaneously; i.e.,

$$m = T_D = \frac{\Omega_p}{T_D}(1+r) + T_D/2$$

This value of Ω_p is a function of T_D and r as follows from equation (27).

$$\Omega_p = \frac{T_D^2}{2(1+r)}$$

This is the limiting condition for Ω_p, since smaller values will always mean an unstable system.

Comparison of rate channel and lead circuit configurations

Lead circuits have a considerable advantage over rate gyros in cost and simplicity. It is therefore interesting to see if a lead circuit configuration can be made as sparing of reaction mass as the rate channel system investigated previously. Figure T-2 shows a lead circuit configuration of the type considered, which is a counterpart to the rate channel system of Fig. T-1.

The Laplace transform of the output of a single stage lead network as shown in Fig. T-2 is:

$$(29) \qquad E_o(s) = \frac{(1+Ts)E_{in}(s)}{\alpha(1+T/\alpha\, s)} - \frac{TV_{oc}}{\alpha(1+T/\alpha\, s)}$$

$$T = R_1 C_1$$

Considering one axis, the vehicle attitude is given by:

$$(30) \qquad \theta = \theta_o + \dot{\theta}_o t + 1/2\, \ddot{\theta}_c t^2$$

where $\ddot{\theta}_c$ is the constant angular acceleration resulting from control moment, and θ_o and $\dot{\theta}_o$ are initial conditions when control is applied. Since input voltage to the lead circuit ($E_{in}(s)$) is to be proportional to the vehicle attitude (θ) then,

$$(31) \qquad E_{in}(s) = K\left(\frac{\theta_o}{s} + \frac{\dot{\theta}_o}{s^2} + \frac{\ddot{\theta}_c}{s^3}\right)$$

Combining equations (29) and (31) we get:

$$(32)\quad E_o(s) = \frac{K\theta_o(1+Ts)}{\alpha s(1+T/\alpha\, s)} + \frac{K\dot{\theta}_o(1+Ts)}{\alpha s^2(1+T/\alpha\, s)}$$

$$+ \frac{K\ddot{\theta}_c(1+Ts)}{\alpha s^3(1+T/\alpha\, s)} - \frac{T V_{oc}}{\alpha(1+T/\alpha\, s)}$$

The inverse Laplace of this is:

$$(33)\quad e_o(t) = \frac{K\theta_o}{\alpha}\left[1 + (\alpha-1)\,\epsilon^{-\frac{\alpha}{T}t}\right]$$

$$+ \left[T\left(\frac{\alpha-1}{\alpha}\right)\left(1-\epsilon^{-\frac{\alpha}{T}t}\right) + t\right]\frac{K\dot{\theta}_{co}}{\alpha}$$

$$+ \frac{K\ddot{\theta}_c}{\alpha}\left[T\left(\frac{1-\alpha}{\alpha}\right)\left(\frac{T}{\alpha} - \frac{T}{\alpha}\,\epsilon^{-\frac{\alpha}{T}t} - t\right) + \frac{t^2}{2}\right]$$

$$- V_{oc}\,\epsilon^{-\frac{\alpha}{T}t}$$

This equation also applies when the control jets are off with $\ddot{\theta}_c = 0$. In normal operation the jets will be off for relatively long periods of time, during the limit cycle, and $\frac{\alpha}{T}$ t will be quite large so that the exponential terms will be negligible. Therefore for "control-off":

$$(34) \quad e_o(t) = \frac{K\theta_o}{\alpha} + \frac{K\dot{\theta}_o}{\alpha}\left[T\,\frac{\alpha-1}{\alpha} + t\right]$$

$$= \frac{K}{\alpha}\left(\theta_o + \dot{\theta}_o t\right) + \frac{KT}{\alpha}\left(\frac{\alpha-1}{\alpha}\right)\dot{\theta}_o$$

Since the control jets are off,

$$\left.\begin{array}{ll} (35) & \theta_o + \dot{\theta}_o t = \theta \\ \text{and} & \\ (36) & \dot{\theta}_o = \dot{\theta} \end{array}\right\} \quad \text{Control jets off}$$

Therefore, with "control-off",

$$(37) \quad e_o(t) = \frac{k}{\alpha}\theta + \frac{kT}{\alpha}\left(\frac{\alpha-1}{\alpha}\right)\dot{\theta}$$

and

$$(38) \quad e_i = k\theta$$

Now

$$(39) \qquad V_{oc} = e_i - e_o = k\theta - \frac{k}{\alpha}\theta - \frac{k}{\alpha}T\left(\frac{\alpha-1}{\alpha}\right)\dot{\theta}$$

$$= k\theta\left(\frac{\alpha-1}{\alpha}\right) - \frac{kT\dot{\theta}}{\alpha}\left(\frac{\alpha-1}{\alpha}\right)$$

The θ and $\dot{\theta}$ of the "control-off equations" (equations (35) thru (39)) are the θ_o and $\dot{\theta}_o$ for the succeeding interval of "control-on". Equation (39) allows us to determine the effect of the capacitor C_1 charge at the initiation of "control-on."

$$(40) \qquad e_o(t) = + \frac{k\theta_o}{\alpha}$$

$$+ \frac{k\dot{\theta}_o}{\alpha}\left[T\left(\frac{\alpha-1}{\alpha}\right) + t\right]$$

$$+ \frac{k\ddot{\theta}_c}{\alpha}\left[T\left(\frac{\alpha-1}{\alpha}\right)\left(t - \frac{T}{\alpha} + \frac{T}{\alpha}\epsilon^{-\frac{\alpha}{T}t}\right) + \frac{t^2}{2}\right]$$

$$= + \frac{k}{\alpha}\left(\theta_o + \dot{\theta}_o t + \ddot{\theta}_c \frac{t^2}{2}\right)$$

$$+ \frac{k}{\alpha}T\left(\frac{\alpha-1}{\alpha}\right)\left(\dot{\theta}_o + \ddot{\theta}_c t\right)$$

$$- \frac{k}{\alpha}T\left(\frac{\alpha-1}{\alpha}\right)\frac{T}{\alpha}\ddot{\theta}_c\left(1 - \epsilon^{-\frac{\alpha}{T}t}\right)$$

$$e_0(t) = \frac{k}{\alpha}\theta + \frac{k}{\alpha}T\left(\frac{\alpha-1}{\alpha}\right)\dot{\theta}$$

$$- k\frac{T^2}{\alpha^2}\left(\frac{\alpha-1}{\alpha}\right)\ddot{\theta}_c\left(1-\epsilon^{-\frac{\alpha}{T}t}\right)$$

This is the exact solution of the lead circuit output.
If we assume that $\epsilon^{-\frac{\alpha}{T}t}$ may be safely ignored when equal to 0.05 or less, then we find that we may ignore it when $t \geq 3T/\alpha$. With T/α generally in the neighborhood of 0.02, this assumption is evidently permissible. We therefore have:

$$(41)\quad e_0(t) = \frac{k}{\alpha}\left[\theta + T\left(\frac{\alpha-1}{\alpha}\right)\dot{\theta} - \frac{T^2}{\alpha}\left(\frac{\alpha-1}{\alpha}\right)\ddot{\theta}_c\right]$$

With equations (37) and (41), we can write expressions for the "pull-on" and "drop-out" lines of the $\dot{\theta} - \theta$ phase plane.

"Drop-Out"

$$(42)\quad \frac{\alpha e_0(t)}{k} = \pm\theta_D = \theta + T\left(\frac{\alpha-1}{\alpha}\right)\dot{\theta} - \frac{T^2}{\alpha}\left(\frac{\alpha-1}{\alpha}\right)\ddot{\theta}_c$$

"Pull-On"

$$(43)\quad \frac{\alpha e_0(t)}{k} = \pm\theta_P = \theta + T\left(\frac{\alpha-1}{\alpha}\right)\dot{\theta}$$

In non-dimensional form (see equations (3), (4), (5) and (6)) these relations become:

"Pull-On"

$$(44)\quad \pm\Omega_P = \pm\Omega \pm M\dot{\Omega}$$

"Drop-Out"

(45)
$$\pm\Omega_D = \pm\Omega \pm M\dot{\Omega} - M_c\ddot{\Omega}_c = r\Omega_p$$

$$= \Omega + M(\dot{\Omega} - c) = r\Omega_p$$

where:

$$M = \tau\left(\frac{\alpha-1}{\alpha}\right) \qquad c = {}^{T}/_{\alpha} \qquad r = \frac{\Omega_D}{\Omega_p} = \text{hysteresis}$$

The equation of the non-dimensional phase plane "pull-on" and "drop-out" lines are therefore, from equations (44) and (45):

"Pull-On"

(46)
$$\dot{\Omega} = \frac{\pm\Omega_p \mp \Omega}{M}$$

"Drop-Out"

(47)
$$\dot{\Omega} = \frac{\pm r\Omega_p - \Omega}{M} + c$$

The "thrust-on" and "thrust-off" lines, which differ from the "pull-on" and "drop-out" lines because of the finite time delays (T_D) due to relay action, solenoid action and thrust buildup are:

"Thrust-on"

(48)
$$\dot{\Omega} = \frac{\Omega_p - \Omega}{M - T_D}$$

"Thrust-off"

$$\dot{\Omega} = \frac{r\Omega_p - \Omega + M(c + T_o) + T_D^2/2}{M - T_D} \tag{49}$$

These equations are similar to the corresponding equations for the rate channel configuration.

This similarity also applies to the important T_{on}/T_{off} relation which may be derived from a phase plane similar to Fig. T-3.

$$\frac{T_{on}}{T_{off}} = \frac{\left[\Omega_p(1-r) + M\left(T_D + \frac{T}{\alpha}\right) - \frac{T_D^2}{2}\right]^2}{2\left[M - T_D\right]^2\left[\Omega_p(1+r) - M\left(T_D + \frac{T}{\alpha}\right) + \frac{T_D^2}{2}\right]}. \tag{50}$$

where $M = T\left(\frac{\alpha - 1}{\alpha}\right)$

If we take a partial differential of equation (50) with respect to T, we find that to find a realizable value of T which makes T_{on}/T_{off} a minimum we must solve a cubic equation as follows:

$$\begin{aligned}
&\left[\frac{(1-1/\alpha)^3}{\alpha} T_D + 2\,\frac{(1-1/\alpha)^2}{\alpha^2} T_D\right]T^3 + \left[\frac{3(1-1/\alpha)^2 T_D^2}{\alpha} + \right. \\
&(1-1/\alpha)^3 T_D^2 + 2\left\{\Omega_p(1+r) + \frac{T_D^2}{2}\right\}\frac{(1-1/\alpha)^2}{\alpha} T_D + \\
&\left. 4\left\{\Omega_p(1+r) - \frac{T_D^2}{2}\right\}\frac{(1-1/\alpha)^2}{\alpha}\right] T^2 + \left[(1-1/\alpha)^2 T_D^3 + \right. \\
&3\left\{\Omega_p(1-r) - \frac{T_D^2}{2}\right\}(1-1/\alpha)^2 T_D - 4\left\{\Omega_p(1+r) + \frac{T_D^2}{2}\right\} \times \\
&\left. \frac{(1-1/\alpha)}{\alpha} T_D - 2\left\{\Omega_p(1-r) - \frac{T_D^2}{2}\right\}\frac{(1-1/\alpha)}{\alpha} T_D\right] T
\end{aligned} \tag{51}$$

[redacted]

(51) continued

$$
\begin{aligned}
&+\Big[-2\left\{\Omega_p(1+r)+\frac{T_D^2}{2}\right\}(1-1/\alpha)T_D^2 \\
&\quad-\left\{\Omega_p(1-r)-\frac{T_D^2}{2}\right\}(1-1/\alpha)T_D^2 \\
&\quad-2\left\{\Omega_p(1+r)+\frac{T_D^2}{2}\right\}\left\{\Omega_p(1-r)-\frac{T_D^2}{2}\right\}(1-1/\alpha)\Big] = 0
\end{aligned}
$$

(This cubic is multiplied by a quadratic, which unfortunately yields negative values of T for positive values of

$$\left[\Omega_p(1-r)-\frac{T_D^2}{2}\right]$$

and

$$\left[\Omega_p(1+r)+\frac{T_D^2}{2}\right]$$

and therefore need not be included.)

[redacted]

The general unwieldiness of the cubic's solution precludes its insertion in equation (50). Equation (50) may be used, however, to show the variation of of $\left(T_{on}/T_{off}\right)$ or $\left(T_{on}/T_{total}\right)$ with T for different values of the lead circuit attenuation factor (α) and deadspot (θ_p), as in Fig. T-7, and the value of T for the $\left(T_{on}/T_{off}\right)$ min checked with the cubic. Figure T-7 shows how the $\left(T_{on}/T_{off}\right)$ min decreases as α is increased until at $\alpha = \infty$ the T_{on}/T_{total} versus T curve is identical to the T_{on}/T_{total} versus m curve of the rate channel configuration.

The upper limit of the lead circuit attenuation factor is determined by the least signal to noise ratio that can be tolerated. Numbers of 10 to 12 are usually given as a practical maximum value, but an α of 40 has been used with no difficulty in the coasting flight attitude control system of a major research rocket.

It is evident therefore that a lead circuit configuration can approach the rate channel system in economy of reaction mass expenditure if the signal to noise ratio can be tolerated.

Derivation of T_{on}/T_{off} for rate channel system

Figure T-3 shows a typical limit cycle as determined by the deadspot (Ω_p), time delay (T_D) hysteresis (1 - r) and rate to displacement gain ratio (m) of an "on-off" control system as shown in Fig. T-1. The two "pull-on" lines are the loci of points representing Ω and $\dot{\Omega}$ signal combinations large enough to actuate their respective jets. The "drop-out" lines represent signal combinations low enough to allow the jets to turn-off. The difference between the "pull-on" and the respective "drop-out" lines is due to hysteresis (1 - r).

The deadspot angle, or angle sufficient for "pull-on" without any rate is Ω_p. By definition:

$$\text{(a)} \qquad m = \frac{K_{\dot{\theta}}}{K_{\theta}} = \frac{\Omega_p}{\dot{\Omega}_p}$$

$\dot{\Omega}_p$ is the rate sufficient for "pull-on" without any displacement. Therefore, the equation of the "pull-on" line is:

$$\text{(b)} \qquad m\dot{\Omega} + \Omega = \Omega_p$$

[redacted]

or

$$\dot{\Omega} = \frac{\Omega_P - \Omega}{m}$$

The equation of the "drop-out" line is:

(c) $$\dot{\Omega} = \frac{r\Omega_P - \Omega}{m}$$

The time delay (T_D) prevents the "pull-on" and "jet-on" lines from being the same. Between the "pull-on" point and "jet-on" point, the vehicle follows a constant rate path on the phase plane whose distance ($\Delta\Omega$) is:

$$\Delta\Omega = \dot{\Omega} T_D$$

Therefore, the equation of the "jet-on" line evolves as follows:

$$m\dot{\Omega} + \Omega = \Omega_P + \Delta\Omega = \Omega_P + \dot{\Omega} T_D$$

$$\dot{\Omega}(m - T_D) = \Omega_P - \Omega$$

$$\dot{\Omega} = \frac{\Omega_P - \Omega}{m - T_D}$$

Between the "jet-on" point and "jet-off" point the vehicle follows a parabolic path in the phase plane. Therefore, there is a parabolic instead of a constant velocity path between the "drop-out" point and the "jet-off" point.

Assume that the "drop-out" line is crossed at point 1 on Fig. T-8, and that the jet actually goes off at point 1A. Since it takes a time T_D to go between 1 and 1A we know from equation (12) ($\Delta T = \Delta\dot{\Omega} = |\Delta t|$) that the distance traversed along the Ω axis is equal to T_D.

[redacted]

The distance travelled along the Ω axis is:

$$\overline{1A-D} = \Delta\Omega = +\frac{1}{2}T_D^2 + \dot{\Omega}_1 T_D$$

where $\dot{\Omega}_1$ is the rate at which the drop-out line is crossed. Since $\dot{\Omega}_{1A} = \dot{\Omega}_1 + T_D$ in this case, we may write $\overline{1A-D} = |\Delta\Omega| =$

$$+\frac{1}{2}T_D^2 + (|\dot{\Omega}_{1A}| - T_D)T_D$$

The point (c) in the drop-out line which is at the same rate (Ω_{1A}) as the point at which the jet turns off (or T_D down the $\dot{\Omega}$ axis) is a distance $(m)(T_D)$ along the Ω axis from the initial point (marked 1). The distance along the Ω axis between the "jet-off" point and the "drop-out" line is therefore:

$$\overline{1A-C} = \frac{1}{2}T_D^2 + (|\dot{\Omega}_{1A}| - T_D)T_D + mT_D$$

$$= (|\dot{\Omega}_{1A}| + m)T_D - \frac{1}{2}T_D^2$$

This shows that the locus of "jet-off" points is a straight line, since its displacement from a straight line (the "drop-out" line) is a linear function.

The slope of the "jet-off" line in Fig. T-8 is:

$$\frac{\overline{-A-F}}{F-1A} = \frac{-\dot{\Omega}}{(F-C)-(1A-C)}$$

$$= \frac{-\dot{\Omega}}{(mT_D - \frac{1}{2}T_D^2 + m\dot{\Omega}) - [(\dot{\Omega} - T_D)T_D + \frac{1}{2}T_D^2 + mT_D]}$$

$$= \frac{-\dot{\Omega}}{\dot{\Omega}\,(m - T_D)}$$

$$= \frac{-1}{m - T_D}$$

This is the same slope as that of the "jet-on" line so the "jet-on" and "jet-off" lines are parallel.

The Ω axis intercept of the "jet-off" line is $B - (m\,T_D - 1/2\,T_D^2)$

$= r\,\Omega p - m\,T_D + 1/2\,T_D^2$

The equation for the "jet-off" line is therefore:

$$\Omega = -(m - T_D)\dot{\Omega} + r\Omega_p - mT_D + \frac{1}{2}T_D^2$$

or

$$\dot{\Omega} = \frac{-\Omega + r\Omega_p - mT_D + \frac{1}{2}T_D^2}{m - T_D}$$

Because of the symmetry imposed by considering the time delay from "pull-on" signal to "jet-on" equal to the delay from "drop-out" and signal to "jet-off", and positive direction thrusts equal to negative direction thrust, it is evident that the rate of movement in one direction with jets off is equal to the rate of movement in the other direction with jets off. Since the rate ($\dot{\Omega}$) at which a jet comes on is equal in value but of opposite sign to the rate at which the jet goes off, it is evident geometrically that the Ω value at which the jets turn on and off is half way between the points of intersection of the "jet on" and "jet off" lines with the axis. This value ( ) is:

$$\Omega_J = \Omega_p - \frac{1}{2}\left[mT_D - \frac{1}{2}T_D^2 + \Omega_p(1 - r)\right]$$

This value of Ω_J is one-fourth of the total distance the vehicle coasts during each limit cycle. Using equation (11), the time per limit cycle with no thrust (T_{off}) is:

$$T_{off} = 4\left(\frac{\Omega_P - 1/2\left[mT_D^2 + \Omega_P(1-r)\right]}{\dot{\Omega}_J}\right)$$

where $\left[mT_D - 1/2\,T_D^2 + \Omega_P(1-r)\right]$ is the distance between the "jet-off" and "jet-on" lines, along a constant $\dot{\Omega}$ line. The absolute value of $\dot{\Omega}_J$ at which the jets turn on and off is therefore:

$$\dot{\Omega}_J = 1/2\,\frac{\left[mT_D - 1/2\,T_D^2 + \Omega_P(1-r)\right]}{m - T_D}$$

This value of $\dot{\Omega}_J$ is equal to one-fourth of the time the jets are on by equation (12). The ratio of T_{on} to T_{off} per limit cycle is therefore:

$$\frac{T_{on}}{T_{off}} = \frac{2\left(\frac{\left[mT_D - 1/2\,T_D^2 + \Omega_P(1-r)\right]}{m - T_D}\right)}{4\left(\frac{\Omega_P - 1/2\left[mT_D - 1/2\,T_D^2 + \Omega_P(1-r)\right]}{1/2\,\frac{\left[mT_D - 1/2\,T_D + \Omega_P(1-r)\right]}{(m - T_D)}}\right.}$$

$$= \frac{\left[mT_D - 1/2\,T_D^2 + \Omega_P(1-r)\right]^2}{4(m-T_D)^2\left[\Omega_P - 1/2\,mT_D + 1/4\,T_D^2 - 1/2\,\Omega_P + 1/2\,r\right]}$$

$$\frac{T_{on}}{T_{off}} = \frac{\left[mT_D - 1/2\,T_D^2 + \Omega_P(1-r)\right]^2}{2(m-T_D)^2\left[\Omega_P(1+r) - mT_D + 1/2\,T_D^2\right]}$$

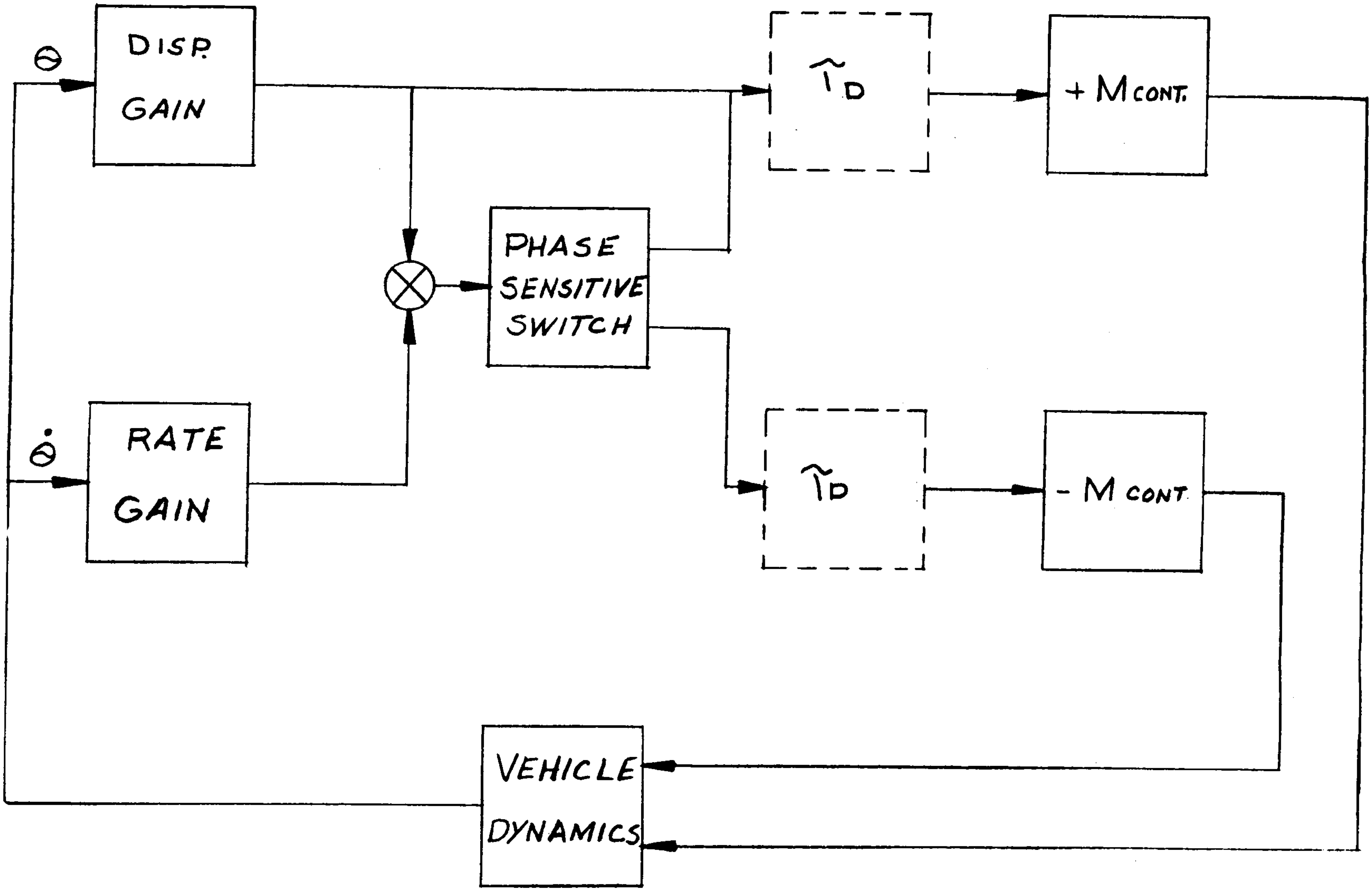
Θ
DISP. GAIN
Θ̇
RATE GAIN
PHASE SENSITIVE SWITCH
τ̃D
+ M CONT.
τ̃D
- M CONT
VEHICLE DYNAMICS

Fig. T-1. Simplified Block Diagram of On-Off Control System

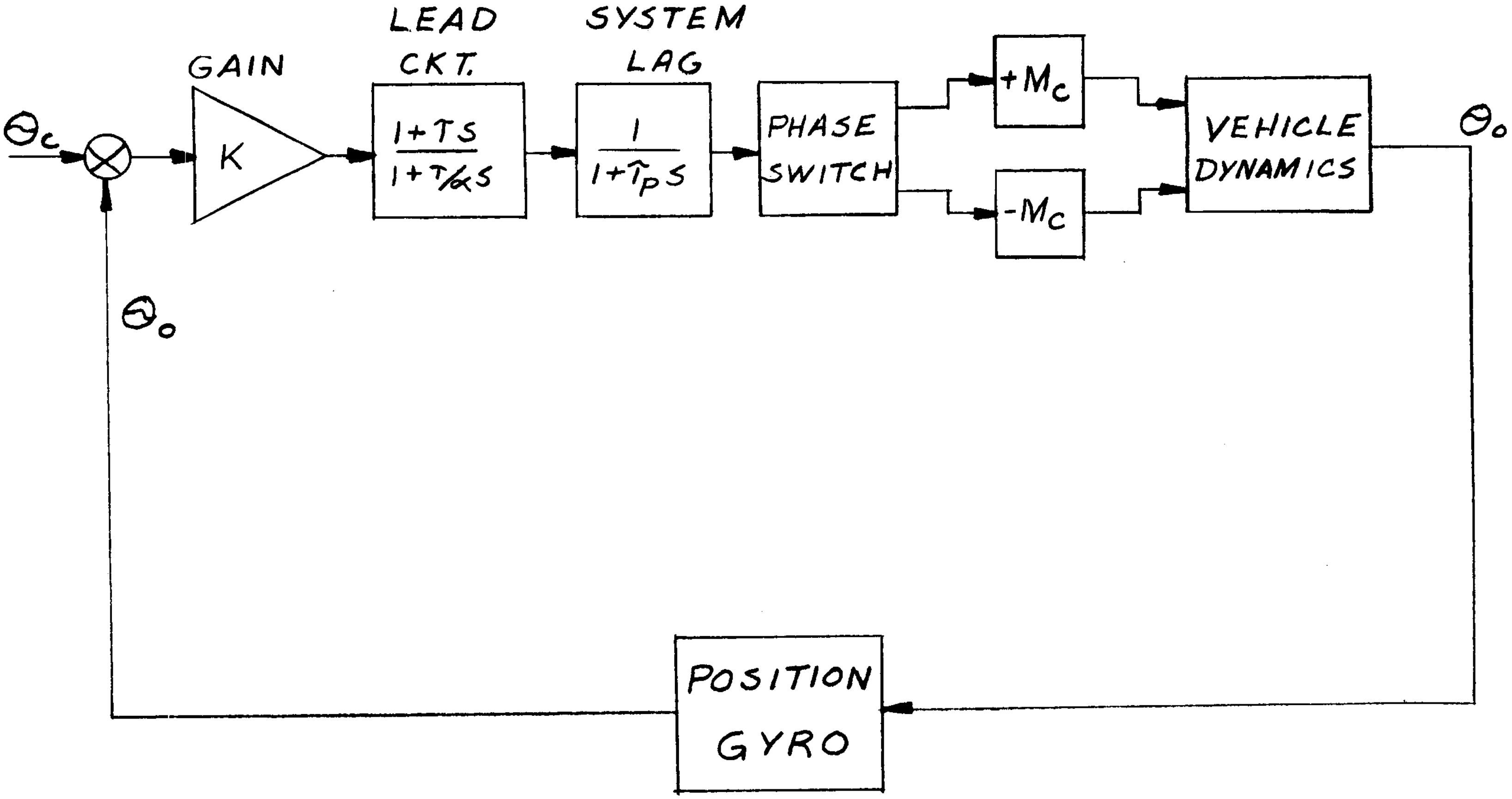
Θ_c
GAIN
K
LEAD CKT.
$\frac{1+TS}{1+T/\alpha S}$
SYSTEM LAG
$\frac{1}{1+\tau_p S}$
PHASE SWITCH
$+M_c$
$-M_c$
VEHICLE DYNAMICS
Θ_o
POSITION GYRO
Θ_o

Fig. T-2. Simplified Block Diagram of a Lead Stabilized Control System

~~CONFIDENTIAL~~

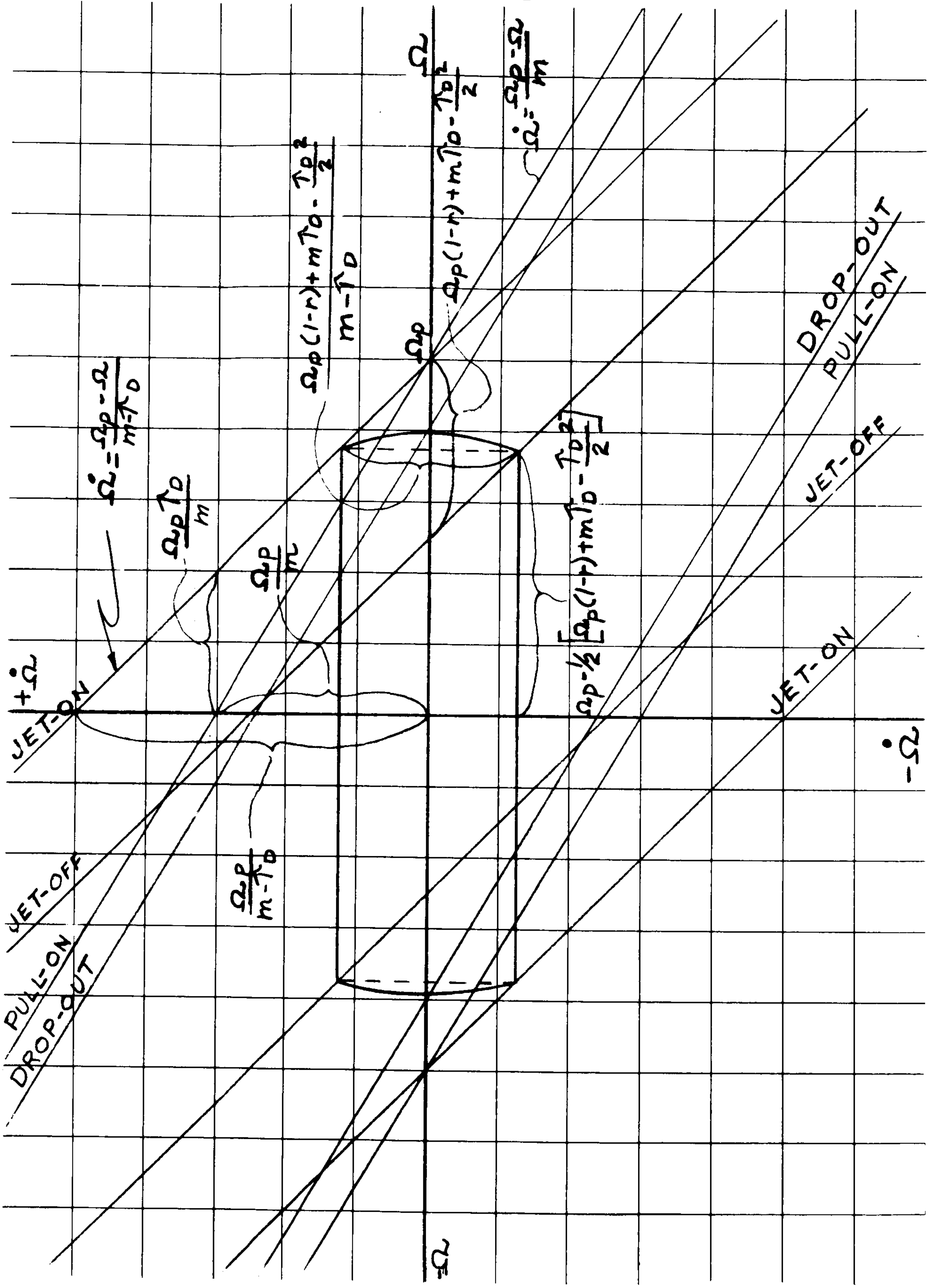

Ω
$-\Omega$
$+\dot{\Omega}$
$-\dot{\Omega}$
Ω_p
JET-ON
JET-OFF
PULL-ON
DROP-OUT
DROP-OUT
PULL-ON
JET-OFF
JET-ON
$\dot{\Omega} = \frac{\Omega_p - \Omega}{m - \tau_D}$
$\dot{\Omega} = \frac{\Omega_p - \Omega}{m}$
$\frac{\Omega_p \tau_D}{m}$
$\frac{\Omega_p}{m}$
$\frac{\Omega_p}{m - \tau_D}$
$\frac{\Omega_p(1-r) + m\tau_D - \frac{\tau_D^2}{2}}{m - \tau_D}$
$\Omega_p(1-r) + m\tau_D - \frac{\tau_D^2}{2}$
$\Omega_p - \frac{1}{2}\left[\Omega_p(1-r) + m\tau_D - \frac{\tau_D^2}{2}\right]$

Fig. T-3. Phase Plane Showing Typical Limit Cycle

[redacted]

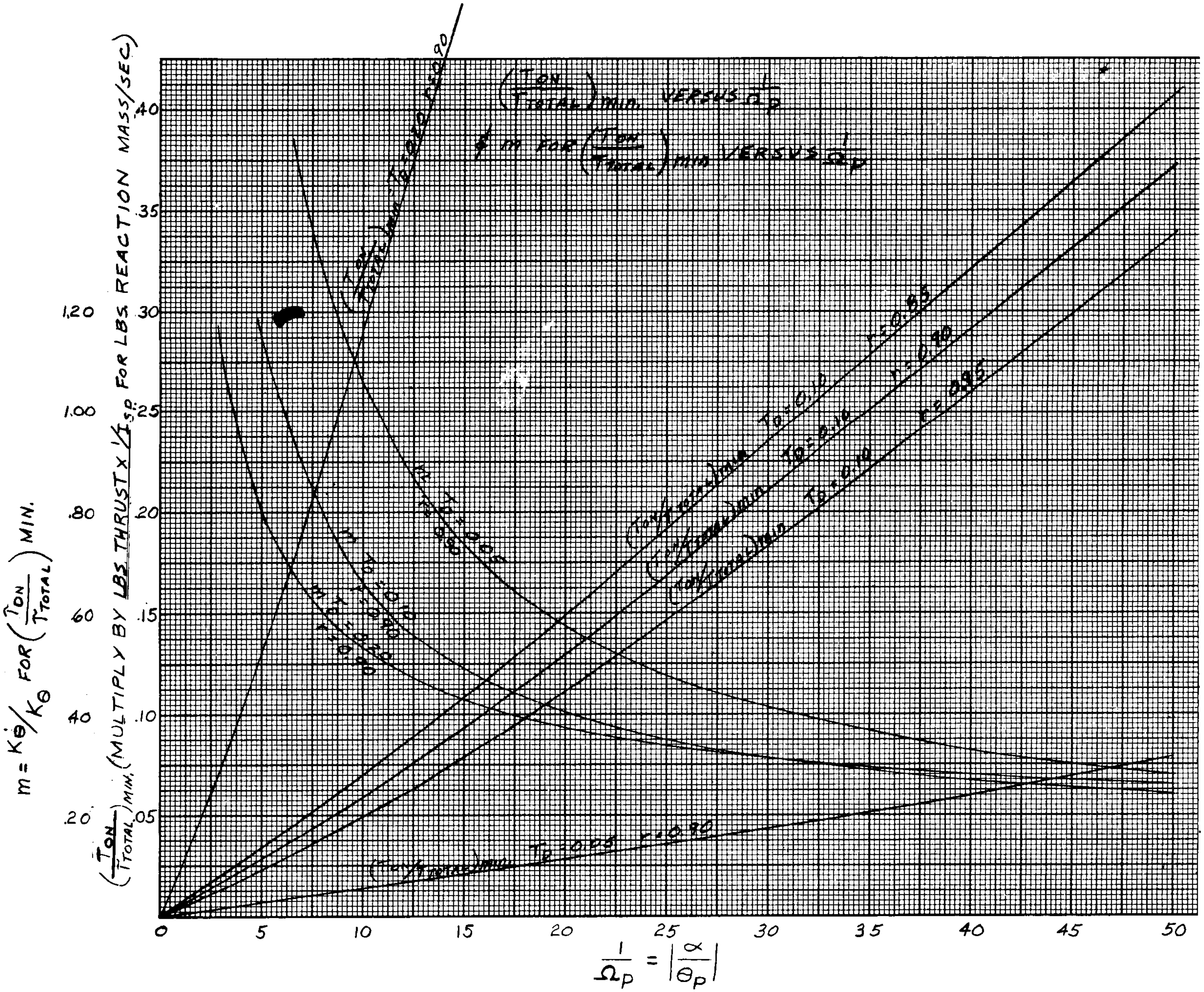

Fig. T-4. Variation of Optimum Design Parameters with Dead Spot

[redacted]

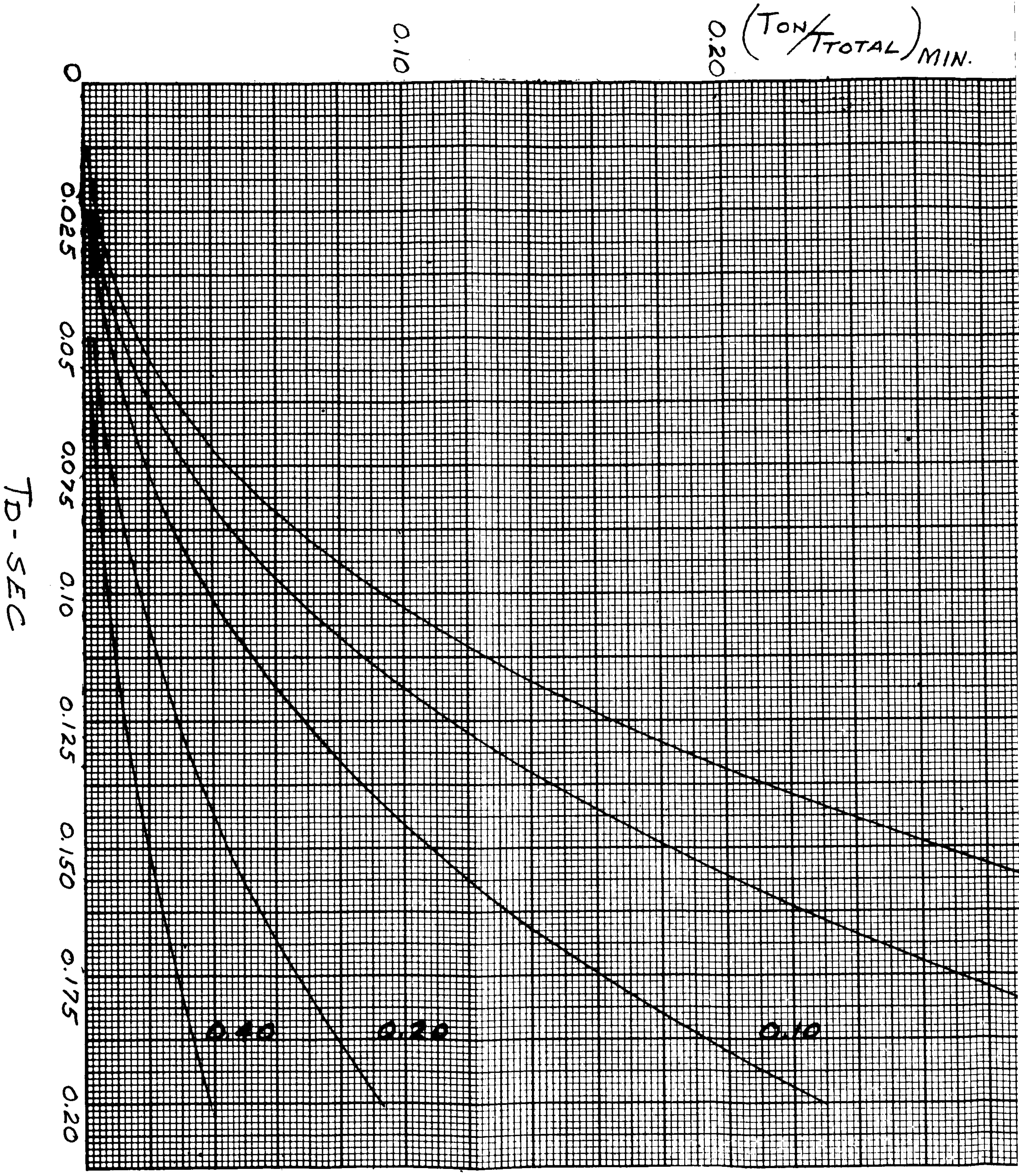
0
0.10
0.20
(TON/TTOTAL)MIN.
0.025
0.05
0.075
0.10
0.125
0.150
0.175
0.20
TD-SEC
0.40
0.20
0.10

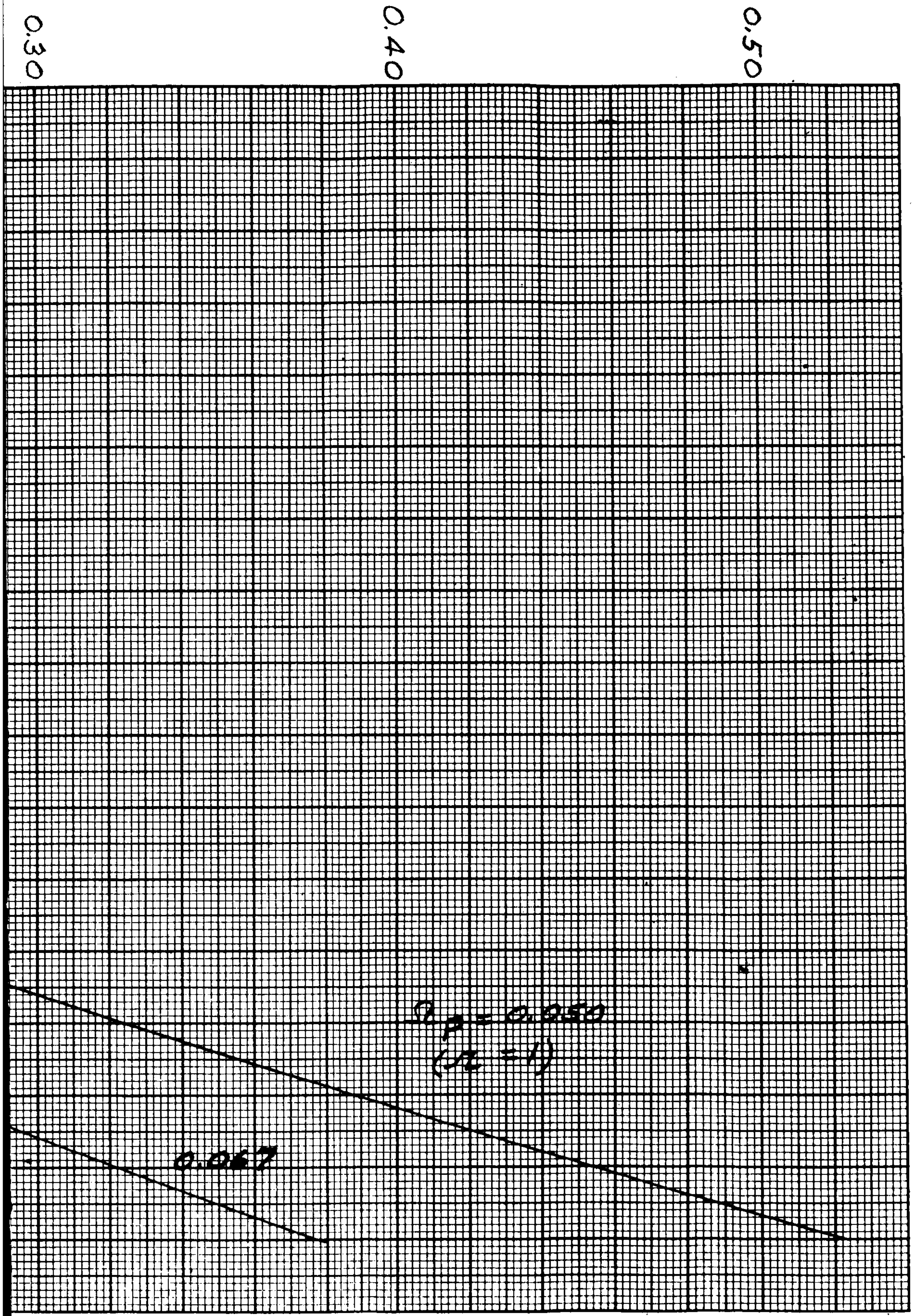

Fig. T-5. $(Ton/T_{total})_{min}$ Versus T_D

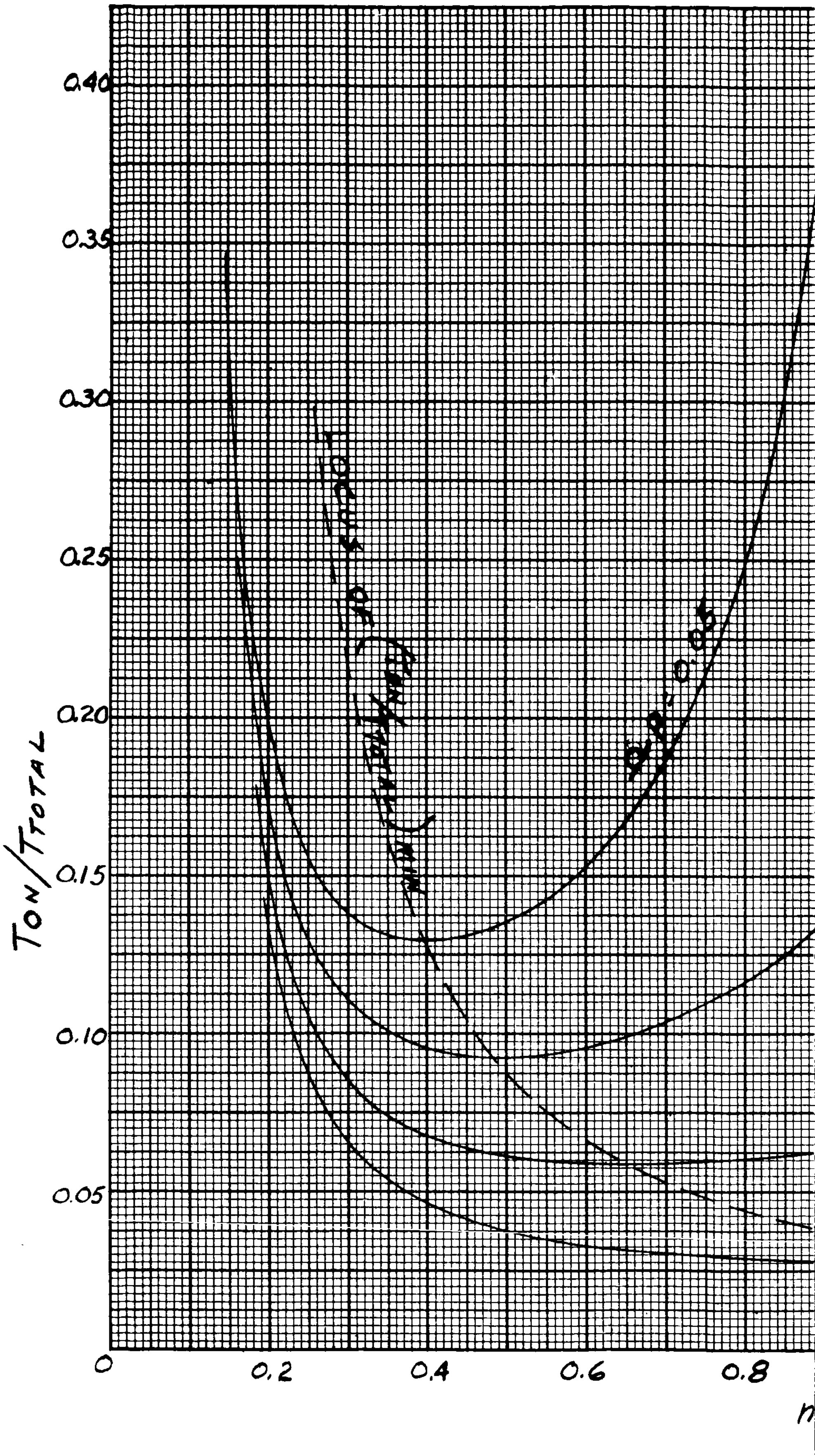

0.40
0.35
0.30
0.25
0.20
0.15
0.10
0.05
0
0.2
0.4
0.6
0.8
T_{ON}/T_{TOTAL}
LOCUS OF MIN (T_{ON}/T_{TOTAL})
Q.B. = 0.05
n

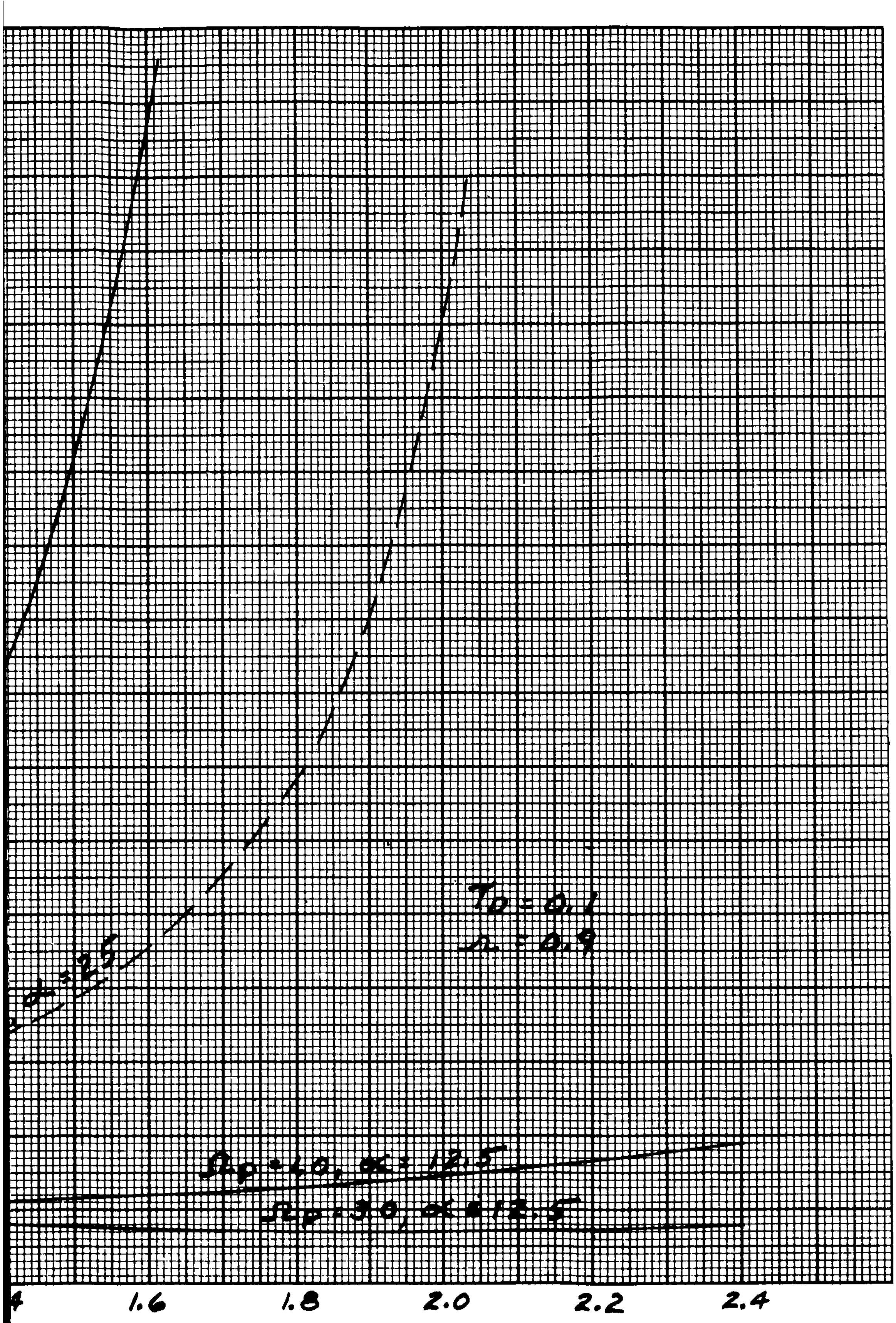

Fig. T-7. Ton/T_{total} Versus T

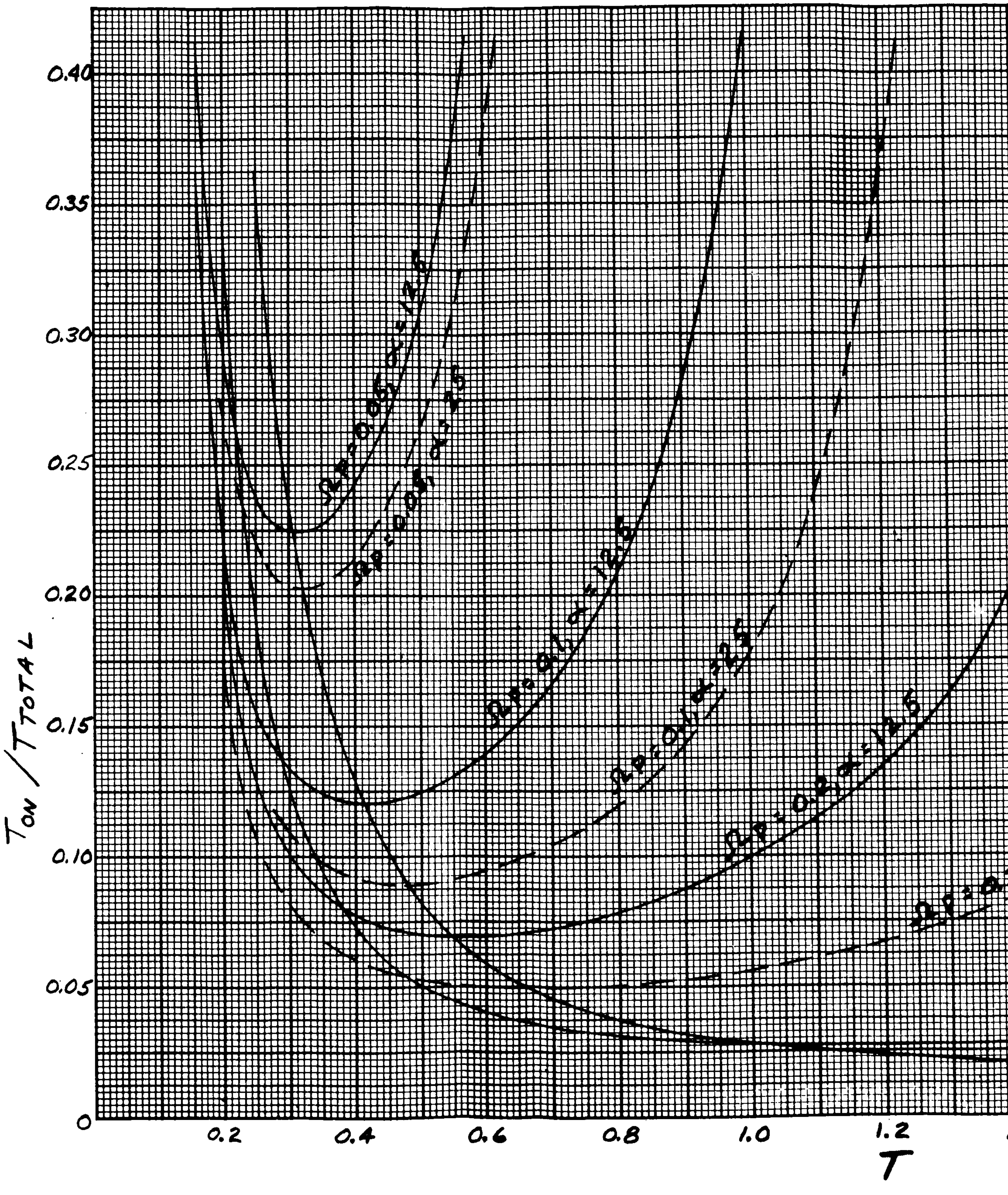
0.40
0.35
0.30
0.25
0.20
0.15
0.10
0.05
0
T_{ON}/T_{TOTAL}
0.2
0.4
0.6
0.8
1.0
1.2
T
ΩP=0.05, α=12.5
ΩP=0.05, α=25
ΩP=0.1, α=12.5
ΩP=0.1, α=25
ΩP=0.2, α=12.5
ΩP=0.

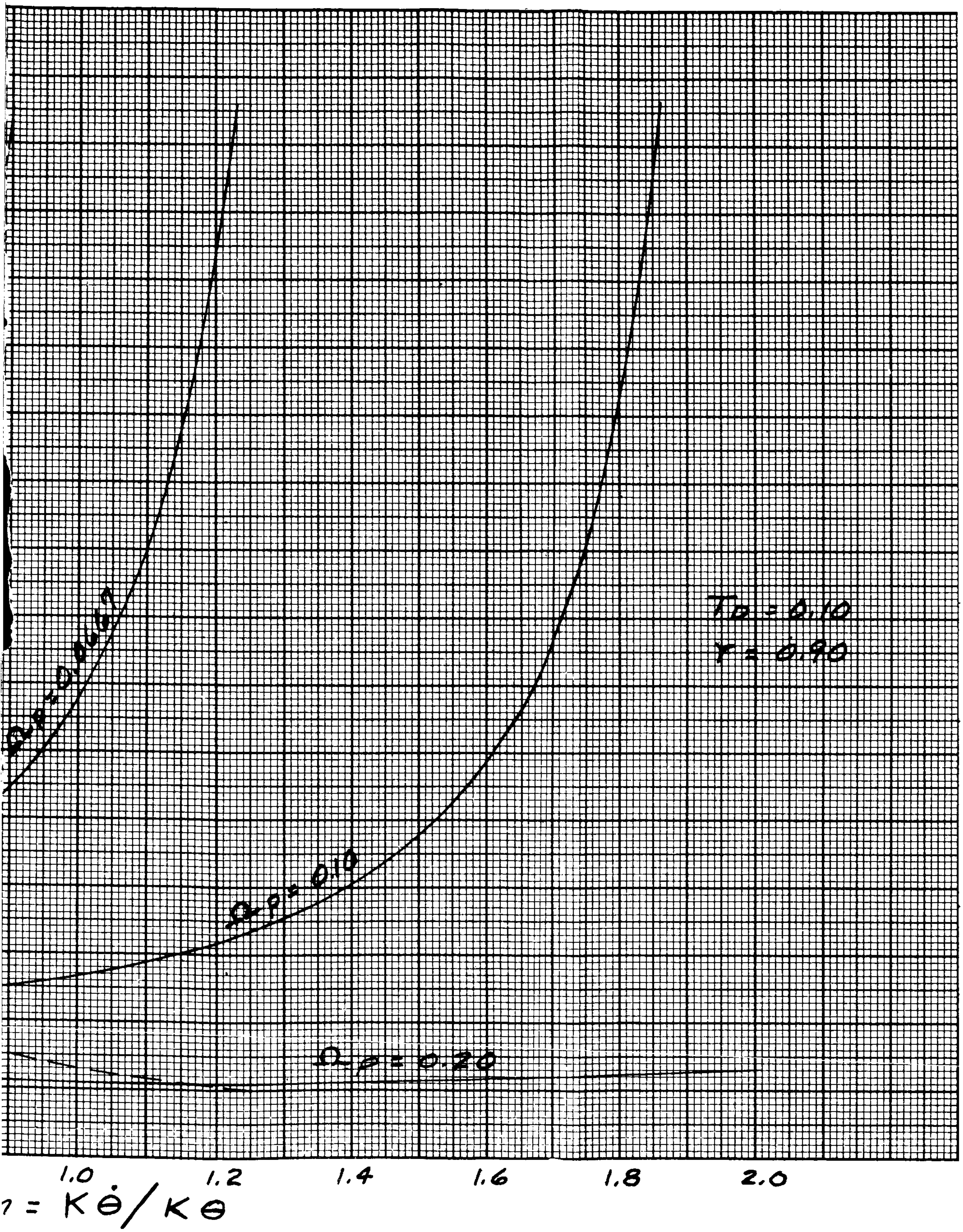

Fig. T-6. Ton/T_{total} Versus M

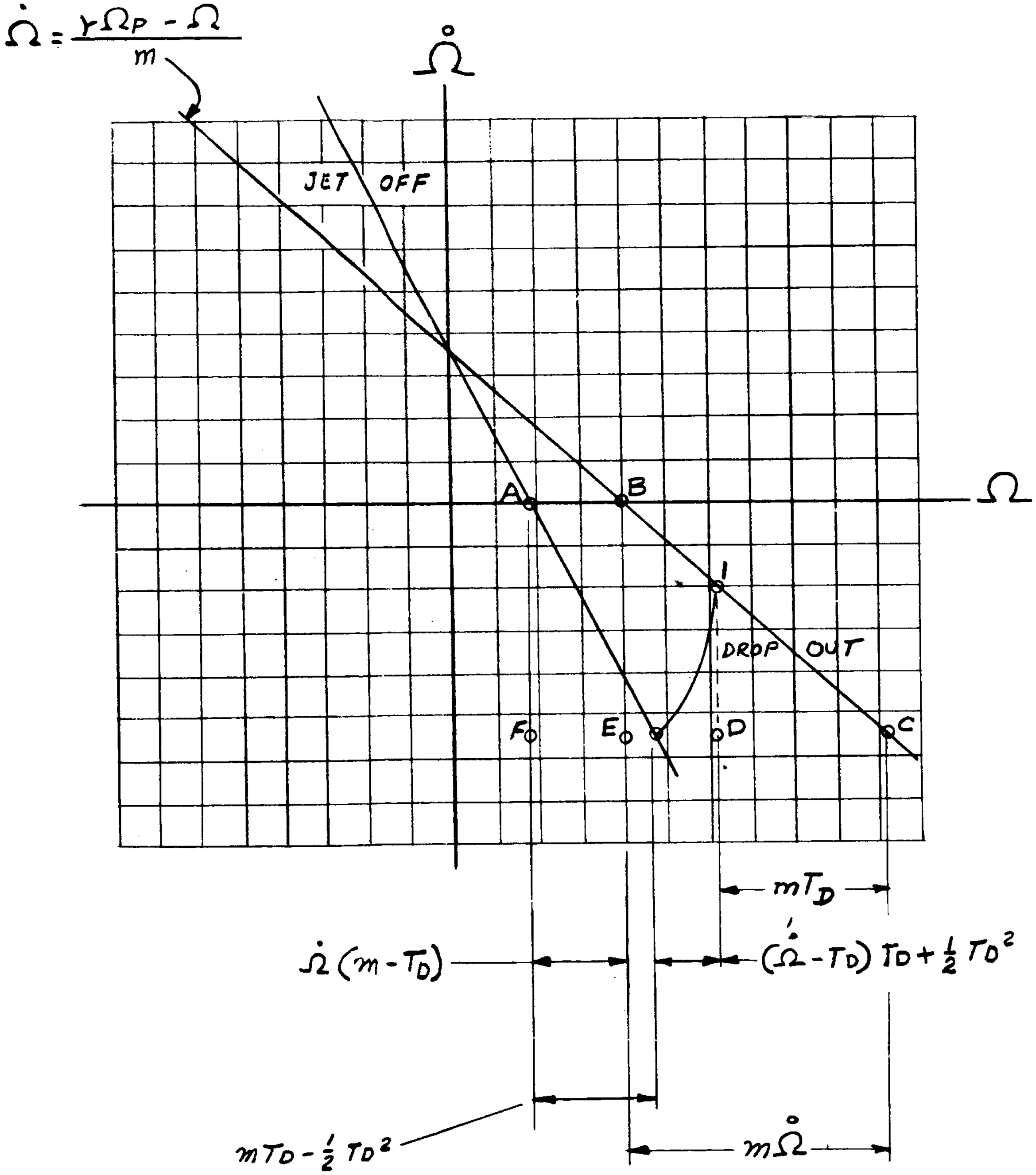
$\dot{\Omega} = \frac{\gamma\Omega_P - \Omega}{m}$
$\mathring{\Omega}$
Ω
JET OFF
DROP OUT
A
B
1
C
D
E
F
mT_D
$\dot{\Omega}(m - T_D)$
$(\dot{\Omega}' - T_D)T_D + \frac{1}{2}T_D^2$
$mT_D - \frac{1}{2}T_D^2$
$m\mathring{\Omega}$

Fig. T-8. Appendix T Section of Phase Plane for Derivation of Ton/T_{off}

APPENDIX U

FUEL EXPENDITURE DURING LIMIT CYCLING WITH A PULSE MODULATED REACTION SYSTEM*

During limit cycle operation, the operation of the pulse rocket will be determined by position error alone. When the vehicle reduces its angular velocity below a fixed dead-band level and the position error is near its dead-band, the system intelligence demands, at most, a single pulse at any one time. If the vehicle is outside its position dead-band, a single pulse is generated in the proper direction to eliminate the error. If the vehicle is within its position dead-band, no pulse is generated. However, if, in this case, the vehicle has a finite angular velocity, the vehicle will eventually drift outside its dead-band and then a pulse will be generated to change the sign of the angular velocity to return the vehicle to its dead-band again. In the absence of outside disturbing torque the vehicle will drift to the opposite side of the dead-band and the same process will be repeated there. These two pulsing operations will have returned the vehicle to its initial velocity condition and the cycle will begin again. Therefore, these two pulses comprise one complete interval of the limit cycle. The phase-plane plot and time history shown in Fig. U-1 illustrate a typical limit cycle.

The fuel expenditure rate during the limit cycle may be derived as follows:

Definition of symbols

F = rocket thrust

$T = Fr$ = applied torque

θ = angular displacement of vehicle

$\Delta\theta$ = dead band (radians)

$\Delta\omega$ = angular velocity change per pulse

f = frequency of limit cycle

I_t = total impulse per pulse

I_{sp} = specific impulse of propellants

r = radius arm of pulse rocket

---

*NOTE: This appendix is taken from work of the Marquardt Corporation and is used with its permission.

$\dot{\varphi}$ = weight flow of propellants

I = vehicle moment of inertia

$$\ddot{\theta} = \frac{T}{I} = \frac{Fr}{I} \qquad (1)$$

$$\int_1^2 \ddot{\theta} dt = \int_1^2 d\dot{\theta} = \frac{r}{I}\int_1^2 F dt \qquad (2)$$

$$\dot{\theta}_2 - \dot{\theta}_1 = \Delta\omega = \frac{r}{I} It \quad \text{where } I_t = \int_1^2 F dt \qquad (3)$$

Given an initial velocity of $\dot{\theta}_1$, the time to traverse the complete dead-band is then:

$$\Delta t_1 = \frac{2\Delta\theta}{\dot{\theta}_1} \qquad (4)$$

similarly, after the direction of drift is changed by a single pulse

$$\Delta t_2 = \frac{-2\Delta\theta}{\dot{\theta}_2} \qquad (5)$$

where

$$\dot{\theta}_2 = \dot{\theta}_1 - \Delta\omega$$

therefore the time required for a complete cycle is

$$\tau = \Delta t_1 + \Delta t_2 = 2\Delta\theta\left[\frac{1}{\dot{\theta}_1} - \frac{1}{\dot{\theta}_1 - \Delta\omega}\right] \qquad (6)$$

$$= \frac{2\Delta\theta\Delta\omega}{\dot{\theta}_1(\Delta\omega - \dot{\theta}_1)}$$

now

$$f = \frac{1}{\tau} = \frac{\dot{\theta}_1(\Delta\omega - \dot{\theta}_1)}{2\Delta\theta\Delta\omega} \qquad (7)$$

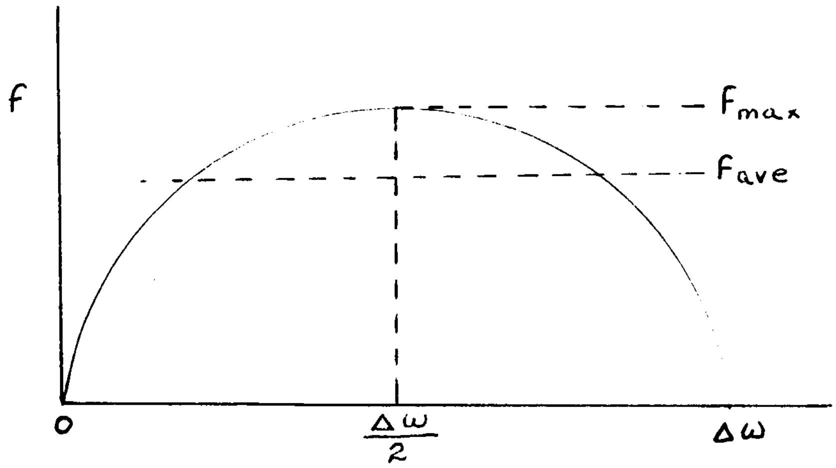

The maximum value of F occurs at

$$F_{max} = \frac{\frac{\Delta\omega}{2}\left(\Delta\omega - \frac{\Delta\omega}{2}\right)}{2\,\Delta\theta\,\Delta\omega} = \frac{\Delta\omega}{8\,\Delta\theta} \qquad (8)$$

If we assume a constant probability of occurance of $\dot{\theta}_1$ in the range of 0 to $\Delta\omega$, the mean frequency is then equal to

$$F_{ave} = \frac{1}{\Delta\omega}\int_0^{\Delta\omega} \frac{\dot{\theta}_1(\Delta\omega - \dot{\theta}_1)}{2\,\Delta\theta\,\Delta\omega}\, d\dot{\theta}_1 = \frac{\Delta\omega}{12\,\Delta\theta} \qquad (9)$$

now,

$$\Delta\omega = \frac{r}{I} I_t$$

and $I_t = W I_{sp}$ where W = propellant weight per pulse

so

$$\Delta\omega = \frac{r}{I} W I_{sp} \qquad (10)$$

and $2FW = \dot{\varphi}$ = effective continuous flow rate of propellants

$$\dot{Q}_{ave} = \frac{2\,\Delta\omega\, I_t}{12\,\Delta\theta\, I_{sp}} = \frac{r\, I_t^{2}}{6\, I\, I_{sp}\,\Delta\theta} \qquad (11)$$

$$\dot{Q}_{max} = \frac{r\, I_t^{2}}{4\, I\, I_{sp}\,\Delta\theta} \qquad (12)$$

when $\Delta\theta$ is converted from radians to degrees

$$\dot{Q}_{ave} = 9.55\ \frac{r\, I_t^{2}}{I\, I_{sp}\,\Delta\theta} \qquad (13)$$

$$F_{ave} = \frac{\Delta\omega}{12\,\Delta\theta} \cdot \frac{r\, I_t}{12\, I\,\Delta\theta} \qquad (14)$$

when $\Delta\theta$ is converted to degrees

$$F_{ave} = 4.77\ \frac{r\, I_t}{I\,\Delta\theta} \qquad (15)$$

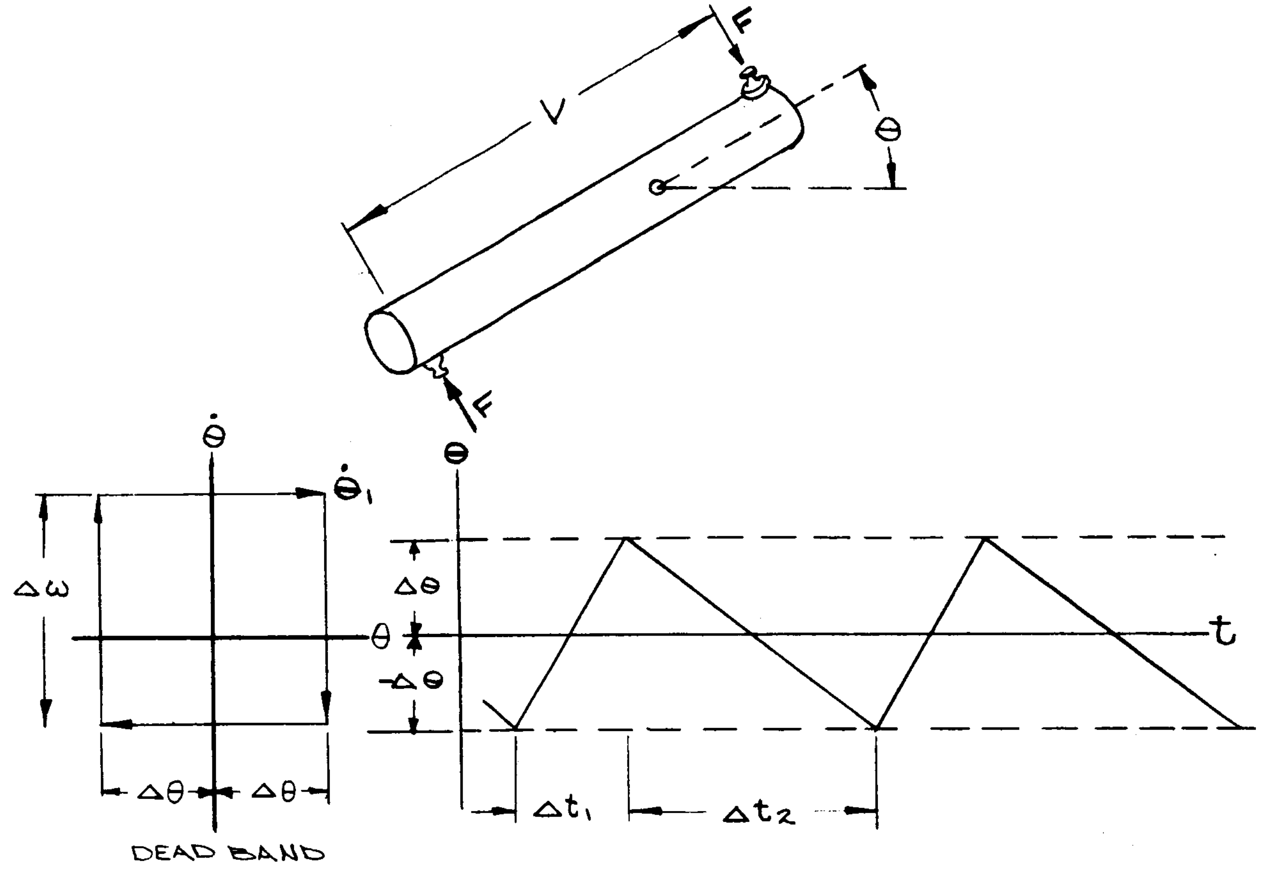
F
V
θ
F
$\dot{\theta}$
$\dot{\theta}_1$
Δω
θ
θ
Δθ
-Δθ
t
Δθ
Δθ
DEAD BAND
Δt_1
Δt_2

Fig. U-1. Configuration and Limit Cycle

APPENDIX V

RELATION BETWEEN EULER ANGLE DERIVATIVES AND BODY RATES

The attitude rate information required to provide the lead necessary for control stability may be obtained by three general methods:

(1) Integration of accelerometer signals

(2) Differentiation of displacement gyro signals

(3) Direct measurement by body mounted rate gyros

The first method, using accelerometers, is usually impractical since the translational and rotational rate inputs must be distiguished. This requires that the accelerometers be used in pairs and that the center of gravity either be fixed or allowances made for any changes. The second method is used whenever possible, since it may be accomplished with simple, reliable and inexpensive R-C networks. The third method, using rate gyros, is superior analytically in some respects, but the rate gyros are expensive and inherently not as reliable as the R-C networks.

A difficulty which sometimes occurs in the use of R-C networks, however, is that the derivatives of the inertial platform Euler angles (which the R-C or "lead" circuits yield) are not exactly equal to the body angle rates under all conditions. The relation between these Euler angle derivatives and the body angle rates may be developed as follows:

Let the body axes be represented by:

(1) $$\begin{pmatrix} x_b \\ y_b \\ z_b \end{pmatrix}$$

and the inertial axis system by:

(2) $$\begin{pmatrix} x_i \\ y_i \\ z_i \end{pmatrix}$$

For a four gimbal platform in which the gimbal order, from inner to outer, is yaw, roll, pitch and roll, the transformation from the inertial to the body axis system is:

(3)
$$\begin{pmatrix} x_b \\ y_b \\ z_b \end{pmatrix} = (\phi_3)(\theta_2)(\phi_1)(\psi_0) \begin{pmatrix} x_i \\ y_i \\ z_i \end{pmatrix}$$

where:

(4)
$$(\psi_0) = \begin{pmatrix} \cos\psi & \sin\psi & 0 \\ -\sin\psi & \cos\psi & 0 \\ 0 & 0 & 1 \end{pmatrix}$$

in which ψ is the inner or yaw gimbal angle,

(5)
$$(\phi_1) = \begin{pmatrix} 1 & 0 & 0 \\ 0 & \cos\phi_1 & \sin\phi_1 \\ 0 & -\sin\phi_1 & \cos\phi_1 \end{pmatrix} = \begin{pmatrix} 1 & 0 & 0 \\ 0 & 1 & 0 \\ 0 & 0 & 1 \end{pmatrix}$$

since the inner roll gimbal is constrained to $\phi_1 = 0$ by a servo,

(6)
$$(\theta_2) = \begin{pmatrix} \cos\theta & 0 & -\sin\theta \\ 0 & 1 & 0 \\ \sin\theta & 0 & \cos\theta \end{pmatrix}$$

where θ_2 is the pitch gimbal angle, and,

(7)
$$(\phi_3) = \begin{pmatrix} 1 & 0 & 0 \\ 0 & \cos\phi_3 & \sin\phi_3 \\ 0 & -\sin\phi_3 & \cos\phi_3 \end{pmatrix}$$

where ϕ_3 is the roll gimbal angle.

Since (ϕ_1) is an identity matrix in the present case, the transformations (3) may be written:

(8)
$$\begin{pmatrix} x_b \\ y_b \\ z_b \end{pmatrix} = (\phi_3)(\theta_2)(\psi_0) \begin{pmatrix} x_i \\ y_i \\ z_i \end{pmatrix}$$

The attitude rates as measured in the body and inertial axis system are related as follows:

(9)
$$\begin{aligned} \Omega &= P\bar{x}_b + Q\bar{y}_b + R\bar{z}_b \\ &= \dot{\psi}\bar{z}_1 + \dot{\phi}_1\bar{x}_2 + \dot{\theta}\bar{y}_3 + \phi_3\bar{x}_3 \end{aligned}$$

where

(10) P = body roll rate

(11) Q = body pitch rate

(12) R = body yaw rate

The relationship demonstrated in equation (9) may be written,

(13)
$$\begin{pmatrix} P \\ Q \\ R \end{pmatrix} = (\phi_3)(\theta_2)(\phi_1)\begin{pmatrix} 0 \\ 0 \\ \dot{\psi} \end{pmatrix} + (\phi_3)(\theta_2)\begin{pmatrix} \dot{\phi}_1 \\ 0 \\ 0 \end{pmatrix} + (\phi_3)\begin{pmatrix} 0 \\ \dot{\theta} \\ 0 \end{pmatrix} + \begin{pmatrix} \dot{\phi}_3 \\ 0 \\ 0 \end{pmatrix}$$

Using the matrix values of (4), (6) and (7) and multiplying, the roll, pitch and yaw body rates are obtained:

(14) $P = \dot{\phi}_3 + \dot{\phi}_1 \cos\theta - \dot{\psi}\sin\theta$

(15) $Q = \dot{\theta}\cos\phi_3 + \dot{\phi}_1 \sin\phi_3 \sin\theta + \dot{\psi}\sin\phi_3 \cos\theta$

(16) $R = \dot{\theta}\sin\phi_3 + \dot{\phi}_1 \cos\phi_3 \sin\theta + \dot{\psi}\cos\phi_3 \cos\theta$

If the roll and pitch Euler angles (ϕ_3 and θ) are small, the following approximations hold:

(17) $P \approx \dot{\phi} - \dot{\phi}_3$

(18) $Q \approx \dot{\theta}$

(19) $R \approx \dot{\psi}$

If the body axis and inertial axis misalignments will not be too great for the small angle approximations, then the Euler angle derivatives, as approximated by a lead circuit, will remain sufficiently close to the actual body rates to be considered the same. In fact, as long as the roll and pitch misalignments do not approach 45°, the Euler angle derivatives may be suitable for control purposes, since the chief effect of the variations will be to change the apparent rate to displacement gain ratio. This may be permissible if the resultant variations in damping are tolerable. However, if the body and inertial axis misalignments are allowed to approach or exceed 45°, then R-C networks will introduce rate cross couplings which are undesirable.

APPENDIX W

APOLLO COASTING AUTOPILOT MECHANIZATION

A. GENERAL

The coasting autopilot produces signals which operate the vehicle reaction jets in response to attitude error and rate signals. Through the moments produced by the six jets, the vehicle attitude is stabilized about the pitch, roll and yaw axes.

The jets can exist in one of two possible states, on or off. Full thrust is produced by a jet when it is on. Since proportional control is desired, it is necessary that the jets be turned on and off in such a manner that the average thrust produced is proportional to the attitude error signals. The jets are oriented on the vehicle in such a way that the moments produced are not orthogonal as far as the yaw and roll axes are concerned. That is, each of the four jets involved produces a moment which causes an acceleration of the vehicle about both the yaw and the roll axes. For this reason, it is necessary to make a special computation in the autopilot, based upon the yaw and roll error and rate signals, to determine the proper signals to supply to each of these four jets. The pitch axis, on the other hand, utilizes jets which produce moments about the pitch axis only, so that this axis is independent of roll and yaw corrections.

To insure satisfactory operation under the environmental stress imposed upon Apollo electronics equipment, the coasting autopilot utilizes silicon semiconductor devices exclusively for all active elements. The key area of concern associated with these devices, relative to environment, is the change in performance when subjected to extreme temperatures and to radiation. The circuits are designed to operate in an ambient temperature of up to + 125°C, which is greater than the expected maximum temperature. Radiation, such as that encountered in the Van Allen Belt, is expected to have little effect due both to the independency of the autopilot performance on semiconductor parameters and to the limitation placed upon the allowable radiation level by the human occupants of the vehicle.

B. SUMMARY OF AUTOPILOT CHARACTERISTICS

(1) General

Control axes, three; yaw, roll and pitch

Type: attitude stabilization

Control modes: linear proportional-plus-rate, limit cycle

Inputs: error magnitude and error rate for each axis (6)

Outputs: six modulated pulse trains (two per axis)

[redacted]

Design technique characterization: transistorized

Power requirements: 20 watts maximum idle

Power output: up to 60 watts per output = 360 watts max.

Gain stability: total variation less than ± 5% up to +125°C

Linearity: within ± 5%

(2) Input characteristics

Frequency: carriers from 400 cps to 1000 cps

Sensitivity: 0.30 vrms produces full 60 watt output

Impedance: adjustable with slight modification, normal 31.6 k ohms

Feedback: no spurious signals fed back

Source impedance: less than 2000 ohms

(3) Output characteristics

Nature of outputs: modulated constant amplitude pulse trains

Load accomodation: greater than 14 ohms resistive, less than 10 henrys inductive

Pulse rise and decay time: less than 100 microseconds

Minimum pulse widths: up to 50 milliseconds, nominally 5 ms.

Maximum pulse frequency: as low as 5 cps (related to width)

Pulse modulation: average value of pulse train is a linear function of the input signals

C. GENERAL DESCRIPTION

A block diagram is given in Fig. W-1. This figure shows the three axes, yaw, roll and pitch, and the six reaction jets. Each axis employs the same basic elements and the three are identical accept for the coupling between the yaw and roll axes. As previously mentioned, this yaw-roll coupling orthogonalizes the system so that the moments produced about any axis are a function of the attitude error and rate about that axis.

[redacted]

The error signals are first mixed, or summed, in each of the three channels. The attitude error signal is added to the attitude rate signal in a proportion that can be set to any desired value. The sum signal is than amplified by the amplifier. The amplifier error is supplied to two demodulators and to a magnitude detector. The demodulators produce dc signals proportional to the magnitude of the ac error signal. One of the two demodulators produces a signal for positive sensed attitude errors only and the other demodulator produces a signal for negative sensed errors. Thus for any given attitude error, only one of the two demodulators produces a dc signal. The magnitude detector measures the absolute magnitude of the ac error signal without regard for the sense of the error. When the error exceeds a preset magnitude the detector produces a sudden change in the dc level at its output. This dc level is employed to control the signal gates.

The demodulator outputs are applied to the signal gates. Due to the operation of the gates and the magnitude detector, the gates produce an output signal only when the error signal exceeds the preset magnitude. Thus, the gate outputs represent the magnitude of the error signal for magnitudes greater than a desired deadspot magnitude. The sense of the error is represented by whichever one of the two gates that is providing an output.

The outputs of the pitch channel gates are supplied directly to the pulse modulators. The roll and yaw channel gate outputs are first summed, and then provided to the pulse modulators. The pulse modulator outputs are amplified by the switches. The switch outputs, as shown, drive the jet control torque motors.

1. Yaw-roll orthogonalization

The results produced by the interconnections between the yaw and roll channels are described best by a few simple relations. The attitude and rate signals for each axis are first summed, resulting in the three signals:

$$Y = \psi + K_{\psi} \dot{\psi} \qquad (1)$$

$$R = \phi + K_{\phi} \dot{\phi}$$

$$P = \theta + K_{\theta} \dot{\theta}$$

These signals are then amplified and applied to the inputs of the demods and magnitude detectors. The gates produce six signals denoted Y^+ Y^-, R^+, R^-, P^+ and P^-. Y^+ signal, for example, is equal to the absolute magnitude of Y for Y greater than some threshold value Y_T and is equal to zero otherwise. The six signals are defined similarly, as follows:

$$
\begin{aligned}
Y^+ &= |Y| && \text{for } Y > Y_T \\
&= 0 && \text{for } Y < Y_T \\
Y^- &= |Y| && \text{for } Y < -Y_T \\
&= 0 && \text{for } Y > -Y_T \\
R^+ &= |R| && \text{for } R > R_T \\
&= 0 && \text{for } R < R_T \\
R^- &= |R| && \text{for } R < -R_T \\
&= 0 && \text{for } R > -R_T \\
P^+ &= |P| && \text{for } P > P_T \\
&= 0 && \text{for } P < P_T \\
P^- &= |P| && \text{for } P < -P_T \\
&= 0 && \text{for } P > -P_T
\end{aligned}
\qquad (2)
$$

Four of the six signals are then summed. The pulse modulators and switches accept the six resulting signals and operate the jet solenoids with signals such that the average thrust produced by the jets are proportional to the six signals. Thus, the average thrusts produced by the jets are proportional to the following functions:

$$\begin{aligned} J_1 &= Y^+ + R^+ \\ J_2 &= Y^+ + R^- \\ J_3 &= Y^- + R^+ \\ J_4 &= Y^- + R^- \\ J_5 &= P^+ \\ J_6 &= P^- \end{aligned} \qquad (3)$$

The jets' physical orientation is such that the moments about the yaw, roll and pitch axes, M_Y, M_R and M_P respectively, are related to the jet average thrust functions J_1, etc. by

$$\begin{aligned} M_Y &= K_Y (J_1 + J_2 - J_3 - J_4) \\ M_R &= K_R (J_1 - J_2 + J_3 - J_4) \\ M_P &= K_P (J_5 - J_6) \end{aligned} \qquad (4)$$

Where K_Y, K_R, K_P are constants of proportionality depending upon the jet characteristics, jet physical locations and vehicle center of gravity location. Substitution of (3) into (4) shows that the movements developed about each control axis depend only upon the corresponding axis error signals and are independent of the other axes. Further substitution of the functions (2) shows that moments are developed only when the corresponding errors exceed the threshhold regions $2Y_T$, etc., which are centered about $Y=O$, etc.

D. COMPONENT CIRCUIT DESCRIPTION

1. Mixer-Amplifier

The mixer-amplifier schematic is shown in Fig. W-1. This amplifier provides mixing of the attitude error with the error rate signals for each of the three channels, as shown in Fig. W-2. The nominal closed loop amplifier gain for R1 = R2 = 31.6 K is 38. The mixing ratio between the displacement and the rate signals is obtained at any desired value by appropriate selection of the values for R1 and R2.

The amplifier utilizes three stages of amplification provided by TR1, TR2 and TR3. The input impedance of the amplifier at the base of TR1 is very low, providing nearly ideal current summing at this point of the a-c signal inputs, the a-c feedback and the d-c feedback. TR3 drives one half of the primary winding of T1, the output transformer. A-c feedback current is obtained from the primary of T1 and flows through R6 and C2 to the input summing point. D-c feedback current flows through R8 and R7 due to the d-c voltage developed across R9, bypassed by C5, and to the d-c drop across the primary of T1. C3 bypasses the a-c signal currents in the d-c feedback path.

TR1 and TR2 both operate in a current mode relative to signal amplification. The collector voltage of TR1 is established by the base voltage of TR2 and the drop across the diode CR1 and is essentially constant. The collector voltage of TR2 is set by avalanche diode CR2, V_{BE3}, and the drop across R11. The resulting a-c current gain is basically the h_{fe} product for the three transistors.

Development tests of the amplifier show a -2.5% change in gain over the temperature range from 25° C to 125°C. Although considered unnecessary, this gain stability could be improved through use of feedback over the transformer and use of more stable resistors for R1, R2 and R6. The d-c operating point (collector current of TR3) varied only 5% over the temperature range.

2. Magnitude Detector

The magnitude detector accepts a 400 cps a-c input signal from the a-c amplifier. When the magnitude of the error is less than some threshold deadspot value, (adjustable from 0.3 vrms upward) the output voltage to the gate is +5 v dc. When the input to the detector is greater than the set level, then the detector output switches from +5 v dc to approximately -14 v dc. The switching time is short, on the order of 10 milliseconds or less, depending upon the deadspot level.

The detector comprises an a-c amplifier, a detector to convert the ac to dc, and an amplitude detector-switch. The schematic for this circuit is shown in Fig. W-3. The a-c input signal is applied to R1 which provides the adjustable deadspot level. Transformer T1 applies the signal to the base of TR1. TR1 operates as a voltage amplifier, common emitter, with an unbypassed emitter resistor for degeneration and gain stability. The quiescent operating point of this stage is established by CR1, a 6.2 volt reference diode V_{BE1}, R4 and R5. The nominal emitter current is 6.7 ma. The quiescent collector voltage of TR1 is nominally +6.9 volts, resulting in a nominal quiescent current for TR2 of 13.4 ma. TR2 operates common collector and provides current amplification sufficient to drive the rectifier circuit comprising CR2, CR3, C3 and R7. The rectifier circuit develops a d-c voltage across R7 which is proportional to the input voltage reduced by the attentuation of R1 and increased by the voltage amplification of T1 and TR1.

Reference diode CR4 establishes a nominally +5 v dc bias at the emitter of TR3. As long as the d-c voltage developed across R7 is less than the voltage across CR4, then TR3 and TR4 will both be cut off. When the d-c voltage across R7 exceeds that of CR4, then base current will flow into TR3 through R10 and TR3 will begin to amplify this current in its collector load resistance R12. A fraction of the TR3 collector current flows into the base of TR4, resulting in a flow of current in the collector of TR4 through the load CR6 and R8. A part of the TR4 collector current is fed back to the base of TR3 through the feedback resistor R11. This feedback is regenerative and causes both TR3 and TR4 to rapidly switch completely into a saturated state as soon as TR3 begins to conduct. When this happens, the output voltage is driven from the +5 v dc initial value to $-15 +V_{CR5} +V_{CE4} +V_{CR6}$ or approximately -13.5 to -14 v dc. This action permits the gate circuit to transfer the signal input to its output.

CR6 and C4 constitute a peak detector which smooths the negative d-c output of the circuit for borderline deadspot level inputs. This is necessary due to the unavoidable ripple in the voltage developed across R7. R2 and R9 provide bias currents for CR1 and CR4.

3. Demodulator and Gate

The basic demodulator circuit is shown in Fig. W-4. This is a well known and conventional configuration, providing accurate operation relatively independant of transistor parameters and a time constant approaching the minimum possible for the 400 cps carrier frequency. The transistors TR1 and TR2 act as a switch which is capable of conduction in either direction. When the excitation provided by T2 is of the proper polarity to forward bias the emitter-base diodes of TR1 and TR2, then a current will flow between the signal provided by T1 and the lead R_L, C if there is any difference between e_s and e_o. For example, if both e_s and e_o are positive but e_s is greater than e_o, then when the current provided by T2 forward biases the emitter-base diodes the collector base diode of TR1 will forward biased and the collector-base diode of TR2 will be reverse biased. Therefore TR1 and TR2 both conduct until $e_o = e_s$ or until the excitation of T2 reverses polarity and reverse biases the emitter-base diodes. When the emitter-base diodes are reverse biased, both transistors are cut off and essentially no current flows between the signal and the lead. Also, in case e_o is greater than e_s, then current will flow from the lead into the source when the transistors are biased into conduction. The capacitor C provides filtering of the pulsating current so that the output current into R_L is substantially dc with a small ripple component.

For the demodulator shown in Fig. W-4, the action is half-wave and the polarity of the output d-c current depends upon the relative phase between the signal voltage and the excitation voltage provided by T2. If these voltages are in phase relative to each other, than a positive d-c output is obtained.

As discussed previously and shown in Fig. W-2, two output signals are required for each channel. One shall exist only for positive sensed attitude errors and the other shall exist only for negative sensed error. To obtain this result, the circuit shown in Fig. W-5 is employed. The resistances identified as R_L are the equivalent load imposed upon the circuit by the summers. The output from each demodulator is required to drive two summer inputs, each comprising a 100K resistance terminated at essentially ground potential. The TR1-TR2 pair and the TR3-TR4 pair each constitute a half-wave demodulator. The excitation provided to each by T3 is in phase with the reference 400 cps voltage so that one of the demodulators produces a negative output for in-phase error signals and the other produces a negative output for out-of-phase error signals. Diodes CR1 and CR2 prevent either demodulator from producing a positive output current.

Transformer T2 is a part of the a-c amplifier circuit of Fig. W-1. Its centertap is biased by the voltage developed at the wiper of potentiometer R3. This bias is used to produce the desired deadspot characteristics previously discussed. For small error signals the output of the magnitude detector is approximately +5 v dc. This voltage excites R3, and according to the setting of R3, results in a positive voltage bias at the centertap of T2. This bias is additive with the signal voltages produced across the secondary of T2. For signals less than the deadspot level, the diodes CR1 and CR2 are reverse biased and no input is provided to the summer. The pulse modulators driven by the summers are therefore cut off and no control is realized. When the signal is slightly in excess of the positive bias, then current flows into the appropriate summers and the corresponding pulse modulators are excited. This is shown in Fig. W-6. For error signals less than the deadspot level, the circuit operates along the coordinate axis between points o and a. For signals in excess of the deadspot, operation is along the curve a-b. At an input slightly greater than point a but less than b the pulse modulator will produce one minimum output pulse. If disturbing ± moments are sufficiently small, this pulse will result in corrective moment sufficient to reverse the vehicle velocity and the error will decrease toward point o. In case the disturbing moments are large or for a command input to the system, as the input error increases from a to b, the pulse modulator output will increase.

Point b of Fig. W-6 represents the operating point of the magnitude detector. When this error level is reached the output of the magnitude detector switches from +5 v dc to -15 v dc. Apparent from Fig. W-5 is that this results in removal of the positive demodulator bias. The wiper voltage of R3 is clamped by CR3 to slightly less than zero. In Fig. W-6 this action is represented by the dashed line b-c. Operation of the demodulator is switched from the biased curve a-b to the unbiased normal curve o-d. For decreasing error signals, due to the hysteresis of the magnitude detector, the switch to the biased condition occurs at point e somewhat less than c. This hysteresis is, however, not critical since it does not affect limit cycle operation. The limit cycle system operation is determined entirely by the biased demodulator curve a-b for all cases except where abnormally large disturbances are encountered.

4. Summer

The summer, shown in Fig. W-7, accepts input signals from two of the gates and develops an output voltage proportional to the sum of the inputs. The output signal is used to control the operating point of the pulse modulator, discussed next. This circuit uses a direct coupled transistor pair to attain a high equivalent h_{FE}. The gain of this circuit is $-R_3/R_1$ for R1 = R2, for each input. The base of TR1 operates at a virtually constant potential very near zero so that the two input currents are almost exactly E_1/R_1 and E_2/R_2. The nominal voltage gain for each of the two inputs is -1.21, The voltage swing required by the modulator for control from off to full on is 13.2 volts, thus requiring a voltage swing of 10.9 v dc of either E_1 or E_2 to produce full control. Diode CR1 serves the purpose both of biasing the base of TR1 to ground potential and of compensating in part for the temperature variations of V_{BE1}.

5. Pulse Modulator

a. General

The function of the pulse modulator is the production of a pulse train whose average value is linearly related to the modulator input signal. If the pulse train comprises a series of equal-amplitude rectangular pulses, then the average value of the train is $T_W F_P$ where T_W is the pulse width and F_P is the pulse repetition frequency. The average value is also called duty cycle. Thus, if λ is proportional to the modulator input signal then

$$T_W F_P = K\lambda \qquad (5)$$

is the required operating law of the modulator where K is a gain constant. In addition to following this law, the modulator must satisfy an additional basic requirement arising from system limit cycle considerations. This is that as λ approaches zero, T_W must approach or equal a finite non-zero pulse width. This minimum value of T_W is denoted $(T_W)_{Min}$ so that

$$\lim_{\lambda \to 0} T_W = (T_W)_{MIN} \qquad (6)$$

Therefore, for operation of the system in a limit cycle mode, when attitude errors exceed deadspot values a pulse of width $(T_W)_{Min}$ is produced.

There are an infinite variety of ways by which the operating law (5) may be satisfied. T_W and F_P are functions of λ, which can be written $T_W(\lambda)$ and $F_P(\lambda)$. Any $T_W(\lambda)$ can be employed so long as $F_P(\lambda) = \frac{K\lambda}{T_W(\lambda)}$. From (6) above, it is clear that $F_P(0^+)$ must be zero.

The modulator circuit to be discussed below follows the following operating laws

$$T_W = \frac{(T_W)_{MIN}}{1 - \frac{\lambda}{\lambda M}}, \quad F_P = 4(F_P)_{MAX}\left(\frac{\lambda}{\lambda M}\right)\left(1 - \frac{\lambda}{\lambda M}\right) \qquad (7)$$

where λ_M is the value of λ required to produce a $T_W F_P = 1$, i.e., the maximum value of λ, and (F_P) max is the maximum frequency of the modulator. (F_P)max occurs for $\lambda = 1/2(\lambda M)$or $T_W F_P = 1/2$, a 50% duty cycle.

The modulator is a relaxation oscillator, similar in respects to the familar gas tube oscillator. The principle of operation is as follows: When a capacitor is charged by a constant current, the change in voltage across the capacitor terminals is $\Delta V = \frac{I\ T}{C}$, where I is the constant current, C is the capacitance, and T is the charging time in seconds. The modulator circuit provides two current sources, $I_1 = I_C \frac{\lambda}{\lambda M}$ and $I_2 = I_C\ (1 - \frac{\lambda}{\lambda M})$, both constant in the sense that changes in the capacitor voltages do not affect either I_1 or I_2. I_C is an invariant constant of the circuit. The pulse train is generated by; first, charging C with I_2 to some voltage change Δ V across C then, second, discharging C with I_1 back to the original capacitor voltage. This is illustrated in Fig. W-8. The time required to charge C with I_2 to ΔV establishes the pulse width T_W. The time required to discharge C with I_1 establishes the pulse off period $(T_P - T_W)$, as shown in Fig. W-9. Thus, since $\Delta V = \frac{I\ T}{C}$

$$T_W = \frac{C\Delta V}{I_2} \qquad (8)$$

$$(T_P - T_W) = \frac{C\Delta V}{I_1} \qquad (9)$$

Substituting into these the relations $I_1 = I_C \frac{\lambda}{\lambda M}$

and $I_2 = I_C\ (1 - \frac{\lambda}{\lambda M})$ yields $T_W = \frac{C\Delta V}{I_C}\left(\frac{1}{1-\lambda/\lambda M}\right)$ (10)

$$F_P = \frac{I_C}{C\Delta V}\left(\frac{\lambda}{\lambda M}\right)\left(1 - \frac{\lambda}{\lambda M}\right) \qquad (11)$$

Comparing these relations to Fig. W-10 shows that

$$(TW)\ \text{Min} = \frac{C\,\Delta V}{I_c} \tag{12}$$

$$(F_P)\ \text{max} = \frac{I_c}{4C\,\Delta V} \tag{13}$$

which are useful in relating circuit values to the modulator operating characteristics. Clearly then

$$(T_W)_{min}\,(F_P)_{max} = 1/4$$

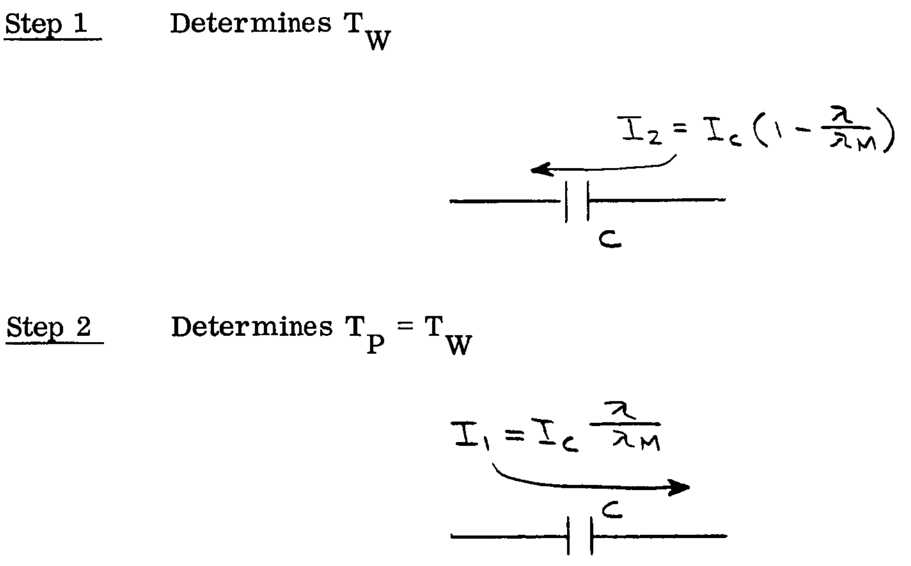
Step 1 Determines T_W
$I_2 = I_c\left(1 - \frac{\lambda}{\lambda_M}\right)$
C
Step 2 Determines $T_P = T_W$
$I_1 = I_c\,\frac{\lambda}{\lambda_M}$
C

Fig. W-8 CAPACITOR CHARGING

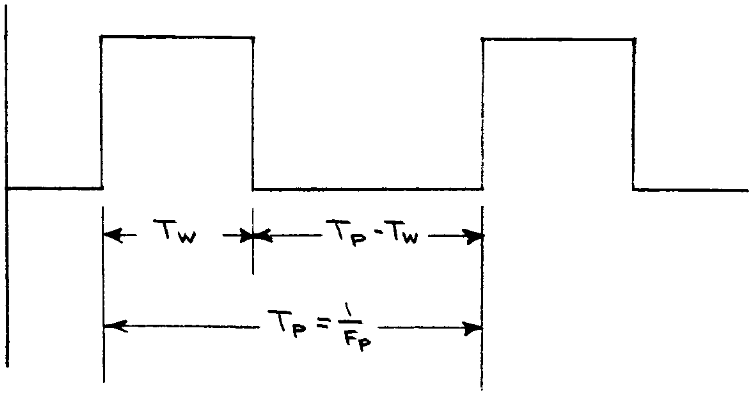

Fig. W-9
MODULATOR WAVEFORM

b. Circuit description

The basic modulator circuit is shown in Fig. W-10. In addition to the "constant" currents I_1, I_2 and the capacitor C as discussed above, two non-linear resistances are required. The diode in Fig. W-10 is conventional and provides a high resistance for V_D less than some small positive voltage on the order of 0.7 volts as shown in Fig. W-12. The "non-linear resistance", shown in Fig. W-10, has the characteristics shown in Fig. W-11. If V_N is initially taken to be zero, then as V_N increases up to the trigger level V_{NT}, no current flows into the resistance. When an applied voltage V_{NT} is reached, the current increases and the voltage V_N decreases as shown. The slope of the $V_N - I_N$ curve is negative and thus represents a negative incremental resistance.

The circuit operation can be explained by first assuming that $I_1 = O$, $I_2 = I_C$ and that I_C all flows into the negative resistance. If $-R_N$ is the slope of the $V_N - I_N$ characteristic, then for these initial conditions $V_N = V_{NT} - I_C$ RN. It is proper to assume that $V_D = 0.7$ volts initially for the approximate diode characteristics assumed in Fig. W-12, since any infinitesimal I_1 or capacitor leakage current will produce this result. I_C flowing thru the capacitor is initially zero.

If a step input in $\frac{\lambda}{\lambda M}$ is assumed at t = O, I_1 will become $I_C \frac{\lambda}{\lambda M}$ and I_2 will be reduced from I_C to $I_C\ (1 - \frac{\lambda}{\lambda M})$. See Fig. W-13 for waveforms. All of I_1 will momentarily flow through the diode and the diode voltage will be approximately unchanged. At T = O, the reduction in I_2 represents a reduction in I_N, yet, the voltage V_N is unchanged since the capacitor voltage cannot change discontinuously. This reduction in I_N at constant V_N requires that I_N be reduced to zero: the negative resistance can be thought of to have "switched" into its low (zero) current state corresponding to the V_N axis of Fig. W-11. Since now $I_N = O$, then I_C must equal I_2 and the capacitor begins to charge toward $V_N = V_{NT}$. This operation is shown in Fig. W-14, where initially the circuit is at point A and switches instantaneously to point B.

The second phase of operation involves the charging of C with I_2 along trajectory B-C of Fig. W-14. During this time V_D is assumed constant at 0.7 volts and $I_D = I_C$. The charging law is $V_N = V_{NT} - \Delta V + \frac{I_2}{C} T_2$.

where I_c Rn is called Δ V.

When the capacitor charges sufficiently for $V_N = V_{NT}$, part of I_2 current will begin to flow into the negative resistance. For the first small increment of I_2 to flow into R_N , the voltage V_N will instantaneously be reduced. Due to the behavior of the capacitor, this requires that V_D also be reduced resulting in $I_D = O$. Since $I_D = O$, I_C must be $- I_1$ and therefore I_N must become instantaneously $I_N = I_1 + I_2 = I_C$. This represents an instantaneous switching of the negative resistance operating point from point C in Fig. W-14 to point A. The voltage V_N has therefore changed instantaneously by $I_C R_N$ or Δ V. The current I_1 flowing into C charges C according to $V_D = 0.7 - \Delta V + \frac{I_1}{C} T_1$. When $V_D = 0.7$ again, as before, the entire cycle will repeat and the R_N operating point will follow the trajectory from point A to B in Fig. W-14. This occurs for $T_1 = \frac{C\,\Delta V}{I_1}$.

In summary, referring to Fig. W-14 there are two timing cycles and two instantaneous switching cycles in the modulator operation. Trajectory A-B is an instantaneous switching cycle. Trajectory B-C is a timing cycle with a time $T_2 = \frac{C\,\Delta V}{I_2}$. Trajectory C-A is instantaneous. Then the operating point dwells at point A for a time $T_1 = \frac{C\,\Delta V}{I_1}$, after which the cycle repeats itself.

The current I_N is used as the output signal of the modulator. $I_N = I_C$ represents the condition of no output pulse. $I_N = 0$ represents an output pulse. Therefore T_1 and T_2 above can be related to T_W and $(T_P - T_W)$ of Fig. W-9 as:

$$T_1 = T_P - T_W \tag{14}$$

$$T_2 = T_W$$

resulting in the modulator operating law given in Equations (10) and (11).

c. Current drive

The "constant" currents I_1 and I_2 required by the modulator are:

$$I_1 = I_C \frac{\lambda}{\lambda M} \tag{15}$$

$$I_2 = I_C \left(1 - \frac{\lambda}{\lambda M}\right)$$

so that their sum is

$$I_1 + I_2 = I_C \tag{16}$$

This result is obtained by utilizing the basic properties of an emitter coupled difference amplifier, a modification of the original circuit credited to D. W. Slaughter of the California Institute of Technology. The configuration is essentially that described by Paul J. Bênêteau of Fairchild Semiconductor Corporation.

The basic difference amplifier circuit is shown in Fig. W-15. A constant current is supplied to the emitters of TR1 and TR2 thus requiring that the sum of their collector currents approximate a constant. For increasing positive signal voltages E_1, the current in TR1 will increase in proportion to the signal and, since the sum is a constant, the current in TR2 will decrease an equal amount. The constant current supplied the circuit is provided by the collector of a transistor operating at constant emitter current.

The circuit used in the modulator is shown in Fig. W-16. The transistors TR1 and TR2 of the circuit in Fig. W-15 are replaced by a NPN-PNP pair which operate substantially as an equivalent NPN high h_{FE}, low I_{CBO} single transistor.

For the transistor pair shown in Fig. W-17, $I_{C1} = h_{FE1} I_{B1}$ and $I_{C2} = h_{FE1} h_{FE2} I_{B2}$. The base current of TR1 is

$$I_{B1} = \frac{E_S - V_{BE1} - E - R_1\left[I_{CB01}(1 + h_{FE1} + h_{FE2} + h_{FE1}h_{FE2}) + I_{CB02}(1 + h_{FE2})\right]}{R_S + R_1(1 + h_{FE1} + h_{FE1}h_{FE2})} \tag{17}$$

and the emitter current of TR2 is

$$\begin{aligned} I_{E2} = {} & \frac{(E_S - V_{BE1} - E)(h_{FE1})(1 + h_{FE2})}{R_S + R_1[1 + h_{FE1}(1 + h_{FE2})]} \\ & + I_{CB01}\frac{(1 + R_1/R_S)(1 + h_{FE1})(1 + h_{FE2})}{1 + R_1/R_S[1 + h_{FE1}(1 + h_{FE2})]} \\ & + I_{CB02}\frac{(1 + R_1/R_S)(1 + h_{FE2})}{1 + R_1/R_S[1 + h_{FE1}(1 + h_{FE2})]} \end{aligned} \tag{18}$$

The condition $(R_1 + R_S) << R_1 h_{FE1}(1 + h_{FE2})$ is easily achieved, for which

$$I_{E_2} = \frac{E_S - V_{BE1} - E}{R_1} + \left(1 + \frac{R_S}{R_1}\right)\left[I_{CB01}\left(1 + \frac{1}{h_{FE1}}\right) + \frac{I_{CB02}}{h_{FE1}}\right] \tag{19}$$

indicating that I_{E2} is independent of h_{FE1} and h_{FE2} and that the I_{cbo} amplifications are low. This will provide nearly ideal operation in the modulator current drive difference amplifier.

In the circuit of Fig. W-16, and from Equation (19) above we have

$$I_1 = I_{E2} = \frac{1}{R_1}(E_1 - V_{BE1} - E) + \left(1 + \frac{R_S}{R_1}\right)\left[I_{CBO1}\left(1 + \frac{1}{h_{FE1}}\right) + \frac{I_{CBO2}}{h_{FE1}}\right] \tag{20}$$

$$I_2 = I_{E4} = \frac{I}{R_1}(E_2 - V_{BE3} - E) + (1 + R_s/R_1) \quad I_{CBO3}(1 + 1/h_{FE3}) + I_{CBO4}/h_{FE3} \tag{21}$$

and due to the constant current source $I_1 + I_2 = I_c$ so that E can be eliminated in these expressions resulting in the approximations

$$I_1 = \tfrac{1}{2}\left[\frac{E_1 - E_2 + V_{BE3} - V_{BE1}}{R_1} + I_c + (I_{CBO1} - I_{CBO3})(1 + R_s/R_1) + \frac{I_{CBO2} - I_{CBO4}}{h_{FE1}}(1 + R_s/R_1)\right] \tag{22}$$

$$I_2 = \tfrac{1}{2}\left[\frac{E_2 - E_1 + V_{BE1} - V_{BE3}}{R_1} + I_c + (I_{CBO3} - I_{CBO1})(1 + R_s/R_1) + \frac{I_{CBO4} - I_{CBO2}}{h_{FE1}}(1 + R_s/R_1)\right] \tag{23}$$

Thus, if the collector cutoff currents and base to emitter voltages of the corresponding transistors are equal then they will have no effect upon the two output currents and (22) and (23) can be written:

$$I_1 = \frac{1}{2R_1}\left(\Delta E_i + E_u\right) + I_c/2 \tag{24}$$

$$I_2 = \frac{1}{2R_1}\left(- \Delta E_i - E_u\right) + I_c/2 \tag{25}$$

where ΔE_i is the difference in input voltages $(E_1 - E_2)$ and E_u is the uncertainty voltage due to the V_{BE} and I_{CBO} differences.

$$E_u = V_{BE3} - V_{BE1} + (R_S + R_1)\left[I_{CBO1} - I_{CBO3} + \frac{I_{CBO2} - I_{CBO4}}{h_{FE1}} \right] \tag{26}$$

Assuming for the moment that $E_u = 0$, the proper signal swing for E_1 is from $E_2 - I_c R_1$ to $E_2 + I_C R_1$ to result in control of I_1 from 0 to I_C. Let E_s denote the signal input voltage to the modulator where

$$E_1 = E_2 - I_c k_1 + E_s \tag{27}$$

and E_s varies from 0 to 21_c R1. Then for I_1 and I_2 in terms of E_s we have

$$I_1 = \frac{E_s}{2R_1} = I_c \left(\frac{E_s}{2R_1 I_c}\right) \tag{28}$$

$$I_2 = \frac{-E_s}{2R_1} + I_c = I_c \left(1 - \frac{E_s}{2R_1 I_c} \right) \tag{29}$$

which is in the same form as equation (15) so that $\lambda = E_s$ and $\lambda_M = 2R_1 I_C$.

The average value of the pulse train will be, from expression (5)

$$T_W f_P = \frac{E_s}{2R_1 I_c} \tag{30}$$

and

$$K = \frac{1}{2R_1 I_c} \tag{31}$$

d. Non-linear resistance

The non-linear resistance providing the voltage - current characteristics shown in Fig. W-11 is obtained from two transistors operating in the circuit shown in Fig. W-18.

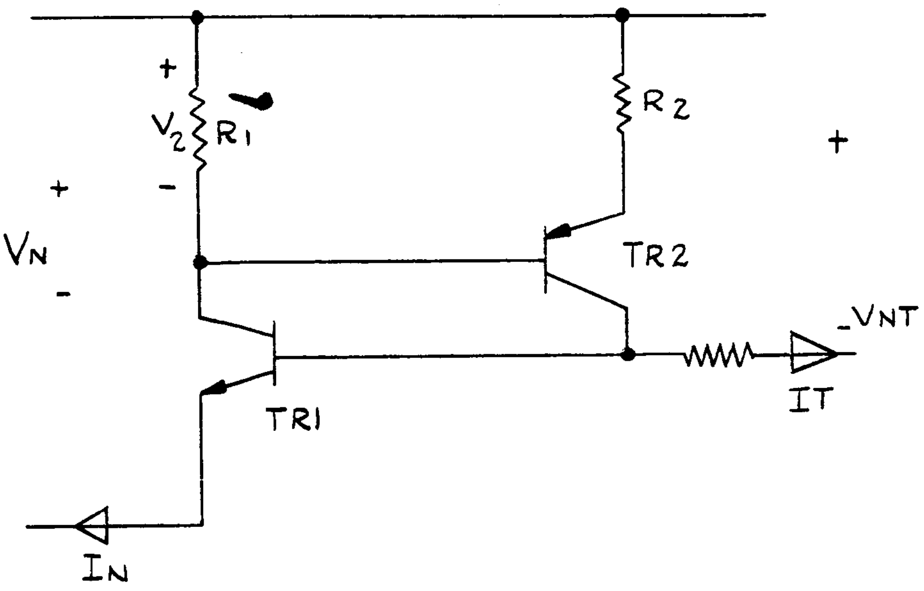

FIGURE W-18

NON-LINEAR RESISTANCE CIRCUIT

The approximate operation of this circuit can be described in three phases. We assume for the moment large h_{FE} and negligible V_{BE} for both transistors.

(1) If $V_N < V_{NT}$ then $I_N = O$ and TR1 is cut off. TR2 is cut off and $I_T = O$ so that $V_1 = V_{NT}$.

(2) When $V_N \geqq V_{NT}$, then TR1 and TR2 will both begin to amplify. Since V_1 must equal V_N (for the assumed negligible V_{BE1}), then $I_T = (V_{NT} - V_N)/ R_N'$. V_2 will equal $I_N R_1$ and $I_{C2} = I_T$ must equal $I_N R_1/R_2$ so that $I_N R_1/R_2 = (V_{NT} - V_N)/R_N'$ and $V_N = V_{NT} - I_N R_N \; R_1/R_2$ so that $V_N = V_{NT} - I_N R_N$ represents the negative resistance where $R_N = R_N' \; R_1/R_2$.

(3) Saturation of TR1 occurs slightly before (for increasing I_N) $I_N R_1 = V_N$ and saturation of TR2 occurs slightly before $I_T R_2 = V_N$. These conditions are identical for $I_T = I_N \; R_1/R_2$ as given in 2) above. Therefore saturation of TR1 and TR2 must occur nearly simultaneously--I_N increases, at $I_N = V_N / R_1$. At this point, the V_N-I_N characteristic assumes a positive slope.

e. Modulator circuit

The actual circuit of the pulse modulator is shown in Fig. W-19, representing a combination of the elements and concepts discussed in the preceeding sections. TR1 to TR4 are the current drive difference amplifier. TR5, a 2N697, furnishes the constant current I_C of 8 ma. CR1 is the diode which furnishes the required non-linear resistance. TR6 and TR7 provide the negative non-linear resistance characteristic. The jet switching amplifier is driven through the resistance-diode network R9 through R12. R8 and CR3, an extremely stable reference diode--IN1530, provide a constant reference voltage of nominally 8.4 v dc at the base of TR3.

f. Summary of characteristics

The modulator produces a constant amplitude pulse train which follows the law

$$T_w f_p = K\lambda = \frac{\lambda}{\lambda_M} \qquad (32)$$

[redacted]

where T_W is the pulse on time, $1/f_P$ is the pulse repetition period, K is a gain constant and λ is proportional to the d-c modulator input signal. The pulse on time T_W is called the pulse width and the quantity f_P is called the pulse repetition frequency.

T_W and f_P are related to λ where $\lambda_M = 1/K$ by

$$T_W = \frac{(T_W)_{min}}{1 - \lambda/\lambda_M} \tag{33}$$

$$f_P = 4(f_P)_{max}\left(\frac{\lambda}{\lambda_M}\right) \tag{34}$$

Equation (32) is, of course, a linear relation between the average value or duty cycle of the pulse train. The jet thrust produced is approximately proportional to this duty cycle. The relation of (33) for pulse width is shown in Fig. W-20 for $(T_W)_{MIN}$ values of 5 and 10 milliseconds. (34) for pulse frequency is given in Fig. W-21 for the same values of $(T_W)_{MIN}$. The relation between T_W and f_P can be related by elimination of λ/λ_M as a variable. These curves are given in Figs. W-22 and W-23. Corresponding values of duty cycle (proportional to input voltages) are shown on the curves. Note that for low values of duty cycle the operation approximates that of an ordinary pulse frequency modulator. For large duty cycles a combined mode of modulation is realized. Straight lines on this graph with a slope of -1 represent lines of constant duty cycle.

As mentioned in 5., a. of this section the minimum pulse width and the maximum frequency are related by

$$(T_W)_{min}(f_P)_{max} = 1/4 \tag{35}$$

[redacted]

This relation is shown in Fig. W-24. For any selected minimum width, the maximum frequency is automatically determined.

As shown in 5., b of this section the negative slope of the non-linear negative resistance characteristic, R_N, the constant current I_C, and the change in voltage V are related by $\Delta V = R_N I_C$ so that from equation (12) the minimum pulse width can be written as

$$(T_w)_{min} = C R_n \qquad (36)$$

which is plotted Fig. W-25. As given in 5., d of this section R_N is the resistance of the Thevenin equivalent source of the network seen by the collector of TR7 looking into R9, etc., in Fig. W-19. For this circuit this resistance is approximately 1063 ohms. C in (36) is C1 of Fig. W-19.

From equation (30) the duty cycle is related to the modulator input voltage by

$$T_W f_P = \frac{E_s}{2 R_1 I_c} \qquad (37)$$

so that λ and λ_M above are

$$\lambda = E_s \qquad \lambda_M = 2 R_1 I_c \qquad (38)$$

R_1 in equation (38) represents R4 and R5 in Fig. W-19. I_C is determined by TR5 and the setting of R3. R3 therefore constitutes a gain adjustment. The nominal gain for this circuit is $K = 1/13.2$ v dc $= 1/2_M$.

Development testing of the modulator circuit was performed employing the summer as a source. All test data included the summer characteristics and inaccuracies. At room temperature (25°C) the maximum deviation of the modulator average value output (duty cycle) from a straight line was 0.76%. This error is sufficiently small that the inaccuracies of the measurement equipment (dc differential voltmeters) and the method cannot be unquestioned. At a temperature of +95°C the maximum linearity error was 1.0% deviation from a straight line. Both of these linearity figures are "terminal" linearity- -relative to a straight line which intersects the actual curve at duty cycles of zero and unity. "Independent" linearity, relative to the best fitting straight line was 0.7% at room temperature and 0.6% 95° C. The gain of the circuit changed at -0.8% over this temperature range. The measured shift in the starting point of the curve, i. e., the value of input voltage which is just sufficient to produce pulses, was 0.010 volts over the same temperature range. These errors are negligible relative to this autopilot application. The circuit operation also adhered closely to the theoretical curve given in Fig. W-22.

g. Jet switching amplifier

The jet switching amplifier accepts the output of the pulse modulator, provides power gain, and drives the reaction jet control torque motors. The circuit offers stable and reliable operation over a wide temperature range, insensitivity to transistor parameters, simplicity in utilizing direct coupled connections, and low idling current with corresponding high efficiency. The transistors in the circuit are either cut off or else operating saturated. Due to the rapid switching inherent in the pulse modulator, no regenerative pulse shaping is required in the switching amplifier. Associated problems are thus avoided. The circuit employs a common emitter output stage, thus driving the inductive torque motor load with a high impedance during the switching transition. This provides a low switching time constant, in the microsecond range, for loads with inductive components as high as 10 henry- -considerably higher than the anticipated jet inductance. The circuit is shown in Fig. W-32.

For the jet off condition, TR1 operates saturated and TR2, TR3, TR4 are cut off. A current equal to the modulator constant current I_C enters the network at the left of Fig. W-32. $I_C = 8$ma. This current added to the current from the +25 v dc supply through R_A flows into the junction of R_C and R_1. Sufficient current flows into the base of TR1 to force it into saturation. V_{CE1} saturated is sufficiently low to keep the remaining transistors cut off. For the jet on condition, the pulse modulator produces an $I_C = 0$. The base current of TR1 then becomes low and TR1 is cut off. Current then flows through R2 into the base of TR2. This in turn turns off TR3 and TR4.

An important consideration with this circuit is its ability to remain turned off under high temperature conditions. The SM72 stabistor provides a reverse

[redacted]

bias for TR4. R4 is selected so that TR4 is always reverse biased and cut off for any I_{CB04} and so that TR3 is also reverse biased by the voltage across R4 compared to that across R3. The cut-off condition of TR3 tends to be stabilized with temperature since the I_{CBO} currents for TR3 and TR4 will track to a certain degree.

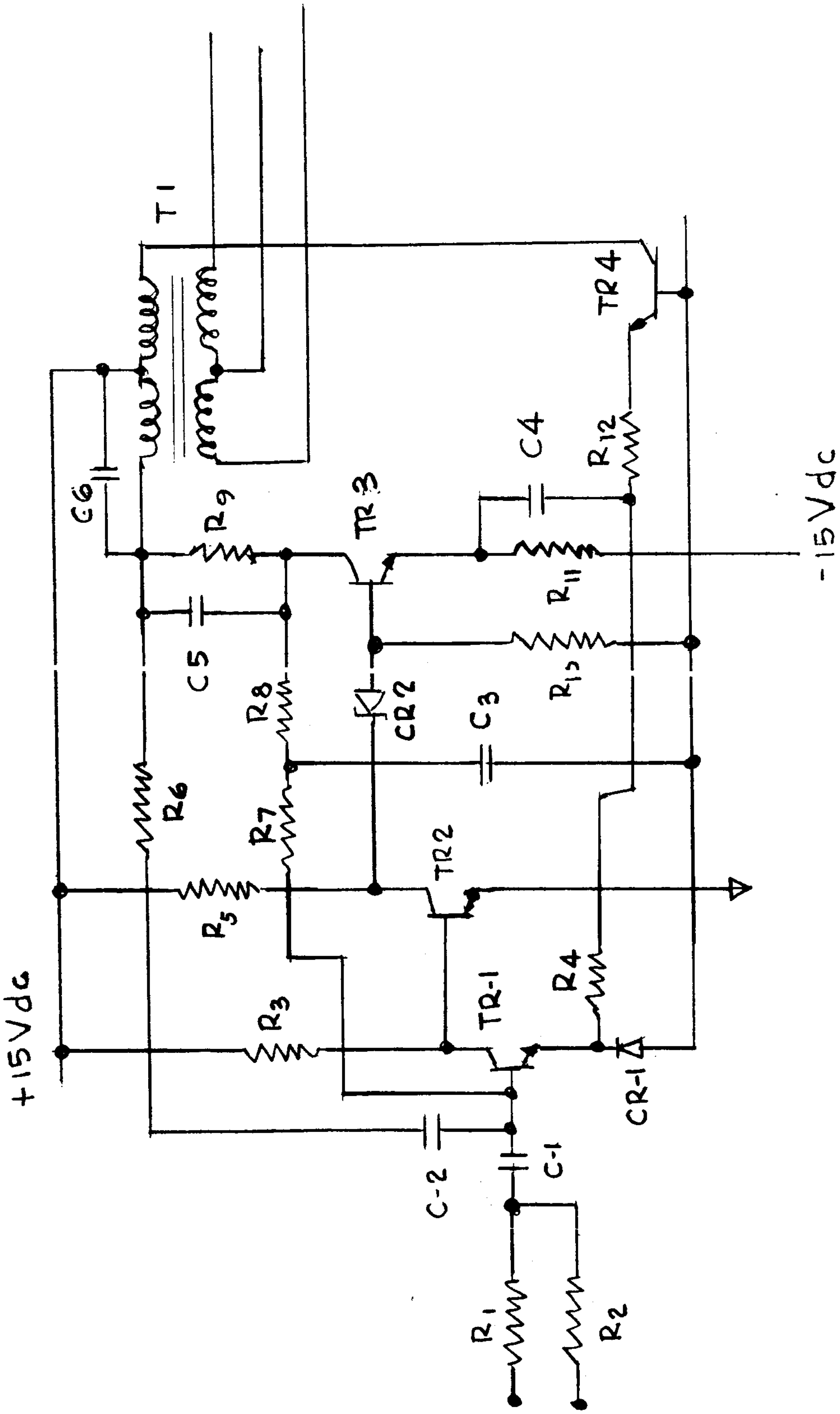
T1
C6
R9
TR3
C4
R12
TR4
C5
R8
CR2
C3
R11
R10
-15Vdc
R6
R7
TR2
R5
R3
TR-1
R4
CR-1
+15Vdc
C-2
C-1
R1
R2

Fig. W-1. Mixer-Amplifier Schematic

[redacted]

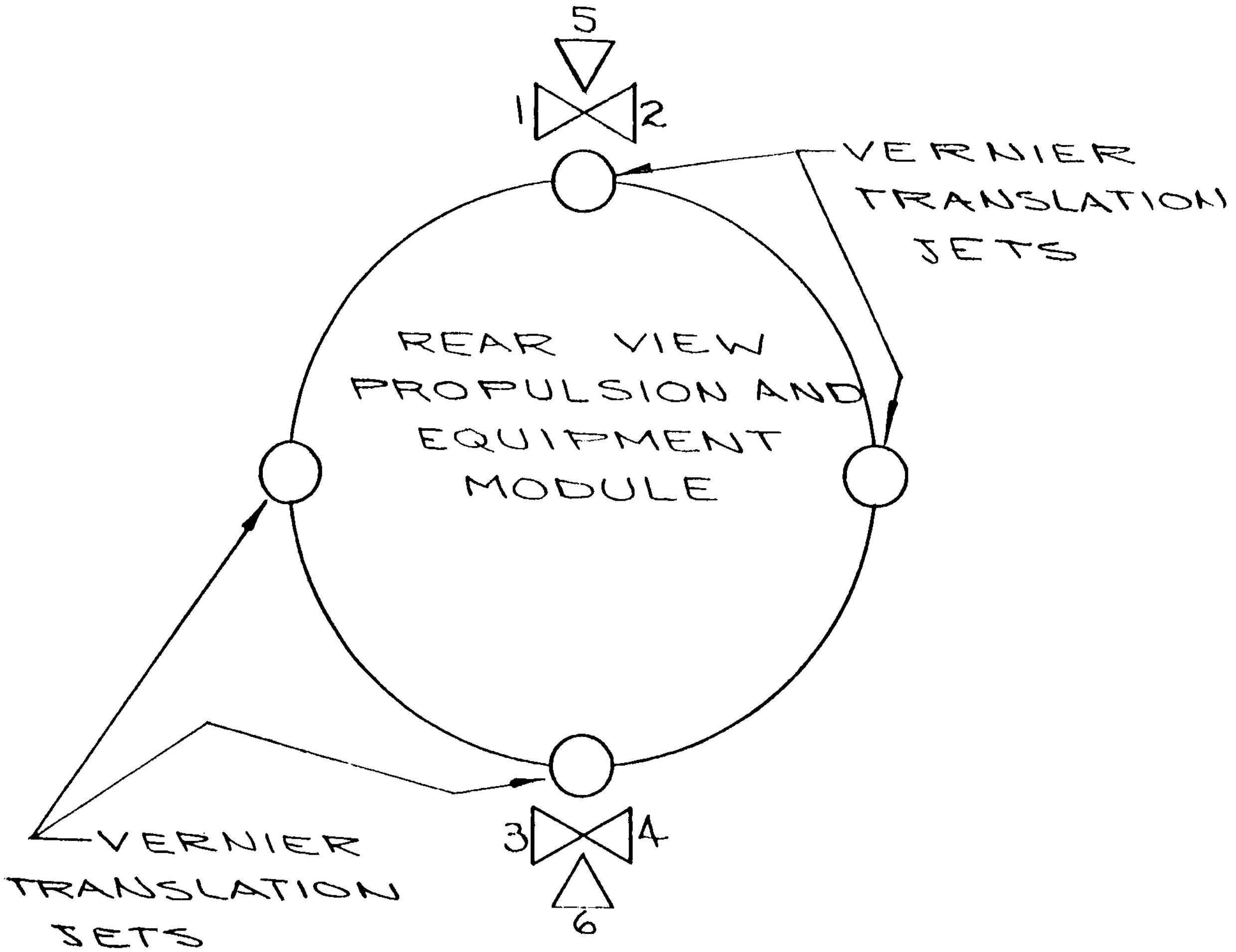
5
1
2
VERNIER TRANSLATION JETS
REAR VIEW PROPULSION AND EQUIPMENT MODULE
VERNIER TRANSLATION JETS
3
4
6

MID-COURSE ATTITUDE JET CONFIGURATION

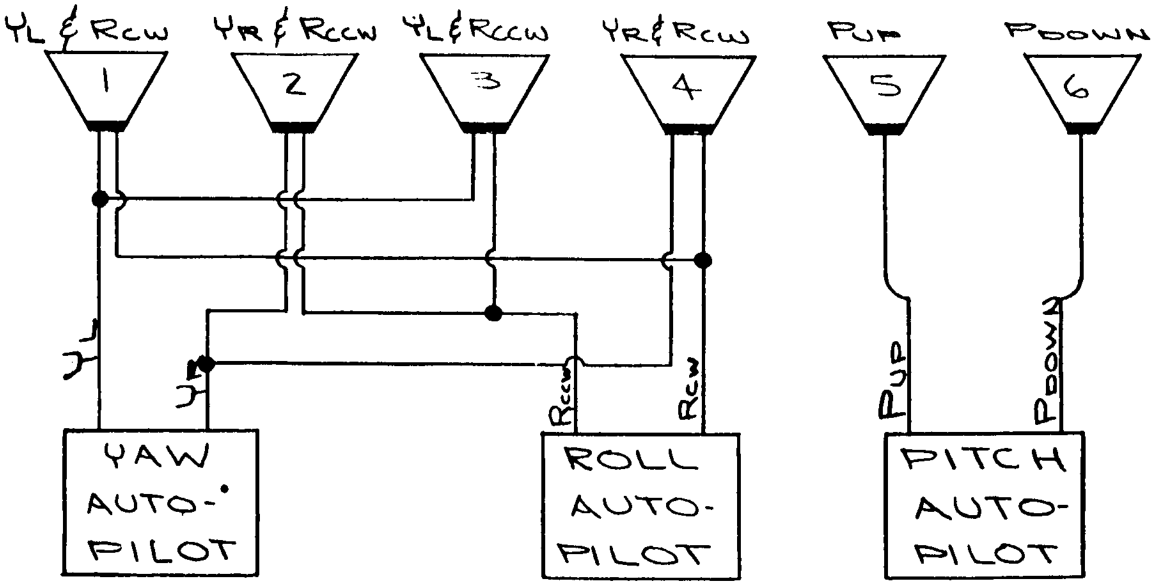
YL & RCW
YR & RCCW
YL & RCCW
YR & RCW
PUP
PDOWN
1
2
3
4
5
6
YL
YR
RCCW
RCW
PUP
PDOWN
YAW AUTO-PILOT
ROLL AUTO-PILOT
PITCH AUTO-PILOT

JET NOZZLES

Fig. W-2. Midcourse Attitude Control Nozzle Configuration

[redacted]

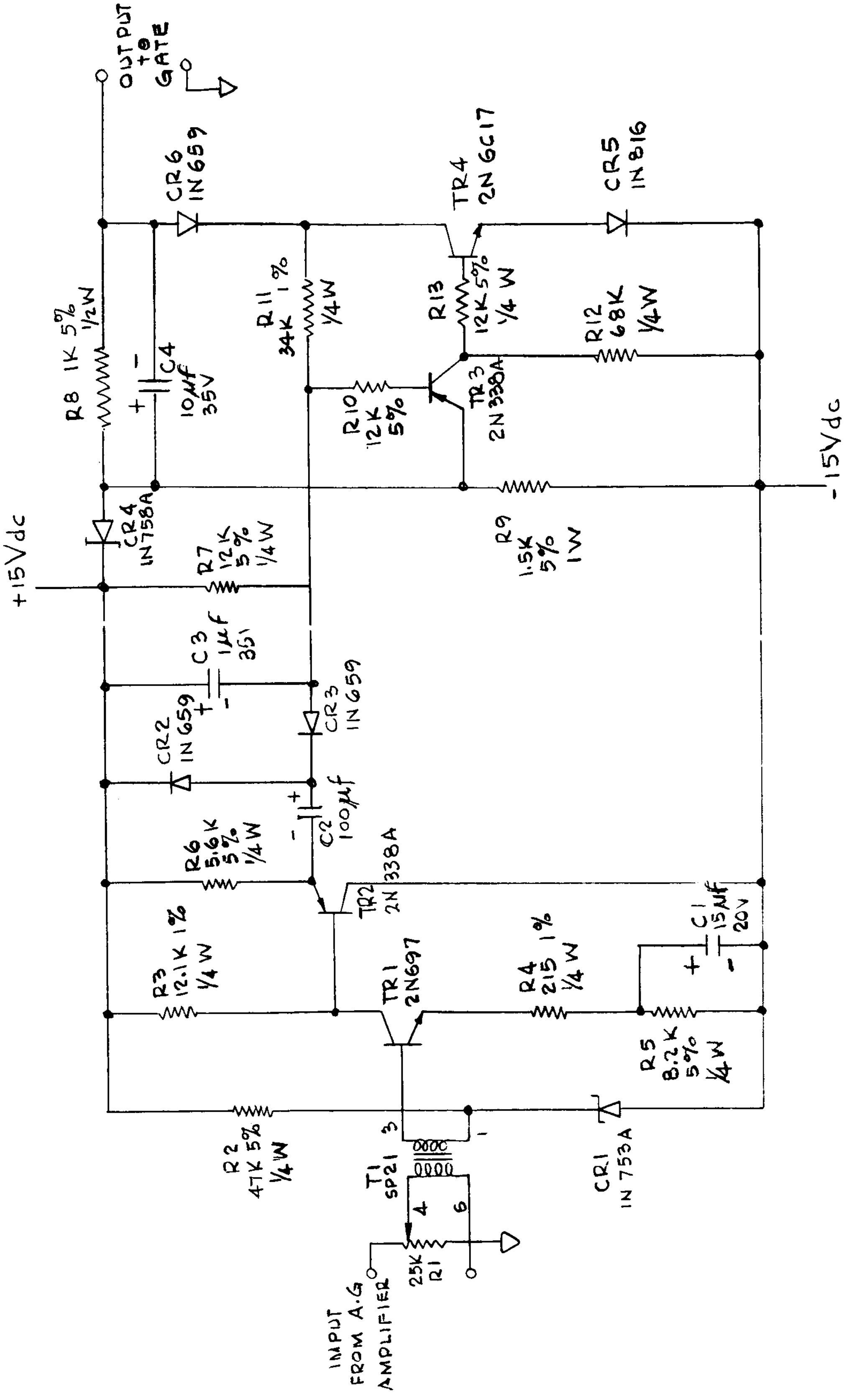
OUTPUT TO GATE
CR6 IN659
TR4 2N GC17
CR5 IN816
R8 1K 5% 1/2W
C4 10μf 35V
R11 34K 1% 1/4W
R13 12K 5% 1/4 W
R12 68K 1/4W
R10 12K 5%
TR3 2N338A
-15Vdc
+15Vdc
CR4 IN758A
R7 12K 5% 1/4W
R9 1.5K 5% 1W
C3 1μf 35V
CR3 IN659
CR2 IN659
C2 100μf
R6 5.6K 5% 1/4W
TR2 2N338A
R3 12.1K 1% 1/4W
TR1 2N697
R4 215 1% 1/4W
C1 15μf 20V
R5 8.2K 5% 1/4W
R2 47K 5% 1/4W
T1 SP21
3
1
4
6
CR1 IN753A
25K R1
INPUT FROM A.G AMPLIFIER

Fig. W-3. Magnitude Detector Schematic

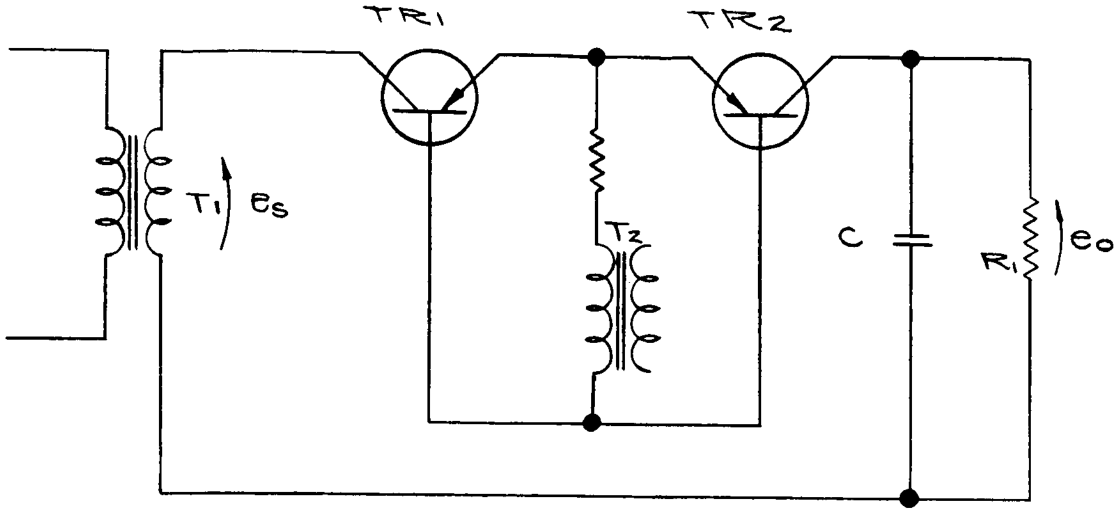
TR1
TR2
T1
es
T2
C
R1
eo

Fig. W-4. Basic Demodulator Schematic

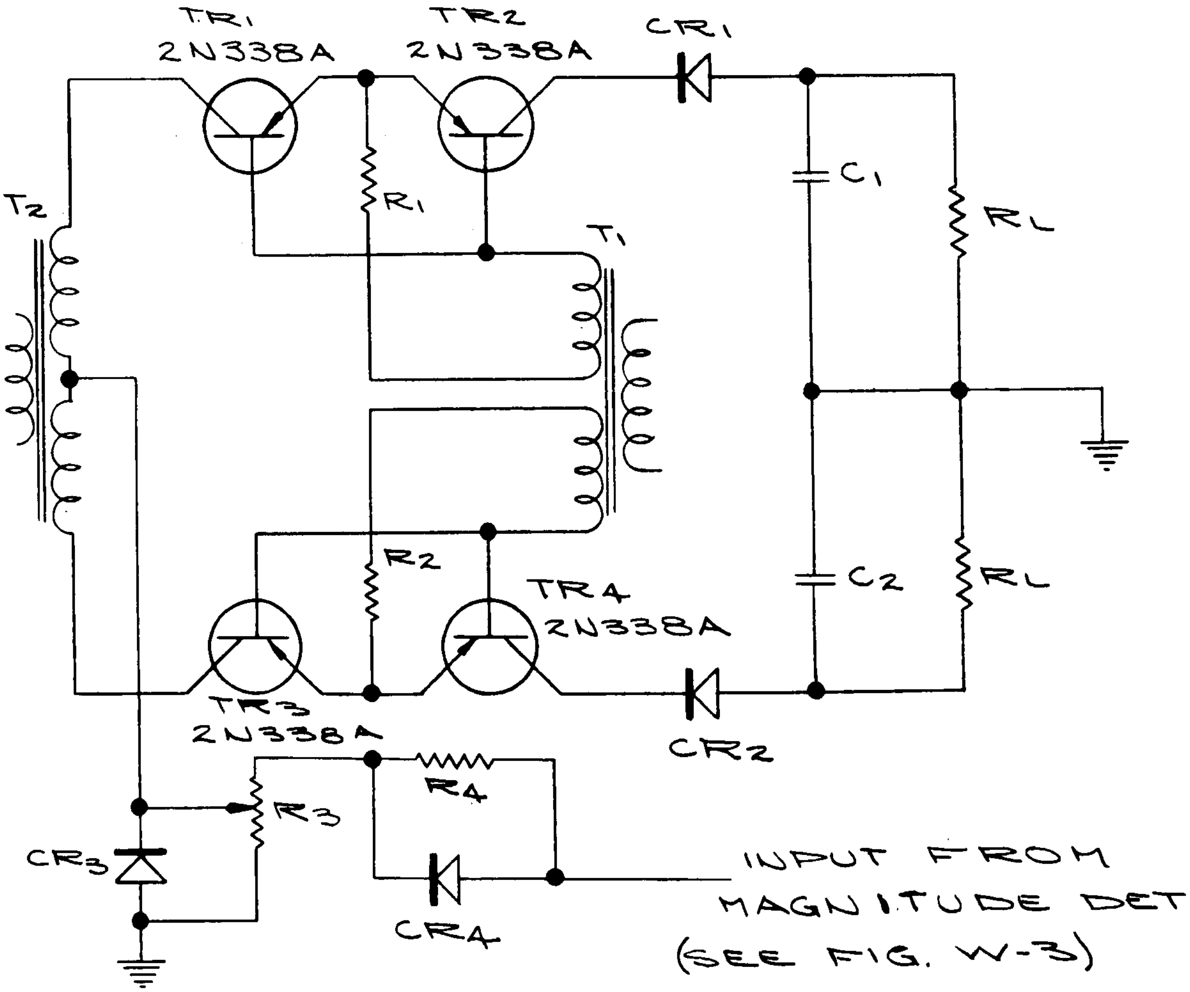
TR1
2N338A
TR2
2N338A
CR1
C1
RL
R1
T2
T1
R2
TR4
2N338A
C2
RL
TR3
2N338A
CR2
R4
R3
CR3
CR4
INPUT FROM
MAGNITUDE DET
(SEE FIG. W-3)

Fig. W-5. Demodulator and Gate Schematic

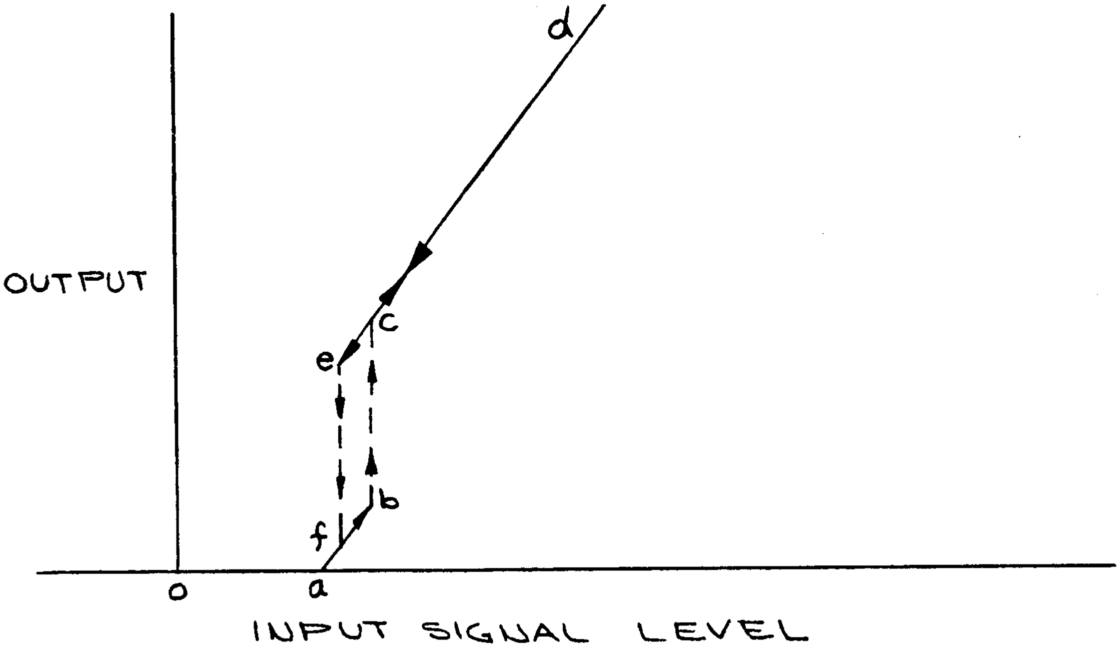

Fig. W-6. Deadspot Operation

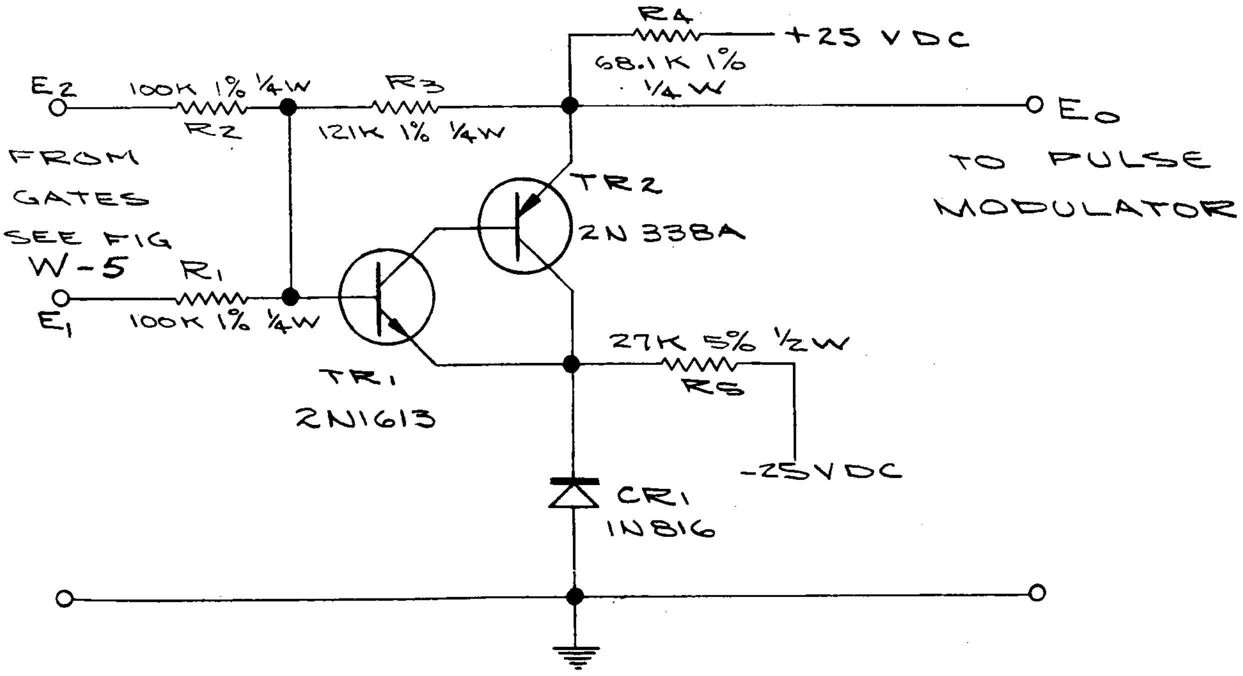
R4
68.1K 1%
1/4 W
+25 VDC
E2
100K 1% 1/4W
R2
R3
121K 1% 1/4W
E0
TO PULSE
MODULATOR
FROM
GATES
SEE FIG
W-5
R1
E1
100K 1% 1/4W
TR2
2N 338A
TR1
2N1613
27K 5% 1/2W
R5
-25VDC
CR1
1N816

Fig. W-7. Summer Circuit Schematic

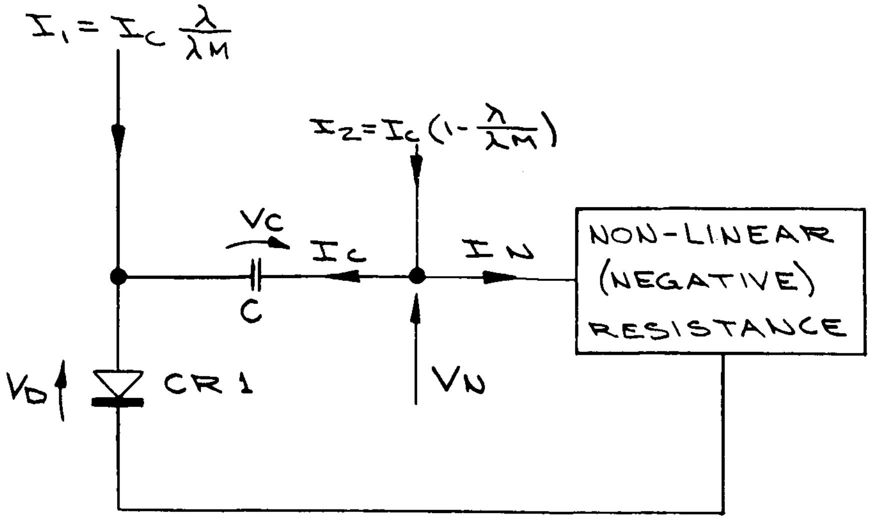
$I_1 = I_C \frac{\lambda}{\lambda M}$
$I_2 = I_C (1 - \frac{\lambda}{\lambda M})$
V_C
I_C
I_N
C
NON-LINEAR (NEGATIVE) RESISTANCE
V_D
CR 1
V_N

Fig. W-10. Basic Modulator Circuit

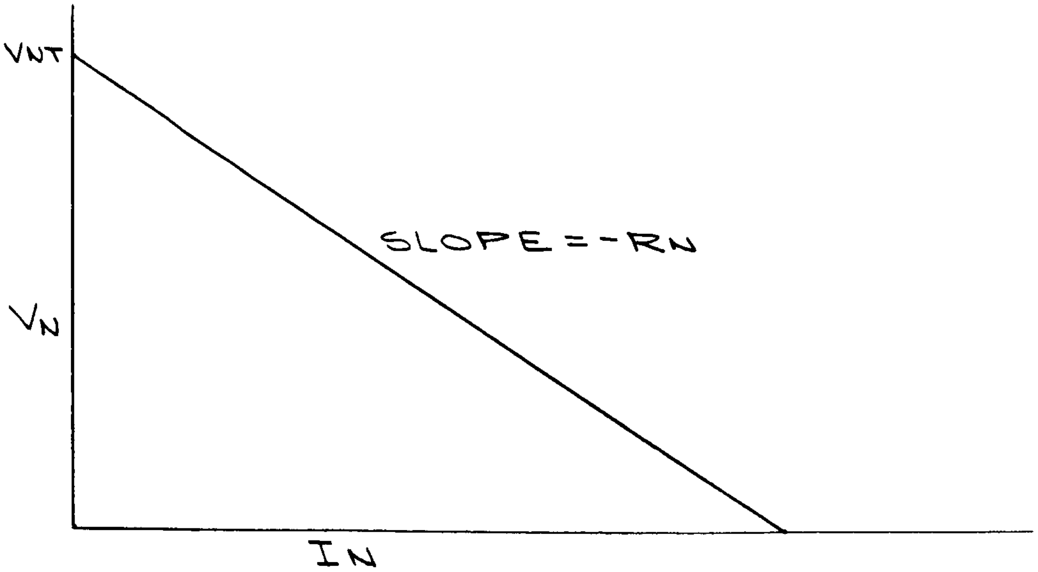

Fig. W-11. Nonlinear Resistance Characteristics

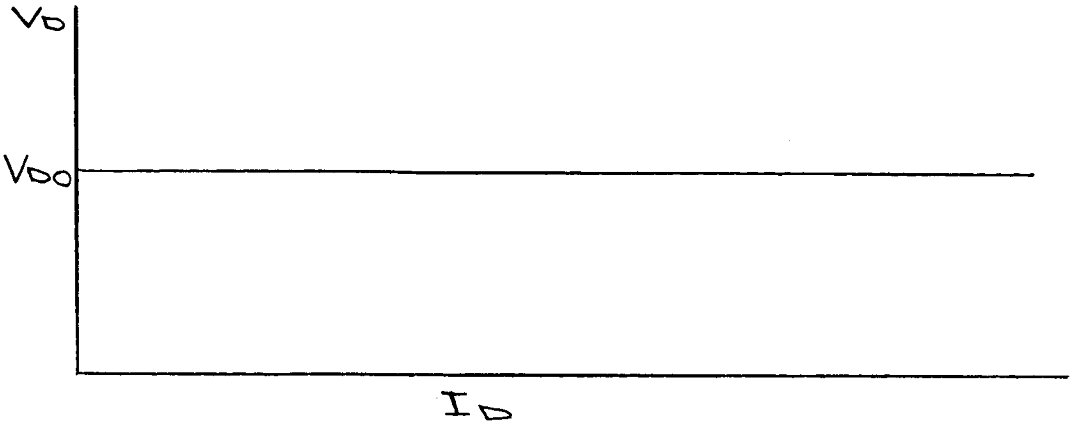

Fig. W-12. Idealized Diode Characteristics

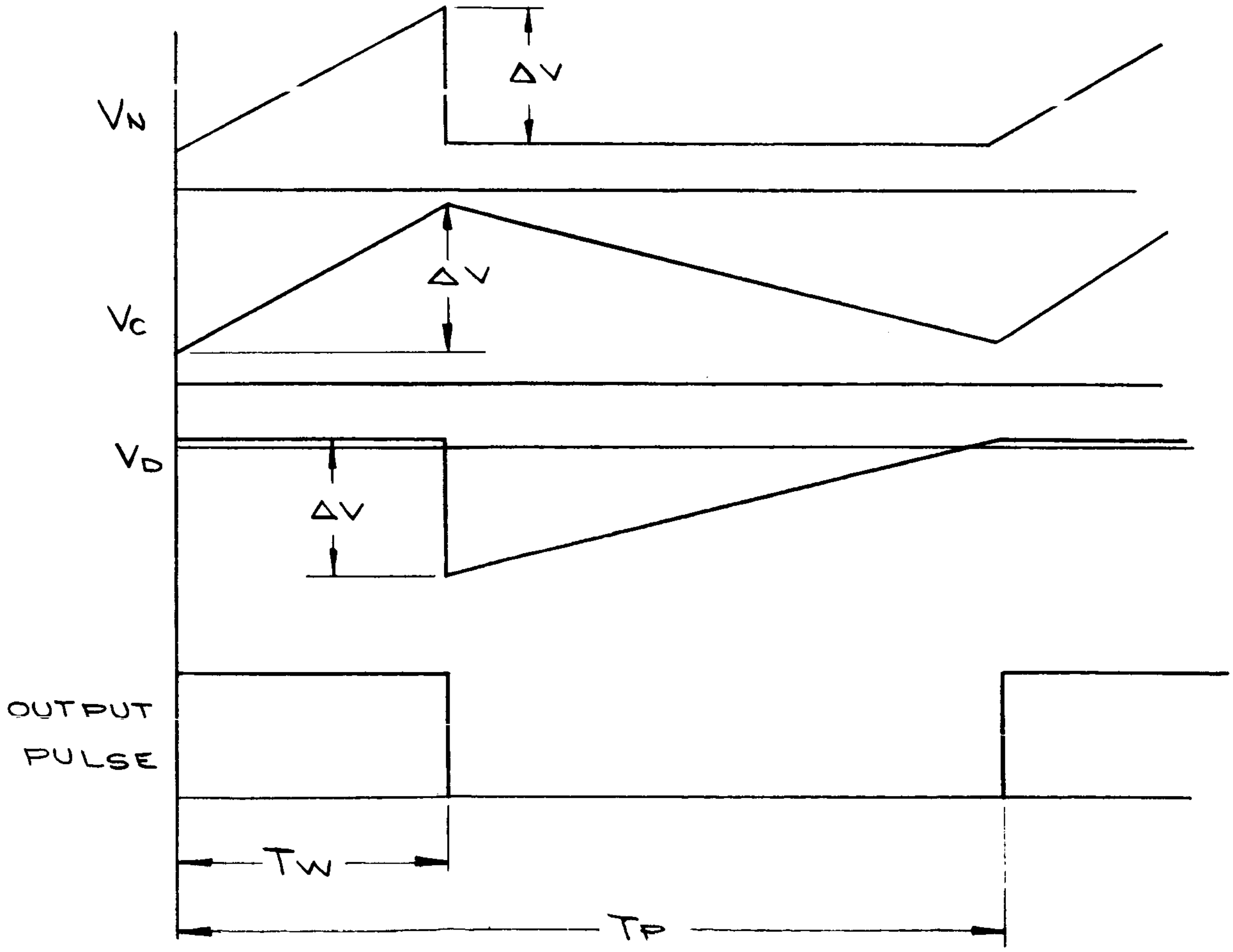
VN
ΔV
VC
ΔV
VD
ΔV
OUTPUT
PULSE
TW
TP

Fig. W-13. Modulator Waveforms

[redacted]

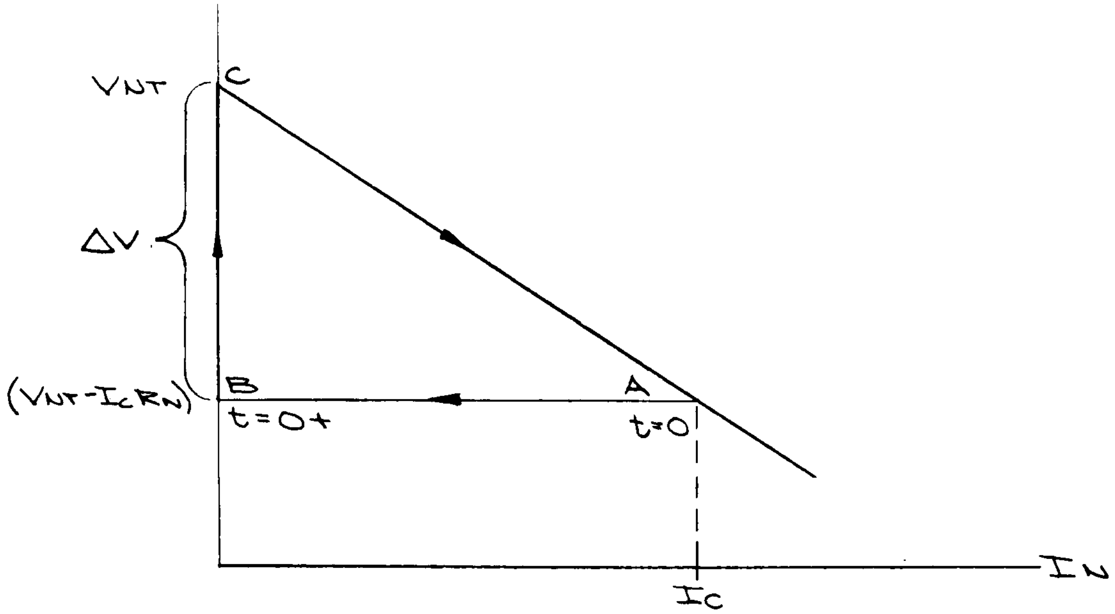
V_NT
C
ΔV
(V_NT - I_C R_N)
B
t = 0+
A
t = 0
I_C
I_N

Fig. W-14. Nonlinear Resistance Operating Characteristics

[redacted]

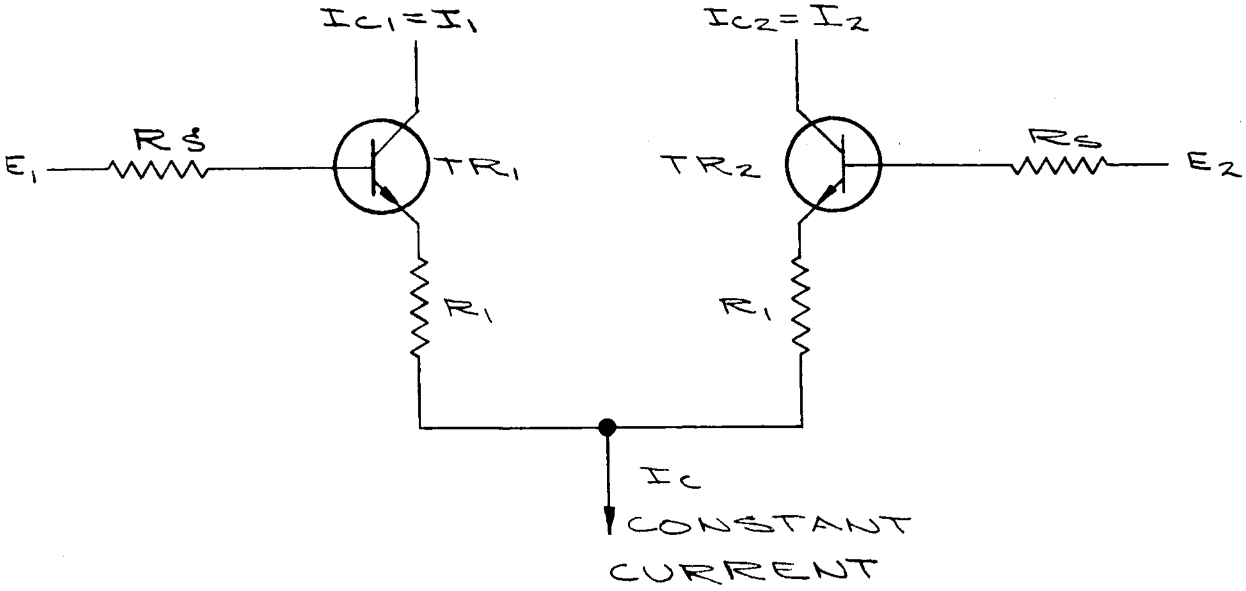

$I_{C1} = I_1$
$I_{C2} = I_2$
RS
E1
TR1
TR2
RS
E2
R1
R1
Ic
CONSTANT CURRENT

Fig. W-15. Difference Amplifier

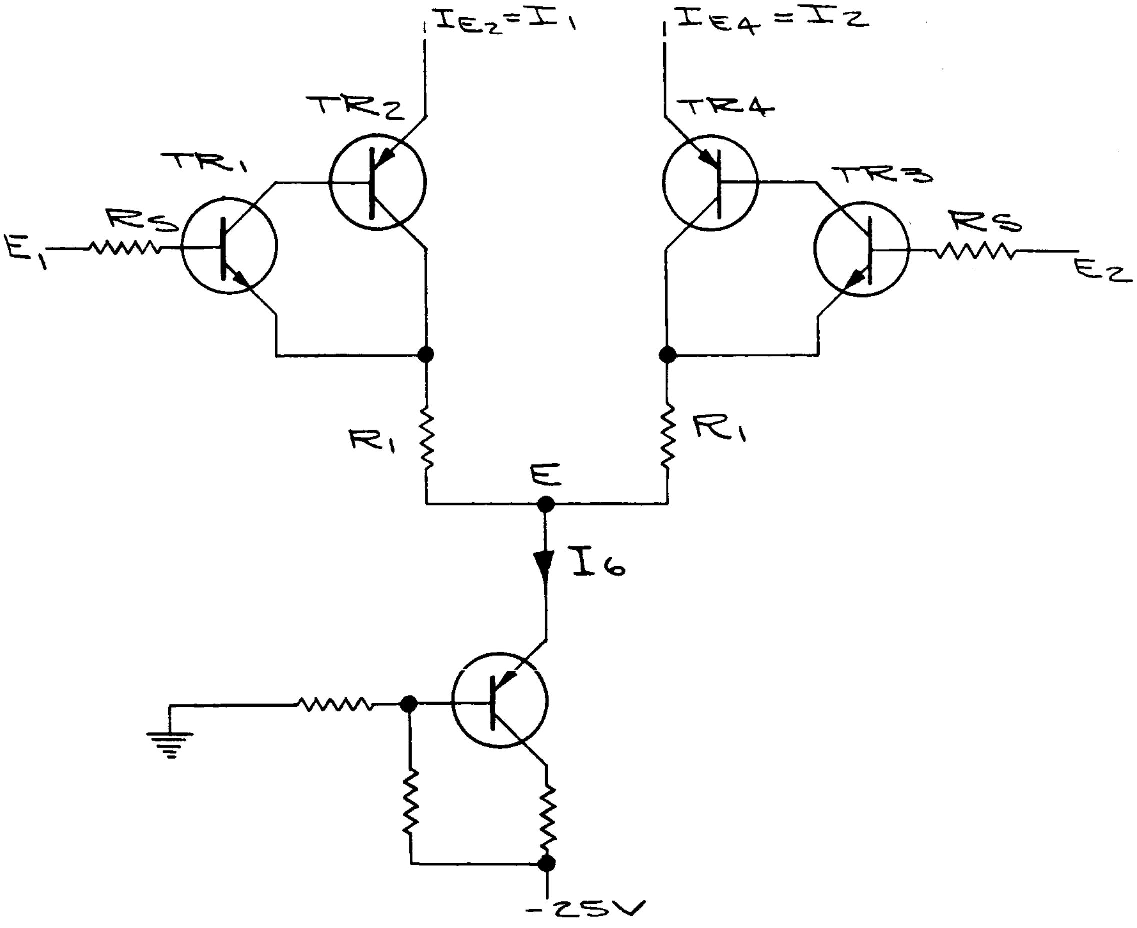

$I_{E2} = I_1$
$I_{E4} = I_2$
TR2
TR4
TR1
TR3
RS
RS
E1
E2
R1
R1
E
I_6
-25V

Fig. W-16. Modulator Current Drive Schematic

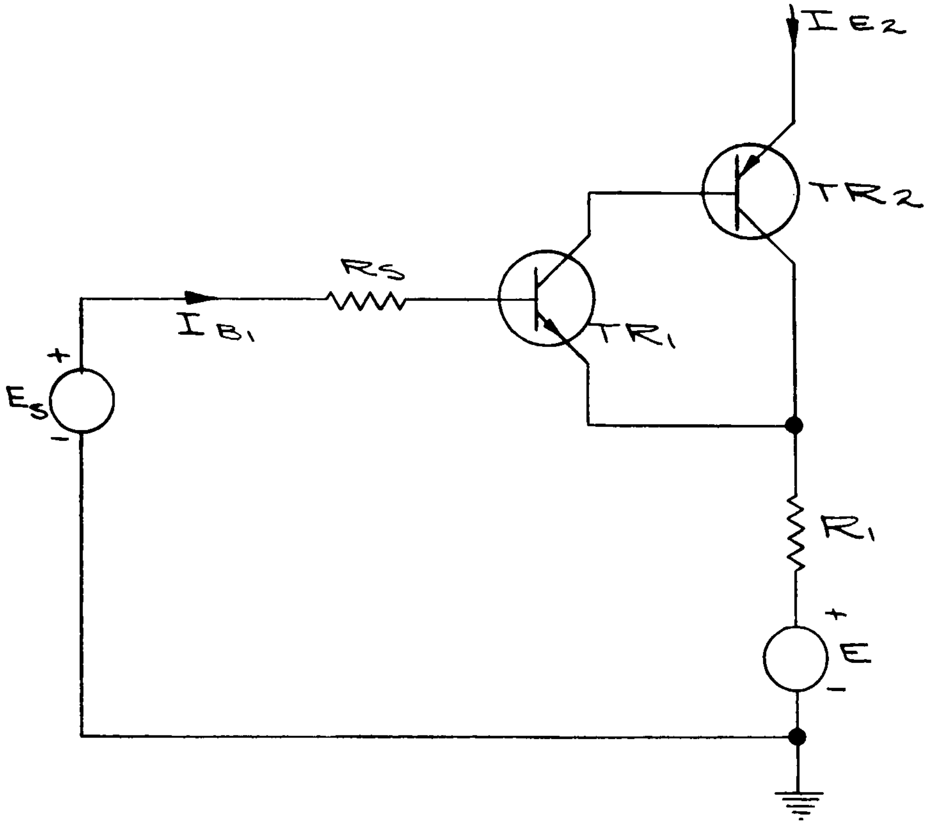
I_{E2}
TR2
R_S
TR1
I_{B1}
+
E_S
-
R_1
+
E
-

Fig. W-17. Basic Transistor Pair

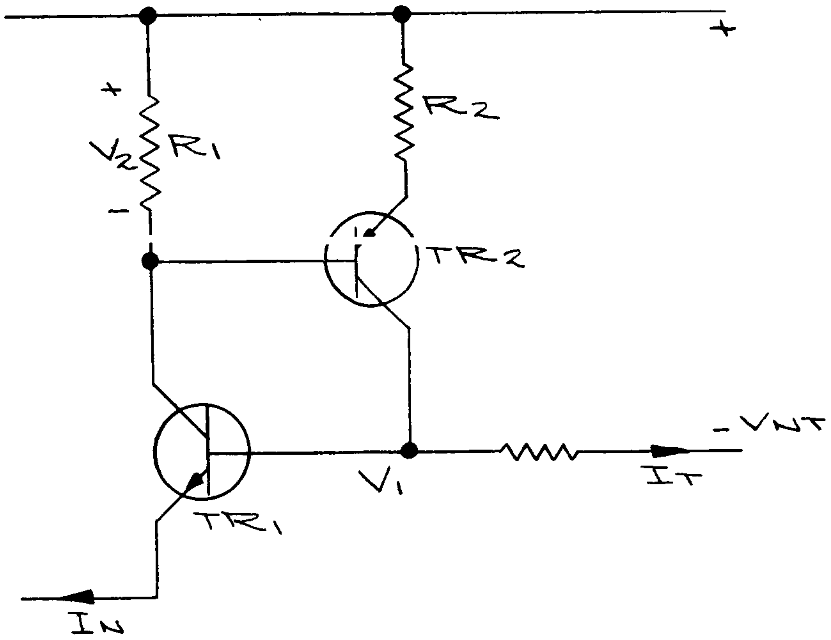
+
+
R2
V2
R1
-
TR2
-VNT
V1
IT
TR1
IN

Fig. W-18. Nonlinear Resistance Circuit

[redacted]

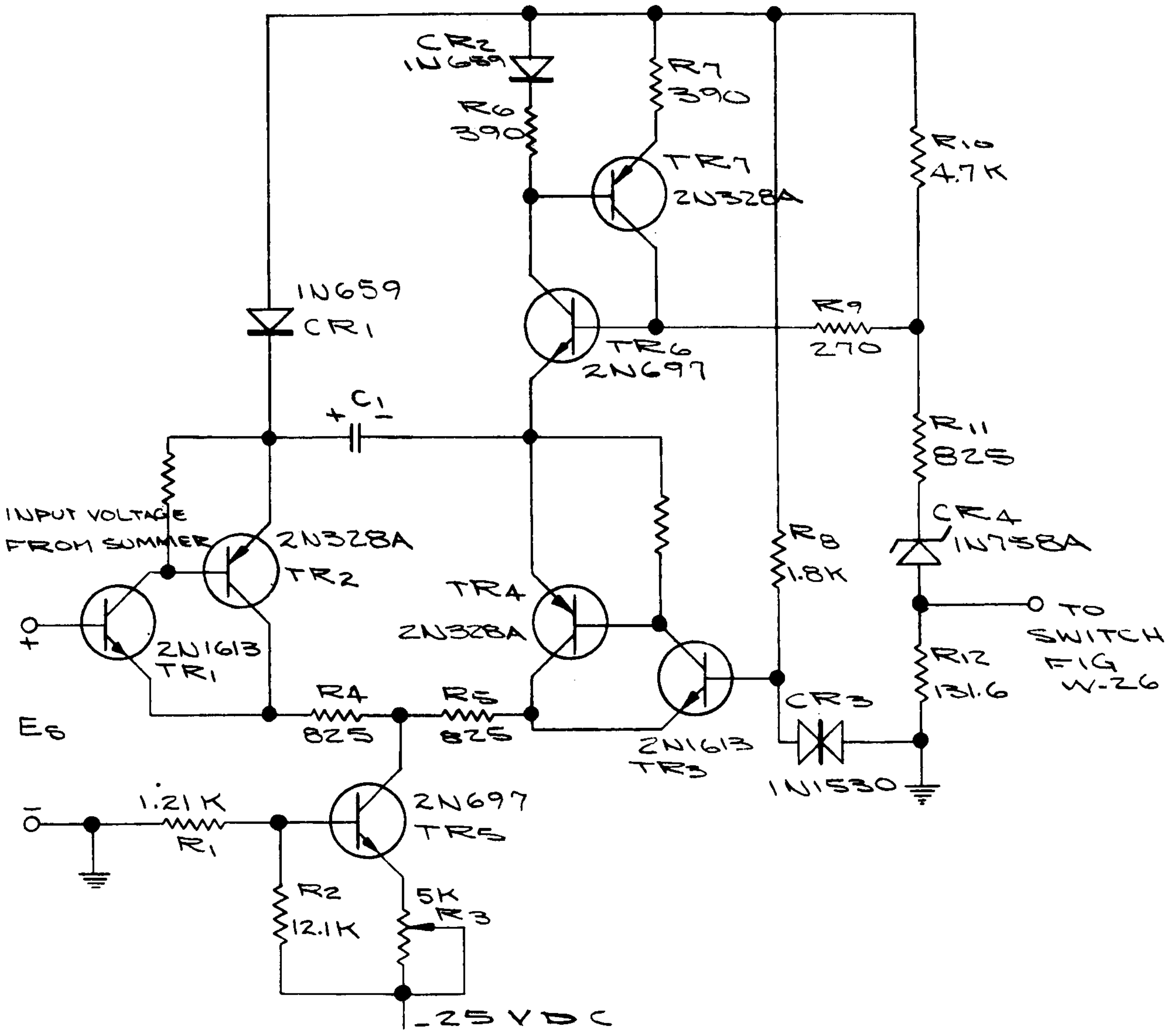
CR2
1N689
R6
390
R7
390
TR7
2N328A
R10
4.7K
1N659
CR1
R9
270
TR6
2N697
C1
+
-
R11
825
CR4
1N738A
INPUT VOLTAGE
FROM SUMMER
2N328A
TR2
TR4
2N328A
R8
1.8K
TO
SWITCH
FIG
W-26
+
2N1613
TR1
R12
131.6
Es
R4
825
R5
825
2N1613
TR3
CR3
1N1530
-
1.21K
R1
2N697
TR5
R2
12.1K
5K
R3
-25 VDC

Fig. W-19. Pulse Modulator Schematic

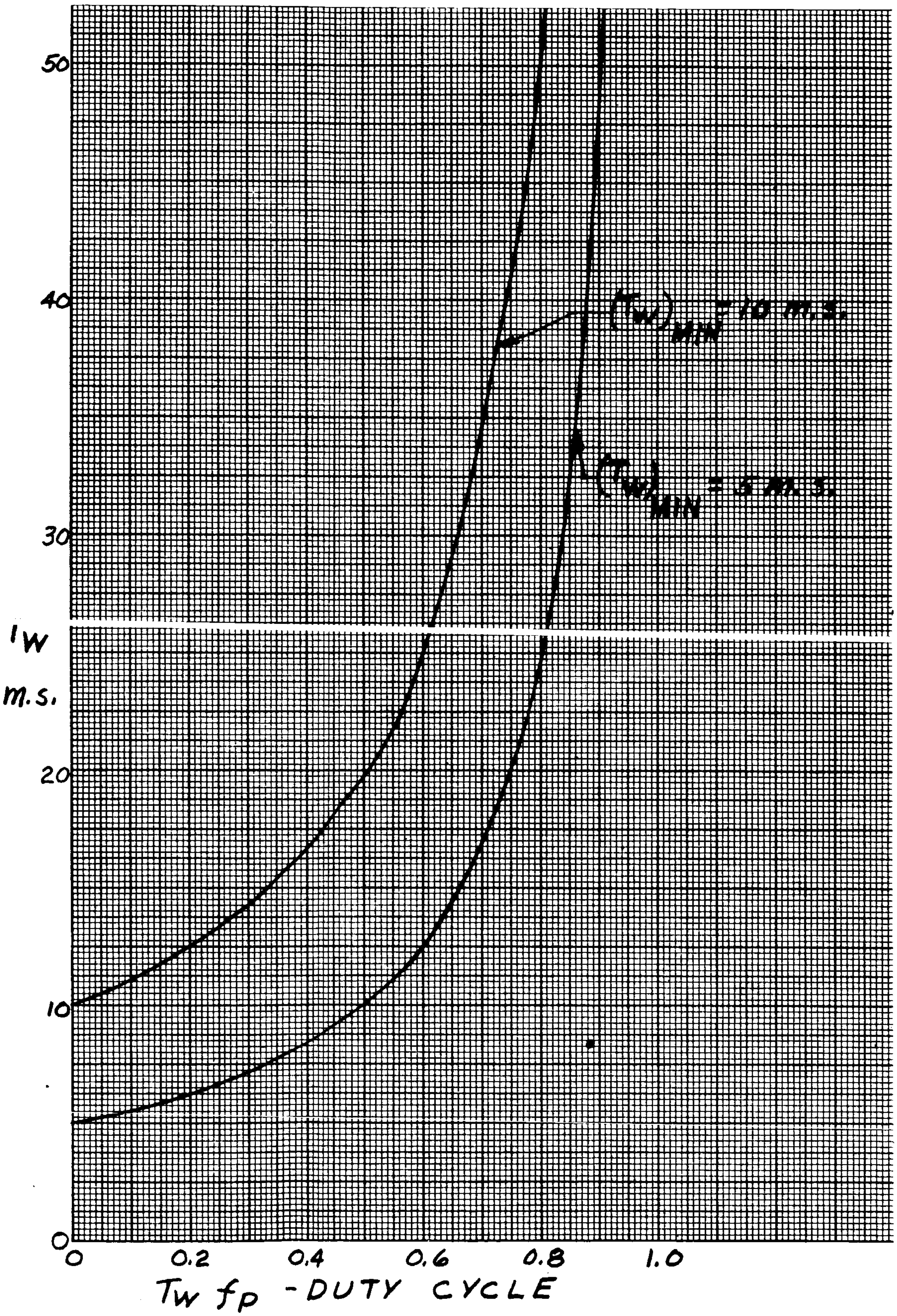

Fig. W-20. Pulse Width Versus Duty Cycle

[redacted]

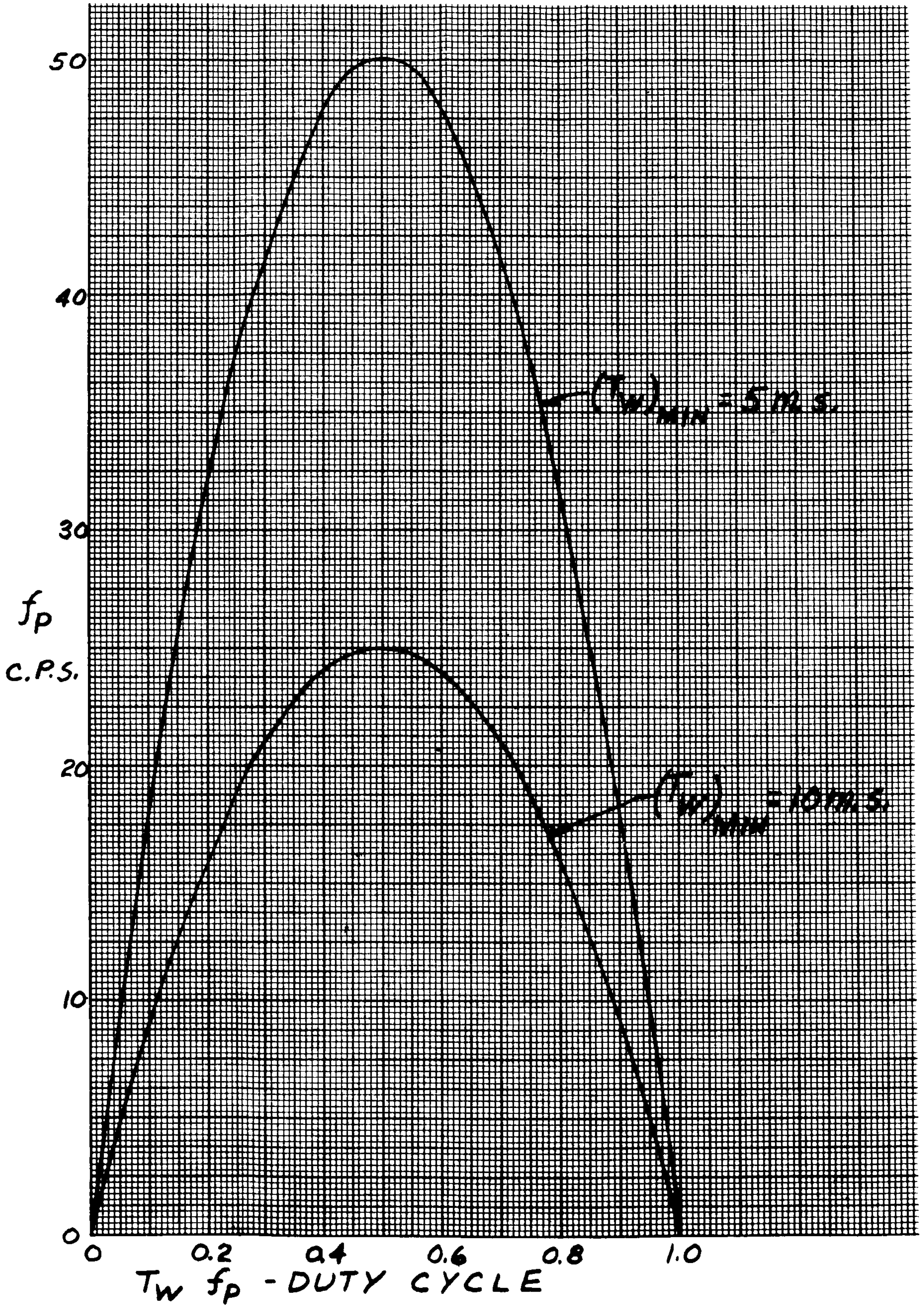

Fig. W-21. Repetition Rate Versus Duty Cycle

[redacted]

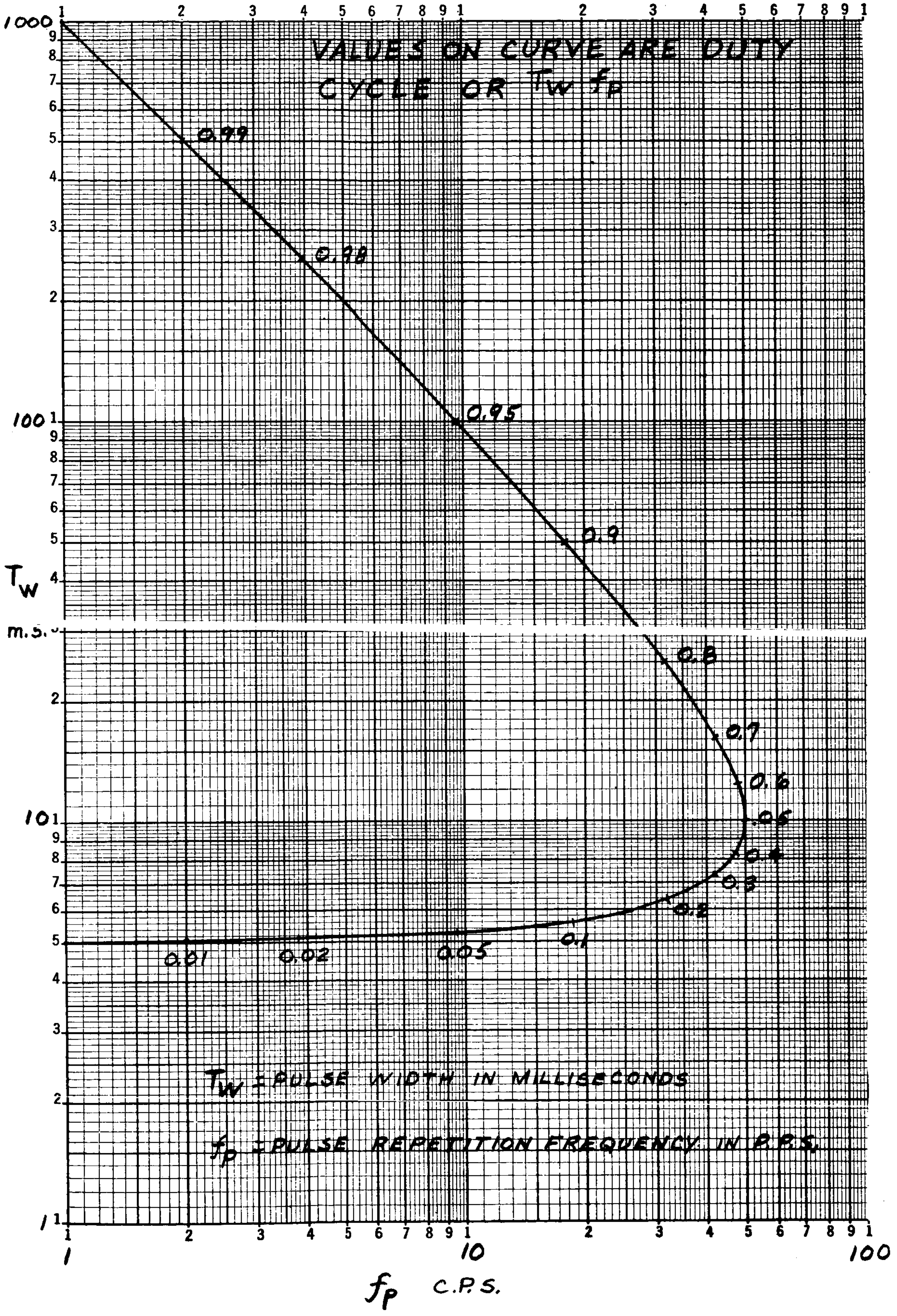

Fig. W-22. Pulse Modulator Operating Curve for 5 Millisecond Minimum Pulse

[redacted]

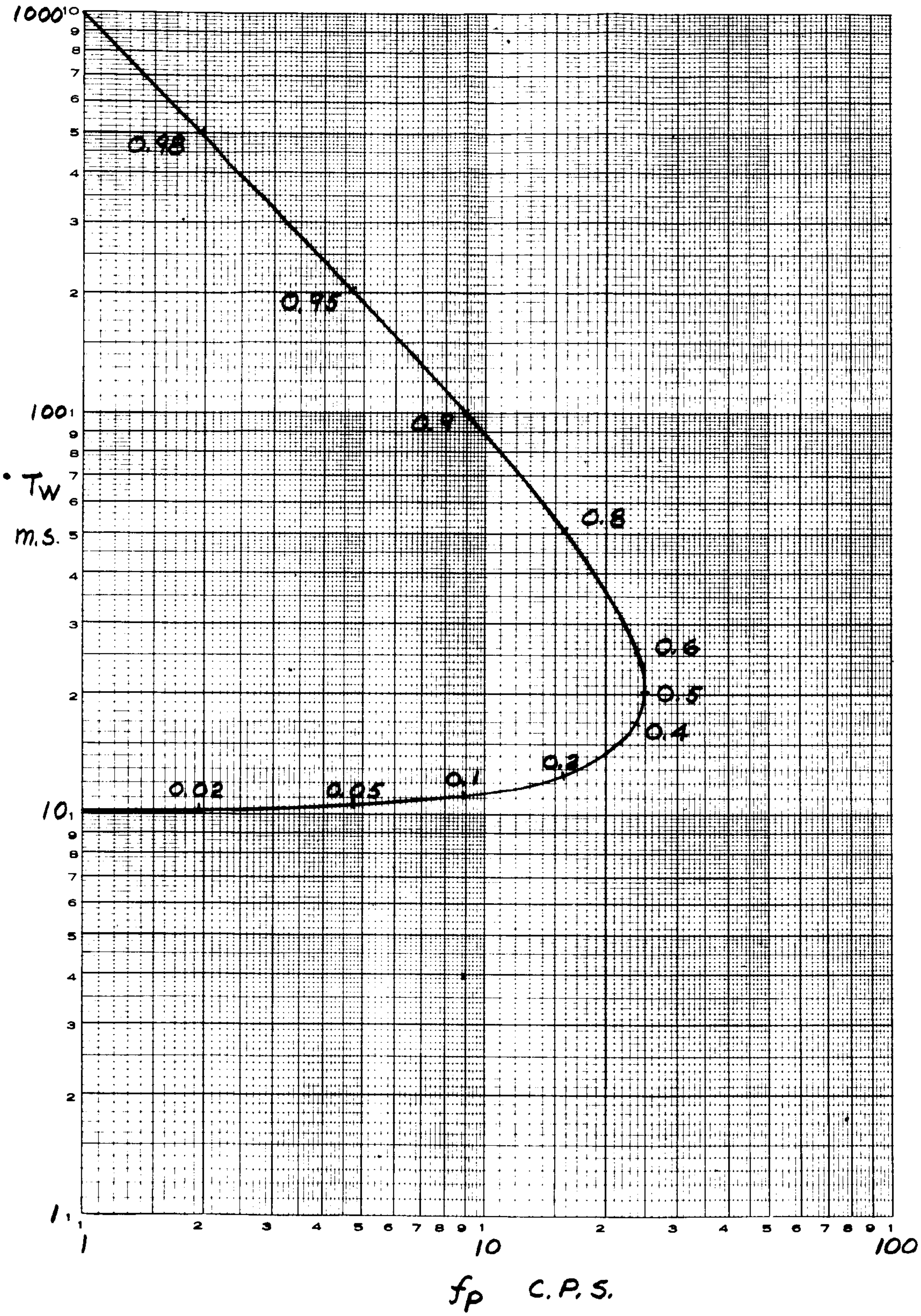

Fig. W-23. Pulse Width Versus Repetition Rate

[redacted]

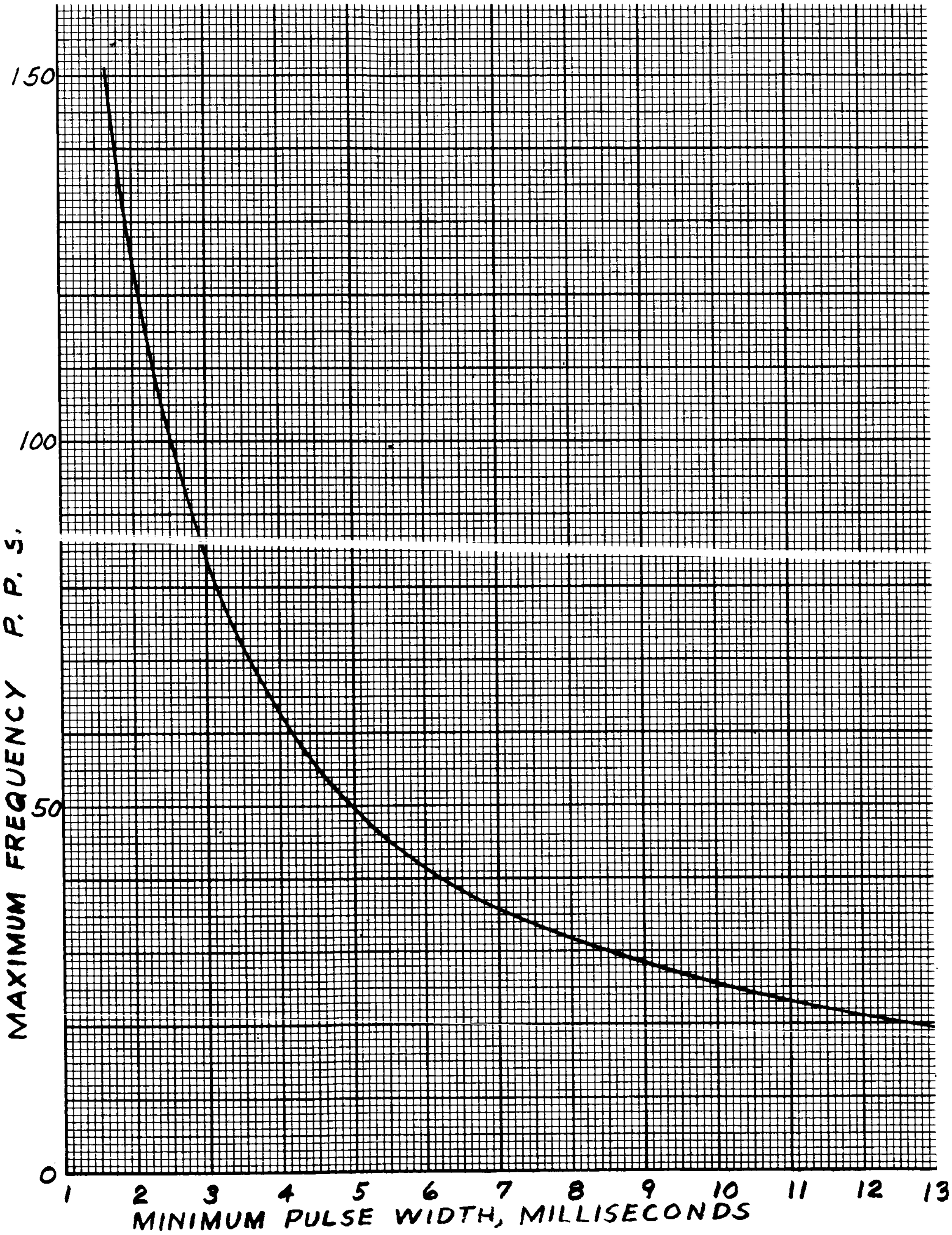

Fig. W-24. Pulse Modulator Minimum Pulse Width—Maximum Frequency Operating Law

[redacted]

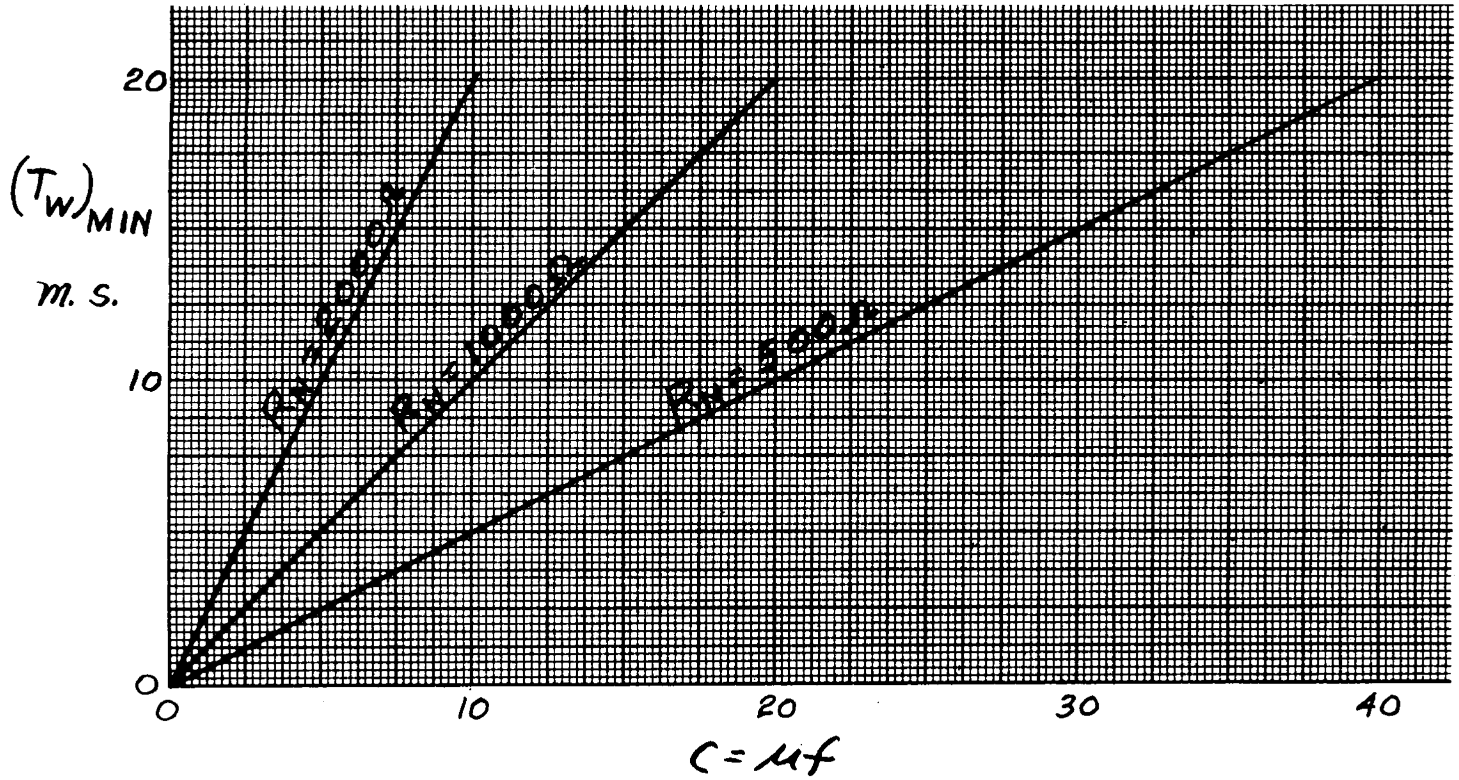

Fig. W-25. (T_W)min Versus C

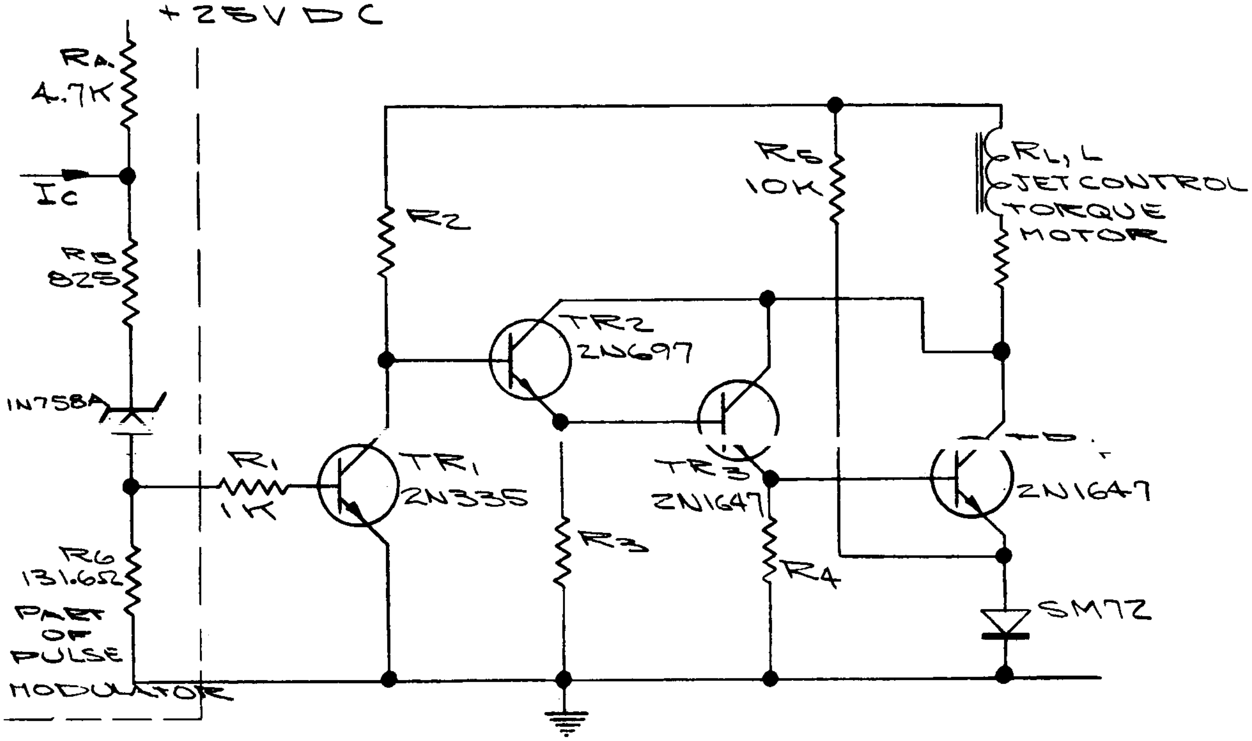
+25VDC
RA
4.7K
Ic
RB
825
1N758A
R1
1K
TR1
2N335
R2
TR2
2N697
R3
TR3
2N1647
R4
R5
10K
RL, L
JET CONTROL
TORQUE
MOTOR
2N1647
SM72
R6
131.6Ω
PART
OF
PULSE
MODULATOR

Fig. W-26. Jet Switching Amplifier Schematic

[redacted]

[redacted]

APPENDIX X

DEVELOPMENT OF LONGITUDINAL TRANSFER FUNCTION

The differential equation for vehicle dynamics in the longitudinal axis using the rigid body assumption is:

(1)

$$\ddot{\theta} + \frac{M_{\dot{\theta}}}{I_{YY}}\dot{\theta} + \frac{M_{\alpha}}{I_{YY}}\alpha = -\frac{M_{\delta}}{I_{YY}}\delta$$

The relation between α and θ is given by:

(2)

$$\theta = \alpha + \gamma$$

$$\dot{\gamma} = \dot{\theta} - \dot{\alpha}$$

(3)

$$\frac{N_{\alpha}}{m}\alpha \approx \frac{V\dot{\gamma}}{g}$$

$$\alpha = \frac{Vm}{N_{\alpha}g}\dot{\gamma} = A(\dot{\theta} - \dot{\gamma})$$

where $$A = \frac{Vm}{N_{\alpha}g}$$

[redacted]

DEFINITIONS

θ = vehicle pitch angle, degrees

α = angle of attack, degrees

γ = flight path angle, degrees

$M_{\dot{\theta}}$ = pitching moment due to the angular pitching rate, ft-lbs

M_{α} = pitching moment due to the angle of attack, ft-lbs

M_{δ} = pitching moment due to flap detection, ft-lbs

N_{α} = normal force due to the angle of attack, lbs

m = mass of vehicle, slugs

v = velocity of vehicle, feet/sec

g = gravitational constant = 32.2 ft/sec^2

$\dot{\theta}$ = vehicle pitch rate, degrees/second

$\dot{\alpha}$ = rate of change of the angle of attack, degrees/second

$\dot{\gamma}$ = rate of change of the flight path angle, degrees/second

$C_{m_{\alpha}}$ = change in pitching moment coefficient per unit change in the angle of attack

$C_{m_{\delta}}$ = change in pitching moment coefficient per unit change in the flap detection

K_{a} = aerodynamic gain

S = Laplace transform variable

I_{yy} = pitch moment of inertia

δ = flap deflection

c = reference length

[redacted]

(3) $\alpha = A\dot{\gamma}$ $\qquad \dot{\gamma} = \frac{\alpha}{A}$

Substitute in (2)

(2)
$$\frac{\alpha}{A} = \dot{\theta} - \dot{\alpha}$$

$$\dot{\alpha} + \frac{1}{A}\alpha = \dot{\theta}$$

Writing equation (2) in Laplace transform notation

(4) $\left(S + \frac{1}{A}\right)\alpha = \dot{\theta}$

(4) $\frac{\alpha}{\dot{\theta}} = \frac{1}{\left(S + \frac{1}{A}\right)}$

Take the Laplace transform of both sides of equation (1) to obtain,

(5)
$$\left[S + \frac{M_{\theta}}{I_{YY}} + \left(\frac{M_{\alpha}}{I_{YY}}\right)\left(\frac{1}{S + \frac{1}{A}}\right)\right]\dot{\theta} = -\frac{M_{\delta}}{I_{YY}}\,\delta$$

(5)

(5)

$$\frac{\dot{\theta}}{-\delta} = \frac{M_\delta/I_{YY}\,(S + 1/A)}{S^2 + \frac{1}{A}S + \frac{M_{\dot{\theta}}}{I_{YY}}\left(S + \frac{1}{A}\right) + \frac{M_\alpha}{I_{YY}}}$$

Since $M_{\dot{\theta}} \approx 0$ and $A \gg 1$, eq. (5) can be approximated by the following expression:

(6)

$$\frac{\dot{\theta}}{-\delta} = \frac{M_\delta/I_{YY}}{S^2 + \frac{M_\alpha}{I_{YY}}} = \frac{M_\alpha}{S^2 + \omega_n^2}$$

Where $K_a = M_\delta / I_{YY}$ and $\omega_n^2 = M_\alpha / I_{YY}$

Both K_a and ω_n^2 are functions of q, where q is the dynamic pressure.

(7)

$$K_a = M_\delta / I_{YY} = \frac{q\,A\,c\,C_{m\delta}}{I_{YY}}$$

(8)

$$\omega_n^2 = \frac{M_\alpha}{I_{YY}} = \frac{q\,A\,c\,C_{m\alpha}}{I_{YY}}$$

[redacted]

[redacted]

APPENDIX Y

DERIVATION OF TRANSFER FUNCTION FOR POSITION - RATE - INTEGRAL CONTROL SYSTEM

Referring to Fig. XII-37, the following transfer functions can be readily derived:

$$\frac{g_i}{\theta_\epsilon} = \frac{K_3}{S} + K_1 + K_2 S \qquad (1)$$

$$\frac{g_i}{\theta_\epsilon} = \frac{K_2 S^2 + K_1 S + K_3}{S} = \frac{K_2 \left(S^2 + \frac{K_1}{K_2} S + \frac{K_3}{K_2}\right)}{S}$$

$$\frac{\delta}{g} = \frac{\frac{NK_4}{S}}{1 + \frac{NK_H}{S}} \qquad (2)$$

$$\frac{\delta}{g} = \frac{NK_H}{S + NK_H}$$

$$\frac{\theta_c}{\theta_\epsilon} = \left(\frac{\theta_c}{\delta}\right) \left(\frac{\delta}{g}\right) \left(\frac{g}{\theta_\epsilon}\right)$$

$$\frac{\theta_c}{\theta_\epsilon} = \left(\frac{K_a}{S^2 + \omega_n^2}\right) \left(\frac{NK_H}{S + NK_H}\right) \left(\frac{K_2 \left(S^2 + \frac{K_1}{K_2} S + \frac{K_3}{K_2}\right)}{S}\right) \qquad (3)$$

$$\frac{\theta_c}{\theta_\epsilon} = \frac{K_2 K_a NK_H \left(S^2 + \frac{K_1}{K_2} S + \frac{K_3}{K_2}\right)}{S \left(S + NK_H\right) \left(S^2 + \omega_n^2\right)}$$

The overall transfer function is

$$\frac{\theta_c}{\theta_i} = \frac{\dfrac{K_2 K_a N K_H \left(S^2 + \frac{K_1}{K_2} S + \frac{K_3}{K_2}\right)}{S(S + NK_H)(S^2 + \omega_n^2)}}{1 + \dfrac{K_2 K_a N K_H \left(S^2 + \frac{K_1}{K_2} S + \frac{K_3}{K_2}\right)}{S(S + NK_H)(S^2 + \omega_n^2)}} \qquad (4)$$

The characteristic equation is

$$1 + \frac{K_2 K_a N K_H \left(S^2 + \frac{K_1}{K_2} S + \frac{K_3}{K_2}\right)}{S(S + NK_H)(S^2 + \omega_n^2)} = 0 \qquad (5)$$

APPENDIX Z

FLIGHT CONTROL SUBSYSTEM

RELIABILITY STUDY

1. Reliability Goal

The flight control subsystem, used throughout the mission, has an allocated reliability goal of 99.65%.

2. Design Analysis

The flight control subsystem is made up of the following equipments:

(1) Autopilot

(2) Electrical/electronic control equipment for the operation of attitude, vernier, and mission control and abort engine along with control components for the operation of aerodynamic surfaces required for re-entry.

(3) Aerodynamic controls, auctuators, and power necessary for control.

Analysis of the preliminary configuration showed several significant reliability problems.

(1) The reliability of the servo actuators, used only for a short period during re-entry, was greatly degraded during the long mission by exposure to hard vacuum and temperature extremes. Of the estimated subsystem reliability of 93.06%, free flight degradations of the hydraulic equipment contributed 84.5% to the unreliability of the total subsystem.

(2) The autopilot backup switch and common electrical components each contributed 4.86% to subsystem unreliability.

Design changes were made: a hot gas system replaced the hydraulic equipment, improved electrical/electronic design and a standby auto pilot were incorporated.

3. Selected Configuration

The flight control subsystem, incorporating duplicate autopilots, duplicate reaction engine control electrical/electronic equipment, and hot gas servo actuators for aerodynamic control, make up the significant components of the chosen configuration. The reliability of this subsystem is estimated to be

[redacted]

99.73%. The reliability analysis summary is shown in Fig. Z-1. The reliability block diagram is shown in Fig. Z-2.

4. Reliability Gains

The substitution of the hot gas servo actuators for the hydraulic equipment alone directly contributed a 100-fold improvement in equipment reliability; negligible degradation in equipment reliability is now encountered during the 338 hour free flight period prior to its use. Indirectly, since hydraulic power generated by means of APU's was no longer necessary, the APU's and radar cells were eliminated and hydrox fuel cell batteries incorporated. By elimination of the APU's alone the reliability of the power subsystem was improved by approximately 50%; and spacecraft flexibility was significantly improved since the mission power could now be supplied in dark periods independent of sunlight.

During the study period, reliability of the flight control subsystem has been improved from 93.06% to 99.73%, equal to a reduction in failure probability of 26.

5. Failure Rate Data

Failure rate data used in analyzing equipment reliability are based on equipment manufacturer's experience data as well as that of The Martin Company. Hydraulic component failure rates are based on data contained in BuAer Report AE61-11, adjusted for the environmental conditions of the Apollo mission.

6. Conclusions

The reliability estimate for the flight control subsystem exceeds the assigned goal and it is anticipated that the operational subsystem will meet or exceed its goal.

[redacted]

[redacted]

Reliability Estimate For Spacecraft Flight Controls Subsystem

one-mission reliability goal 99.65%

one-mission predicted reliability 99.73%

Equipment / Component	Equivalent Mission Phase Failure Rate X 10^{-6}									Predicted Failure Rate Per Mission x 10^{-6}	% Total Subsystem Failure Rate Per Mission	Predicted Reliability In Missions Between Failure
	Countdown	Boost	Coast	Translunar Flight	Lunar Orbit	Transearth Flight	Re-Entry	Landing	Recovery			
Autopilot	--	-	-	8	15	16	47	NA	NA	86	3.2	11628
Common Electrical	4	15	1.7	83	168	82	133	"	"	486.7	18.0	2055
Hot Gas Generator	1.6	27.0	0.8	33.2	67.2	41	565.4	"	"	736.2	27.2	1358
Servoactuator Switch	--	-	-	-	-	-	199.5	"	"	199.5	7.4	5012
Servoactuators	--	-	-	-	-	-	798	"	"	798	29.5	1253
Surface Controls	-	-	-	-	-	-	399	"	"	399	14.7	2506
Predicted Phase Failure Rate	5.6	42.0	2.5	124.2	250.2	139	2141.9	NA	NA	Σ = .0027054		
Predicted Phase Reliab. In Missions Between Failure	178571	23810	400,000	8052	3997	7194	467	NA	NA		- 0027054	

Missions Between Failure 370

[redacted]

[redacted]

[redacted]

APPENDIX AA

DETERMINATION OF RENDEZVOUS EQUATIONS OF MOTION

The acceleration of a "point" as viewed from a rotating coordinate system is given by

(1) $$\ddot{P}_r = \ddot{P}_m + 2\omega \times \dot{P}_m + \omega \times (\omega \times P)$$

$\ddot{P}_r$ = acceleration in reference (inertial) space

$\ddot{P}_m$ = acceleration as measured in moving (rotating) space

ω = angular rate of rotation of rotating system

$\dot{P}_m$ = velocity in moving space

P = position in reference space

Thus, if we have a satellite and a rendezvous vehicle, and thrust is acting on the vehicle only:

(2) $$\ddot{P}_{rs} = \ddot{P}_{ms} + 2\omega \times \dot{P}_{ms} + \omega \times (\omega \times P_s) = G_s$$

(3) $$\ddot{P}_{rv} = \ddot{P}_{mv} + 2\omega \times \dot{P}_{mv} + \omega \times (\omega \times P_v) = G_v + \frac{T_v}{m_v}$$

G_s = accel. of satellite due to gravity

G_v = accel. of vehicle due to gravity

T_v = thrust applied to vehicle

[redacted]

[redacted]

Solving for $\ddot{P}_{mv} - \ddot{P}_{ms}$

(4) $$\ddot{P}_{mv} - \ddot{P}_{ms} = G_v - G_s + \frac{T_v}{m_v} - 2\omega \times \dot{P}_{mv} - \omega \times (\omega \times P_v)$$
$$+ 2\omega \times \dot{P}_{ms} - \omega \times (\omega \times P_s)$$

Let
$$\ddot{P}_{mv} - \ddot{P}_{ms} = \ddot{r}$$
$$\dot{P}_{mv} - \dot{P}_{ms} = \dot{r}$$
$$P_v - P_s = r$$

Substituting the above relation, the following general equation is obtained:

(5) $$\ddot{r} = (G_v - G_s) + \frac{T_v}{m_v} - 2\omega \times \dot{r} - \omega \times (\omega \times r)$$

$(G_V - G_S)$ may be expanded into the following approximate terms:

(6) $$(G_v - G_s)_x \approx \frac{-\mu r_x}{R_o^3} = -\omega^2 r_x$$

(7) $$(G_v - G_s)_y \approx \frac{-\mu r_y}{R_o^3} = -\omega^2 r_y$$

(8) $$(G_v - G_s)_z \approx \frac{2\mu r_z}{R_o^3} = 2\omega^2 r_z$$

Where (9) R_o = radius from earth center to satellite orbit (considered circular) and (10) $\omega = \left(\frac{\mu}{R_o^3}\right)^{1/2}$ the angular frequency of the satellite.

(ω) consists only of rotation about the lateral (x) axis of the local vertical system. Then:

[redacted]

(11) $$\omega \times \dot{r} = -j\,\omega_x \dot{r}_z + k\,\omega_x \dot{r}_y$$

and

(12) $$\omega \times (\omega \times r) = -j\,\omega_x^2 r_y - k\,\omega_x^2 r_z$$

let

(13) $$\omega_x = \omega$$

in subsequent notation.

Then, for the no thrust case we have

(14) $$\ddot{r}_x = -\omega^2 r_x + \frac{T_{vx}}{m_v}$$

(15) $$\ddot{r}_y = 2\omega\dot{r}_z + \frac{T_{vy}}{m_v}$$

(16) $$\ddot{r}_z = 3\omega^2 r_z - 2\omega\dot{r}_y + \frac{T_{vz}}{m_v}$$

Where the polarity is as shown in Figure AA-1.

The solutions of equations 14), 15) and(16) without thrust terms are:

(17) $$r_x(t) = r_{x_0}\cos\omega t + \frac{\dot{r}_{x_0}}{\omega}\sin\omega t$$

(18) $$\dot{r}_x(t) = -\omega r_{x_0}\sin\omega t + \dot{r}_{x_0}\cos\omega t$$

(19)
$$\begin{aligned} r_y(t) = {} & r_{y0} + \dot{r}_{y0}\left(\frac{4}{\omega}\sin\omega t - 3t\right) \\ & + r_{z0}(6\omega t - 6\sin\omega t) \\ & + \dot{r}_{z0}\left(\frac{2}{\omega} - \frac{2}{\omega}\cos\omega t\right) \end{aligned}$$

(20)
$$\begin{aligned} \dot{r}_y(t) = {} & 4\dot{r}_{y0}\cos\omega t - 3\dot{r}_{y0} \\ & + 6 r_{z0}(\omega - \omega\cos\omega t) \\ & + 2\dot{r}_{z0}\sin\omega t \end{aligned}$$

(21)
$$\begin{aligned} r_z(t) = {} & \dot{r}_{y0}\left(\frac{2}{\omega}\cos\omega t - \frac{2}{\omega}\right) \\ & + r_{z0}(4 - 3\cos\omega t) \\ & + \dot{r}_{z0}\left(\frac{1}{\omega}\sin\omega t\right) \end{aligned}$$

(22)
$$\begin{aligned} \dot{r}_z(t) = {} & -2\dot{r}_{y0}\sin\omega t \\ & + 3 r_{z0}\,\omega\sin\omega t \\ & + \dot{r}_{z0}\cos\omega t \end{aligned}$$

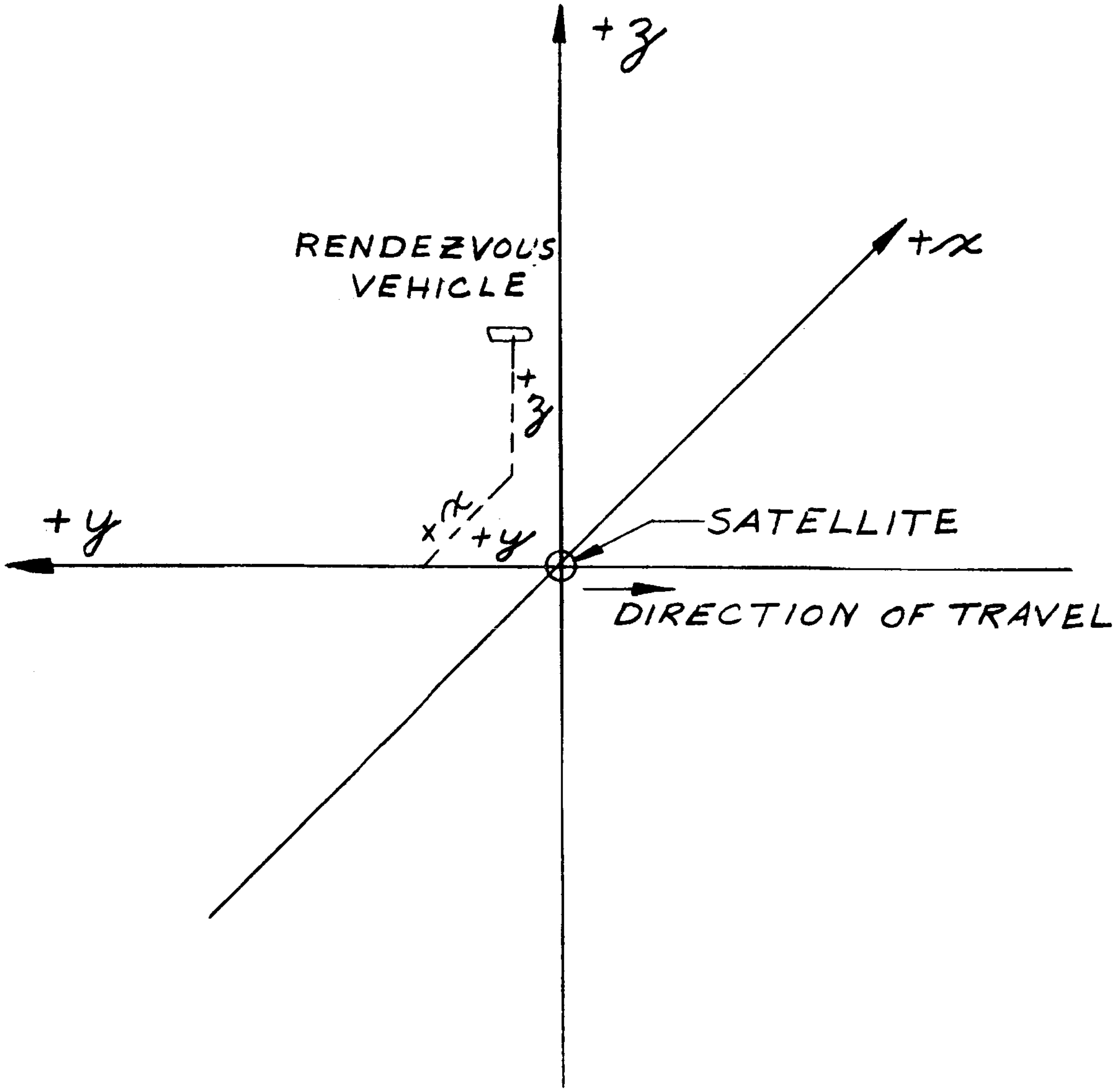
+z
+x
RENDEZVOUS VEHICLE
+z
x
+y
+y
SATELLITE
DIRECTION OF TRAVEL

Fig. AA-1 Rendezvous Reference System

[redacted]

[redacted]

APPENDIX BB

LIST OF REFERENCES

II-1 "Study Report, Navigation and Guidance System for NASA Apollo Vehicle, Vol. I, Technical Report," prepared by ARMA, A Division of American Bosch Arma Corporation, Arma Document #CX-13, 184; AG1-16, April 21, 1961 (Confidential).

II-2 "Technical Proposal, Optical-Inertial Guidance for The Martin Company Apollo," revised 5 May 1961, Autonetics Report EM-6741 (Secret).

II-3 "An Introduction to Celestial Mechanics," F.R. Moulton, The Macmillan Company, Second Edition, N.Y., 1923.

II-4 "Three-Body Problem: Earth-Moon Space Ship," Astronautica-Acta, W.F. Grobner, Vol. 5, No. 5, 1959, pp. 287-312.

II-5 "Asymptotic Expansion of the Solutions of the Equations of Motion in Earth-Moon Space," A. Yukerman, No. 61-8, January 1961.

III-1 "Divergence from Equilibrium Glide Path at Supersatellite Velocities," by R. Morth and J. Speyer, ARS Journal, Vol. 31, No. 3, March 1961.

III-2 "An Approximate Analytical Method for Studying Entry Into Planetary Athmospheres" NASA Technical Report R-11 by Dean R. Chapman.

III-3 "An Analysis of the Corridor and Guidance Requirements for Supercircular Entry into Planetary Atmospheres," NASA Technical Report R-55 by Dean R. Chapman.

III-4 "Piloted Simulator Tests of a Guidance System which can Continuously Predict Landing Point of a Low L/D Vehicle During Atmosphere Re-entry," NASA TN D-787 by R.C. Wingrove and R.E. Coate.

III-5 "An Analytical Method for Studying the Lateral Motion of Atmosphere Entry Vehicles," NASA Technical Note D-325 by R.E. Slye.

III-6 "Gradient Theory of Optimal Flight Paths," American Rocket Society Preprint No. 1230-60, by H.J. Kelley.

III-7 "Determination of the Lift or Drag Program that Minimizes Re-entry Heating with Acceleration or Range Constraints Using a Steepest Descent Computation Procedure," Institute of Aeronautical Sciences Preprint No. 61-6, by A.E. Bryson, W.F. Denham, F.J. Carroll, and K. Mikami.

III-8 "A Proposal to Determine Optimum Re-entry Trajectories and to Develop a Trajectory Control System for Project Apollo," BR-1176, Prepared by Raytheon Company.

III-9 "Centrifuge Study of Pilot Tolerance to Acceleration and the Effects of Acceleration on Pilot Performance," NASA TN-337, by Creer, Smedal, and Wingrove.

III-10 "Synthesis and Flight Test of a Ballistic Missile Adaptive Flight Control System," by Ordway B. Gates, Jr. and Orrin C. Kaste, IAS Paper No. 59-124.

III-11 "Automatic Feedback Control System Synthesis," McGraw-Hill Company, Truxal, 1955.

IV-1 Technical Description, Litton P-300 Inertial Subsystem, Publication No. 1453, Guidance and Control Systems Division, Litton Systems, Inc., March 1961.

IV-2 "Proposal for an Earth-Moon Theodolite-Sextant," KIC-ED-882, Kollsman Instrument Corporation, 9 May 1961.

IV-3 "Proposal for Apollo Altimeter Equipment," Aerospace Communication and Controls Division, Defense Electronics Products, Radio Corporation of America, 20 April 1961.

V-1 "Astronomy" by Russel, Dugan, and Stewart, Gunn and Co.

V-2 Star Tables and Tables as follows:

Zweiter Katalog der Astronomischen Gesellschaft-Hamberg
Bergedorf 1951

Yale Zone Catalogue, Yale Observatory, Conn.

The General Catalog of 33,342 Stars for Epoch 1950

The American Ephemeris and Nautical Almanac,
U.S. Government Printing Office, Wash. 25 D.C.

Bonn 1886 Star Charts, Steindruck von A. Henry
in Bonn, 1886

Berlin 1898 Star Charts Ausgabe mit Verbesserungen aller bis zum Jahre 1898 bekannt gewordenen Fehler

V-3 "Sky and Telescope," American Astronomers Report, pp 134-135 April 1950.

V-4 "The Earth's Equatorial Radius and the Distance of the Moon" by John O'Keefe, Astronautical Journal, Page 108, Vol. 57, 1952.

V-5 "Predicting and Observing Lunar Occultations" by Flora Sadler, Sky and Telescope, Dec. 1959.

V-6 "The Practical Use of Ephemeris Time" by G.M. Clemence, Sky and Telescope, Jan. 1960.

V-7 Transactions of the International Astronomical Union, Vol. X. 1958; Vol. IX, 1955; Vol. VIII, 1952; Vol. VII, 1948 Cambridge Univ. Press.

V-8 "Geodetic Applications of Eclipses and Occultations" by W.D. Lambert, Bulletin Geodestique 13, 1 Sept. 1949, pp 274-292.

V-9 "Occultations and Lunar Mountains" by Davis S. Evans, A.J. 60 (11), 432-440, 1950.

V-10 Technical Report on Occultations, Army Map Service (available in June 1961.

VI-1 Final Report-Human Factors Analysis and Recommendations for Project Apollo, MPG, Minneapolis-Honeywell Regulators Company, April 29, 1961.

VIII-1 "Typical Kearfott Gyrodynamics Products," GTO - 115A, Kearfott Division, General Precision Incorporated.

VIII-2 Honeywell Subminiature Platform, GG-8029, MH Aero Document R-ED 28050, Military Products Group, Minneapolis-Honeywell Regulator Company, 5 December 1960.

VIII-3 Computer for Apollo to The Martin Company, Federal Systems Division, IBM, 10 May 1961.

VIII-4 A Digital Computer for the Apollo Program, Proposal to The Martin Company, Baltimore, Maryland, CDC No. 30704, Litton Systems, Inc.

VIII-5 Proposal to Furnish Digital Flight Controller for the Apollo, Proposal No. A61-143, Apparatus Division, Texas Instruments Incorporated, 29 April 1961.

VIII-6 Technical Description of the LN-5 Astro-Inertial Navigational System, Publication 1253, Litton Industries.

XI-1 "Centrifuge Study of Pilot Tolerance to the Effects of Acceleration on Pilot Performance," by Brent Y. Creer, Capt. Harold A. Smedal and Rodney C. Wingrove, NASA TN D-337.

XI-2 Man's Ability to Apply Certain Torques While Weightless by Ernest Daendolet and John F. Rievley, WADC Technical Report 59-94.

XI-3 Manual Application of Impulse While Tractionless by Ernest Daendolet, WADC Technical Report 60-129.